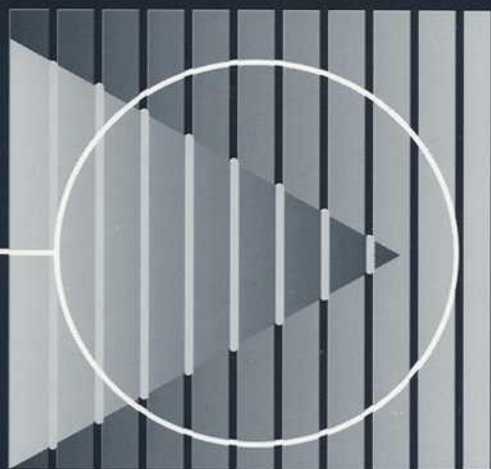


Techniques to Assess the  
**Corrosion Activity**  
**of Steel Reinforced**  
**Concrete Structures**



**Neal S. Berke**  
**Edward Escalante**  
**Charles K. Nmai**  
**David Whiting**  
EDITORS



**STP 1276**

STP 1276

# *Techniques to Assess the Corrosion Activity of Steel Reinforced Concrete Structures*

*Neal S. Berke, Edward Escalante, Charles K. Nmai, and  
David Whiting, Editors*

ASTM Publication Code Number (PCN):  
04-012760-07



ASTM  
100 Barr Harbor Drive  
West Conshohocken, PA 19428-2959  
Printed in the U.S.A.

Library of Congress Cataloging-in-Publication Data

Techniques to assess the corrosion activity of steel reinforced  
concrete structures / Neal S. Berke ... [et al.], editors.  
(STP ; 1276)

“ASTM publication code number (PCN) 04-012760-07.”

Includes bibliographical references and index.

ISBN 0-8031-2009-5

1. Reinforcing bars--Corrosion--Testing. 2. Reinforced concrete--  
Corrosion--Testing. # Steel, Structural--Corrosion--Testing.  
I. Berke, Neal Steven, 1952- . II. Series: ASTM special technical  
publication ; 1276

TA445.5.T43 1996

620.1'3723--dc20

96-35303

CIP

Copyright © 1996 AMERICAN SOCIETY FOR TESTING AND MATERIALS, West Conshohocken, PA. All rights reserved. This material may not be reproduced or copied, in whole or in part, in any printed, mechanical, electronic, film, or other distribution and storage media, without the written consent of the publisher.

#### Photocopy Rights

**Authorization to photocopy items for internal, personal, or educational classroom use, or the internal, personal, or educational classroom use of specific clients, is granted by the American Society for Testing and Materials (ASTM) provided that the appropriate fee is paid to the Copyright Clearance Center, 222 Rosewood Drive, Danvers, MA 01923, Tel: 508-750-8400; online: <http://www.copyright.com/>.**

#### Peer Review Policy

Each paper published in this volume was evaluated by three peer reviewers. The authors addressed all of the reviewers' comments to the satisfaction of both the technical editor(s) and the ASTM Committee on Publications.

To make technical information available as quickly as possible, the peer-reviewed papers in this publication were prepared "camera-ready" as submitted by the authors.

The quality of the papers in this publication reflects not only the obvious efforts of the authors and the technical editor(s), but also the work of these peer reviewers. The ASTM Committee on Publications acknowledges with appreciation their dedication and contribution to time and effort on behalf of ASTM.

# Foreword

This publication, *Techniques to Assess the Corrosion Activity of Steel Reinforced Concrete Structures*, contains papers presented at the symposium of the same name, held on 7 December 1994. The symposium was sponsored by ASTM Committees G-1 on Corrosion of Metals and C-9 on Concrete and Concrete Aggregates. Neal S. Berke of W. R. Grace and Company in Cambridge, MA; Edward Escalante of NIST in Gaithersburg, MD; Charles K. Nmai of Master Builders in Cleveland, OH; and David Whiting of Construction Technology Labs in Skokie, IL, presided as symposium chairmen and are editors of the resulting publication.

# Contents

<b>Overview—N. S. BERKE</b>	vii
<b>MODELING</b>	
<b>Modeling the Measured Time to Corrosion Cracking—C. D. NEWHOUSE AND R. E. WEYERS</b>	3
<b>Progress on Design and Residual Life Calculation with Regard to Rebar Corrosion of Reinforced Concrete—C. ANDRADE AND C. ALONSO</b>	23
<b>Predicting Times to Corrosion from Field and Laboratory Chloride Data—N. S. BERKE AND M. C. HICKS</b>	41
<b>Computer Modeling of Effect of Corrosion Macrocells on Measurement of Corrosion Rate of Reinforcing Steel in Concrete—A. A. SAGÜÉS AND S. C. KRANC</b>	58
<b>Finite Element Modeling of Ground Level Potential Measurements of Galvanic Cells on Concrete Pipe—E. J. CARLSON, R. G. STRINGFELLOW, AND S. C. HALL</b>	74
<b>CORROSION RATE MEASUREMENTS</b>	
<b>Field Measurement of the Corrosion Rate of Steel in Concrete Using a Microprocessor Controlled Unit with a Monitored Guard Ring for Signal Confinement—J. P. BROOMFIELD</b>	91
<b>Electrochemical Methods for On-Site Determinations of Corrosion Rates of Rebars—S. FELIÚ, J. A. GONZÁLEZ, AND C. ANDRADE</b>	107
<b>Assessment of Corrosion of Steel in Concrete Structures by Magnetic Based NDE Techniques—A. GHORBANPOOR AND S. SHI</b>	119
<b>Tests for Evaluation of the Effectiveness of Penetrating Sealers in Reducing Penetration of Chlorides into Concrete—D. WHITING AND M. A. NAGI</b>	132

<b>Combined Bulk and Interfacial Studies of the Cement/Steel System by Impedance Spectroscopy—S. J. FORD AND T. O. MASON</b>	146
--	-----

CASE STUDIES

<b>Preliminary Corrosion Investigation of Prestressed Concrete Piles in a Marine Environment: Deerfield Beach Fishing Pier—P. D. KRAUSS AND C. K. NMAI</b>	161
--	-----

<b>Field Experience with Rebar Probes to Monitor Performance of Sprayed Zinc Galvanic Anodes on Concrete—A. A. SAGÜÉS AND R. G. POWERS</b>	173
--	-----

<b>A Case Study: Assessment of Ice Rink Refrigerant Tubing Corrosion Using Half Cell Techniques—W. J. BRICKEY</b>	185
---	-----

# Overview

---

The deteriorating infrastructure is a topic of major importance throughout the world. Steel reinforced concrete is one of the most widely used construction materials, and as such, many of the deteriorating structures are of reinforced concrete. This has occurred even though steel-reinforced concrete is very durable, because this very durability has led to its use in aggressive environments.

The purpose of the symposium, in which the papers in this special technical publication (STP) were presented, is to explore techniques to determine the corrosion activity of steel in reinforced concrete field structures. This is not an easy task due to the fact that the steel is not visible, concrete has a high resistivity, and the structures are in use. Furthermore, the structures are orders of magnitude larger than typical laboratory specimens and traditional techniques, such as mass loss measurements and visual appearance of embedded steel are not practical.

ASTM Committees G-1 on Corrosion of Metals, in particular G01.14 on Rebar Corrosion, and C-9 on Concrete jointly sponsored the symposium. Both committees have active efforts in determining corrosion rates and other factors such as permeability to the ingress and chloride as well as other concrete properties that could affect performance. These committees have been involved in producing several STPs related to the performance of concrete and steel-reinforced concrete in the environment.

There are 13 papers in this STP that have been grouped into three major headings: Modeling, Corrosion Rate Measurements, and Case Studies. All of the papers address more than one of these topics and several others; however, the major emphasis is in the area of the major heading. Several of the papers address new methods of assessment or look at older methods with new approaches, that are in some cases, controversial. The editors encourage the readers to evaluate for themselves conclusions based upon the evidence given in the papers and the included references. As a whole, the papers presented give a broad overview that can be used in the assessment of steel-reinforced concrete in the field.

## Modeling

The five papers in the Modeling section deal with using assessment information to predict remaining service life, service life of similar newer structures, or current condition. They combine the use of electrochemical measurements such as corrosion potential and corrosion rate measurements.

The papers by Newhouse and Weyers and Andrade and Alonso address using corrosion rate measurements to predict time to cracking. The first paper showed that chloride contents and changing environmental conditions played major roles and that corrosion rate measurements were far from accurate. They also showed that Bazant's model for time to cracking underestimated the times.

Andrade and Alonso looked at various approaches used to predict chloride ingress or carbonation front movement. These techniques were combined with corrosion rate measurements and predicted corrosion product build-up to develop models to predict remaining service life or service life of new structures.

Berke and Hicks determined chloride profiles for several field structures to calculate effective diffusion coefficients. These values were used to predict future chloride profiles from which time to corrosion initiation could be estimated. They showed that laboratory predictions of diffusion coefficients based upon Test Method for Electrical Indication of Concrete's Ability to Resist Chloride Ion Penetration (ASTM C 1202) were in good agreement with field measurements on the same concrete. The potential benefits of using corrosion inhibitors to significantly increase the threshold value of chloride for corrosion initiation were shown.

Kranc and Sagüés, and Hall et al. discussed the use of models based on finite element analyses. Kranc and Sagüés show how finite difference computations can be used to correct underestimations of the corrosion rates in large marine structures. Hall et al. use finite element analysis of corrosion potential data on buried pipe to detect corroding areas and to identify the detection limits of potential surveys.

### **Corrosion Rate Measurements**

Five papers are included in this section. Two examine the use of guard ring electrodes, one looks at electrochemical impedance spectroscopy, one at a magnetic-based nondestructive technique, and the last paper at techniques to evaluate sealers. It should be noted by the reader that corrosion rate measurements are at best indicative of conditions existing at test time, and given the changes in environment that occur in the field, can vary significantly from day to day or even within a few hours due to changing moisture, temperature, and chloride contents.

Broomfield et al. and Feliú et al. compare the use of guard ring electrodes to conventional counter electrode and reference electrode techniques in determining corrosion rates of steel in field structures. The papers show that the guard ring confines the current to a more well-defined area during polarization resistance so that a more accurate determination of the area polarized can be made. This results in a more accurate representation of the corrosion rate.

Broomfield et al. use the guard ring electrode to evaluate the performance of several rehabilitation techniques that were applied to field structures.

Feliú et al. show that the corrosion rates are significantly lower at low corrosion rates for the guard ring electrode. At higher corrosion rates or with larger counter electrodes the corrosion rate without the guard ring approaches that of the guard ring. It is useful to review the Newhouse and Weyers papers which showed that the guard ring underestimated corrosion rates and the conventional techniques overestimated corrosion rates.

Ghorbanpoor and Shi showed that a magnetic field technique can determine a 3% reduction in cross-sectional steel area. More research is needed with this new application that could offer an additional nondestructive technique that shows cumulative corrosion damage to the time of measurement.

Ford and Mason use electrochemical impedance spectroscopy to examine steel in cement pastes. They use ultra-high frequencies in the MHz range to determine diffusivity and permeability of the paste. Frequencies in the Hz range provide information on the interfacial zone between the steel and paste, and the lower frequencies mHz provide information on passivity. Even though the techniques discussed are more suited for laboratory studies, predictions of permeability from laboratory data might be applicable to estimating service life.

The paper by Whiting and Nagi assesses the performance of penetrating sealers with two new test techniques. One is a resistivity measurement and the other is based upon the absorption of water. Both techniques can be used in the field. Though not a corrosion technique, the evaluation of the condition of sealers over time in the field can be used as a predictor of future corrosion activity due to the ingress of chloride.

## Case Studies

Three papers on case studies are given. Two involve marine concrete structures and one is of a corroding ice rink.

Krauss and Nmai provide an initial evaluation of a new fishing pier with an amine and fatty acid admixture to reduce corrosion. They employed visual, chloride, and corrosion potential analyses. They showed that high negative corrosion potential are not indicative of corrosion activity in concrete submerged in sea water and that the initial condition of the structure is good. The importance of developing base-line information for future studies is emphasized.

Sagüés and Powers evaluated the use of spray zinc anodes in several field locations in Florida. They used short embedded rebar probes with switchable connectors so that various cathodic protection parameters could be determined.

Brickey used corrosion potential mapping, chloride analyses, microscopy, and destructive techniques to document and determine the cause of corrosion-induced damage in an ice rink. The paper is useful in showing how to combine multiple techniques to solve a real world problem.

The papers outlined here will give the reader a good background into the latest techniques used in assessing steel-reinforced concrete structures and in modeling future service life based upon the assessment. The reader will also see that considerable work remains in refining techniques to accurately measure corrosion activity. I wish to thank my co-editors Ed Escalante, NIST; Charles K. Nmai, Master Builders, Inc.; and David Whiting, Construction Technology Laboratories, for help in getting speakers, running sessions, reviewing papers, and selecting reviewers. They join me in gratefully acknowledging the efforts of the authors and ASTM personnel that have made this publication possible.

*Neal S. Berke*

Co-editor and Chairman, G01.14 on Rebar Corrosion,  
Grace Construction Products.

# **Modeling**

Charles D. Newhouse<sup>1</sup> and Richard E. Weyers<sup>2</sup>

## MODELING THE MEASURED TIME TO CORROSION CRACKING

---

**REFERENCE:** Newhouse, C. D. and Weyers, R. E., “**Modeling the Measured Time to Corrosion Cracking**,” Techniques to Assess the Corrosion Activity of Steel Reinforced Concrete Structures, ASTM STP 1276, Neal S. Berke, Edward Escalante, Charles K. Nmai, and David Whiting, Eds., American Society for Testing and Materials, 1996.

**ABSTRACT:** The deterioration models for reinforced concrete structures include a period for time to corrosion cracking: time from initiation of corrosion to first cracking. Theoretical equations for determining the time to corrosion cracking have been presented but never validated. This paper reports on a study which was initiated to validate or modify a set of theoretical equations for field linear polarization, unguarded and guarded, corrosion rate devices. The test variables included six corrosion rates, two concrete cover depths, two reinforcing steel bar diameters and spacings, two exposure conditions (indoors and outdoors), and one design concrete strength (water to cement ratio). Influence of temperature and chloride content on the measured corrosion rates are presented. Corrosion rates increase with increasing chloride content and corrosion rates vary significantly with annual changes in temperature, highest in the spring and lowest in the winter. Measured metal loss measurements were compared with the calculated metal loss based on monthly corrosion rate measurements for both devices. The 3LP device significantly over-estimated the amount of metal loss and the Geocor 3 device significantly under-estimated the amount of metal loss based on average monthly measurements. The theoretical time to corrosion cracking equations significantly under-estimated the time to corrosion cracking using a uniform corrosion rate based on the measured metal loss.

**KEYWORDS:** corrosion, concrete cracking, chloride, corrosion measurement, corrosion rate

---

---

<sup>1</sup>Graduate Student, Charles E. Via, Jr. Department of Civil Engineering, Virginia Polytechnic Institute and State University, Blacksburg, VA 24061-0105.

<sup>2</sup>Professor, Charles E. Via, Jr. Department of Civil Engineering, Virginia Polytechnic Institute and State University, Blacksburg, VA 24061-0105.

The problem of chloride induced corrosion of reinforcing steel in concrete structures is well known. The mechanism requires a threshold concentration of the chloride ion to initiate corrosion, oxygen and moisture as the electrolyte. The severity of the problem is illustrated by the condition of United States bridges. Forty percent of 576,665 bridges on the federal aid system are structurally deficient or functionally obsolete [1]. Corrosion of the reinforcing steel in concrete bridges accounts for 40 percent of the deficient bridges, 92,266 deficient bridges [1].

Limited resources requires cost-effective management of the protection, repair, and rehabilitation of concrete bridges and other structures. Service lives and initial costs are needed to cost-effectively manage our infrastructure. Service lives may be estimated from deterioration models. The deterioration models for the chloride-induced corrosion of steel reinforced concrete bridges consist of a rapid initial deterioration related to construction procedures and quality, a chloride diffusion time period to a specified depth based on a percentage of the reinforcing steel, a corrosion period (time from initiation to cracking) followed by a rate of deterioration to a cumulative damage defined as the end-of-functional-service-life [2,3].

Methods have been developed for estimating the amount of initial damage, the chloride diffusion period, the rate of damage and definition of end-of-functional-service-life for concrete bridges [3]. However, the corrosion period has not been determined and thus presently can only be estimated [3]. This paper presents results from a study that was initiated to estimate the time-to-corrosion cracking from measurements with an unguarded and guarded linear polarization device and unvalidated theoretical equations.

## THEORETICAL EQUATIONS

Bazant presented the following theoretical equation for estimating the time to corrosion cracking [4].

$$t_{\text{corr}} = \rho_{\text{corr}} \frac{D\Delta D}{Sj_r} \quad (1)$$

where

- $t_{\text{corr}}$  = time to corrosion cracking,
- $\rho_{\text{corr}}$  = function of the mass density of steel and rust,
- $D$  = reinforcing bar diameter,
- $\Delta D$  = increase in bar diameter,
- $S$  = bar spacing,
- $j_r$  = rate of rust production per unit length of bar.

The increase in bar diameter ( $\Delta D$ ) is a function of cover depth ( $L$ ), concrete strength ( $f_c$ ), bar diameter ( $D$ ), and bar hole flexibility ( $\delta_{pp}$ ). If the bar spacing is greater than  $6D$ , which is the condition for all cases in this study, the increase in bar diameter is equal to the following:

$$\Delta D = 2 f_c \frac{L}{D} \delta_{pp} \quad (2)$$

and the bar hole flexibility is equal to:

$$\delta_{pp} = \left[ \frac{D(1 + \phi_{cr})}{E} \right] (1 + \nu) \cdot D^2 \left[ \frac{2}{S^2} + \frac{1}{4L(L+D)} \right] \quad (3)$$

where

- $\phi_{cr}$  = creep coefficient of concrete,
- $\nu$  = Poisson's ratio of the concrete,
- $E$  = elastic modulus of the concrete.

The theoretical failure mode for a condition in which the bar spacing ( $S$ ) is greater than 6 times the bar diameter ( $D$ ) is incline cracking.

### CORROSION RATE DEVICES

The corrosion rate devices used in this study do not measure the rate of corrosion or rate of metal loss directly. The devices measure the corrosion current density ( $i = \text{amp/cm}^2$ ) which is directly proportional to the rate of metal loss, Faraday's First Law:

$$\text{Weight of metal loss} = k I_{\text{corr}} t \quad (4)$$

where

- $k$  = electrochemical constant,
- $I_{\text{corr}}$  = corrosion current, amps,
- $t$  = time.

The devices, 3LP and Geocor 3, used in this study employ the linear polarization method to measure an instantaneous polarization resistance and the corrosion current

density is calculated from the Stern-Geary equation:

$$i_{\text{corr}} = \frac{k}{R_p} \quad (5)$$

where

$k$  = constant based on the Tafel slopes,

$R_p$  = polarization resistance.

The 3LP and Geocor 3 employ different Tafel slope values in the calculation of the constant,  $k$ . Also, the Geocor 3 uses a guard ring to confine the polarization current to a defined bar length and the polarization rate is automatically determined and applied based on the rate of corrosion. The 3LP device does not use a guard ring and the rate of polarization is operator dependent within a set of operational guidelines. Thus, the magnitude of the corrosion current densities measured by the devices are significantly different, particularly for the more passive conditions where the polarization currents tend to spread out further over the assumed bar polarization length [5].

The operational manuals of the devices present the following interpretation of the measured corrosion rates. Here liberties are taken, corrosion rate is really corrosion current densities.

### 3LP Device

Measured $i_{\text{corr}}$ , ( $\mu\text{A}/\text{cm}^2$ )	Expectation
< 0.18	No damage expected
0.18 - 0.93	Damage possible in 10-15 years
0.93 - 9.3	Damage possible in 2-10 years
> 9.3	Damage possible < 2 years

### Geocor 3

Measured $i_{\text{corr}}$ , ( $\mu\text{A}/\text{cm}^2$ )	Expectation
< 0.1	No active corrosion
> 0.2	Active corrosion

## EXPERIMENTAL DESIGN

A sensitivity analysis of Eq. 1 demonstrated that the rate of rust production ( $j_r$ ) significantly influenced the estimated time to corrosion cracking ( $t_{\text{corr}}$ ), whereas the other

parameters have a minor influence on the time to corrosion cracking [6]. Thus, the study included 6 corrosion rates, 2 reinforcing bar spacings, 2 reinforcing bar diameters, 2 concrete cover depths, 2 exposure conditions (outdoors and indoors), and 1 concrete strength (water to cement ratio). The corrosion rates were controlled by the amount of admixed chloride. A total of 56 slabs were constructed. The slabs are 188 cm square and 20 cm thick. Each slab contained 5 steel reinforcing bars as the reinforcing steel, all other reinforcement, top temperature and bottom reinforcement and temperature, was fiberglass bar. The 5 top steel reinforcing bars were electronically isolated and thus only micro-cell corrosion could take place on the steel bar surfaces. A type T thermocouple was placed at both of the center steel reinforcing bars in the center of the slab. Tables 1 and 2 summarize the experimental design. Table 3 presents the average fresh and hardened concrete properties. The coarse aggregate is a crushed limestone and the fine aggregate a natural silicious sand, ASTM C33 #57 stone and sand, respectively.

TABLE 1--Outdoor slab matrix

Admixed Chloride, kg/m <sup>3</sup>	Bar Size, mm	Bar Spacing, cm	Number of Specimens Cover Depth, cm	
			5	7.6
0.00	13	20	2	2
0.35	13	20	3	3
0.71	13	20	3	3
0.71	13	15	3	...
0.71	16	20	3	...
1.4	13	20	3	3
2.8	13	20	3	3
5.7	13	20	3	3

TABLE 2--Indoor slab mixture

Admixed Chloride kg/m <sup>3</sup>	Bar Size, mm	Bar Spacing, cm	Number of Specimens
			Cover Depth, cm
			5
0.00	13	20	2
0.35	13	20	3
0.71	13	20	3
1.4	13	20	3
2.8	13	20	3
5.7	13	20	2

TABLE 3--Concrete mixture

Batch Weights, kg/m <sup>3</sup>			
Ingredient	Weight	Property	
Cement	376	W/C	0.45
Water	169	Air content, %	5
Coarse Aggregate	1056	Slump, cm	10
Fine Aggregate	710	Compressive Strength @ 28 days, MPa	35

An initial series of corrosion rate measurements demonstrated that the rate of corrosion along a bar and within a slab were relatively uniform with the greatest variability being between slabs for a given series, matrix cell [6]. Thus, the number of corrosion rate measurements were reduced to 2 or 3 measurements each month for each specimen. Thus, 7 or 8 monthly corrosion rates were measured for each specimen series, matrix cell, over the 2 year time period are presented in this paper.

## RESULTS

Figs. 1, 2, and 3 present the average measured corrosion rates for the 3LP and Geocor 3 devices as a function of time and season for the outdoor, 5 cm cover, 13 mm bar, 20 cm spacing and the 0.0, 1.4, and 5.7 kg/m<sup>3</sup> admixed chloride content series, respectively. The results presented in Figs. 1, 2, and 3 are typical for each matrix cell specimens within an outdoor admixed chloride series. The indoor admixed chloride series had the same corrosion rate magnitudes but the corrosion rates were relatively uniform because the temperature and the moisture content of the indoor concrete were more uniform than the outdoor specimens [7].

As shown in Figs. 1, 2, and 3, the measured corrosion rates for the 3LP was always greater than the Geocor 3 measurements, regardless of the admixed chloride content. In general, the 3LP measurements were 15 to 20 times greater than the Geocor 3 measurements. Factors which contributed to the difference in measured values are different assumed Tafel slope values, differences in assumed bar polarization length (unguarded versus guarded electrode), and rate of polarization. Tafel slope values and guard electrodes would account for about a factor of 4 between the measurements [7]. Thus, a significantly large portion of the difference between the devices may be related to the difference in the rate of polarization between the devices.

Figs. 1, 2, and 3 illustrate the influence of admixed chloride content, time and season (moisture-temperature) effects on the rate of corrosion. In all cases, the initial corrosion rate was relatively high and decreased with time. For the zero admixed chloride content, this observation may be attributed to the formation of the passive layer which may have taken as long as 9 months to completely form. After 9 months, the corrosion rates were relatively constant considering seasonal effects. For the 1.4 and 5.7 admixed chloride cases, the decreasing of corrosion rate with time may be related to reduction of the cathode to anode area and the time for corrosion products to diffuse through a rust layer.

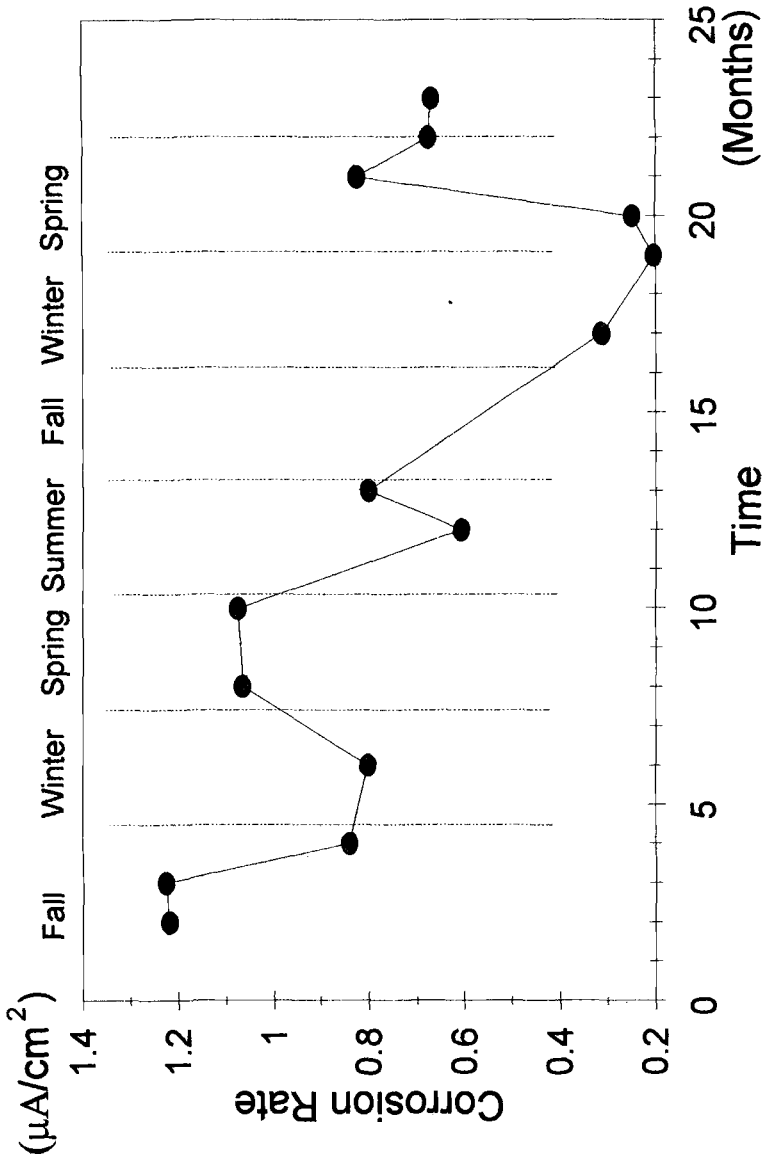


Fig. 1A--Typical 3LP monthly average corrosion rate profile for the 0.00 admixed chloride series.

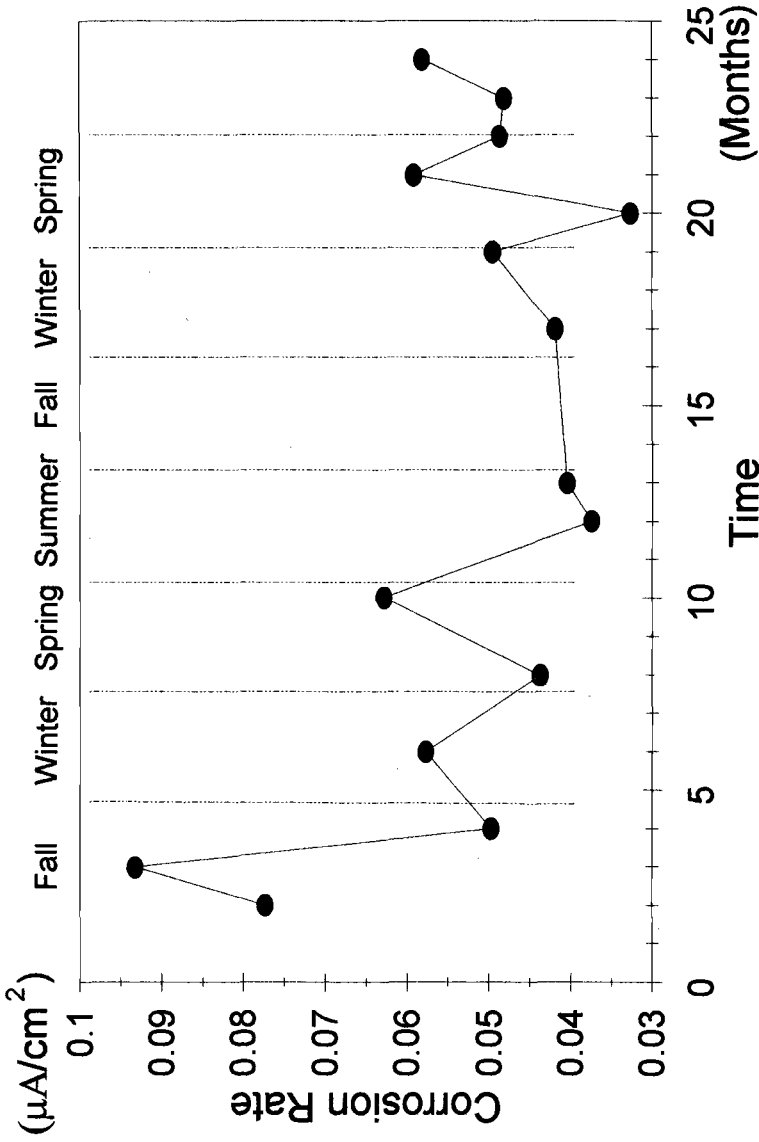


Fig. 1B--Typical Geocor 3 monthly average corrosion rate profile for the 0.00 admixed chloride series.

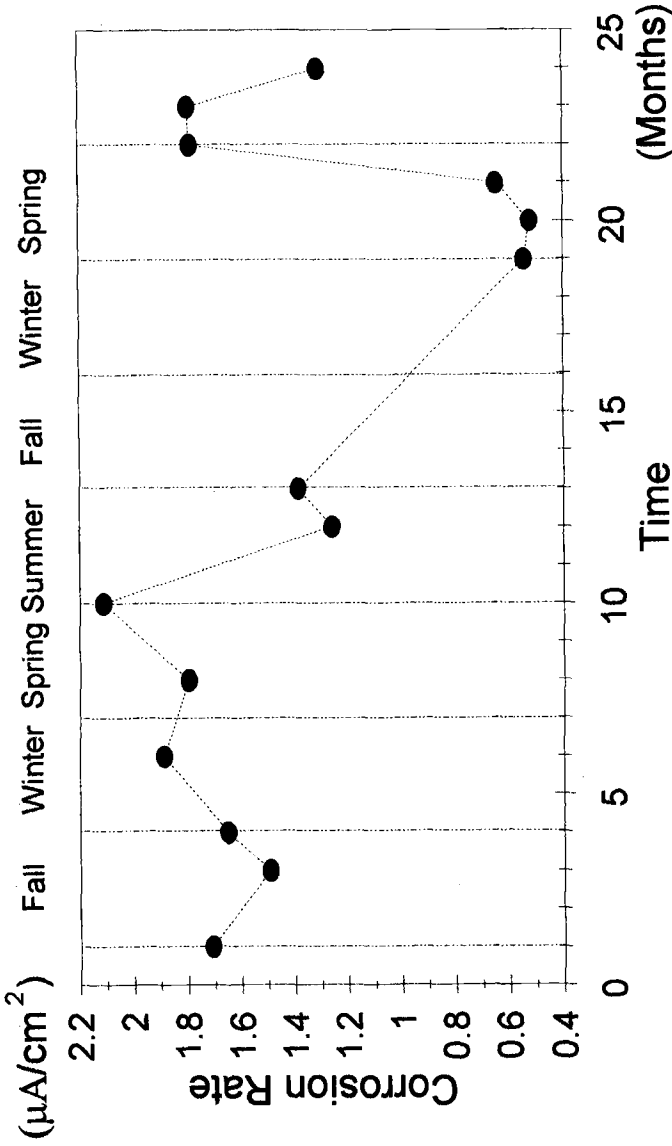


Fig. 2A--Typical 3LP monthly average corrosion rate profile for the 1.4 admixed chloride series.

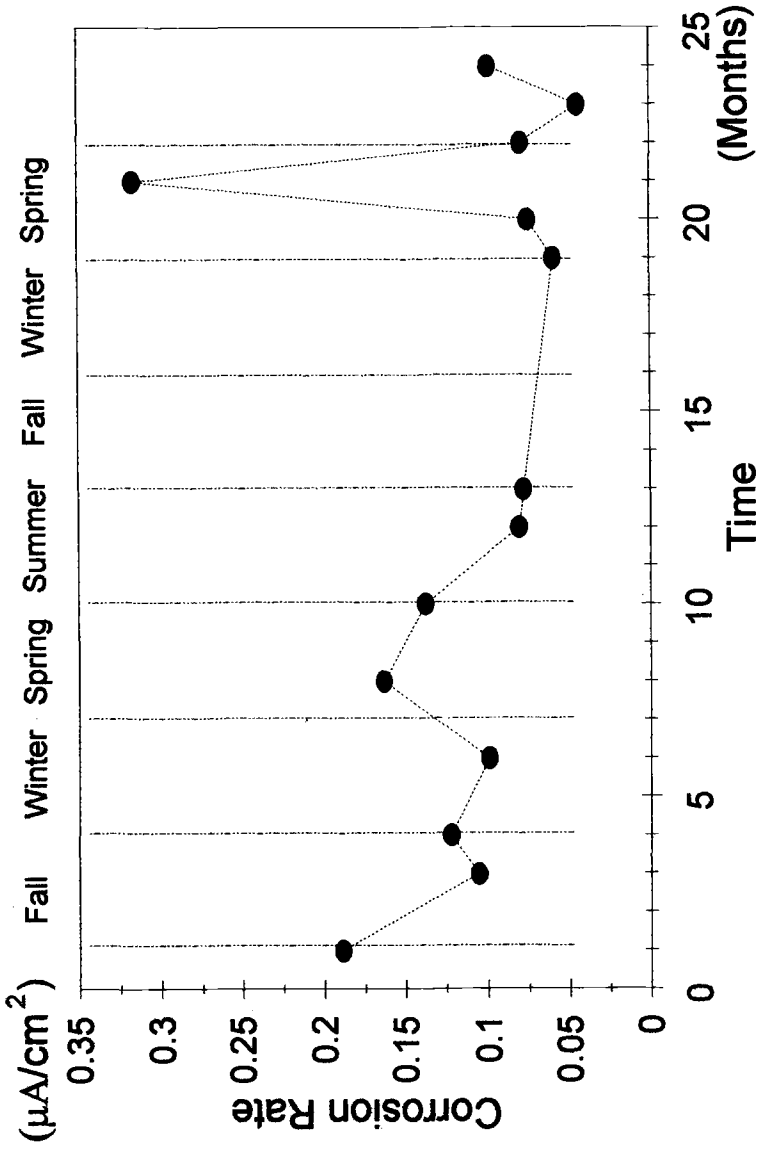


Fig. 2B--Typical Geocor 3 monthly average corrosion rate profile for the 1.4 admixed chloride series.

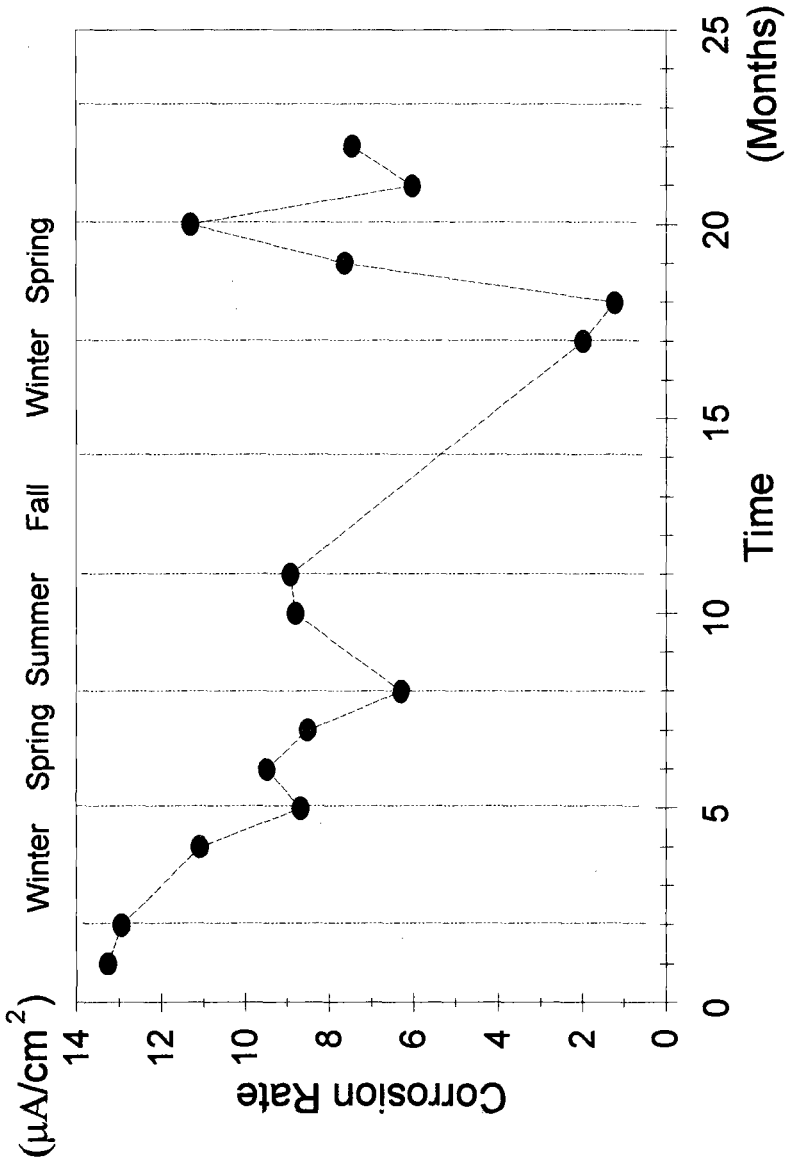


Fig. 3A--Typical 3LP monthly average corrosion rate profile for the 5.7 admixed chloride series.

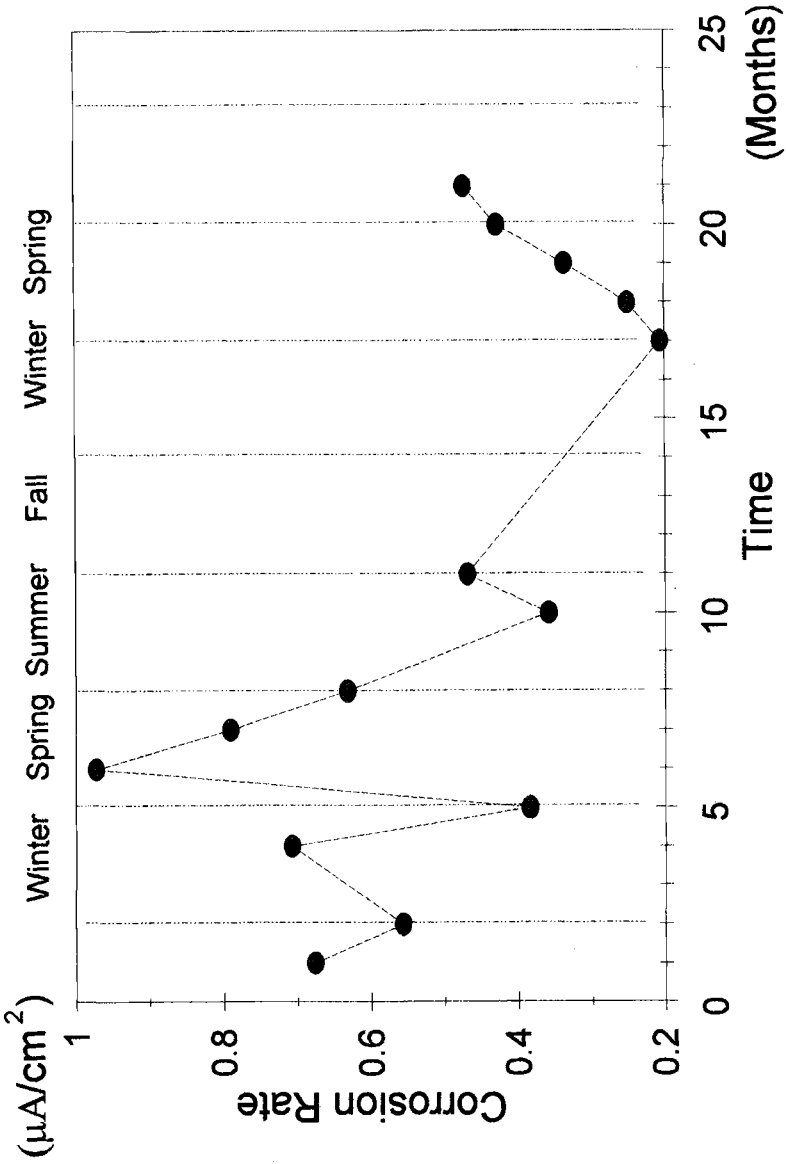


Fig. 3B--Typical Geocor 3 monthly average corrosion rate profile for the 5.7 admixed chloride series.

Relative to admixed chloride content, as shown in Figs. 1, 2, and 3, corrosion rates increase with increasing admixed chloride content. Note that the 0.35 series is approximately equal to the 0.0 admixed chloride series and the 0.71 series lies in between the 0.35 and 1.4 admixed chloride content series [7]. Figs. 1, 2, and 3 also show the influence of seasonal effects, the interaction between temperature and moisture of the concrete on the measured corrosion rate. The highest corrosion rates generally occur during the Spring when temperatures and moisture increased in the outdoor exposure area, at Virginia Tech in Blacksburg, Virginia. As Summer approaches, temperatures increase but moisture decreases, as the concrete moisture content decreases, the corrosion rate decreases because the resistance of the corrosion cell decreases. During Fall, temperatures decrease and moisture increases but the corrosion rate decreases because temperature is the controlling factor, during Winter the corrosion rate continues to decrease because temperatures continue to decrease. The lowest corrosion rate occurs during the Winter and the highest during the Spring. The annual corrosion rate may vary by a factor of 4 to 6 and appears to interact with the chloride content, higher factors for higher chloride content.

Measured corrosion rates presented in Figs. 1A, 2A, and 3A would be interpreted as possible damage in 10-15, 2-10, in less than 2 years, respectively. Fig. 1A is the corrosion profile for the 0.0 admixed chloride series where no corrosion damage would be expected. Thus, one must question the accuracy of the interpretations presented in the 3LP users manual. For the Geocor 3, as shown in Figs. 1B, 2B, and 3B, only the 5.7 admixed chloride series appears to be actively corroding, based on the criteria presented in the user's manual.

Figs. 4 and 5 present the average monthly corrosion rates for the same 5.7 admixed chloride series presented in Fig. 3 as a function of concrete temperature measured at the bar depth. The measurements are presented separately for the time periods 1-9 months and 11-23 months to illustrate the significant effect a decreasing cathode to anode area ratio and diffusion of corrosion products through the rust layer has on the measured values during the early months, see Figs. 1, 2, and 3. Measured corrosion rates are less variable after 10 months. As shown in Fig. 4A, 3LP, 1-9 month measurements, the corrosion rate appears to at best decrease with increasing time, however, electrochemical reactions are known to increase with increasing temperature. For the 1-9 month Geocor measurements presented in Fig. 5A, there appears to be a slight increase with increasing temperature. However, after 10 months, both the 3LP and Geocor 3 measurements increase with increasing temperature, as would be expected. The 3LP measurements increase by about a factor of 5 from 50 to 100°F (10 to 38°C) whereas the Geocor 3 measurements increase by a factor of about 3 over the same temperature range, see Figs. 4B and 5B. Note that the above observed temperature factors are not the influence of temperature alone because the specimens were stored outdoors where moisture and temperature vary as would be the case for field structures.

At 22 months, the outdoor, 5 cm cover, 20 cm spacing, 13 mm bar, 5.7 admixed chloride series cracked. Cracking was vertical above the bar, not inclined cracking as present in Bažant's equation. This was the only series to crack during the 24 month measurement period reported here. Vertical cracking occurred in all 3 specimens in the series within about a two week period. Three 5 cm bar sections were removed from the

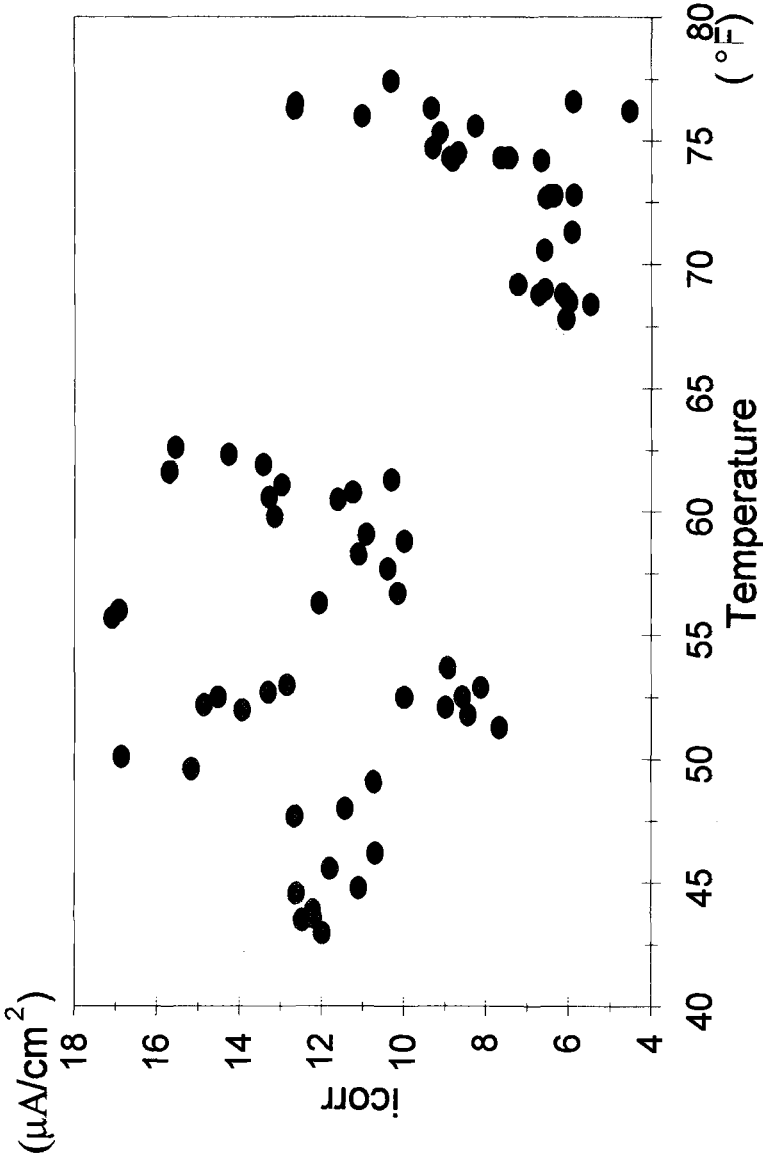


Fig. 4A--3LP average monthly corrosion rate for months 1-9 as a function of concrete temperature for the 5.7 admixed chloride series presented in Fig. 3A,  $^{\circ}C = 5/9(^{\circ}F - 32)$ .

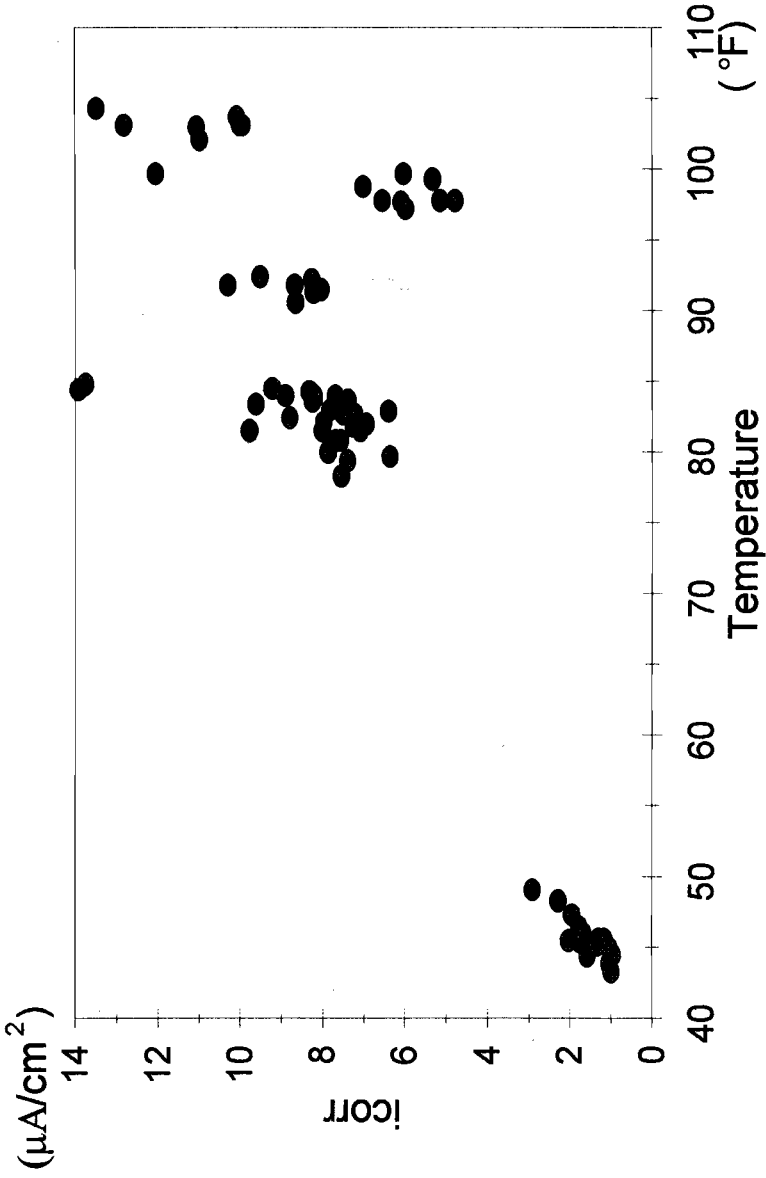


Fig. 4B--3LP average monthly corrosion rate for months 11-23 as a function of concrete temperature for the 5.7 admixed chloride series presented in Fig. 3A,  $^{\circ}\text{C} = 5/9(^{\circ}\text{F} - 32)$ .

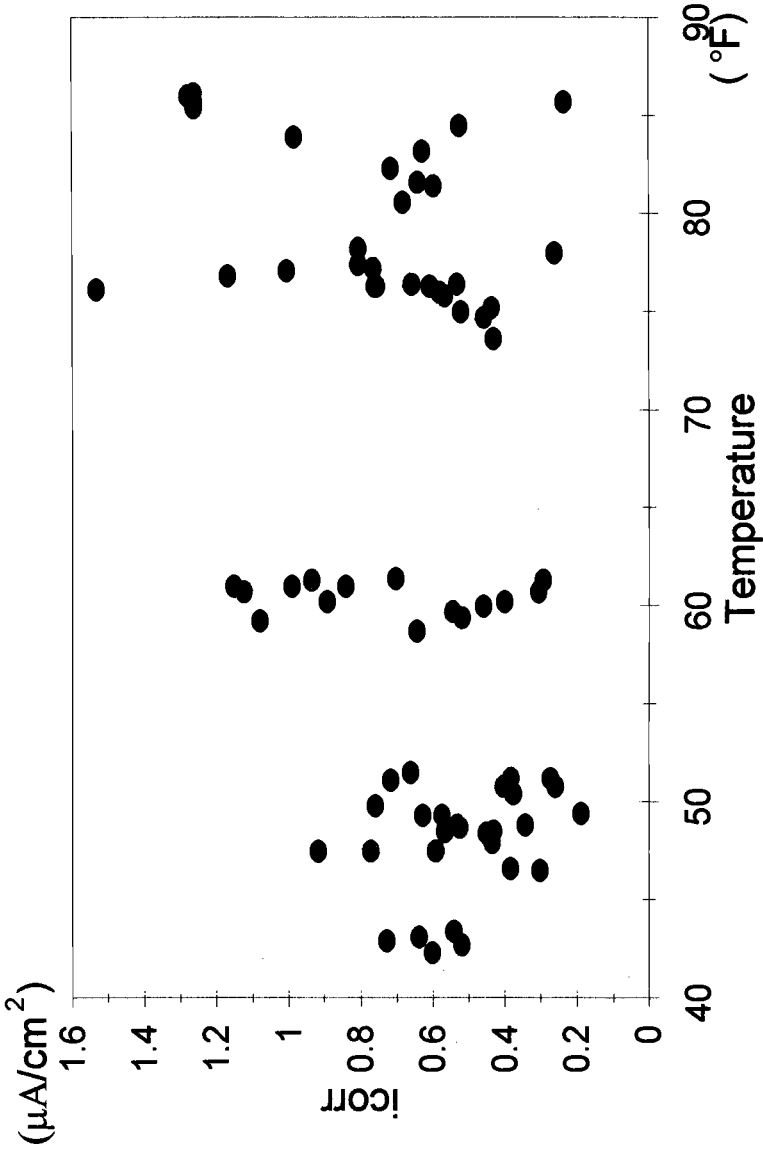


Fig. 5A--Geocor 3 average monthly corrosion rate for months 1-9 as a function of concrete temperature for the 5.7 admixed chloride series presented in Fig. 3B, °C = 5/9(°F - 32).

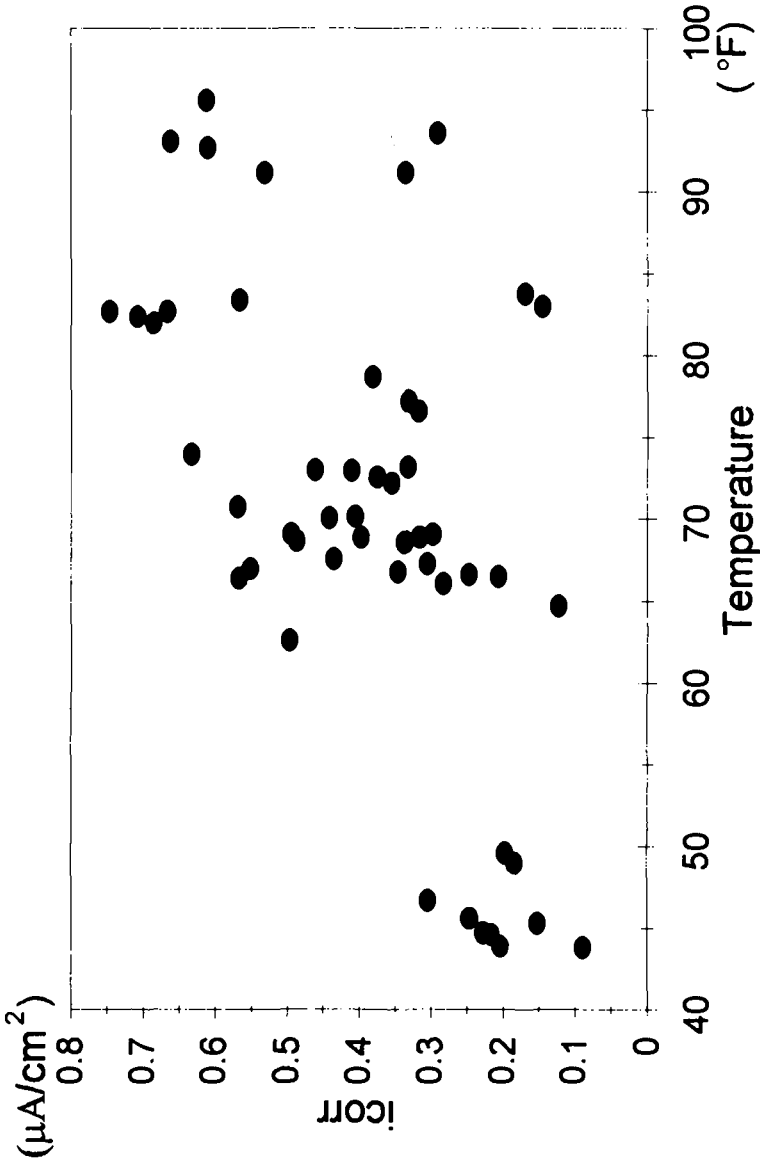


Fig. 5B--Geocor 3 average monthly corrosion rate for months 11-23 as a function of concrete temperature for the 5.7 admixed chloride series presented in Fig. 3B,  $^{\circ}C = 5/9(^{\circ}F - 32)$ .

outdoor, 5 cm cover, 20 cm spacing, 13 mm bar series. A bar section was removed from each of the 3 slabs within an admixed chloride matrix cell. Weight loss of the bar sections were determined in accordance with ASTM G1-90, Standard Practice for Preparing, Cleaning and Evaluating Corrosion Test Specimens, Method C.3.5 which removed the mortar and the rust products but not the mill scale on the bar sections. Also, the chloride content, acid and water soluble, was determined for each admixed chloride matrix cell in accordance with standard ASTM procedures.

Average corrosion rates were determined by integrating the area under the measured corrosion rate profiles and using Faraday's First Law for the corrosion weight measurements. Results of the chloride content and corrosion rate measurements are presented in Table 4.

TABLE 4--Chloride content and corrosion rate for an outdoor admixed chloride slab series

Admixed Chloride, kg/m <sup>3</sup>	Chloride Content, kg/m <sup>3</sup>		Average Corrosion Rate $\mu\text{A}/\text{cm}^2$		
	Acid	Water	Weight Loss	3LP	Geocor 3
0.00	0.00	0.00	0.00	0.71	0.046
0.35	0.36	0.04	0.00	0.88	0.049
0.71	1.0	0.29	0.00	1.09	0.070
1.4	1.4	0.78	0.00	1.33	0.096
2.8	3.2	2.0	0.00	3.77	0.267
5.7	4.9	4.7	2.18	7.77	0.403

As shown in Table 4, the measured acid soluble chlorides generally agree with the target admixed concentrations. Whereas, at low admixed chloride concentrations, less than 1.4 kg/m<sup>3</sup>, half or more of the chlorides were bound up within the cement hydration products. Also, as the chloride concentrations increased the ratio of acid to water soluble chlorides decreased, thus indicating that the cement hydration products had a limiting amount of chlorides which can be bound up within the cement matrix.

Also of interest is that no corrosion weight loss occurred within any of the admixed chloride series except for the highest concentration of 4.9 kg/m<sup>3</sup> acid soluble chlorides, over the 22 month measurement period. The weight loss measurements are in general agreement with published admixed sodium chloride corrosion threshold levels of 1.5 to 3.0 kg/m<sup>3</sup> [8]. In all cases, the 3LP measured corrosion rates over-estimated the weight loss corrosion rates and the Geocor 3 under-estimated the weight loss corrosion rates when measurements were taken once a month. Perhaps more frequency measurements would show better agreement but even once a month measurements are impractical for concrete bridges. Both the 3LP and Geocor 3 user manual interpretations of corrosion rates do not agree with weight loss corrosion rates, as shown in Table 4. Note, weight loss measurements were taken at measurement locations.

Other observations made during the removal of the bar sections from the concrete were as follows:

1. Corrosion products were mixed green, black, and rust red.
2. Corrosion products were found as far away as 6.35 cm from the bar and in void areas adjacent to the bar.
3. Only the 4.9 kg/m<sup>3</sup> acid soluble (4.7 kg/m<sup>3</sup> water soluble) chloride content slabs showed any visual signs of corrosion.

The average weight loss corrosion rate, 2.18  $\mu\text{A}/\text{cm}^2$ , was used to test the validity of Bažant's time to corrosion cracking equations. In doing so, two conditions must be accounted for. First the corrosion rate,  $i_{\text{corr}}$  (corrosion current density) is corrosion current per surface area of the bar. Whereas, Bažant's corrosion rate term,  $j_r$ , is for a unit length of bar. Second, Faraday's First Law determines weight loss from corrosion current,  $L_{\text{corr}}$ . Whereas, Bažant's corrosion rate term,  $j_r$ , is rate of rust production instead of rate of metal loss. Considering both of these conditions, Bažant's equation may be expressed at [7].

$$t_{\text{corr}} = \rho_{\text{corr}} \frac{\Delta D}{i_{\text{corr}}} \quad (6)$$

For the conditions of vertically cracked slabs, with  $\rho_{\text{corr}} = 0.590 \text{ g}/\text{cm}^3$  and  $\Delta D = 9.23 \times 10^{-3} \text{ cm}$  and 2.18  $\mu\text{A}/\text{cm}^2$  being equal to 5.88  $\times 10^{-5} \text{ g}/\text{cm}^2/\text{days}$  [7], Bažant's predicted time to cracking is 93 days, whereas the observed time to cracking was 671 days. The difference is most likely related to the corrosion observations that not all the corrosion products produce internal pressure (corrosion products were observed in uncracked concrete voids as far as 5 cm away from the reinforcing bar), nor do they result in the same volume increase.

## CONCLUSIONS

The following conclusions may be gleaned for this reported study period.

1. Corrosion rate increases with increasing chloride concentrations.
2. Corrosion rate is strongly influenced by seasonal changes, interaction between concrete temperature and moisture content.
3. Corrosion rate is highest in the Spring and lowest in the Winter, rates differ by at least a factor of 4 to 5 annually.
4. Corrosion rate is strongly influenced by the cathode to anode ratio and the rate of diffusion of corrosion products through a rust layer.
5. Corrosion observations for admixed chlorides agree with published chloride threshold concentrations.
6. Corrosion observations for admixed chlorides do not agree with interpretations of measured corrosion rates presented in the 3LP and Geocor 3 user's manuals.
7. Bažant's equations significantly under-estimated time to corrosion cracking for the single vertical cracking case.

**REFERENCES**

- [1] ENR Washington Observer, Engineering New Record, Vol. 27, No. 2, July 15, 1991, p. 7.
- [2] Cady, P. D. and Weyers, R. E., Journal of Transportation Engineering, Vol. 110, No. 1, January 1984, pp. 34-45.
- [3] Weyers, R. E., Prowell, B. D., Sprinkel, M. M., and Vorster, M. C., "Concrete Bridge Protection, Repair, and Rehabilitation Relative to Reinforcement Corrosion: A Methods Application Manual," Strategic Highway Research Program, National Research Council, Washington, D. C., 1993, pp. 268.
- [4] Bažant, Z. P., "Physical Model for Steel Corrosion in Concrete Sea Structures - Theory," Journal of the Structural Division, June 1979, pp. 1137-1153.
- [5] Flis, J., Sehgal, A., Li, D., Kho, Y. T., Sabol, S., Pickering, H., and Osseo-Asare, K., "Condition Evaluation of Concrete Bridges Relative to Reinforcement Corrosion," Strategic Highway Research Program, National Research Council, Washington, D. C., 1992, pp. 105.
- [6] Peterson, J. E., "A Time to Cracking Model for Critically Contaminated Reinforced Concrete Structures," Master of Science Thesis, Virginia Polytechnic Institute and State University, December 1993.
- [7] Newhouse, C. D., "Corrosion Rates and the Time to Cracking of Chloride-Contaminated Reinforced Concrete Bridge Components," Master of Science Thesis, Virginia Polytechnic Institute and State University, December 1993.
- [8] ACI 222R-89, Corrosion of Metals in Concrete, Part 1, Materials and General Properties of Concrete, 1991, p. 222R-13.

C. Andrade<sup>1</sup> and C. Alonso<sup>2</sup>

## **PROGRESS ON DESIGN AND RESIDUAL LIFE CALCULATION WITH REGARD TO REBAR CORROSION OF REINFORCED CONCRETE**

---

**REFERENCE:** Andrade, C. and Alonso, C., “**Progress on Design and Residual Life Calculation with Regard to Rebar Corrosion of Reinforced Concrete,**” Techniques to Assess the Corrosion Activity of Steel Reinforced Concrete Structures, ASTM STP 1276, Neal S. Berke, Edward Escalante, Charles K. Nmai, and David Whiting, Eds., American Society for Testing and Materials, 1996.

**ABSTRACT:** The increasing amount of structures presenting distress due to reinforcement corrosion is urging the establishment of more accurate calculation methods for the service life of concrete structures. In the present paper, a summary of the different approaches is presented that are able to calculate the expected life of new structures, in certain aggressive environments or the residual life of already corroding structures. The methods are based on the proper calculation of the carbonation front or chloride penetration and on the steel corrosion rate.

**KEYWORDS:** Service life prediction, reinforced concrete, durability design, residual life, corrosion.

---

When reinforced concrete started to be industrialised, the pioneers were convinced to have found a material with unlimited durability, as concrete supposes a chemical protection for the steel in addition to providing the rebar with a physical barrier against contact with the atmosphere.

However, in spite of the good performance noticed over this century it is also evident that the amount of concrete structures presenting insufficient durability is increasing, the corrosion of reinforcement being the main distress observed.

Therefore, service life prediction is becoming an area of increasing interest. The pioneering proposals from the sixties [1][2] were followed by North American initiatives, which led into the publication of the ASTM E 632-81: "Standard practice for developing accelerated tests to aid prediction of the service life of building components and materials". These initial proposals were mainly philosophical, dealing with definitions and methodologies but not giving any method of quantification. More recently, several codes (ACI, Eurocode II) are starting to introduce these concepts into design rules.

---

<sup>1</sup>Professor and <sup>2</sup>Researcher, Institute "Eduardo Torroja" of Construction Sciences, CSIC, Serrano Galvache, s/n, 28033 Madrid, Spain.

## STANDARD AND REFINED METHODS FOR SERVICE LIFE PREDICTION

In spite of the fact that codes and recommendations are starting to define the concept of service life, the design of new concrete structures is still based on the traditional methodology of fixing limiting values for one or several of the following concrete requirements: concrete grade, minimum cement content, maximum water/cement ratio, air content, cover thickness, and maximum structural crack width.

This approach for providing a certain durability can be called the "**standard method**". However, as following this leads to concrete performance that is not always satisfactory, new methods have to be developed in order to predict and quantify the structural service life. These more sophisticated methods are called "**refined methods**" by the CEN Committee CEN TC 104/WG1/TG1: "**Concrete durability**". The fundamentals of these methods will be described in the present paper.

In the case of already deteriorating structures, a "simplified" and a "refined method" for predicting Residual Life are both feasible. These will also be briefly presented in the second part of the paper.

### Refined Method for Durability Design of the Reinforcement in New Structures

The most well known service life model for concrete reinforcements is that K. Tuutti published in 1982 [3] and which is shown in Fig. 1. The initiation period comprises the time taken by the aggressives (chlorides or the carbonation front) to reach the reinforcement and depassivate the steel. This is the relevant period if depassivation is identified as the end of the service life. In consequence, the penetration of chloride or carbonation front would be the rate determining parameter.

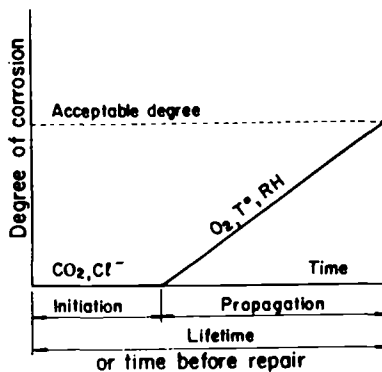


FIG. 1 - Service life model for reinforcement corrosion [3]

However, if a certain amount of steel deterioration is considered as part of the design service life, or in the case of already deteriorating structures, then the steel corrosion rate is also a determining parameter of the service or residual life.

In his original work, Tuutti [3] tried to quantify both periods and gave some limiting values of steel cross-section loss or crack widths indicative of having reached the maximum tolerable amount of damage.

This first proposal has been improved by later studies [4-7,16-17]. The most common methodology followed at present when trying to design for reinforcement corrosion protection by a refined method, has at least the following steps:

- 1) Identification of aggressivity of the environment
- 2) Definition of the length, in years, of the service life in addition to considering some special actions of maintenance.
- 3) Consideration of a calculation method for the attack progression
- 4) Implementation of calculation results into concrete requirements
- 5) Supplementary protection methods

## **1. Identification of Aggressivity of the Environment**

Environmental actions are responsible of the lack of durability of reinforced concrete. In general, no significant damage is noticed in dry indoor conditions, although indoor environment may be very different depending upon heating regimes or external climate.

In outdoor environment, the main aggressive agents in relation to steel corrosion are: carbon dioxide ( $\text{CO}_2$ ) concentration, chloride ( $\text{Cl}^-$ ) proportion and RH-T° (humidity-temperature) cycling. Proper values of  $\text{CO}_2$ , and  $\text{Cl}^-$  are needed in order to be introduced into the mathematical expressions that will be described later. RH-T° cycling is also relevant as it defines the concrete depth at which humidity remains constant.

In this respect, the identification of the fact that only the "skin" of the concrete has the ability to "breathe" is comparatively recent [5][6][8] That is, as the concrete wets quickly and dries slowly, RH daily cycles produce a gradient of moisture along the concrete cover until a certain depth at which the concrete moisture content is insensitive to external RH changes [8]. This depth depends on concrete quality and varies from 1 to 2 cm in ordinary concretes. This means that if the rebar has a cover of  $\geq 2$  cm, the moisture at this level remains almost unaltered along the yearly seasons.

Therefore, along the cover a humidity gradient is produced which greatly influences the rate of entrance of the aggressives. The whole picture is idealised in Fig.2.

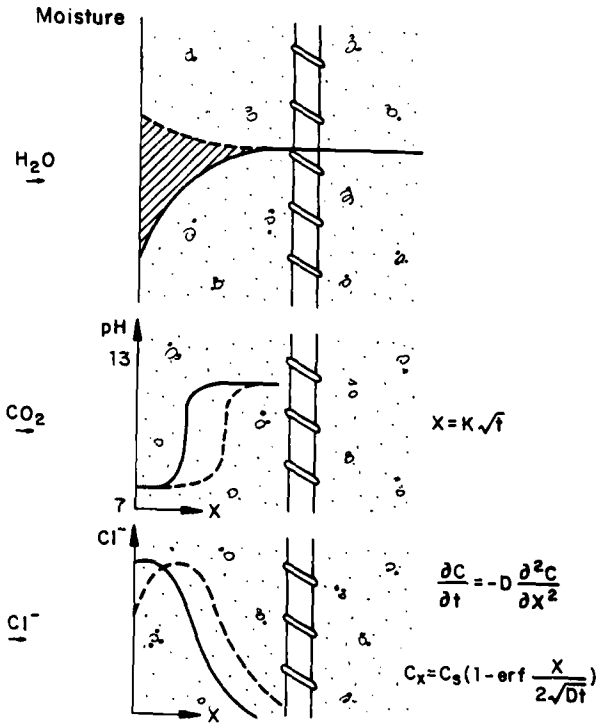


FIG. 2. Figurative profiles of moisture, carbonation and chloride in the concrete

**2. Length of Service Life**

The definition of service life has technical as well as economical and legal implications, as responsibilities are involved. Dealing with only the technical aspects, the Task Group 1 of CEN TC 104 has recently agreed on proposing a **nominal service life of 75 years** as the reference. Shorter or longer lives may be taken into account for particular cases.

The nominal life is considered if the maintenance regime is minimum and implies any unexpected cost of repair. A more intensive maintenance regime may be considered with the consequent change in the referred length of service life.

**3. Calculation Methods for Attack Progression**

Two aspects have to be considered here: 1) The identification of the mechanism of the attack and 2) the definition of the maximum tolerable amount of damage.

Regarding **mechanisms of attack**, there are three processes by which the aggressive agents mentioned in 1 may penetrate into concrete. These are: diffusion, absorption and permeability.

Carbonation usually progresses by a diffusion mechanism while chlorides may penetrate also with a combination of absorption and diffusion (tidal or splash zones). That is, from these three mechanisms the most common are diffusion and absorption. Both are known to follow the law of the "square root of time":

$$x = K \sqrt{t} \quad (1)$$

where:  $x$  = attack penetration depth, mm

$t$  = time, s, and,

$K$  = constant depending on concrete and ambient characteristics [3][5][6].

This square root law may be plotted in a log-log scale as in Fig. 3 as Tuutti suggested [3], which is very convenient and general:

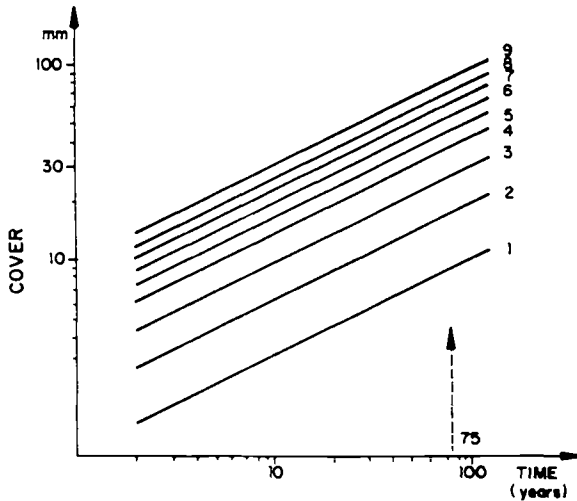


FIG. 3. Representation of a square root law in log-log diagrams. The numbers in the parallel lines of slope 0.5 represent the values of the constant  $K$  [3].

Considering now the modelling of every type of attack it has to be recognised that the carbonation rate has been modelled by many researchers, although only three models have been considered by the CEN TC 104/WG1/TG1/Panel 1. Those are the models proposed by: Tuutti [3], Bakker [5] and Parrott [6]. The three models have as input factors the concrete requirements and climatic (humidity) loads.

**Tuutti [3]** bases his method on the known diffusion theory of "moving boundaries", which offers the following expression for the calculation of the rate of advance of the carbonation front:

$$\frac{C_s}{C_x} = \sqrt{\pi} \left[ \frac{x/\sqrt{t}}{2\sqrt{D}} \right] \exp \left[ \frac{x^2}{4Dt} \right] \operatorname{erf} \left( \frac{x/\sqrt{t}}{2\sqrt{D}} \right) \tag{2}$$

- $C_s$  = CO<sub>2</sub> concentration in the atmosphere, mol/kg
- $C_x$  = amount of bound CO<sub>2</sub> (cement phases plus pore solution), mol/kg,
- $D$  = CO<sub>2</sub> diffusion coefficient, m<sup>2</sup>/s
- $x$  = Carbonation depth, mm, and
- $t$  = time, s

**Bakker [5]** bases his proposal in a diffusion solution of the first order, but taking into account the internal moisture content of the concrete due to the RH cycling. This leads to the introduction of the concept of "effective time" of action of the carbonation, as it is known that carbonation cannot progress in wet concrete. The expression reached is:

$$x_n = \sqrt{\frac{2D_c}{a} (c_1 - c_2) \left[ t_{d1} + t_{d2} - \left(\frac{x_1}{B}\right)^2 + t_{d3} - \left(\frac{x_2}{B}\right)^2 \dots + t_{dn} - \left(\frac{x_{n-1}}{B}\right)^2 \right]}$$

$$B = \sqrt{\frac{2D_v}{b} (c_3 - c_4)} \tag{3}$$

- $x_i$  = carbonation depth, mm,
- $a$  = CaO content in the cementitious materials, mol/kg,
- $b$  = amount of water which evaporates from concrete, (kg/m<sup>3</sup>)
- $D_c$  = diffusion coef. of CO<sub>2</sub> at a particular RH in concrete, m<sup>2</sup>/s
- $D_v$  = diffusion coef. of water vapour at a particular RH in concrete, m<sup>2</sup>/s
- $C_1 - C_2$  = difference of CO<sub>2</sub> concentration between air and concrete, mol/kg
- $C_3 - C_4$  = difference in RH between air and concrete

**Parrott [6]** follows a different approach offering an empirical solution based on the gas permeability of the concrete. Thus, he obtains an "empiric expression" by mathematical fitting of carbonation depths measured in real structures. His fitting considers the 95% confidence range and the expression reached in function of the gas permeability is:

$$x = 64 \frac{k^{0.4} t^{0.5}}{c^{0.5}} \quad (4)$$

$x$  = carbonation depth, mm,       $k$  = oxygen permeability coefficient,  $m^2/s$   
 $t$  = time, years,                       $c$  = CaO content in the cement, mol/kg

When applying Eqs. (2)(3) and (4) to real data obtained from carbonated concrete, they give very similar results, as shown in Fig.4. The choice of preference depends on the available input data.

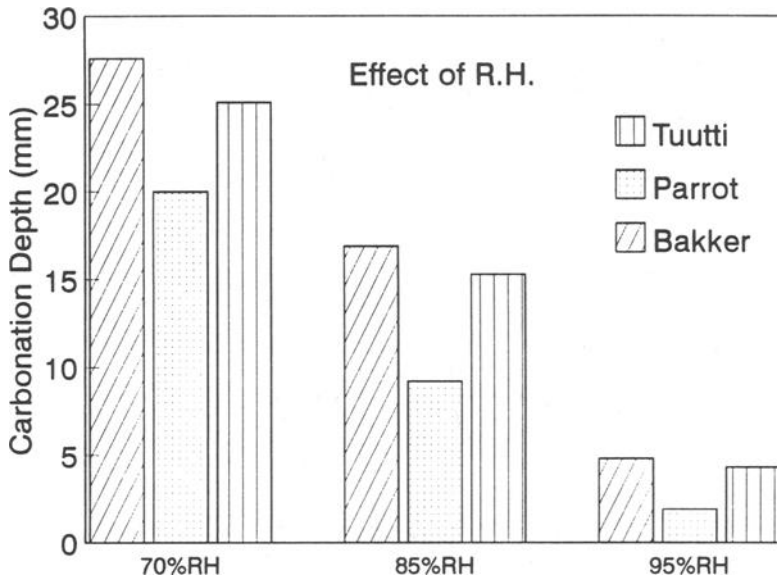


FIG. 4. Carbonation depth results in concrete specimens obtained by means of the formulae proposed by Bakker (B), Parrot (P) and Tuutti (T) for the carbonation rate.

In the case of chlorides the agreement on the mathematical model is much wider and in general all accept the solution of the second Fick's law in a semi-infinite medium as the most suitable model [3,4].

$$C_x = C_s \left(1 - \operatorname{erf} \frac{x}{2\sqrt{Dt}}\right) \quad (5)$$

- $C_s$  = surface chloride concentration, %,  
 $C_x$  = proportion of chlorides at a certain depth, %,  
 $D$  = chloride diffusion coefficient,  $\text{m}^2/\text{s}$ ,  
 $x$  = depth of penetration, m,  
 $t$  = time, s,

In general, the  $D$  value for a particular concrete is considered as the rate determining parameter.

In spite of the wide use of this model, it has to be recognised that there are limitations in its use as a predictive model:

- The  $C_s$  is not always a constant as it may increase with time
- if  $C_s$  is not constant, the  $D$  value cannot be used for comparative purposes as it depends on the  $C_x/C_s$  ratio.
- The  $D$  value is not a constant. It changes with the proportion of chlorides and time.
- No absorption period effect is considered in this model.
- It has not been related  $D$  to the concrete mix proportions.

All these shortcomings limit the use of the model for predictive purposes as the  $D$  value should be established in previous laboratory experiments. The trials undertaken until now indicate that  $D$  values obtained in young concrete are much higher than values obtained in cores taken from old real structures [9].

Other more comprehensive and sophisticated models, [10] as well as accelerated methods based on the application of an electrical field [11], are being now experimented.

Regarding the **maximum tolerable amount** of corrosion, in the case of new structures, both carbonation and chloride attack have to be considered separately. While in the case of carbonation a certain propagation period can be considered as part of the design service life, (as the expected corrosion is homogeneous), no propagation period should be considered in the case of localised attack due to chlorides. This is because the uncertainties linked to how much localised and deep the corrosion pits may be, do not allow at present the acceptance of such a risk from the design phase of the structure.

With regard to a limit for the case of the carbonation attack, a general suggestion considered by CEN TC 104/WG1/TG1 is to accept a corrosion penetration depth of about 100-200  $\mu\text{m}$ . Assuming a corrosion rate of about 5  $\mu\text{m}/\text{year}$ , this would aim at propagation periods of 20-40 years [12]:

$$t = \text{service life} = t_i + t_p = K_c \sqrt{t} + \frac{PL}{CR} \quad (6)$$

where:

$t_i$  = corrosion initiation time, years,  
 $t_p$  = corrosion propagation time, years,  
 $K_c$  = carbonation coefficient  
 PL = Penetration limit, mm,  
 CR = Corrosion rate,  $\mu\text{m}/\text{year}$

If  $PL = 200\mu\text{m}$  and  $CR = 5\mu\text{m}/\text{year}$  and  $t = 75$  years,  $t_p = 200/5 = 40$  years is deduced and then  $t_i = 35$  years, which means that for a cover of  $x = 30\text{mm}$ , instead of using a concrete having a  $K_c = 30\sqrt{75} = 3.5 \text{ mm year}^{-0.5}$ , another one having a  $K_c = 30\sqrt{35} = 5 \text{ mm year}^{-0.5}$  can be used.

#### 4. Concrete requirements

The availability of refined calculation methods provide the possibility of trying different concrete qualities in order to obtain the same durability. This is known as a "trade-off" of concrete requirements, mainly between: cover thickness, mechanical strength, w/c ratio, amount of cement or ambient humidity..

In fact, the final aim of using refined methods is the adequate selection of concrete characteristics and of minimum cover for a particular environment. This is now feasible in the case of carbonation applying eq.(2)(3) or (4). However, for chloride contamination it appears still to be far from possible.

#### 5. Supplementary Protection Methods

In very aggressive environments it may happen that concrete cover itself is not sufficient protection to the design life time. Then, at the design phase it will be necessary to define the supplementary protection methods to provide the structure with the adequate durability.

The main additional protection methods are: 1) cathodic protection, 2) galvanising, 3) stainless steel rebars, 4) epoxy coated rebars, 5) corrosion inhibitors, 6) concrete coatings

The description of these protection methods is out of the scope of the present paper although Fig. 5 summarises their main features [25].

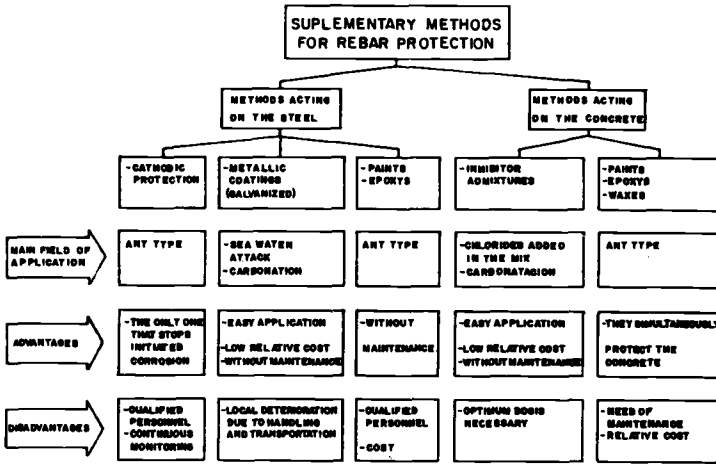


FIG. 5. Summary of supplementary methods for rebar protection.

**RESIDUAL LIFE PREDICTION OF STRUCTURES SUFFERING CORROSION**

The assessment of structures already suffering deterioration due to reinforcement corrosion, is even more difficult as their structural behaviour, at different damage levels, have not been adequately tested or analysed.

Fig. 6 summarises the consequences of the corrosion at the material level which are:

- In the reinforcement: 1) loss of load-bearing section and 2) loss of ductility [13].
- In the concrete interface and the cover: 3) loss in bar/concrete bond and 4) concrete cracking.

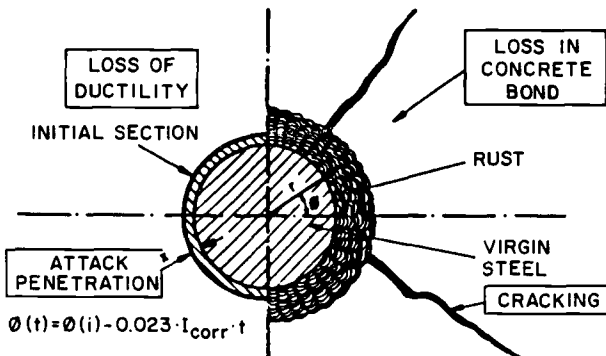


FIG. 6. Consequences of rebar corrosion.

These immediate consequences of the corrosion will affect the load-bearing structural capacity in different ways, which are still not well known. This lack of knowledge explains why the approaches used at present are merely empirical, or simply based in engineering experience or intuition. Therefore it seems appropriate to distinguish two types of methodologies to ascertain the residual life of corroding structures:

- 1) That used at present, based in the experience and rough evaluation of the structural load-carrying capacity, which may be labelled "simplified method". This methodology has been described in the Bulletin 162 of the CEB [23].
- 2) That, which in opposition, may be named "refined method". It should be based in a rigorous establishment of the deterioration evolution of the four corrosion consequences previously mentioned and in the calculation of their influence in the loss of load-carrying capacity of the structure.

### Simplified Method of Residual Life Assessment

In general, the methodology followed for the appraisal of a deteriorating structure considers the following steps: 1) Inspection, 2) Diagnosis, 3) Prognosis: determine urgency of intervention, 4) Options of repair, 5) Maintenance and surveillance regime.

As it has been mentioned, at present, steps 1 and 2 can be developed with enough quantitative accuracy at a material level. Thus, on-site analysis and instrumentation, core extraction and laboratory test procedures in the case of the simplified method are developed enough to enable to draw a damage classification map of the structure to assess present situation of the deterioration level (point A in Fig. 7).

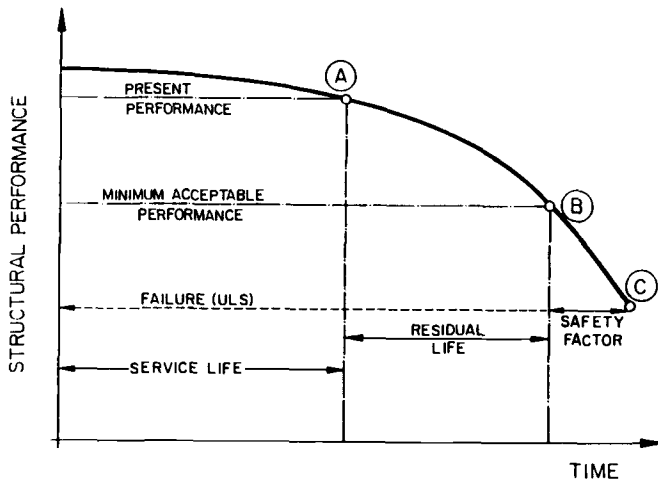


FIG. 7. Simplified figuration of evolution of residual load-bearing capacity of concrete structures.

From this "damage map" and the diagnosis of the causes of the corrosion, a classification in "levels of intervention urgency" or risk levels has to be established in order to further decide upon the optimal moment and option of repair and on surveillance regimes. These levels of urgency may differ from one structure to another, or have to be adapted to owner's requirements.

An exercise of application of this simplified method of residual life prediction was made in Spain, in the case of floors fabricated around the sixties with calcium aluminate cement, CAC, . The joists of these floors have prematurely deteriorated and corroded. A general survey was undertaken in order to find out the real risk of collapse [14][15].

### **Refined Method of Residual Life Prediction**

Due to the lack of quantitative information on the structural behaviour of elements suffering reinforcement corrosion, a quantitative model based on a rigorous structural analysis does not exist but is urgently needed.

Several years ago, the authors have suggested [16][17] that the determining parameter of the deterioration rate of a corroding structure, should be the corrosion rate,  $i_{corr}$ , if a rigorous appraisal of the phenomenon is considered. This assumption was derived from Fig. 6, since the rate of steel cross section loss is the factor provoking the other effects: loss of ductility, loss in concrete bond, concrete cracking.

In fact, corrosion rate means the amount of metal lost per area and time units ( $g/cm^2$  year or  $\mu A/cm^2$  or  $\mu m/year$ ). This progressive loss can be measured currently by means of an electrochemical method based on the Polarisation Resistance,  $R_p$ , technique which is non-destructive [21]. Measurements carried out on real structures [19] confirm previous findings in the laboratory and enable the determination of the normal values of corrosion rates: values smaller than  $1\mu m/year$  mean negligible corrosion and higher than  $10\mu m/year$  have to be considered as high [16].

After this first suggestion, the methodology is being developed step by step. At present it is under BRITE funding in collaboration with the partners named in the acknowledgements [18][19][20]. The general framework developed up to now, will be described next.

The pattern of the methodology consist in connecting the corrosion rate to decrease bond, steel ductility and section loss as well as generation of cover cracking. From the mathematical functions derived, the structural deterioration evolution is described or calculated.

The flow chart of the methodology of assessment is shown in Fig. 8 and may be summarized as follows:

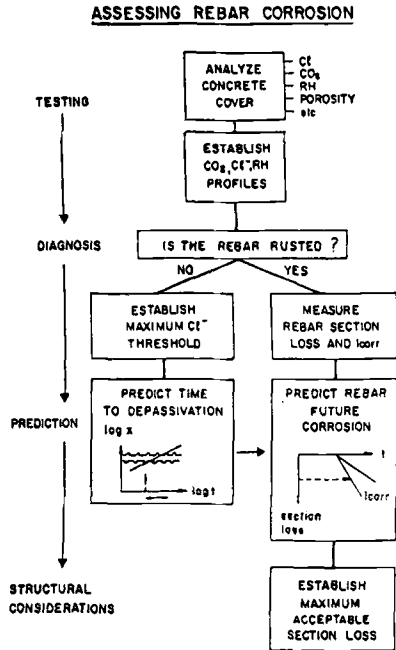


FIG. 8. Steps in the spection and assessment of rebar corrosion.

- **Inspection and Diagnosis**- at these step, the characteristic corrosion rate has to be established first by the accurate on-site measurement of this parameter and with further statistical analysis in order to establish a limiting value to represent the 95% probability of occurrence. By means of "the characteristic corrosion rate" value, or by simple visual observation, the present steel cross-section loss has to be calculated.
- **Prognosis** - at this step, the models relating the consequences of corrosion (bond, steel ductility and section loss, and cover cracking) to the  $I_{corr}$  previously measured, have to be established. The mathematical expression for these relations are now under research. As an example the decrease in steel cross section showed in Fig. 9 and the influence in the bending moment of a beam, Fig. 10, based in the general expression found for the progressive loss in diameter is [17]:

$$\varnothing(t) = \varnothing_1 - 0.023 I_{corr} \cdot t \tag{7}$$

where:

$\varnothing (t)$  = remaining diameter at time  $t$ , mm,  
 $\varnothing i$  = initial diameter, mm,  
 $i_{corr}$  = corrosion rate,  $\mu\text{m}/\text{year}$ , and,  
 0.023 is a factor to translate  $\mu\text{A}/\text{cm}^2$  into  $\mu\text{m}/\text{year}$ .

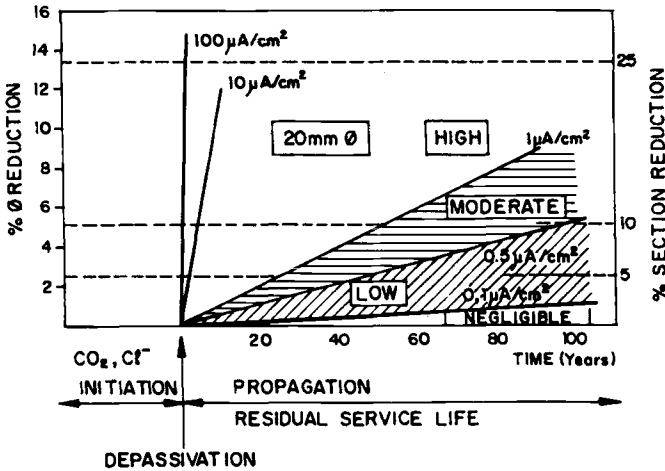


FIG. 9. Decrease with time of rebar diameter (left) or section (right) as function of the corrosion rate. The risk is classified as: negligible, low, moderate and high.

Another example may be given on cover cracking due to the expansive character of the iron oxides. It has been found [22] that just 10-50  $\mu\text{m}$  of corrosion penetration is enough to produce a visible crack (0.05 mm width) for cover/diameter = 20-30mm. Fig. 11 shows times to cracking for different corrosion rates and cover/bar diameter ratios.

As soon as these relationships are fully developed, the structural deterioration evolution can be known and therefore, the maximum tolerable amount of damage, could be also established. This assists in judging the urgency of intervention.

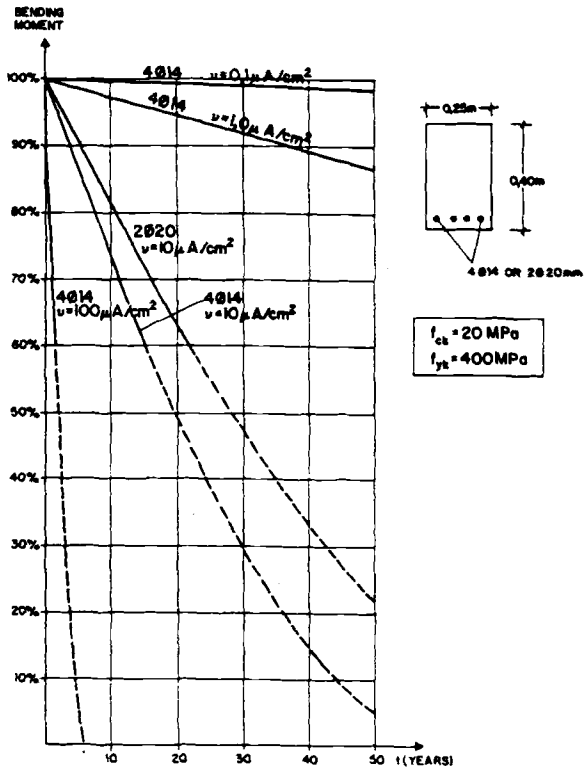


FIG. 10. Decrease in the bending moment resisted in time, for different corrosion rates.

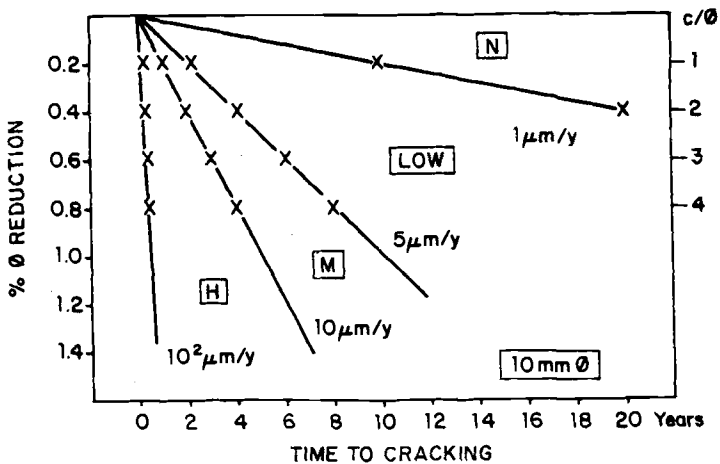


FIG. 11. Times to cracking as function of % Ø reduction for cover/bar diameter ratios of 1, 2, 3 and 4.

However, in the case of a refined method this urgency is recommended to be statistically supported. The statistical analysis may be made effect by effect or element by element. Research on statistical treatments is also needed [24].

The options of repair and surveillance regimes may be drawn up in a similar manner that was described for the simplified methodology.

## ACKNOWLEDGEMENTS

The authors are grateful to the partners of the BRITE Project BREU-92-0591 "The Residual life of Reinforced Concrete Structures" for fruitful discussions and especially to DG-XII of the EU for the partial financial support of this research. They are also grateful to the CICYT of Spain for the funding provided.

Finally, C. Andrade would like to acknowledge the contributions of members of Panel 1 of the CEN Committee TC 104/WG1/TG1 and of RILEM TC-130.

## REFERENCES

- [1] Valenta, O., "General Analysis of the methods of testing the durability of concrete," Rilem Symposium of Durability of Concrete. Paper A-3, Vol. 1 (1969).
- [2] Fagerlund, F., " Prediction of the service life of concrete exposed to frost action," Studies on Concrete Technology - Swedish Cement and Concrete Research Inst. Stockholm, (1979): pp. 249-276.
- [3] Tuutti, K., "Corrosion of steel in concrete," Swedish Cement and Concrete Institute (CIB) n° 4-82. Stockholm (1982).
- [4] Masters, L., "Prediction of service life of building materials and components," Materials and Structures. Vol. 19 n° 114, (1986): pp. 417-422 .
- [5] Bakker, R., "Prediction of service life reinforcement in concrete under different climatic conditions at given cover," Corrosion and Protection of Steel in Concrete International Conference, Sheffield (UK), R.N. Swamy Ed., (1964)
- [6] Parrott, L.J. "Design for avoiding damage due to carbonation - included corrosion," SP-145-15 International Congress on Durability of Concrete, Nice (France) - CANMET- Malhotia Ed., (1994): pp. 283-298.

- [7] Clifton, J., "Methods for predicting remaining life of concrete in structures". Report NISTIR 4954 NIST-US Dept. of Commerce - USA (1992).
- [8] Hedenbland, G., "Determination of moisture permeability in concrete under high moisture conditions," Nordic Concrete Research. Publication n° 7. Norwegian Concrete Ass. Oslo, (1988).
- [9] Mangat, P.S., Molloy, B.T., "Prediction of long term chloride concentration in concrete". Materials and Structures, vol.27, 1994, pp.338-346.
- [10] Sdetta, A.V., Scotta, R.V., Vitaliani, R.V., "Analysis of chloride diffusion into partially saturated concrete," ACI Materials Journal, (1993): pp. 441-451
- [11] Andrade, C., "Calculation of chloride diffusion coefficients in concrete from ionic migration measurements". Cement and Concrete Research. Vol. 28, n° 3, (1993): pp. 724-742
- [12] Alonso, C., Andrade, C., "Life time of rebars in carbonated concrete", Progress in the understanding and prevention of corrosion, Ed. Costa, J.M. and Mercer ., vol. 1, (1993) pp. 634-641
- [13] Andrade, C., Alonso, C., García, D. and Rodríguez, J. "Remaining life time of reinforced concrete structures: Effect of corrosion on the mechanical properties of the steel". Symposium on Life Prediction of corrodible structures. Cambridge (U.K.) (1991).
- [14] Andrade, C., "Corrosion of reinforcement and its inspection in High Alumina Cement," (in Spanish), Informes de la Construcción. (Madrid) Vol. 44 n° 422 (Nov-Dec) (1992): pp. 40-48.
- [15] Ortega, L.M., García, A.M., Rodríguez, J., "Applicability of rebar corrosion rate measurement to the assessment of High Alumina Cement floors," (in Spanish), Informes de la Construcción. Vol. 44 n° 422 (Nov-Dic) (1992): pp. 61-69.
- [16] Andrade, C., Alonso, C., González, J.A., "An initial effort to use corrosion rates measurements for estimating rebar durability," Corrosion Rates of Steel in Concrete ASTM STP 1065. Berke, Chacher and Whithing D. (1990): pp. 29-37.
- [17] Andrade, C., Alonso, C., Rodríguez, J., "Remaining service life of corroding structures", IABSE Symposium on Durability, Lisboa, (Sep 1989): pp. 359-363.
- [18] Andrade, C., Alonso, C., Petterson, K., Sommerville, G., Tuutti, K., "The practical assessment of damage due to corrosion," Concrete Across Borders

International Congress, Odense (Denmark), (June 1994): pp. 337-350.

- [19] Rodríguez, J., Ortega, L.M, García, A.M. "Assessment of structural elements with corroded reinforcements," Corrosion and Protection of steel in concrete, International Congress Sheffield (U.K.), R.N. Swamy Ed, (1994): pp. 171-185.
- [20] Fagerlund, G., Somerville, G., Tuutti, K., "The residual service life of concrete exposed to the combined effect of frost attack and reinforcement corrosion", Concrete Across Borders International Congress, Odense (Denmark), pp. 351.
- [21] Andrade, C., González, J.A., "Quantitative measurements of corrosion rate of reinforcing bars embedded in concrete by polarization resistance measurements", Werkstoffe und Corrosion 29. (1978): pp. 515-519
- [22] Alonso, C., Andrade, C., Rodríguez, J., Casal, J., García, A.M., "Rebar Corrosion steel time to cover cracking," Concrete Across Borders, International Conference - Odense (Denmark) (1994): pp. 301-319.
- [23] Comité Eurointercontinental du Béton (CEB) - Bulletin 162 - "Durable concrete structures"
- [24] Siemes, A.J.M., Vrouwenvelder, A.C., Van den Beukel, A., "Durability of buildings: a reliability analysis", Heron 30, n° 3, 1985.
- [25] Andrade, C. et all. "Inspección de obras dañadas por corrosión de armaduras", Edt. ACUR. CSIC, (1989) pp 5-12.

## **PREDICTING TIMES TO CORROSION FROM FIELD AND LABORATORY CHLORIDE DATA**

---

**REFERENCE:** Berke, N. S. and Hicks, M. C., “**Predicting Times to Corrosion from Field and Laboratory Data,**” Techniques to Assess the Corrosion Activity of Steel Reinforced Concrete Structures, ASTM STP 1276, Neal S. Berke, Edward Escalante, Charles K. Nmai, and David Whiting, Eds., American Society for Testing and Materials, 1996.

**ABSTRACT:** Corrosion of steel in concrete is one of the major causes of the premature failure of steel reinforced concrete. In marine and deicing salt environments the ingress of chloride is the primary cause for the breakdown of passivity and the onset of severe corrosion. In this paper, we show how to develop effective diffusion coefficients for chloride ingress based on chloride profiles from several marine structures. Predictions of the times to reach chloride levels associated with initiation of severe corrosion are made.

Chloride profiles using effective diffusion coefficients determined in other studies are given for bridge decks and parking structures. There are significant benefits of increased concrete cover and the use of corrosion inhibitors in increasing the time to corrosion. Finally, comparisons of Standard Test Method for Electrical Indication of Concrete's Ability to Resist Chloride Ion Penetration (ASTM C 1202) coulomb values with effective diffusion coefficients, determined from field and laboratory studies, indicate that effective diffusion coefficients for low permeability concretes can be estimated using simple modifications of this test method. Thus, we demonstrate that knowledge of the chloride profile is useful to assess the future performance of existing structures that are not undergoing active corrosion, and in predicting the time to corrosion initiation of new structures.

**KEYWORDS:** concrete, steel reinforcing, field structures, bridge and parking decks, marine piles, chlorides, diffusivity, permeability, calcium nitrite, modeling, service life.

---

<sup>1</sup>Research Manager, W. R. Grace & Co., Conn., Construction Products Division, 62 Whittemore Avenue, Cambridge, MA 02140.

<sup>2</sup>Senior Research Engineer, W. R. Grace & Co., Conn., Construction Products Division, 62 Whittemore Avenue, Cambridge, MA 02140.

Initiation of severe corrosion of steel in concrete begins when chloride levels reach 0.9 to 1.2 kg/m<sup>3</sup> (1.5 to 2 lb/yd<sup>3</sup>) [1]. The first signs of corrosion appear typically within five years of the initiation of severe corrosion [2]. Therefore, one way to assess the future corrosion activity of steel in concrete is to determine the present chloride profile and use this information to model the chloride ingress as a function of time.

One of the first researchers to model chloride ingress and time to corrosion as a function of environment, depth of cover, and concrete quality was Stratfull [3]. He used an empirical model to determine time to corrosion damage. Browne used diffusion coefficients determined from concretes in the North Sea to develop a nomograph indicating times to critical chloride values [4]. Several others, including the authors of this paper, have shown that diffusion of chloride into concrete describes the overall chloride profiles for concretes typically used in severe chloride exposures, and have modeled the ingress of chloride [5-12].

In this paper, diffusion coefficients were calculated, and chloride profiles were determined for several field structures. In some cases the chloride contents indicate that corrosion might be occurring, though not visible at the time of these measurements. For these cases future corrosion rate measurements are planned. Diffusion coefficients were used to predict the time for corrosion initiation in those cases where chloride levels at the reinforcement level were below corrosion initiation threshold values.

Also, for two of the field exposures "rapid chloride" permeability data are available on the concretes as determined by the Rapid Determination of the Chloride Permeability of Concrete (AASHTO T-277-89, American Association of State Highway and Transportation Officials, AASHTO Standard Specifications, Part II Tests, Washington, DC, 1990) or by the Standard Test Method for Electrical Indication of Concrete's Ability to Resist Chloride Ion Penetration (ASTM C 1202-94, American Society for Testing and Materials, 1994, Vol. 04.02, Concrete and Aggregates) or a modified version of the test. Several researchers have shown that there are good relationships between the values determined using this technique or slightly modified versions and the diffusion coefficient [9-10,13-16], and that trend is evident in the field-determined chloride diffusion coefficients. A simple analysis of the integrated chloride content, as suggested by some researchers [17,18], does not adequately differentiate the concretes due to the universally high chloride contents near the surface.

Finally, the data and calculated diffusion coefficients are excellent modeling tools for new construction. Examples of extending the projected service-life using calcium nitrite corrosion inhibitor are given, based upon values in Table 1 [19].

TABLE 1 -- Calcium nitrite dosage rates vs. Chloride protection

Calcium Nitrite (30% sol.) L/m <sup>3</sup> (gal/yd <sup>3</sup> )	Chloride Ion kg/m <sup>3</sup> (lb/yd <sup>3</sup> )
10 (2)	3.6 (6.0)
15 (3)	5.9 (9.9)
20 (4)	7.7 (13)
25 (5)	8.9 (15)
30 (6)	9.5 (16)

### EXPERIMENTAL METHOD

The effective diffusion coefficients used in this study were calculated from chloride concentrations that were measured in various concrete structures which had been in service for several years. The chloride analyses were made on cores taken from the structure using either a core drill or a rotohammer. Samples of concrete powder were then obtained either by crushing 13 or 25 mm thick slices cut from the cores, or by drilling 13 mm diameter holes in the core with a masonry drill. In either case, the powder was ground until it passed through a # 50 (0.3 mm) sieve. The total chloride content of the concrete powder was determined using the test method for Sampling and Testing for Total Chloride Ion in Concrete and Concrete Raw Materials (AASHTO T260-84, Standard Specifications for Transportation Materials and Methods of Sampling and Testing, Vol. II, American Association of State Highway and Transportation Officials, Washington DC, August 1986), which entails digesting the powder sample with a nitric acid solution followed by titration of the resulting filtrate with silver nitrate.

Rapid chloride permeability values were obtained using the methods described in AASTHO T-277 and ASTM Test Method C 1202 or a modified version of them. The modification was to apply a 60 volt electrical potential across the specimen for 5 minutes instead of the 6 hours recommended by the standard methods. We and others [13, 15, 18] found that, for coulomb values below 1000, this time-saving step caused no appreciable difference in the results.

## RESULTS AND DISCUSSION

The transport of chlorides through a porous medium follows Fick's second law of diffusion [9], which, for a semi-infinite slab, may be written:

$$C(x, t) = C_o [1 - \operatorname{erf}(\frac{x}{2\sqrt{D_{\text{eff}} \cdot t}})] \quad (1)$$

where:  $C(x, t)$  = chloride concentration at depth  $x$  and time  $t$   
 $C_o$  = chloride concentration at the surface  
 $D_{\text{eff}}$  = effective diffusion coefficient  
 $\operatorname{erf}$  = error function

When chloride values at various depths are known, this equation can be solved by iteration to determine the diffusion coefficient. This procedure was used to obtain the diffusion coefficients for various types of concrete from a knowledge of the chloride concentration at various depths in samples of known exposure time.

Conversely, once the diffusion coefficient is known, chloride profiles can be generated to predict the amount of chloride at a particular depth at some future time, for an assumed value of  $C_o$ . In the case of chloride ingress being unidirectional (bridge decks, parking garages, marine walls), a one-dimensional diffusion model can be used for solving equation (1). In the case of marine piles, where chloride ingress is from two sides, a numerical solution to a two-dimensional model was used.

### Parking Garage - Northern Midwest, USA

This facility was built and went into service in September, 1988. The concrete mixture used included 7.5% silica fume by weight of cement. The 28-day rapid chloride permeability was 1100 coulombs. However, in specimens made at the time the structure was built and tested in the laboratory, this value decreased to around 600 coulombs at about 100 days, and 350 coulombs at 147 days.

Chloride contents at three different locations were determined at four depths after the structure was in service for six years. The data obtained are given in Table 2. The diffusion coefficients were calculated using an iterative method to solve equation (1) for the apparent surface concentration and diffusion coefficient. Figure 1 shows the good agreement between the measured chloride values and those calculated using the diffusion coefficient which resulted from solution of equation (1) for one of the locations.

TABLE 2 --Chloride concentration ( $\text{kg/m}^3$ )of a parking garage at various depths

Depth (mm)	Location 1	Location 2	Location 3
0 - 13	4.0	5.3	3.7
13 - 25	0.6	0.8	0.4
25 - 38	0.12	0.09	0.02
38 - 51	0.09	0.09	0.09
Diff. Coefficient ( $\times 10^{-8} \text{ cm}^2/\text{s}$ )	0.31	0.33	0.25
Surface concentration ( $\text{kg/m}^3$ )	7.1	9.5	12

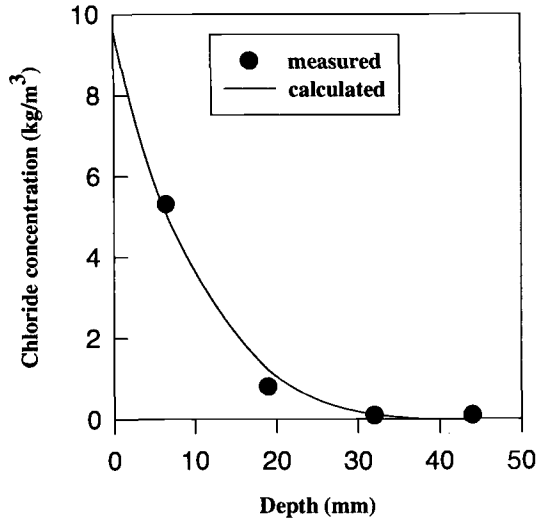


Fig. 1 -- Chloride concentration profile fitted to the complementary error function

The average of the diffusion coefficients for the three locations was calculated to be  $(0.29 \pm 0.14) \times 10^{-8} \text{ cm}^2/\text{s}$ . Diffusion coefficients of this magnitude are typically found in silica fume concretes [20] and correspond to concrete with rapid chloride permeability lower than 500 coulombs, which compares well with the 147-day value measured for concrete obtained for this parking facility at the time it was built. The predicted chloride profiles are shown for a depth of 38 mm in Figure 2.

The chloride profiles indicate that the corrosion initiation threshold (chloride concentration of  $0.9 \text{ kg/m}^3$ ) will be reached after 20 to 45 years of service (average of about 28 years). This is a significant improvement over what a typical 0.4 water to cement ratio (W/C) would provide, in which the average predicted time to corrosion would be around 19 years, as can be seen from Figure 2. The time to corrosion initiation expected for a similar structure could be extended considerably by addition of  $15 \text{ L/m}^3$  of a 30 percent solution of calcium nitrite corrosion inhibitor to this silica fume concrete.

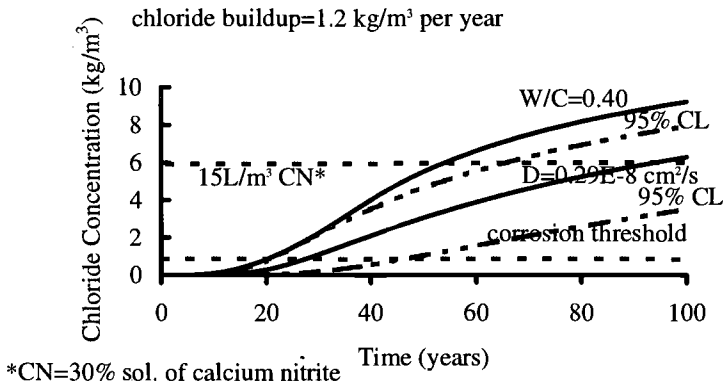


Fig.2 -- Estimated chloride profiles of a parking garage in the Midwest at 38 mm depth

Marine Piles and Decks

Southern California --Chloride concentrations obtained from 610 mm (24 in.) marine piles which had been in service for 32 (piles A to D) and 73 years (piles G to I) are given in Table 3. The cores were taken at the splash/tidal zone which is where the steel reinforcing is more severely attacked. Chloride profiles were obtained from the center of the face so that the data could be analyzed using a one-dimensional model for chloride diffusion. The location of the cores was chosen to avoid further exposing the steel to the chloride action.

TABLE 3 -- Chloride concentration ( $\text{kg}/\text{m}^3$ ) for marine piles in Southern California

Depth (mm)	Pile A 32 yrs	Pile B 32 yrs	Pile C 32 yrs	Pile D 32 yrs	Pile G 73 yrs	Pile H 73 yrs	Pile I 73 yrs
0 - 25	10.2	9.6	7.5	8.0	20.3	20.3	12.9
25 - 51	7.2	7.1	4.4	7.9	11.2	5.1	0.92
51 - 76	5.8	3.3	3.8	3.8	2.1	0.85	0.37
Calculated $D \times 10^{-8} \text{ cm}^2/\text{s}$	4.2	2.0	2.8	3.9	0.38	0.16	0.071
Surface conc. ( $\text{kg}/\text{m}^3$ )	11.3	11.7	8.3	9.7	27	32	27

The average diffusion coefficient for piles A to D was found to be  $3.23 \times 10^{-8} \text{ cm}^2/\text{s}$ . This value can now be used to determine the chloride profiles along the diagonal of the pile where concentrations are a maximum (chloride arrives from two surfaces). Expected chloride concentrations over time are given Figure 3 for depths of 64 mm (2.5 in.) and 76 mm (3 in.) which are typically the concrete covers encountered in a marine environment. As can be seen, the corrosion threshold chloride concentration of  $0.9 \text{ kg}/\text{m}^3$  will be attained after about 5-7 years of service. Addition of a corrosion inhibitor in a dosage of  $30 \text{ L}/\text{m}^3$  would extend the life of such a structure considerably. These profiles were based upon the diagonal and as such, chloride concentrations would be higher than in the face due to a 2-dimensional chloride ingress.

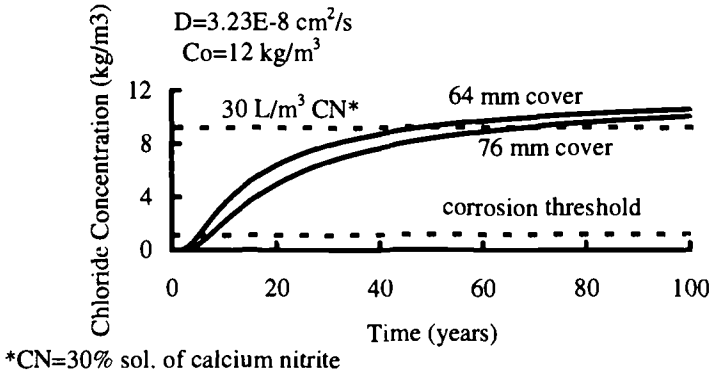


Fig. 3 -- Estimated chloride profile of marine piles in Southern California, at two depths; data obtained from 32 year old piles

The average diffusion coefficient for piles G, H and I was  $0.203 \times 10^{-8} \text{ cm}^2/\text{s}$ . The calculated coefficient was used to calculate the amount of chloride present at depths of 64 mm (2.5 in.) and 76 mm (3 in.) up to 100 years. The resulting curves are shown in Figure 4. As can be seen, in this case corrosion initiation is expected after 60 years service or longer, as this older concrete has a very low diffusion coefficient compared to that found in the newer piles.

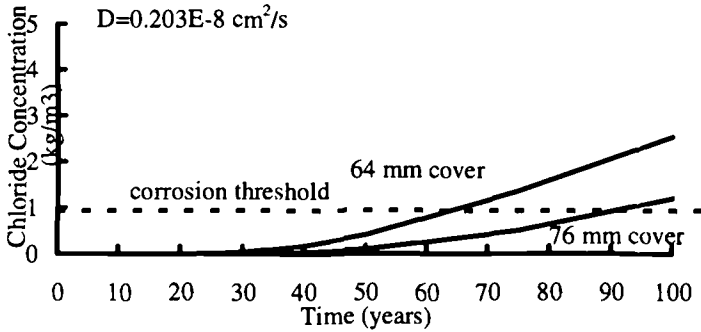


Fig. 4 -- Estimated chloride profile of marine piles in Southern California for two depths of concrete cover; data obtained from 73 year old piles

**Northern California** -- Concrete cores were obtained from piles and decks which had been in service from 19 to 84 years in Northern California. Chloride concentrations and calculated diffusion coefficients are listed in Table 4. Average diffusion coefficients were used (data from piles B-E were used, as pile A had an extremely high value), in a similar manner to those obtained from piles in Southern California, to calculate chloride vs. time for depths of 64 mm (2.5 in.) and 76 mm (3 in.). The profiles are shown in Figure 5. Corrosion of the reinforcing could start at around ten years at 76 mm of cover. The use of calcium nitrite corrosion inhibitor in dosages of 25 L/m<sup>3</sup> would extend the life of such structures considerably.

TABLE 4 -- Chloride concentration (kg/m<sup>3</sup>) of concrete piles and decks in the No. California area

Depth (mm)	Pile A	Pile B	Pile C	Pile D	Pile E	Deck A	Deck B
Age→	27 yrs	19 yrs	84 yrs	60 yrs	27 yrs	84 yrs	27 yrs
0 - 25	10.8	3.8	11.6	9.4	8.0	1.1	5.6
25 - 51	9.5	2.2	11.0	6.4	4.6	0.72	0.42
51 - 76	6.7	0.56	7.2	4.4	2.8	0.72	0.12
Calculated							
Dx10 <sup>-8</sup> cm <sup>2</sup> /s	7.7	1.7	2.4	1.7	2.0	2.0	0.18
C <sub>o</sub> (kg/m <sup>3</sup> )	12.1	5.0	13.5	10.4	9.5	1.2	11.6

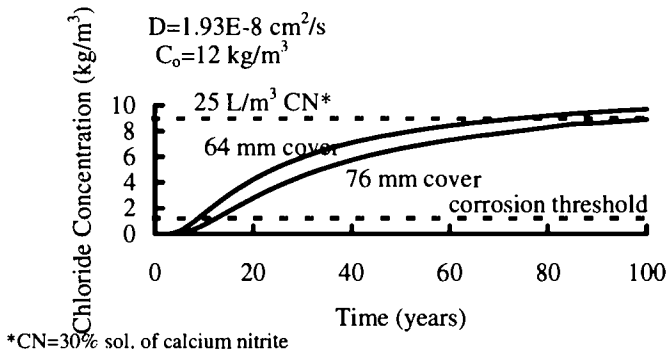


Fig. 5 -- Estimated chloride profile of marine piles in Northern California for two depths of concrete

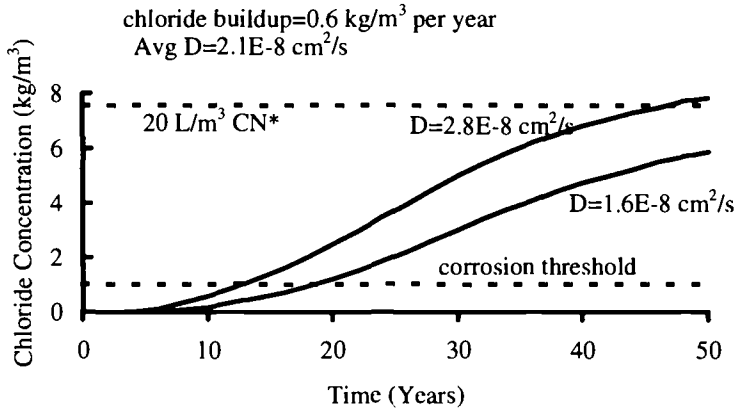
Bridge Decks

Kentucky Bridge Decks -- These bridges contain 20 L/m<sup>3</sup> of a 30% solution of calcium nitrite. Chloride concentrations were obtained from concrete cores received from two bridges which had been in service for 5.5 years. The measured data are given in Table 5 along with the calculated diffusion coefficients and surface concentrations. The average diffusion coefficient is  $(2.13 \pm 0.64) \times 10^{-8}$  cm<sup>2</sup>/s and the average surface concentration is 3.3±1.14 kg/m<sup>3</sup>. The surface concentration corresponds to a chloride buildup at the surface of 0.6 kg/m<sup>3</sup> per year, a value which is typically used to generate chloride profiles at later ages.

Calculated chloride profiles for a depth of 51 mm are shown in Figure 6, and indicate that corrosion would start between 12 and 18 years service, if no corrosion protection were employed. The service life of these decks will be extended considerably, as 20 L/m<sup>3</sup> of calcium nitrite corrosion inhibitor protects to a chloride level of 7.7 kg/m<sup>3</sup> chloride, according to the values listed in Table 1.

TABLE 5 -- Chloride concentration (kg/m<sup>3</sup>) for bridge decks in Kentucky

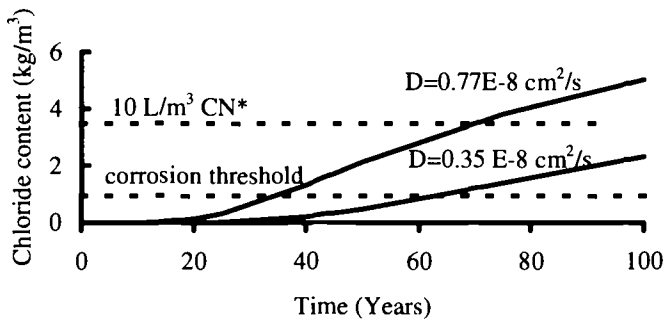
Depth (mm)	A	B	C	D	E	F
6 - 19	2.2	2.8	2.4	3.3	1.7	0.71
19 - 32	1.8	1.2	0.95	1.7	0.59	0.24
32 - 44	0.41	0.71	0.65	0.88	0.30	0.30
44 - 57	-	0.59	0.59	0.65	0.30	0.30
Calculated						
Dx10 <sup>-8</sup> cm <sup>2</sup> /s	1.7	2.3	2.5	2.6	1.4	2.3
Surface conc.(kg/m <sup>3</sup> )	3.7	4.1	3.4	4.9	2.8	1.0



\*CN=30% solution of calcium nitrite

Fig.6 -- Estimated chloride profile of Kentucky bridge decks  
51 mm below deck top surface

Pennsylvania Bridge Decks -- Weyers and Cady [11], reported diffusion coefficients for several bridge decks in Pennsylvania. We found their average effective diffusion coefficient to be  $0.56 \times 10^{-8}$  cm<sup>2</sup>/s (0.0275 in<sup>2</sup>/yr). The 95% confidence limits for their data are  $\pm 0.21 \times 10^{-8}$  cm<sup>2</sup>/s. Using the model for diffusion given above, it is seen that chloride levels of 0.9 kg/m<sup>3</sup> will be reached in over 30 years at 64 mm depth (Fig. 7). Thus, it was not surprising that corrosion had not initiated at 8-9 years time of their study. 10 L/m<sup>3</sup> calcium nitrite would provide protection for a long time.



\* CN=30% solution of calcium nitrite

Fig. 7 -- Estimated range of chloride profiles of Pennsylvania bridge decks  
64 mm depth

Data from other structures

Concrete blocks were exposed to circulating cooling water at 38 C (100 F) for four years at a power station in Florida which uses brackish water for cooling. The high chloride concentration, the abundance of oxygen, and the elevated temperature make this a particularly harsh environment. The cooling tower is in operation from about March to December. The chloride concentrations at the several depths tested are given in Table 6, along with the calculated diffusion coefficients and surface concentrations.

TABLE 6 -- Chloride concentration ( $\text{kg/m}^3$ ) of concrete blocks ponded in cooling tower water at 38 C (100 F) in Florida

Depth (mm)	A	B	C	D	E	F	G	H	I
6 - 19	6.3	6.9	8.4	6.3	3.9	2.0	2.3	4.9	4.2
19 - 32	1.2	1.4	4.4	3.3	0.77	0.40	0.53	2.2	2.7
32 - 44	0.5	0.5	2.0	1.0	0.41	0.36	0.3	0.71	0.53
44 - 57	0.5	0.4	0.4	0.3	0.3	0.3	0.36	0.3	0.3
57 -76	0.4	0.4	0.4	0.2	0.18	...	...	...	...
Calculated $D \times 10^{-8} \text{ cm}^2/\text{s}$	0.86	0.88	2.6	2.4	0.90	1.1	1.1	1.9	2.5
Surface conc. ( $\text{kg/m}^3$ )	15.3	16.3	13.2	10.1	9.2	4.3	4.9	8.4	6.8
Rapid $\text{Cl}^-$ Permeability (Coulombs)	691	216	1123	1512	518	173	518	778	1383
Silica Fume (%)	10	15	10	5	10	20	20	15	10
Calcium Nitrite ( $\text{L/m}^3$ ) (30% sol)	20	0	0	20	10	0	30	0	10

Rapid chloride permeability data were obtained at the times the blocks were manufactured. Some of the blocks were made with concrete containing calcium nitrite, which typically tends to yield higher values for the rapid chloride coulomb value. These data are also included in Table 6. The diffusion coefficient is shown as a function of the rapid chloride permeability in Figure 8, which also shows the higher rapid chloride permeability values for concrete containing calcium nitrite without an increase in permeability. There is excellent agreement between the modified rapid chloride test results and the actual diffusion coefficients when the coulombs measured are below 2000.

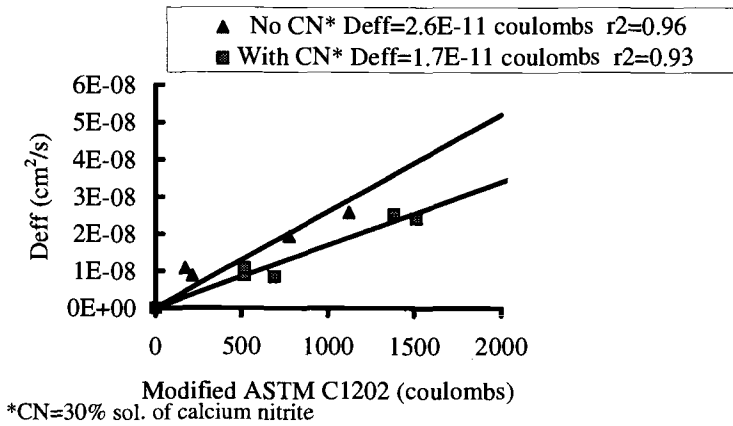


Fig. 8 --  $D_{eff}$  vs. modified ASTM C 1202

## FURTHER DISCUSSION

The effective chloride diffusion coefficients for piles in Southern California are an order of magnitude lower for concretes produced over 70 years ago than for that found in 27 year-old piles. This is most likely due to a change in mixture proportioning, curing procedures, and materials. This improvement is not seen in the Northern California piles, which is an indication that this may not be common to all marine piles made at early ages. However, regardless the cause, it shows that projections of chloride ingress for new structures needs to be based upon the concrete that is being produced today, and not necessarily on the older pile data.

One method to predict future chloride ingress is based upon ASTM Test Method C1202, known as the rapid chloride permeability method. Previous laboratory data showed a good correlation between the effective diffusion coefficient and this method when the coulombs passed were under 2000 [10]. Analyses of two field cases indicate that a good correlation holds. However, effective diffusion coefficients predicted by the rapid chloride permeability method are estimates. Effective diffusion coefficients for the parking garage were actually less than predicted by the original ASTM Test Method C1202 test values, and similar results have been noted for some laboratory specimens [10]. Thus, the test values might be slightly overestimating the diffusion coefficients, and as such are conservative.

The good correlation between diffusion coefficient and the electrical conductivity of concrete is expected from an examination of the Nernst-Einstein equation which relates conductivity to diffusion and is given below:

$$\frac{\sigma_i}{D_i} = \frac{n_i(z_i e)^2}{k_B T} \quad (2)$$

where,

- $D_i$  = diffusion coefficient of species
- $\sigma_i$  = electrical conductivity
- $z_i$  = number of charges of diffusing species
- $e$  = electrical constant
- $n_i$  = concentration of diffusion species
- $T$  = temperature

The addition of calcium nitrite increases  $n_i(z_i e)^2$  leading to an increase in conductivity without a corresponding increase in the diffusion coefficient. This was clearly demonstrated for the power plant field specimens as shown in Figure 8.

Examination of the various chloride profiles, especially those in Figures 2, 6, and 7, shows that increasing the chloride corrosion initiation threshold value with calcium nitrite is much more effective in increasing service life than decreasing the diffusion coefficient by a factor of 2 to 4. Low permeability concrete combined with calcium nitrite has long projected times to corrosion initiation, even in adverse environments.

One point that might not be evident in the predicted chloride profiles shown is that concrete cover is critical. The chloride values in Tables 2-6, are well beyond corrosion initiation threshold values for the lower depths. This occurs regardless of quality and exposure time. Thus, even good quality concrete requires cover over the steel at or above 38 mm (1.5 in.) to resist chloride ingress.

Future work is centered upon performing more complete examination of some of the piles with high chloride contents. This will include petrographic analyses, corrosion potential mapping and corrosion rate measurements based upon polarization resistance. Also, the chloride profiles generated will be used as a guide as to when to inspect the structures that are not currently showing high chloride contents or distress.

## CONCLUSIONS

This work demonstrates that analysis of the chloride contents in field structures can provide a useful tool in predicting future chloride ion profiles, as a means of predicting the initiation of corrosion and future repair of the existing structures. However, it was shown that existing concrete could be a poor predictor of the performance of new concretes. Comparisons of effective diffusion coefficients to ASTM Test Method C 1202 results show that a good correlation exists when the coulomb values are under 2000. Thus, it is possible to estimate the performance of new structures. Finally, it was shown how calcium nitrite corrosion inhibitor can be used to extend the projected time-to-corrosion for reinforced concretes using effective chloride diffusion coefficients. Since the protection provided by calcium nitrite is significantly greater than that obtained by non order of

magnitude changes in the effective diffusion coefficient, its use lessens the effects of minor errors in the estimation of the chloride distribution as a function of time.

## ACKNOWLEDGMENTS

The authors wish to thank the Research Technical Service Group and Alan Dressler for their help in obtaining the chloride data, and Ken Nigro and Mike Weber for providing specimens for analyses. We would also like to thank Sheng-Yi Lee and D. Meyers, from W. R. Grace Washington Research Center for analyzing the same chloride data and developing computer programs which were used in this paper.

## REFERENCES

- [1] Hansen, T. C., "designed to Fail-Marine Concrete in Hot Climates," in *Advances in Cement Manufacture and Use*, E. Gartner, ed., Engineering Foundation, New York, NY, pp. 189-193, 1989.
- [2] Purvis, R. L., Babaei, K., Clear, K. C. and Masrkow, M. J. , *SHRP-S-377 Life-Cycle Cost Analysis for Protection and Rehabilitation of Concrete Bridges Relative to Reinforcement Corrosion*, Strategic Highway Research Program, National Research Council, Washington DC, 1994
- [3] Stratfull, R. F., Jurkovich, W. J. and Spellman., D. L., California Transportation Laboratory, Research Report, CA-DOT-TL-5116-12-75-03, (1975).
- [4] Browne, R. D., "Design Prediction of the Life for Reinforced Concrete in Marine and Other Chloride Environments, "Durability of Building Materials, V. 1, pp. 113-125 (1982).
- [5] Bamforth, P. B., "Prediction of the Onset of Reinforcement Corrosion due to Chloride Ingress", *Concrete Across Borders*", Odense, Denmark, June 1994
- [6] Bamforth, P. B. and Chapman-Andrews, J.F., "Long Term Performance of R.C. Elements under UK. Coastal Exposure Conditions", International Conference on Corrosion and Corrosion Protection of Steel in Concrete, University of Sheffield, England, July 1994.
- [7] Bamforth, P. B., and Price, W.F., "Factors Influencing Chloride Ingress into Marine Structures", presented at Economic and Durable Construction Through Excellence, Dundee, Scotland, September 1993.
- [8] Bamforth, P. B., and Pocock, D. C., "Minimizing the Risk of Chloride Induced Corrosion by Selection of Concreting Materials", Third International Symposium on Corrosion of Reinforcement in Concrete Construction, Wishaw, England, May 1990.

- [9] Berke, N. S. and Hicks, M. C., "Predicting Chloride Profiles in Concrete", *Corrosion*, pp. 234-239, March 1994.
- [10] Berke, N. S. and Hicks, M. C., "Estimating the Life Cycle of Reinforced Concrete Decks and Marine Piles using Laboratory Diffusion and Corrosion Data", STP 1137, *Corrosion Forms and Control of Infrastructure*, Victor Chaker Editor, ASTM, Philadelphia, pp. 207-231, 1992.
- [11] Weyers, R. E., and Cady, P. D., "Deterioration of Concrete Bridge Decks from Corrosion of Reinforcing Steel", *Concrete International*, pp. 15-20, January, 1987.
- [12] Cady, P. D. and Weyers, R. E., "Chloride Penetration and the Deterioration of Concrete Bridge Decks", *Cement, Concrete and Aggregates*, Vol. 5, pp. 81-87, 1983.
- [13] Arup, H., Sorensen, B., Frederiksen, J. and Thaulow, N., "The Rapid Chloride Permeation Test - An Assessment", *Corrosion 93*, Paper No. 334, NACE, New Orleans, March 1993.
- [14] Andrade, C., Sanjuan, M. A. and Alonso, C., "Measurements of Chloride Diffusion Coefficient from Migration Tests", *Corrosion 93*, Paper, No. 319, NACE, New Orleans, March 1993.
- [15] Feldman, R., et al., "An Investigation of the Rapid Chloride Permeability Test," *Proceedings of the 3rd Canadian Symposium on Cement and Concrete*, Ottawa, August 1993, National Research Council, Canada, Ottawa, 1993.
- [16] Ozyildirim, C., "Rapid Chloride Permeability Testing of Silica Fume Concrete," *Cement, Concrete and Aggregates*, 1994, Vol. 16, No. 1, pp. 53-56.
- [17] Whiting, D., "Permeability of Selected Concretes", *Permeability of Concrete*, SP-108, American Concrete Institute, Detroit, MI, pp. 195-222, 1988.
- [18] Pfeifer, D. W., McDonald, D. B. and Krauss, P. D., "The Rapid Chloride Permeability Test and its Correlation to the 90-Day Chloride Ponding Test", *PCI Journal*, pp. 38-47, January-February 1994.
- [19] Berke, N. S., Pfeifer, D. W. and Weil, T. G. "Protection Against Chloride-Induced Corrosion," *Concrete International*, Vol. 10, No. 12, pp. 45-55. December 1988.
- [20] Berke, N. S., Hicks, M. C. and Hoopes, R. J., "Condition Assessment of Field Structures with Calcium Nitrite," Philip D. Cady International Symposium *Concrete Bridges in Aggressive Environments*, SP-151, American Concrete Institute, Detroit, MI, 1994, pp. 43-72.

- [21] Bamforth, P. B., "Concrete Classifications for R. C. Structures Exposed to Marine and Other Salt-Laden Environments," presented at Structural Faults and Repair-93, Edinburgh, June 29-July 1, 1993, 20 pp.

Alberto A. Sagüés<sup>1</sup> and S.C. Kranc<sup>1</sup>

## COMPUTER MODELING OF EFFECT OF CORROSION MACROCELLS ON MEASUREMENT OF CORROSION RATE OF REINFORCING STEEL IN CONCRETE

---

**REFERENCE:** Sagüés, A. A. and Kranc, S. C., “**Computer Modeling of Effect of Corrosion Macrocells on Measurement of Corrosion Rates of Reinforcing Steel in Concrete,**” Techniques to Assess the Corrosion Activity of Steel Reinforced Concrete Structures, ASTM STP 1276, Neal S. Berke, Edward Escalante, Charles Nmai, and David Whiting, Eds., American Society for Testing and Materials, 1996.

**ABSTRACT:** The corrosion rate of steel in concrete can be significantly underestimated if corrosion is non-uniform, because of short-range uneven distribution of the excitation current during polarization measurements. This effect occurs in addition to large scale current distribution problems originating from the use of small counter electrodes or similar causes. Short range macrocells create zones that at low frequencies have much smaller interfacial impedance than the remainder of the steel. However, the impedance is small and uniform at high frequencies due to the presence of interfacial capacitance. The resulting variation of current distribution pattern with frequency prevents correct application of solution resistance compensation techniques. Finite difference computation of current distribution are combined with matrix analysis of the a.c. current distribution to illustrate this behavior. Calculations of the degree to which corrosion is underestimated as a function of system parameters are presented.

**KEYWORDS:** corrosion, concrete, measurement, computation, impedance, polarization, errors, macrocells, current distribution

---

## INTRODUCTION

Electrochemical techniques are highly valuable for the measurement of corrosion rate of steel in concrete, because an assessment of the corrosion condition of the reinforcement can be made nondestructively and with high sensitivity. Specifically, polarization techniques (Polarization Resistance Method (PRM), Electrochemical Impedance Spectroscopy (EIS)) can give an indication of the actual rate of corrosion of the steel. Because these techniques assess corrosion indirectly,

---

<sup>1</sup>Professors, Dept. of Civil Engineering and Mechanics, University of South Florida, Tampa, FL 33620

they are based on a number of assumptions that can, in many cases, be satisfied only partially and cause significant interpretation error. It is therefore important to examine the impact that corrosion modalities have on the applicability of measurement techniques, so that appropriate allowance for errors (or if possible suitable corrections) can be made while interpreting results. The advent of powerful computers has permitted the quantitative determination of the extent of error that can result when applying simplified theoretical treatments to corrosion test results in a variety of corrosion morphologies commonly encountered for steel in concrete. This paper examines in particular the effect of the presence of short-range corrosion macrocells on the value of corrosion rate that would be obtained by application of the Stern-Geary relationship [1] to small amplitude polarization measurement results.

Short-range corrosion macrocells can develop for example when, upon external contamination, the chloride concentration at the steel surface has just reached the threshold value for active corrosion initiation at only a few spots, and the rest of the steel surface is still in the passive condition. The onset of localized corrosion causes an overall potential drop that also affects the surrounding passive areas. As a result, those areas may require a greater amount of chloride contamination (compared to that needed for creating the first active spot) before the breakdown potential matches the newly established local macrocell potential. The macrocells are then somewhat stable, preserving the concentrated character of corrosion until chloride ion contamination becomes more severe. It is not uncommon to observe localization of corrosion in spots that can be only a few mm or cm in length, while the rest of the bar surface remains corrosion free.

The measured electrochemical response of the system provides little indication of the localized nature of the corrosion. On first approximation, it could be speculated that the overall result of a polarization measurement is about the same as if the total amount of corrosion were taking place uniformly over the steel surface examined. Thus if the measured charge transfer resistance (or polarization resistance if appropriate) corresponding to a total steel area  $A$  is  $R$ , then the apparent total corrosion current  $I_{app}$  could be considered to be

$$I_{app} = B/R \quad (1)$$

where  $B$  is the Stern Geary coefficient which is an appropriate function of the Tafel slopes of the reactions involved. An average corrosion current density  $i_{app} = I_{app}/A$  could then be computed as the final result of the polarization measurement. However, several recent computational investigations [2-6] indicate that the actual corrosion current  $I_{corr}$  of the system may differ significantly from  $I_{app}$  depending on the degree of corrosion localization. The evidence, which involves a variety of system geometries, is analyzed here with a view to establish quantitative procedures for appropriate interpretation of polarization measurements for the evaluation of corrosion rates.

## PROCEDURE

The approach used to examine the effect of corrosion geometry in the investigations leading to the present work consisted of the following steps:

1. **D.C Modelling:** Create a computational model to predict the static polarization behavior of the system to be simulated. The model output provided the value of the electrical potential and oxygen concentration at all points in the electrolyte; processing of this information provided in turn the value of the metal dissolution and oxygen consumption rates at all points of the steel surface.
2. **Surface Impedance Modelling:** Assign a local impedance value to each element of the steel surface. The local impedance was formulated as the combination of Faradaic and non-Faradaic terms. The value of the Faradaic terms was obtained from the local rate of the electrochemical reactions (from Step 1) and from the system dimensions. The non-faradaic term was approximated by assigning a value to the interfacial capacitance of the element. The impedance of each surface element was evaluated for a series of test frequencies spanning the range to be investigated.
3. **Equivalent Circuit Building:** Create a composite equivalent circuit of the system by representing the bulk of the concrete by a three-dimensional resistor network connected to the surface impedance elements at the steel surface (from Step 2), and to the counter electrode position at the external concrete surface.
4. **Alternating Current (a.c.) Response Computation:** Solve the alternating current distribution matrix of the equivalent circuit for each of the test frequencies, assigning to the counter electrode nodes an a.c. amplitude and phase representative of the excitation voltage applied to the system during a measurement. The output of the calculation consisted of the alternating potential (amplitude and phase) present at each node of the equivalent circuit. The total alternating current (amplitude and phase) delivered by the counter electrode was computed by post processing.
5. **Impedance Spectrum Computation:** The complex impedance of the system was obtained at each test frequency by dividing the value of the complex potential at a designated node or nodes (corresponding to one or several selected positions of the reference electrode) by the total complex alternating current.

The investigations included a number of simulations, of which 4 main cases have been selected for analysis here. These cases approximate diverse conditions that are encountered in laboratory test specimens or field systems. In each of Cases 1-3 a reinforcing steel bar was placed along the axis of a cylindrical concrete body. The bar contained an active steel region that extended for a portion of the bar length. The rest of the bar surface was in the passive condition. Variations in the length and placement of the active region constituted subcases; both the cases and subcases are described in Table I. In Case 4 the steel was considered to be in the form of a closely spaced rebar mat, approximated by the limit case of a pervious steel sheet. The mat was

placed halfway between the faces of a wide concrete cylinder. The mat steel was considered to be active in a disk centered on the cylinder axis; the rest of the mat was considered to be passive. Variations in the size of the active region resulted in subcases as shown in Table I. For all cases, counter electrodes were placed on the external concrete surface, at the positions shown in Table 1. The reference electrodes were assigned positions at the concrete surface, also indicated in Table I.

Cases 1, 2 and 4 concerned systems in which the concrete resistivity and oxygen diffusivity were constant through the bulk of the concrete. Case 3 simulated a system in which an oxygen diffusivity and concrete resistivity gradient existed along the cylinder body, as in a specimen placed so that only its lower part is in contact with water.

In all cases only two electrochemical reactions were assumed to exist on the steel surface: Cathodic oxygen reduction ( $O_2 + 2 H_2O + 4e \rightarrow 4 OH^-$ , current density  $i_c$ ) and anodic iron dissolution ( $Fe \rightarrow Fe^{++} + 2e$ , current density  $i_a$ ). The reverse reactions were considered to be negligible in the potential range of interest. Both reactions were assumed to obey Butler-Volmer kinetics, with only the oxygen reduction subject to mixed activation/concentration polarization:

$$i_c = i_{oc}(C_s/C_o) \exp [(2.303/\beta_c) (E-E_{oc})] \quad (2)$$

$$i_a = i_{oa} \exp [(2.303/\beta_a) (E_{oa}-E)] \quad (3)$$

where  $i_{oc}$ ,  $\beta_c$ ,  $E_{oc}$  and  $i_{oa}$ ,  $\beta_a$ ,  $E_{oa}$  are the exchange current density, Tafel slope, and equilibrium potential for the cathodic and anodic reactions respectively.  $C_s$  and  $C_o$  are the oxygen concentrations at the steel surface and at the external concrete surface respectively. Oxygen was assumed to be transported by simple Fickian diffusion, with an effective diffusion coefficient  $D$ . The magnitudes  $E$  and  $C_s$  were a function of position in the concrete, while  $i_c$ ,  $i_a$  were a function of position on the steel surface. Values of selected magnitudes are listed in Table I; a detailed listing is given in Refs. [2-5].

After solution of the D.C. problem the local current densities of the cathodic and anodic reactions were obtained for each point of the steel surface by differentiation. The local admittance for each surface element was assigned by [2-5]:

$$Y_{el} = j\omega C_{el} + \frac{1}{\frac{\beta_a}{2.303 I_{ael}}} + \frac{1}{\frac{\beta_c}{2.303 I_{cel}} + \frac{\beta_c \sqrt{j\omega}}{2.303 (I_{lel} - I_{cel}) \sqrt{\tanh(j\omega)}}} \quad (4)$$

TABLE I

Case [Ref]	L (cm)	x (cm)	c (cm)	2a (cm)	2b (cm)	$\rho$ (K $\Omega$ -cm)	D (cm <sup>2</sup> /sec)	$\beta_c$ (mV)	$\beta_a$ (mV)	A <sub>r</sub>	I <sub>corr</sub> ( $\mu$ A)	I <sub>app</sub> ( $\mu$ A)	U <sub>r</sub>	P	R <sub>r</sub>	SYSTEM
1.1 [2]	30	0.2	10	1	11	10	10 <sup>-5</sup>	160	60	.0067	57	15.3	0.21	1	0.75	
1.2	"	0.6	"	"	"	"	"	"	"	.013	68	16.8	0.25	1	0.9	
1.3	"	1	"	"	"	"	"	"	"	.02	70	17.5	0.25	1	0.92	
2.1 [4]	30	0.25	7.8	1.3	7.6	3-30	10 <sup>-5</sup> -10 <sup>-3</sup>	160	60	.015	93.5	26.3	.28	0.97	0.79	
2.2	"	5.3	"	"	"	"	"	"	"	.31	164	100	.60	0.83	1.37	
3.1 [3]	102	6.3	102†	1.9	9.5	10	10 <sup>-4</sup>	160	60	.0625	860	237	.27	0.72	1.14	
3.2	"	"	"†	"	"	"	"	"	"	.0625	760	270	.35	0.68	1.0	
3.3	"	"	"†	"	"	"	"	"	"	.0625	640	237	.37	0.62	0.83	
4.1 [5]	12	7	200	7	200	10	10 <sup>-4</sup>	100	60	.00123	1390	180	.13	0.7	0.16	
4.2	12	7	30	7	200	"	"	"	"	.00123	1390	319	.23	0.7	5.04	
4.3	12	7	7	7	200	"	"	"	"	.00123	1330	418	.31	0.7	45.7	

\*Estimated Analytically

†Various Counter Electrode Polarizability Subcases

R: Reference Electrode Position

\*\* Spatially Variable Parameter (minimum - maximum)

A: Active Steel (Anode)

P: Passive Steel (Cathode)

c: Size of Counter Electrode

m: 10.5 cm(Subcases 2.1 and 2.2)

in which  $u = \omega d^2/D$ ,  $\omega$  is the angular frequency, and  $I_{ce1}$  and  $I_{ae1}$  are the cathodic and anodic currents of the element.  $I_l$  is the effective limiting current density for the element, obtained by approximate consideration of the characteristic diffusion distance  $d$  and the diffusion coefficient  $D$ .  $C_{el}$  is the interfacial capacitance of the element.

Solution of the a.c. problem yielded the overall impedance for the system (as sensed from the reference electrode position) over a range of  $\omega$  values.

## RESULTS

The DC modelling of all four cases resulted in reaction current distributions consistent with the assumed geometries and rate equations. The potential of the concrete immediately next to the steel surface showed strong variation when moving from passive to active steel regions. The potential profile was considerably smoother at the external concrete surface. The oxygen concentration showed gradients from the external surface toward the steel surface. The gradient was usually strongest at the anodic regions, where oxygen consumption was greatest because of the less noble potentials. Macrocell currents flowing through the bulk of the concrete concentrated in the anodic regions. The total corrosion current was computed in each case by integration of the iron dissolution current density over the anodic area. The corrosion current  $I_{cor}$  results are shown in Table 1 for each of the subcases. The values obtained were comparable with those commonly obtained in actual systems.

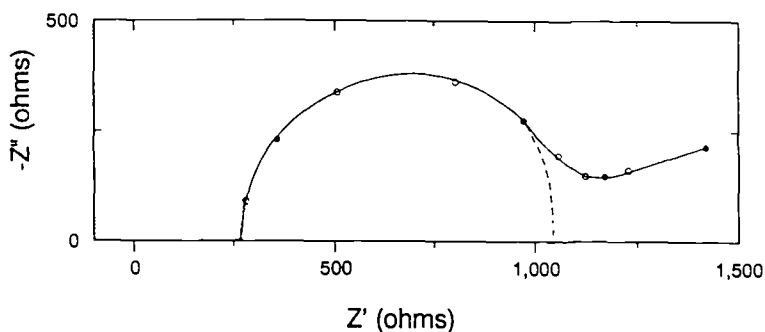


FIG. 1 -- EIS behavior computed for Subcase 1.2. The lowest frequency used was 0.0001 Hz. The points for increasing frequency decades (up to 1 Hz) are marked with solid symbols.

Figure 1 exemplifies the output of the computational procedure for Subcase 1.2. The Nyquist diagram exhibits the features expected from a system with combined activation-concentration polarization of the cathodic reaction, including a high frequency arch and the start of a diffusional low frequency arch.

In a discrete system stabilized at the corrosion potential ( $E=E_{\text{corr}}$  ;  $i_a = i_c = i_{\text{corr}}$ ) the high frequency arch would be associated with  $i_{\text{corr}}$  and the activation parameters of the cathodic and the anodic reactions ( $\beta_c, \beta_a$ ). In the presence of an ideal interfacial capacitance, the high frequency arch would furthermore be a semicircle with diameter  $R_{\text{ct}}$  (corresponding to the non-surface normalized charge transfer resistance) such that

$$I_{\text{corr}} = [\beta_a \beta_c / (\beta_a + \beta_c)] / 2.303 R_{\text{ct}} \quad (5)$$

The high frequency arch in Figure 1 is approximately semicircular. Graphically fitting a semicircle to the arch yields an apparent charge transfer resistance  $R_{\text{app}}$  (equal to the fitted semicircle diameter). Formal application of Eq. 4 using  $R_{\text{app}}$  instead of  $R_{\text{ct}}$  gives an apparent corrosion current  $I_{\text{app}}$ . The value of  $I_{\text{app}}$  obtained by this procedure is shown in Table 1 for all the subcases examined. Comparison with the DC-modelled values revealed that  $I_{\text{app}}$  was consistently smaller than  $I_{\text{corr}}$ . The apparent/actual corrosion current ratio  $U_f = I_{\text{app}} / I_{\text{corr}}$  ranged from 0.6 to as low as 0.13 .

## DISCUSSION

### Sources of Error due to Excitation Current Distribution.

Assuming that experimental implementation is adequate and that a system exhibits causal behavior, discrepancies between the actual corrosion current of a system and the value estimated by simplified EIS interpretation can result from numerous sources. Those sources may be classified into the following broad categories: 1) Insufficient consideration of all reactions involved in the corrosion process (for example, neglecting the presence of an additional cathodic reaction); 2) Disregarding the modality of reactions (for example, ignoring the effect of transport on cathodic reactions) 3) Improper consideration of non-Faradaic currents (such as failing to account for the non-ideal nature of the interfacial capacitance); 4) Treating an extended system as a discrete electrode, consequently ignoring current distribution effects.

The present work uses ideal systems capable of examining all four categories of error sources, some of which have been examined in detail in Refs. [2 to 5]. Specific examples have been selected to concentrate on the fourth category. Within this category, one can distinguish between current distribution problems that arise from the size and placement of the counter electrode, and problems that remain even after using a counter electrode that covers the entire rebar assembly. Problems related to the size of the counter electrode occur when the electrode is so small that only a portion of the rebar surface is affected to any significant extent by the excitation signal. In those cases there may be uncertainty as to the size of that portion; upon completion of a test the value of  $I_{\text{corr}}$  obtained would have then to be divided by an area that is not precisely known. This particular problem has been well recognized

and various means to better define the area of rebar excited have been implemented [5,7,8]. This discussion concerns primarily the problems that remain even after the overall area of current excitation has been determined. The following sections will address this issue for circumstances of increasing complexity .

### Distributed Electrodes in a Non-resistive Electrolyte.

If the electrolyte that surrounded the rebar were non-resistive, the a.c. excitation current density  $\bar{i}_L$  at any point of the steel surface would be given simply by the ratio of the excitation voltage  $V_e$  to the local interfacial impedance  $Z_L$ :

$$\bar{i}_L = V_e / Z_L \quad (6)$$

where  $V_e$  is independent of position by virtue of the lack of electrolyte resistance. The total a.c. excitation current  $\bar{I}$  is given by

$$\bar{I} = \int_A \bar{i}_L dA = V_e \int_A (1/Z_L) dA = V_e \int_A Y_L dA \quad (7)$$

where  $A$  is the overall steel area, and  $Y_L = 1/Z_L$  is the local interfacial admittance. The local charge-transfer admittance  $Y_{ct}$  and  $Y_{al}$  of the cathodic and anodic reactions respectively is given by:

$$Y_{ct} = 2.303 i_c / \beta_c \quad (8)$$

$$Y_{al} = 2.303 i_a / \beta_a \quad (9)$$

Since those are the only two reactions considered, then the local charge-transfer admittance  $Y_{ct}$  is simply  $Y_{ct} = Y_{ct} + Y_{al}$ . As a result, the Faradaic a.c. current  $\bar{I}_{ct}$  at the charge-transfer limit is given by integration of (7) by

$$\begin{aligned} \bar{I}_{ct} &= V_e \int_A (Y_{ct} + Y_{al}) dA = V_e [(2.303/\beta_c) \int_A i_c dA + (2.303/\beta_a) \int_A i_a dA] = \\ &= V_e (2.303/\beta_c) I_c + V_e (2.303/\beta_a) I_a = \bar{I}_{ctc} + \bar{I}_{cta} \end{aligned} \quad (10)$$

Since  $I_c = I_a = I_{corr}$ , the charge transfer admittance  $Y_{ct}$  is given by

$$Y_{ct} = R_{ct}^{-1} = \bar{I}_{ct} / V_e = I_{corr} 2.303 (\beta_c^{-1} + \beta_a^{-1}) \quad (11)$$

Which reduces to the same relationship as for a discrete electrode (Eq.(5)).

### Resistive Electrolyte

If the electrolyte is resistive, the magnitude  $V_e$  must be replaced with  $V_L$  which is no longer independent of position and Eqs. (7-11) are not warranted. Instead,

$$\bar{I} = \int_A \bar{I}_L dA = \int_A V_L (1/Z_L) dA = \int_A V_L Y_L dA \quad (12)$$

The distribution of  $V_L$  is a complicated function of the frequency, the electrolyte resistance distribution, and the interfacial impedance distribution [3-5,9]. A greatly simplified view of such system could be examined by assuming that the sites for the anodic and cathodic reactions are physically separate and discrete, and that separate discrete and frequency-invariant solution resistances exist for each of the two sites. Naming those solution resistances  $R_{sc}$  and  $R_{sa}$  for the cathodic and anodic sites respectively, the total admittance of the system at the charge transfer limit would be

$$Y_{ct} = (R_{sc} + \beta_c/2.303 I_{corr})^{-1} + (R_{sa} + \beta_a/2.303 I_{corr})^{-1} \quad (13)$$

At frequencies high enough that the interfacial capacitance causes the interfacial impedance to be negligible, the system would exhibit an effective solution admittance  $Y_s$  and effective solution resistance  $R_s$  given by

$$Y_s = (R_{sc}^{-1} + R_{sa}^{-1}) = R_s^{-1} \quad (14)$$

It should be noted that in the special case when  $R_{sc}$  and  $R_{sa}$  are such that:

$$R_{sc} / R_{sa} = \beta_c / \beta_a \quad (15)$$

then Eq.(13) would reduce to  $Y_{ct} = (R_s + R_{ct})^{-1} = Z_{ct}^{-1}$ . The value of the actual charge transfer resistance could then be obtained by simple subtraction of the high frequency impedance limit from the charge transfer impedance limit ( diameter of the high frequency arch), and formal application of Equation (5) would give  $I_{app} = I_{corr}$ .

### Localized Corrosion; Large Cathode-to-Anode Area Ratios

The assumptions leading to Eqs. (13-15) are not adequately satisfied when corrosion is very localized. While formal values of  $R_{sc}$  and  $R_{sa}$  can be proposed for each frequency, the values of those magnitudes become frequency-dependent, because the interfacial capacitance causes the current distribution pattern in the electrolyte to vary with frequency. This variation is illustrated in Figure 2 [3], corresponding to Case 2.1 (a cylindrical reinforced concrete specimen with a counter electrode covering the entire lateral surface of the cylinder).

At the high frequency limit (which can be as low as  $\sim 1$  Hz in concrete) the a.c. amplitude equipotential lines are roughly parallel, indicating a nearly uniform current flow between the counter and working electrodes. This current distribution results from the uniformly low impedance of the working electrode surface at high frequencies, dictated by the presence of the interfacial capacitance. The a.c. current flow approaches then that expected to exist between two cylinders each at a uniform and different a.c. potential. The equivalent electrolyte resistance (for a reference electrode placed at the outer concrete surface) is then simply  $R_s = \rho \ln(b/a)/2\pi L$ ,

where  $b$ ,  $a$  and  $L$  are respectively the cylinder radius, the rebar radius, and the length of the cylinder.

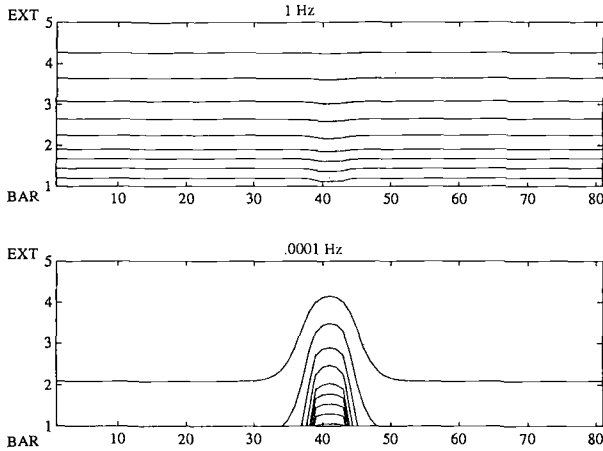


FIG.2 -- Equipotential (a.c.) lines at 1 mV intervals computed for Subcase 3.1 [3] for 1 Hz and 0.0001 Hz. Shown on a longitudinal section of the cylinder between external concrete surface (EXT), on which the counter electrode was placed, and the steel surface (BAR). Positions of radial (1 to 5) and axial (1 to 81) computational nodes are shown in coordinate axes. Potential at the external surface was 10 mV a.c. The aspect ratio was modified for clarity.

At low frequencies approaching the charge-transfer limit the a.c. potential pattern is dramatically different from the previous condition. At low frequencies the interfacial admittance is no longer dominated by interfacial capacitance, but is determined instead by the extent of the Faradaic reactions. At the charge transfer limit, and considering for the moment completely separated cathodic and anodic regions, the admittance of cathode and anode would be:

$$Y_c = 2.303 I_{corr} / \beta_c \tag{16}$$

and  $Y_a = 2.303 I_{corr} / \beta_a \tag{17}$

respectively. In the following the terms  $A_c$  and  $A_a$  designate the areas of the anodic and cathodic regions respectively (it will be assumed that only one of each region exists). The area ratio  $A_r$  is defined as  $A_r = A_a / A_c$ . The specific admittance for both regions would then be given approximately by  $Y_{cL} \sim Y_c / A_c$  and  $Y_{aL} \sim Y_a / A_a$ . When corrosion is highly localized,  $A_a \ll A_c$ , and the specific admittance of the anodic region is much greater than that of the cathodic region. Because of the greater specific admittance, a.c. current concentrates in the anodic region, as revealed by the potential pattern at low frequencies in Figure 2. This current concentration results in an equivalent low frequency solution resistance for the anode (called  $R_{ssa}$  for this case) that is much greater than if it were uniformly distributed along the entire bar surface. The current distribution on the remaining, cathodic surface of the bar is relatively

uniform, and does correspond to an equivalent resistance for the cathode which is roughly the same as that of an electrode uniformly distributed along the bar surface (which is in turn roughly equal to the value of  $R_s$  obtained for the entire system at the high frequency limit).

From the above discussion, the impedance limits for the system with  $A_c \gg A_a$  would be therefore given by the following:

$$\text{High frequency: } Z_{\text{hf}} = R_s = \text{uniform flow resistance.} \quad (18)$$

$$\text{Charge-transfer: } Z_{\text{ct}} \sim [ (R_s + Y_c^{-1})^{-1} + (R_{\text{ssa}} + Y_a^{-1})^{-1} ]^{-1} \quad (19)$$

in which  $R_{\text{ssa}} \gg R_s$ . In the case of extreme current localization at the anode,  $R_{\text{ssa}} \rightarrow \infty$  and the impedance behavior of the system near the charge transfer limit would be dominated by the cathodic reaction. The charge-transfer limit impedance in such extreme would be given by  $Z_{\text{ct}} = R_s + Y_c^{-1}$ , and the apparent charge-transfer resistance for the system would then be  $R_{\text{app}} = Z_{\text{ct}} - R_s = Y_c^{-1}$ . Use of such value in place of  $R_{\text{ct}}$  in equation (4) would result in a value of  $I_{\text{app}}$  that is equal to  $I_{\text{corr}}$  multiplied by a factor  $U_f \sim \beta_a / (\beta_c + \beta_a)$ .

#### Localized Corrosion, Intermediate Cathode-to-Anode Area Ratios

The underestimation of  $I_{\text{corr}}$  for anodic regions of intermediate size can be roughly evaluated from the effective resistance of the cathode and anode as a function of the relative area of both regions. When  $A_r = 1$ , it will be assumed that  $R_{\text{sc}}$  and  $R_{\text{sa}}$  are both approximately equal to  $2 R_s$ . As  $A_r$  approaches zero,  $R_{\text{sc}}$  approaches  $R_s$  and  $R_{\text{sa}}$  tends to  $\infty$ . Because of the relatively small change in  $A_c$  (factor of 2), a simple linear relationship

$$R_{\text{sc}} = R_s (A_r + 1) \quad (20)$$

will be proposed for the interval  $0 \leq A_r \leq 1$ . As indicated elsewhere [2-6,9], current distribution effects cause  $R_{\text{sa}}$  at the low frequency limit to be smaller than a value that would be simply inversely proportional to the area ratio. For small spots facing a much larger counter electrode, the effective solution resistance tends to depend only on the linear dimensions of the spot. For example, for a disk-shaped spot of radius  $r$  facing a semi-infinite medium of resistivity  $\rho$ , the effective solution resistance is [9]:

$$R_{\text{sr}} = \rho / 4 r \quad (21)$$

For a cathodic region of area  $A_c$ , a characteristic radius on the order of  $\frac{1}{2} A_c^{1/2}$  can be proposed. Substituting in Eq.(21) yields for the anode  $R_{\text{sa}} = \rho / 2 A_c^{1/2}$ . Considering that  $R_{\text{sa}} = 2 R_s$  when  $A_c = 1$ , then by substitution and rearrangement:

$$R_{\text{sa}} = R_s [ 2 (1 + 1/ A_c) ]^{1/2} \quad (22)$$

The impedance of the system at the charge-transfer limit then becomes:

$$Z_{ct} = \frac{1}{\frac{1}{R_s(A_r+1)+Y_c^{-1}} + \frac{1}{R_s\sqrt{2(1+A_r^{-1})+Y_a^{-1}}}} \quad (23)$$

The value of  $I_{app}$  can then be obtained by application of Eq.(5) using  $R_{app} = Z_{ct} \cdot R_s$ . This permits estimating the ratio  $U_f = I_{corr} / I_{app}$  as a function of  $A_r$  and the system parameters.

### Effect of Mixed Polarization at the Anode

The preceding sections apply to anodic and cathodic regions in which only one of either reaction is possible. While the cathodic region may be reasonably considered to be the site of only cathodic reactions (passive steel, negligible rate of metal dissolution), the anodic site is likely to support both metal dissolution and oxygen reduction. The simulations for Cases 2 to 4 incorporated the possibility of both reactions in the anodic region. For those cases, the calculations showed that the anodic region was supporting between 3% and 40% of the total cathodic reaction of the steel. The total current flowing through the concrete between the predominantly cathodic and anodic regions was called the macrocell current  $I_{mac}$ . Table I shows the ratio  $p = I_{mac} / I_{corr}$  for each of the Cases. The range of  $p$  values obtained agrees with representative values from experimental observations in similar systems [10].

The effect of mixed polarization at the anode can be estimated by noting that if the rate of the reactions were uniform within the cathode and anode, then the admittance of each region could be modified to values  $Y_{mc}$  and  $Y_{ma}$  respectively such that:

$$Y_{mc} = p Y_c \quad (24)$$

$$Y_{ma} = (1-p) Y_c + Y_a \quad (25)$$

And as a result at the charge-transfer limit:

$$Z_{ct} = \frac{1}{\frac{1}{R_s(A_r+1)+(pY_c)^{-1}} + \frac{1}{R_s\sqrt{2(1+A_r^{-1})+((1-p)Y_c+Y_a)^{-1}}}} \quad (26)$$

Figure 3 incorporates the observations from Cases 1 to 4, showing the current ratio  $U_f$  as a function of the area ratio  $A_r$ . Superimposed to the results are the

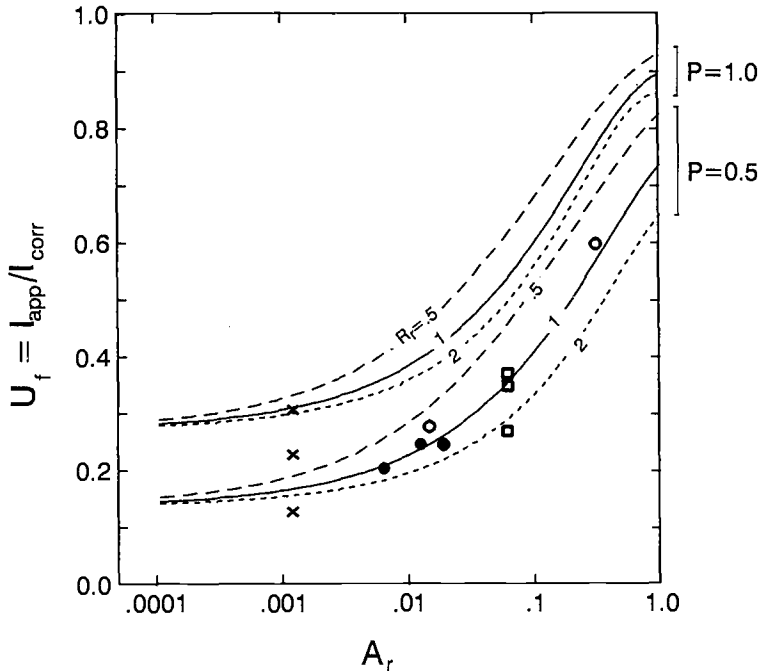


FIG. 3 -- Ratio  $I_{app} / I_{corr}$  as a function of anode-to-cathode area ratio  $A_r$  for the 4 Cases examined (Case 1: solid circles; Case 2: open circles; Case 3: open squares; Case 4: crosses). The lines show the values predicted by Eq. (26) using the resistance ratio  $R_r$  and anode-cathode separation factor  $p$  as parameters.

predictions of Eq.(26) for both  $p=1$  (same as Eq.(23)) and  $p=0.5$ . The calculations were made for  $\beta_c = 0.160$  V and  $\beta_a = 0.060$  V, which correspond to Cases 1 to 3 and approximate Case 4. Examination of Eqs.(16-17, 26) shows that the result of the calculations can be parameterized based on the ratio  $R_r = R_s / R_p$  (with  $R_p = (Y_a + Y_c)^{-1}$ , the polarization resistance that would have been observed if the electrolyte effects on EIS behavior were not present). The ratio  $R_r$  indicates how large the apparent solution resistance  $R_s$  is compared with the "true" polarization resistance of the system. The values of  $R_r$  for each case are shown in Table I. In Figure 3 the results of applying Eq.(23) for  $R_r$  ranging from 1/2 to 2 are shown.

The results from the detailed numerical simulations of Cases 1 to 4 fall generally within the predictions of the simplified treatment leading to Eq.(23) for a reasonable range of values of  $p$ . The variations in  $R_r$  have a relatively small effect on the overall predictions. The results show that concentration of corrosion on a small spot can lead to significant underestimation of the corrosion rate, and that the underestimation is worse as  $A_r$  becomes smaller. The extent of the error was usually smaller than one order of magnitude. While this level of uncertainty may be relatively tolerable in some applications, it can be important when the results of EIS or PRM

measurements are used (for example) to rank alternative rebar materials, or to evaluate the relative merits of various corrosion inhibitors. In those instances corrosion may be relatively uniform under some of the test variables, and non-uniform under others, with consequently different degrees of underestimation of the corrosion current. Erroneous material or process ranking may therefore result.

### Additional issues

The above treatment assumed that the values of the Tafel slopes were known beforehand. The corresponding value of  $B$  (Eq.(1)) was 0.019 V for Cases 1 to 3, and 0.016 V for Case 4. In actual applications it is common to use an empirical value from gravimetric information for  $B$ , often equal to 0.026 V for steel that has reached active behavior [11]. Application of  $B=0.026$  V to the test cases yielded the values of the apparent corrosion current designated by  $I_{app-26}$  in Table I. Those values were somewhat larger than  $I_{app}$ , but still significantly smaller than  $I_{corr}$  in all cases with small  $A_r$ . Interestingly, a value of  $B=0.052$  V has been proposed for estimation of  $I_{corr}$  in "passive" steel [11] also based on empirical gravimetric correlations. Because very localized corrosion at a few spots is most likely to result just after the transition from active to passive behavior, it is possible that the larger value of the empirical constant for "passive" behavior than for active corrosion is the result of indirectly adjusting for underestimation of the corrosion rate due to the mechanism considered here. For specimens experiencing advanced corrosion  $A_r$  is expected to be eventually smaller, which would explain the reasonably gravimetric correlation when a value of  $B=0.026$  V is used.

In EIS measurements the charge-transfer limit behavior is in principle identifiable. It should be pointed out that if the actual polarization resistance limit behavior were to be used instead (with  $R=R_{pol}$  in Eq. (4)), the value of  $B$  is not a simple function of the Tafel parameters unless complete diffusional control of the cathodic reaction is present [12]. In such case  $B=\beta_c/2.303$  and underestimation of  $I_{corr}$  comparable or worse to that estimated earlier would result from corrosion localization. In PRM measurements the potential scan rates commonly used result in conditions approaching the charge transfer limit [13], and the general considerations indicated above apply.

The cases selected for examination involved anodic spots placed immediately below or relatively near the counter electrode. Only the total corrosion currents were discussed. The additional issue of which value of rebar surface area should be used to compute average current densities is beyond the scope of this paper. A quantitative treatment of that issue has been presented by the authors in Reference [5].

A final consideration applies to the case of localized corrosion in which numerous small anodic regions exist in a mostly passive bar. If there are  $N$  roughly equal spots, each will have an area  $A_s \sim A_a / N$ , and a characteristic radius  $\sim 1/2 (A_a)^{1/2} / N^{1/2}$ . As a result, the resistance of each spot varies proportional to  $N^{1/2}$ , but since the number of spots varies as  $N$ , the overall anodic resistance can be expected to decrease

with  $N^{1/4}$ . The extent of  $I_{\text{corr}}$  underestimation is therefore also expected to decrease accordingly. Not surprisingly, a much finer distribution of anodes would result in behavior approaching that of uniformly distributed corrosion with no important current underestimation. Relatively coarse anode-cathode distributions similar to those addressed in the model systems (linear anodic spots sizes ~ 0.1 to 1 cm; linear cathodic region sizes one order of magnitude larger or more) are more likely to produce the type of effects addressed in this paper.

## CONCLUSIONS

1. The computed a.c. excitation current distribution in polarization tests of reinforcing steel with localized corrosion was strongly frequency-dependent.
2. A variety of test cases showed that excitation current concentration caused the effective anode resistance to be high compared to the apparent solution resistance of the system. This resulted in overestimation of the charge transfer resistance of the anode, with consequent underestimation of the corrosion current.
3. Analysis of a simplified system predicted the extent to which the corrosion current is underestimated, as a function of anode-to-cathode area ratio, concrete resistance, extent of corrosion, and extent of separation of anodic and cathodic reactions.
4. Both the numerical computations and simplified analytical treatment indicated that the apparent corrosion current in reinforced concrete can be several times smaller than the actual corrosion current. The predicted effect was greatest at small anode-cathode area ratios and for relatively coarse spatial anode-cathode distributions.

## ACKNOWLEDGMENT

This work was partially supported by the Florida Department of Transportation (FDOT) and Engineering Computing Services of the University of South Florida (USF). The opinions, findings and conclusions expressed herein are those of the authors and not necessarily those of FDOT or USF.

## REFERENCES

- [1] Mansfeld, F., "The Polarization Resistance Technique", in Advances in Corrosion Science and Technology, Vol. 6, M.Fontana and R.Staehle, Eds., Plenum Press, New York, 1976.
- [2] Kranc, S.C. and Sagüés, A.A., "Computation of Corrosion Macrocell Current Distribution and Electrochemical Impedance of Reinforcing Steel in Concrete", in Computer Modelling in Corrosion, ASTM STP 1154, R.S. Munn, Ed., American Society for Testing and Materials, Philadelphia, p. 95, 1992.

- [3] Kranc, S.C. and Sagüés, A.A., "Calculation of Extended Counter Electrode Polarization Effects on the Electrochemical Impedance Response of Steel in Concrete", p. 365 in Electrochemical Impedance: Interpretation and Analysis, ASTM STP 1188, D.C. Silverman, J.R. Scully and M.W. Kendig, Eds., American Society for Testing and Materials, Philadelphia, 1993.
- [4] Kranc, S.C. and Sagüés, A.A., "Computational Modelling of the Electrochemical Impedance Response of Macroscopic Reinforcing Steel in Concrete Systems", p.263, Proceedings of the 1st. Pan-American Corrosion and Protection Congress, Vol.1, Argentine Corrosion Association and National Association of Corrosion Engineers, V. Rascio, Editor, Mar del Plata, Argentina, 1992.
- [5] Kranc, S.C. and Sagüés, A.A., Electrochimica Acta, Vol. 38, p.2055, 1993.
- [6] Sagüés, A. and Kranc, S.C., Corrosion, Vol. 48, 1992.
- [7] Flis, J., Sabol, S., Pickering, H., Sehgal, A., Osseo-Asare, K., and Cady, P., Corrosion, Vol.49, p.601, 1993.
- [8] Feliu, S., Gonzalez, J., Feliu Jr., S., and Andrade, M.C., ACI Materials Journal, Vol. 87, p.457, 1990.
- [9] R. Oltra and M. Keddami, Corrosion Science, Vol.28, p.1, 1988.
- [10] Andrade, C., Maribona, I., Feliu, S., Gonzalez, J. and Feliu Jr, S., Corrosion Science, Vol. 33, p. 237, 1992.
- [11] Andrade, C., Castelo, V., Alonso, C. and Gonzalez, J., "The Determination of the Corrosion Rate of Steel Embedded in Concrete by the Polarization Resistance and AC Impedance Methods", p.43, in Corrosion Effects of Stray Currents and the Techniques for Evaluating Corrosion of Rebars in Concrete, ASTM STP 906, V. Chaker, Ed., ASTM, Philadelphia, 1986
- [12] Epelboin, I., Gabrielly, C., Keddami, M. and Takenouti, H., "AC Impedance Applied to Corrosion Studies", in Electrochemical Corrosion Testing, p.150, ASTM STP 727, F. Mansfeld and U.Bertocci, Eds., ASTM, Philadelphia, 1981.
- [13] Sagüés, A. "Corrosion Measurements Techniques for Steel in Concrete", Paper No.353, Corrosion/93, National Assoc. of Corrosion Engineers, Houston, 1993.

Eric J. Carlson<sup>1</sup>, Richard G. Stringfellow<sup>1</sup>, and Sylvia C. Hall<sup>2</sup>

## FINITE ELEMENT MODELING OF GROUND LEVEL POTENTIAL MEASUREMENTS OF GALVANIC CELLS ON CONCRETE PIPE

---

**REFERENCE:** Carlson, E. J., Stringfellow, R. G., and Hall, S. C., “**Finite Element Modeling of Ground Level Potential Measurements of Galvanic Cells on Concrete Pipe,**” *Techniques to Assess the Corrosion Activity of Steel Reinforced Concrete Structures*, ASTM STP 1276, Neal S. Berke, Edward Escalante, Charles K. Nmai, and David Whiting, Eds., American Society for Testing and Materials, 1996.

**ABSTRACT:** Ground potential surveys are used to monitor for the presence of corrosion activity on buried pipe. Questions arise as to the relationship between the measured potentials and anode size, detectable anode size, and the parameters which influence the magnitude of the potential. In this study, surface center-line and side-drain potentials were calculated for galvanic cells in buried concrete pipe using a 3-D finite element model. The model was calibrated using the results from potential surveys conducted on buried pipe with implanted anodes. Soil cover, anode size, and anode location are the dominant variables affecting surface potential. The analyses reveal the detection limits of potential surveys for the given range of parameters studied.

**KEYWORDS:** prestressed concrete pipe, galvanic cell, corrosion monitoring, finite element modeling, three-dimensional

---

## INTRODUCTION

Buried pipelines are critical components of the national infrastructure, transporting oil, gas, water, and sewage. The failure of these pipelines is, of course, a critical concern. The definition of failure depends on the application, but may range from catastrophic failure with long-term loss of service to short-term loss of service, when the reserves of the critical fluid are exceeded. For example, in the metropolitan Boston area, a single reinforced concrete pressure pipe supplies 90% of the drinking

---

<sup>1</sup> Senior Consultants, Arthur D. Little, Cambridge, MA 02140

<sup>2</sup> Director, Engineering Development Center, Ameron, South Gate, CA 90280

water supply to Boston[1]. Loss of service beyond 20 hours would produce hardships for the local population. The aqueduct has been in service for over 50 years without incident, yet the question has been asked: "Can it continue to provide service for 10 to 20 years until a new aqueduct comes on-line?" The ability to monitor the condition of older pipelines is essential to insuring reliable service.

Materials of construction for pipelines include: steel, reinforced concrete, prestressed concrete, and more recently plastic. As corrosion prevention technology has evolved, coatings and cathodic protection have been used, individually or in concert, to protect pipe structures. However, a large population of systems were installed before coatings and cathodic protection were mandated or became accepted practice. In the case of concrete pipe, cathodic protection cannot generally be retrofitted to older systems because pipe segments were not electrically bonded at the time of installation. Consequently, in areas where the environment has proven to be corrosive, periodic assessment of the pipe condition allows implementation of corrective actions prior to failure.

Degradation of the steel may occur in many ways, including: uniform corrosion, crevice corrosion, stress corrosion cracking, and galvanic corrosion. In concrete, the alkalinity of the cement normally protects the steel reinforcing or prestressing wire by passivation. The ingress of chlorides, carbonation of the cement, sulfate attack, acidic soil, or leaching may reduce the protective properties of the cement leading to initiation of corrosion. Cracking of the cement cover by the stresses from the precipitation of corrosion products further accelerates ingress of the environment and the spread of corrosion.

For uncoated concrete pipe, galvanic cells are the primary corrosion concern. Galvanic potentials arise from gradients in pH, oxygen, steel passivity, and chloride. Gouda and Mourad[2-5] showed by laboratory experiments that the driving force of galvanic cells in concrete range from 300 to 500 millivolts (measured without current flow).

Two potential survey techniques are commonly used for the detection of corrosion on buried structures:

- Pipe-to-Soil (P/S), and
- Cell-to-Cell.

P/S potential surveys are particularly appropriate for concrete pipe, where the onset of corrosion coincides with a shift from passive to active potentials. However, the concrete pipe segments must be electrically bonded for use of P/S potential measurements. In those situations where pipe segments are not bonded, Cell-to-Cell techniques can be used to detect the presence of galvanic corrosion cells.

Potential gradients along the ground surface can be detected with two reference electrodes placed in contact with the ground. The measurement typically takes two forms. In the first, using a moving reference electrode potentials are measured as a function of distance away from a fixed reference electrode. Measurements are taken down the centerline of the pipe and/or offset (2 to 6 m) on both sides. In the second method, both reference cells are moved along the pipe, with one cell over the centerline, and the other offset. Both techniques rely upon the generation of surface potential gradients due to galvanic currents.

The reliability and accuracy of both the P/S and Cell-to-Cell potential survey techniques have been challenged. Recently, the American Concrete Pressure Pipe Association (ACPPA) sponsored a round robin evaluation of potential survey techniques on a 240 foot (73 m) line made up of ten 48 inch (1.2 m) diameter by 24 foot (7.3 m) long sections covered by 6 feet (1.8 m) of soil[6]. Four small inert anodes were placed at the midpoint of each pipe segment at the top, bottom, and "east-

west" springlines. Electrically bonded and unbonded pipelines could be simulated by making or breaking connections to adjacent pipe. Simulated galvanic currents were then passed between the anode or anodes to the pipe. The study indicated that the extent to which galvanic corrosion cells can be monitored for corrosion depends upon the intensity of corrosion and the location of the anode on the pipe circumference.

Figure 1 shows a typical potential response recorded for an anode on the top of an unbonded pipe using the Fixed Cell-Moving Cell method with 5 foot (1.5 m) intervals between measurements and a galvanic current of 80 milliamperes. The peak height was approximately 35 millivolts above the baseline. The potential distribution extended over approximately 1½ pipe lengths. During the potential surveys, the soil resistivity ranged from 25,000 to 40,000 ohm-cm during the trials.

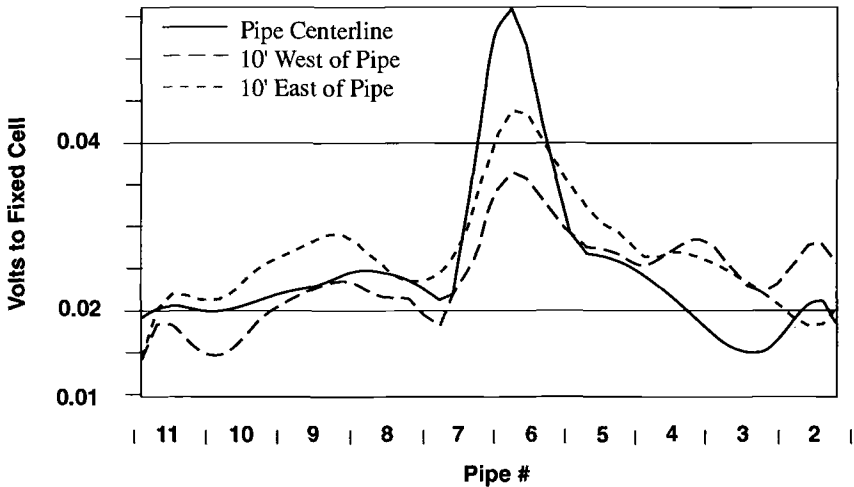


FIG. 1--Typical response from ACPPA potential survey (anode at top of pipe).

We suggested that the ACPPA experimental results could be used to calibrate a computer model of ground level potentials arising from galvanic cells on pipe. Once calibrated, the limits of the potential survey techniques could be studied using the computer model to explore the effects of variation in pipe diameter, location and size of anodic areas, depth of ground cover, soil conductivity, and corrosion current. The results of this parametric experiment are presented in the discussion which follows.

## APPROACH

The distribution of current and potential in the soil surrounding the buried pipeline was determined using three-dimensional finite element methods. The commercially-available ABAQUS finite element program was used to carry out the calculations on a DEC 3100 workstation computer. The equations governing electrostatic fields are analogous to those which govern conductive heat transfer, with: electrical conductivity analogous to thermal conductivity; potential analogous to temperature; and current density analogous to heat flux. Through this analogy, the heat transfer analysis capabilities of ABAQUS were used for the calculations.

The kinetic and diffusion processes occurring at the anode and cathode were not modeled. Instead, the cathodic reaction rate and distribution were assumed to be limited by diffusion and IR losses respectively.

### Calibration

The ACPPA experiment for which only the anode at the top of the pipe was activated and for which the pipe sections were electrically unbonded (Figure 1) was used to validate the finite element analysis methodology. The finite element mesh for modeling of the ACPPA experiment is shown in Figure 2. A great deal of mesh refinement was required to accurately capture the potential gradients and current distribution around the small (1.5 mm diameter x 5.1 cm long) anode. At the same time, it was necessary to extend the mesh far enough away from the pipe that current flow diminished entirely. The model pictured uses over 13,000 8-noded "brick" elements to discretize the pipe mortar and surrounding soil. A potential difference of 160 volts was assigned between the anode and cathode surfaces, as was done experimentally. A linear, steady-state calculation was then performed to determine the corresponding potential field and current distribution.

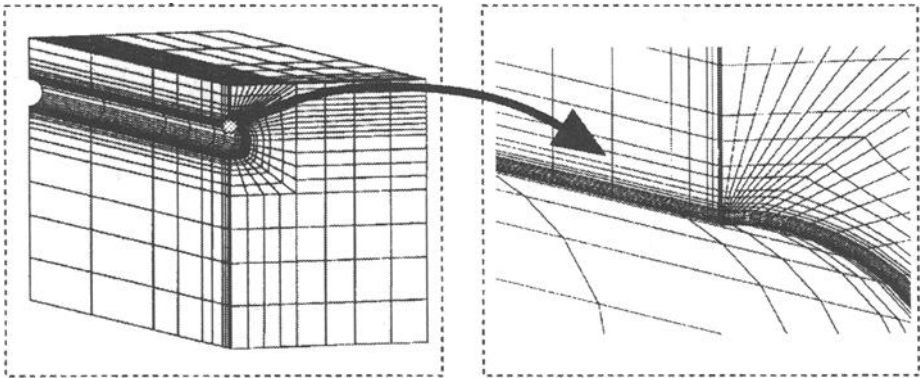


FIG. 2--Mesh pattern used to model the ACPPA experiment.

### Parametric Study

The model in the parametric study required a less detailed mesh (5000 elements) because of the larger anode size — 1 ft<sup>2</sup> to 10 ft<sup>2</sup> (0.093 m<sup>2</sup> to 0.93 m<sup>2</sup>).

For the parametric study, the application of nonlinear boundary conditions, representing limiting cathodic currents, was first investigated. Under such conditions, it was necessary to solve the analogous nonlinear, transient heat transfer problem in an iterative fashion, supplying a "guess" of the anode and cathode potential distributions as initial boundary conditions, and then iterating until steady-state conditions in which current flow patterns and associated potential distributions satisfying limiting current conditions were reached. The convergence of the nonlinear 3-D calculations was extremely slow, and because of the large size of the problem, such calculations were impractical given the limits of computer time. The slow convergence rate is likely attributable to the fact that nonlinear boundary conditions of this sort are not common

in heat transfer analysis, and are not effectively handled in ABAQUS’s solution procedures.

Further analysis showed that the nonlinear solutions could be approximated to within a few percent using linear calculation methods by simply separating the anode and cathode by about an inch. In this manner, the singular nature of the current at the anode/cathode interface was eliminated, and the area within which the cathodic current reached levels exceeding limiting values was restricted. With this linear approximation, the results can be scaled by the level of the applied voltage.

**RESULTS/DISCUSSION**

Modeling of ACPPA Experimental Data

In setting up the model to simulate the potential distributions measured in the ACPPA experiment, initial use of a uniform resistivity for the mortar coating over the prestressing wire and for the soil cover failed to fit the data. The surface potential profile could be reproduced for the specified current flow but the total applied voltage exceeded that of the field experiment. Consequently, an additional resistance zone adjacent to the wire in which the resistance could be varied separately from the soil was incorporated into the model. Physically, the lower porosity and higher conductivity of the alkaline mortar relative to the surrounding soil can result in a lower mortar resistivity.

Figure 3 shows the surface potential profiles predicted for a mortar resistivity of 8,000 ohm-cm and a soil resistivity of 30,000 ohm-cm. Soil resistivities measured at the time of the experiment ranged from 25,000 to 40,000 ohm-cm. The simulated potential profiles are consistent with the measured values shown in Figure 1.

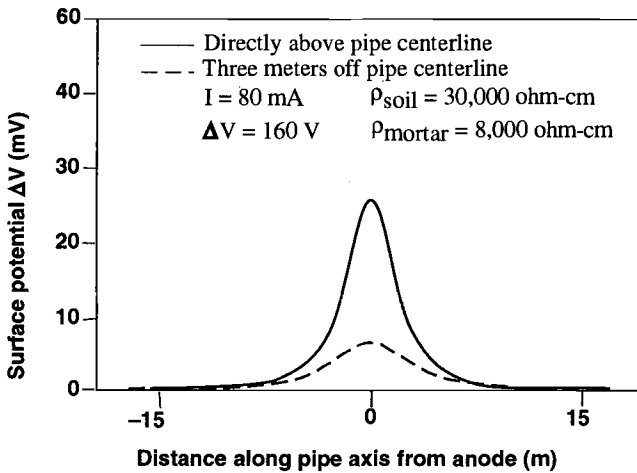


FIG. 3--Separate soil and mortar resistivities resulted in a fit to the ACPPA data.

The cathodic current distribution was limited to within a few inches of the anode. Cathodic current as a function of distance around the pipe circumference is shown in Figure 4 for two axial positions: at the surface of the anode and 0.4 inches away from the anode.

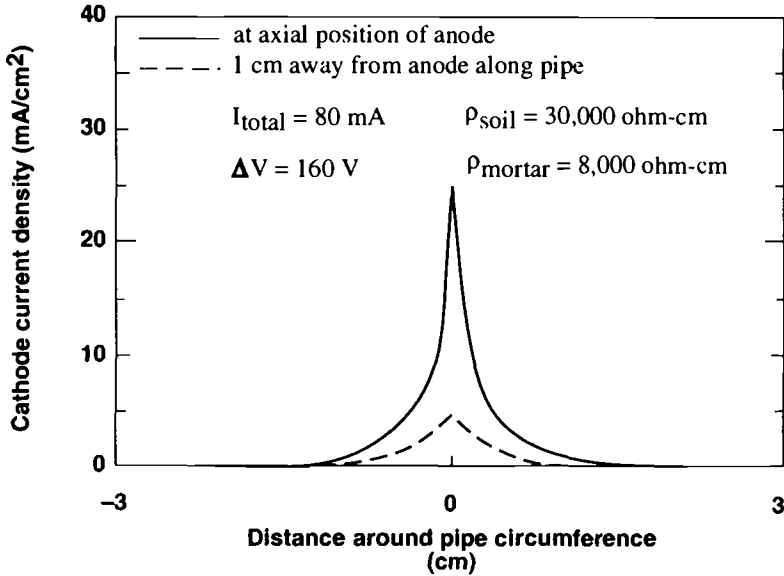


FIG. 4--Cathodic current distribution calculated for two axial positions.

From a modeling perspective, the use of a larger anode size — on the order of 1 ft<sup>2</sup> (0.093 m<sup>2</sup>) — in future experiments of this nature would allow for more accurate verification of the modeling techniques. The singular nature of the anode (2.4 cm<sup>2</sup>) also produced unrealistically high anode current densities (33,000 μA/cm<sup>2</sup>). Values on the order of 10 to 100 μA/cm<sup>2</sup> are typically found in field corrosion cells.

Parametric Study

For purposes of displaying the data, the potential and current distribution calculations are based on a galvanic potential of 1 volt. Since the linear calculations assume resistance (IR) losses control the current distribution, the potentials generated can be scaled by the current.

Results of the parametric study are displayed in Figures 5 through 15. Calculated surface potentials were found not to depend upon the resistivity of the soil. The effect of opposing trends in resistance and current cancel, since the surface potential is the product of soil resistance and current flow. In contrast to surface potential, total anodic current decreased with increasing resistivity (Figure 5) for a fixed driving voltage.

In reality, maintenance of good ionic continuity between the reference electrodes and the soil establishes the lower limits of soil resistivity for reliable potential measurements.

The cathodic current distribution, which was not limited by electrode size, dropped rapidly within a distance of about 25 cm for both of the anode sizes considered (Figure 6). The current density then approached zero over the next 25 cm. The finite element model does not include kinetic expressions to simulate electrode reactions at either the anode or cathode, which might further alter the current distribution on each electrode.

Estimated surface potentials (calculated using the fixed-reference method) increase with increasing anode size, but not in a linear fashion (Figure 7). The potentials shown in this figure can be scaled by the driving voltage selected for the galvanic couple or environmental conditions. At a cell voltage of 500 millivolts, an anode size of one square foot probably represents the lower limit of detection (25 millivolt peak surface potential). The graph also shows that potential sampling should be performed several times within the 20 foot length in order to capture the peak voltage and shape of the curve.

Figure 8 illustrates the anticipated surface potential distribution measured with moving-cell-to-moving-cell techniques. This technique essentially takes the slope of the potential curves. Potentials are lower than those calculated for the fixed-reference method.

Shifting the anode away from the top of the pipe also lowers the surface potential (Figure 9). An anode on the side of the pipe produces a peak potential, approximately 1/6 of the magnitude of the potential for an anode on the top of the pipe. An anode of the same size on the bottom of the pipe would not be detected. Moving the anode away from the top of the pipe results in a non-symmetric potential distribution on the surface, detectable by the side drain potentials measurements (Figure 10).

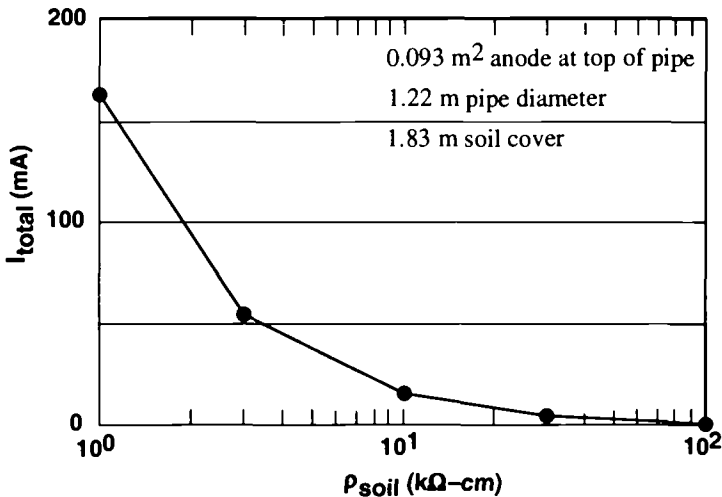


FIG. 5--As soil resistance increases, the total corrosion current decreases.

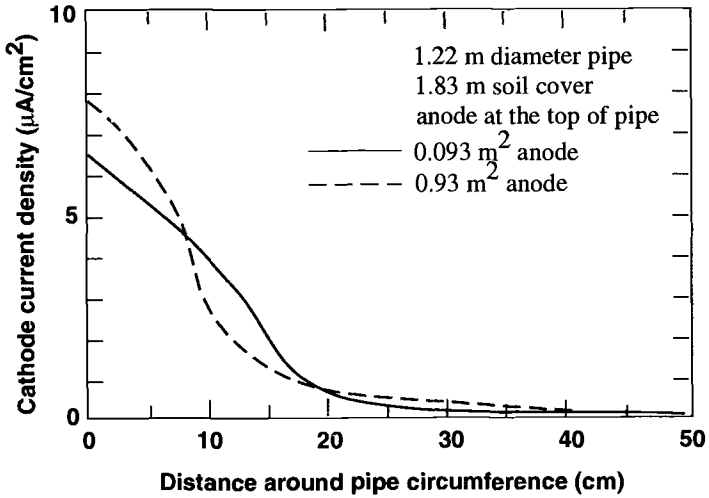


FIG. 6--Cathodic current decreased in a circumferential path away from the electrode interface.

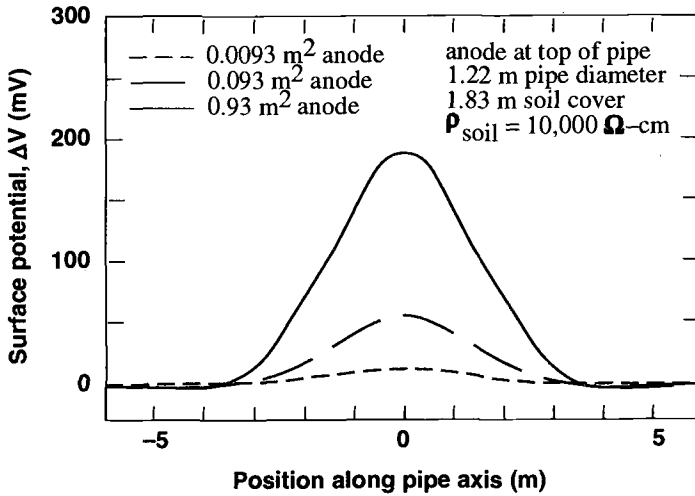


FIG. 7--Surface potential down pipe centerline versus anode area for (anode on top of the pipe).

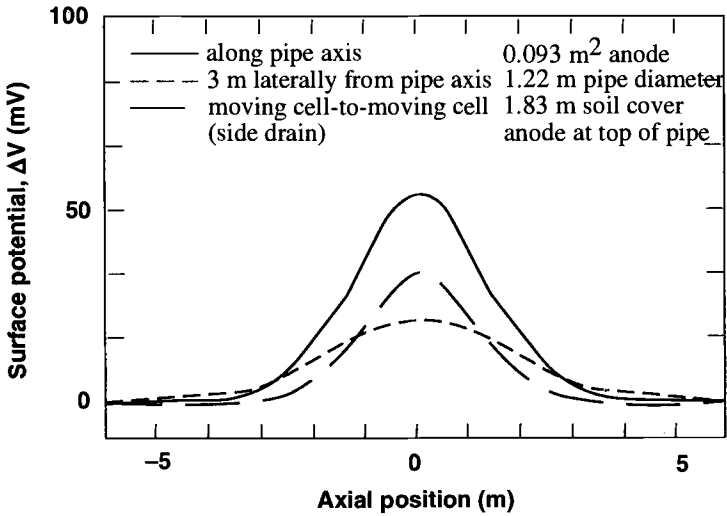


FIG. 8--Moving Cell-to-Moving Cell surface potential with anode on top of the pipe.

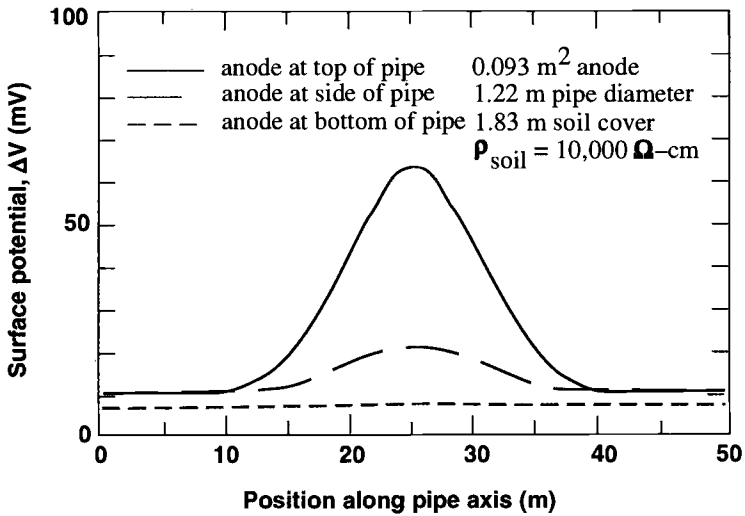


FIG. 9--Peak potential decreases as the anode moves from the top to bottom of pipe.

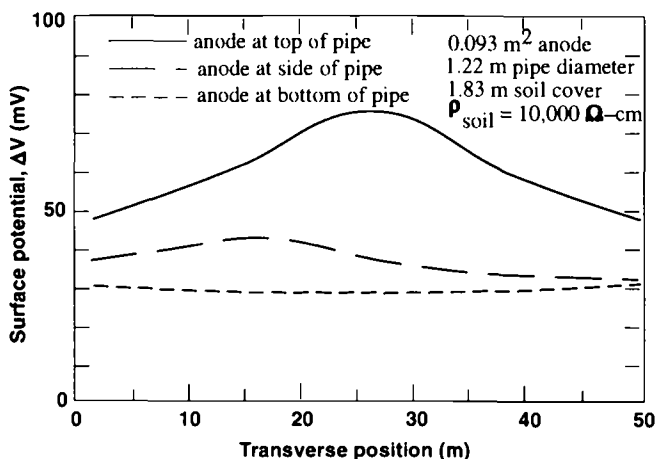


FIG. 10--Asymmetry in transverse potential profile indicates anode location.

Isocontour potential plots in a cross-section of the pipe and soil for three anode locations are shown in Figures 11—13. Current flow can be visualized by drawing current lines which intersect the potential lines at right angles. When the anode is located at the top of the pipe, the cross-sectional potential distribution for the anode is symmetric, with the largest gradient over the top of the pipe (Figure 11).

As the anode moves away from the top of the pipe, the magnitude of the potential gradient on the surface decreases, and the asymmetry of the distribution increases. For an anode at the side of the pipe, the highest gradients are below the surface because some of the current lines do not reach the surface (Figure 12). For the same anode parameters as for the top and side cases, the anode on the bottom of the pipe (Figure 13) results in the smallest potential gradient on the surface and produces a change in the sign of the surface potential because the direction of current flow changes.

Location of anodic and cathodic areas on a pipeline depends upon many factors, including: height of the water table, distribution of soil types, design of the trench, and excavation procedures. Several factors, including height of the water table and the formation of a French drain by the trench, produce higher moisture levels below the springline of pipelines. Consequently, the higher moisture levels result in lower ingress of aggressive species, limiting cathodic reaction rates, and lowering the probability that corrosion will initiate. These factors lessen the likelihood that anodes will form below the springline, and concerns about detectability.

Conversely, factors such as: wet/dry cycling, higher probability of installation damage, and more porous backfill, make the pipe areas above the springline more prone to initiation of corrosion. Fortunately, these areas are also more easily detected.

From a measurement perspective, only the potential on the surface is useful. Figures 14 and 15 show the surface potential distribution above the pipeline. As in previous plots, the anode on the top of the pipe produces a symmetric potential distribution. (The slight asymmetry of the contours is a numerical artifact.) Moving the anode to the side shifts the surface potentials laterally.

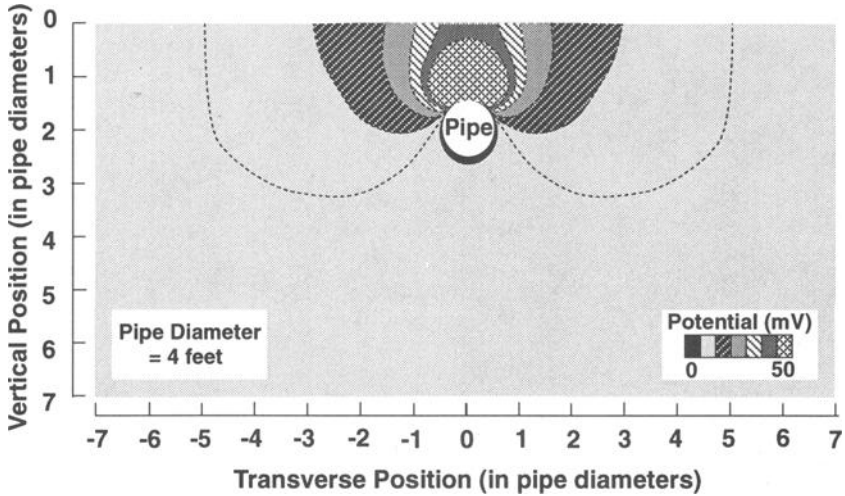


FIG. 11--Isocontour plot of transverse potentials for an anode on top of the pipe.

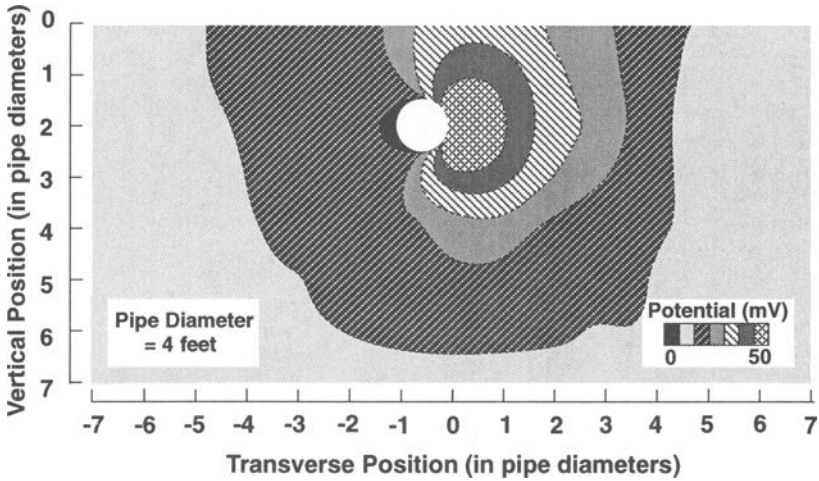


FIG. 12--Isocontour plot of transverse potentials for an anode on side of the pipe.

For electrically isolated pipe segments, anodes placed at the pipe ends produced asymmetric potential distributions, but with similar potential magnitudes as the centrally located anodes.

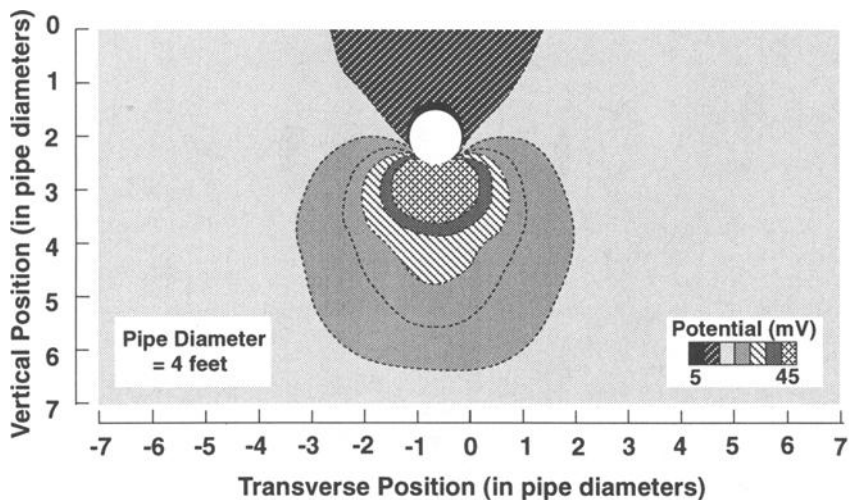


FIG. 13--Isocontour plot of transverse potentials for an anode on bottom of the pipe.

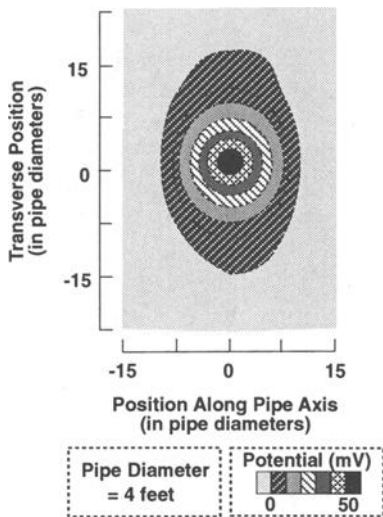


FIG. 14--Surface potentials for an anode on the top of the pipe.

Table 1 summarizes the results of the parametric study with regard to three measures: peak surface potential, total corrosion current, and anodic current density. Soil cover, anode position, and anode area have the most significant impact on the calculated surface potential. As soil cover increases, surface potentials decrease, but the total current remains constant. In our model, the soil is simply a conductor and as

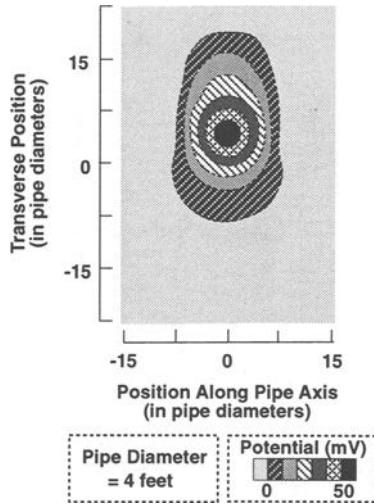


FIG. 15--Surface potentials for an anode on the side of the pipe.

TABLE 1--Summary of the effects of parameter variation on peak surface potential, total corrosion current, and average anode current density.

Variable	Anode	Anode Area (ft <sup>2</sup> )*	Soil Resistance (kohm-cm)	Pipe Diameter (in)*	Soil Cover (in)*	$\Delta V_{\text{surface}}$ (MV)	$I_{\text{total}}$ (mA)	$I_A$ (mA/cm <sup>2</sup> )
Soil Resistance	top	1.0	1	48	72	57.0	163.0	175.0
			3			58.0	55.0	59.0
			10			59.0	17.0	18.0
			30			60.0	5.7	6.0
			100			62.0	1.8	1.9
Pipe Diameter	top	1.0	10	48	72	59.0	17.0	18.0
				96		72.0	15.0	16.0
				252		79.0	18.0	19.0
Soil Cover	top	1.0	10	48	72	59.0	17.0	18.0
					120	23.0	18.0	19.0
					240	6.0	20.0	21.0
Anode Position	top	1.0	10	48	72	59.0	17.0	18.0
	side	1.0				11.0	15.0	18.0
	bottom	1.0				-3.4	18.0	19.0
	bottom	10.0				-9.4	45.0	4.8
Anode Area	top	0.1	10	48	72	11.0	6.7	72.0
		1.0				59.0	17.0	18.0
		10.0				187.0	44.0	4.7

\* 1 ft<sup>2</sup> = 929 cm<sup>2</sup>; 1 inch = 2.54 cm

its cross-sectional area increases the voltage drop decreases. Some increase in current occurs as soil cover increases because the total resistance of the system is decreasing. Anode position is clearly a critical variable because of the effect of position on the distribution of current relative to the ground surface. In essence, the plane of symmetry of the potential distribution rotates with the anode position. As the anode moves from the top to the bottom, only fringe currents reach the ground surface. Total current increases as anode area increases, consequently the current flow and potential drops along the ground surface increase. Soil resistivity and pipe diameter have less of an effect on surface potentials. Soil resistivity, within the resolution of the model, does not affect the measured surface potential; however, corrosion current decreases as the soil resistivity increases. In the simple "conductor" model, increases in resistance are balanced by decreases in current with no net effect on voltage. As soil resistance increases due to drying, the corrosion rate may decrease in a nonlinear manner due to lack of moisture at the anode surface. (Currents at the cathode will go through a maximum due to increased diffusion of oxygen through the partially saturated concrete or mortar.) However, too dry a soil can create measurement difficulties in establishing stable ionic (electrical) continuity between the reference electrodes and the soil. As the pipe diameter increases, for a constant soil cover, the peak surface potential increases. In reality, larger pipe tend to be buried deeper and the effects of greater soil cover will dominate.

In this analysis, the impact of anode and cathodic reaction rates, and the impact of stray currents on the measurement have not been considered. Electrode reaction rates were lumped together as a voltage loss which lowers the driving force of the galvanic cell. Impact of electrode reactions then has a linear effect on the surface potentials measured. The effect of diffusion limitations on the cathodic current distribution were also not included in the model, since cathodic currents were found to be on the order of  $10 \mu\text{A}/\text{cm}^2$  in a limited region immediately around the anode.

## CONCLUSIONS

The results demonstrate the physical basis of surface potential measurement techniques. With a "relatively" simple numerical model, the effect of pipe geometry, corrosion cell size and position, and pipe environment (soil resistance) on surface potentials arising from galvanic cells has been demonstrated.

Surface potential measurements do not provide a definitive picture of the corrosion rate or corrosion cell dimensions, but rather serve as an indicator of corrosion activity. Asymmetry in the surface potential distribution, lateral and across the pipe centerline measurements, can be used as an indicator of anode position. Model results as presented here help in defining the limits of detection for a given pipe application.

### Next Steps

Validity of the model should be checked by further comparison with pipeline measurements. Installation of larger artificial anodes on an experimental line such as that used in the ACPA experiment would allow the design of controlled experiments. Otherwise, comparison with actual field measurements on working pipelines in which excavations have been performed to repair or inspect suspected areas of corrosion would provide confirmation of the model.

Improvements to the model, such as inclusion of nonlinear boundary conditions (electrode kinetics and diffusion), would eliminate the need to assume a driving force

for the galvanic cell. Inclusion of electrode reaction rate modeling complicates the model additionally by introducing parameters such as concrete pH, chloride concentrations, and permeability of the concrete or mortar to oxygen. Increasing model complexity allows more fundamental questions to be answered, but lessens its utility as a field tool.

The computer model developed for this study could be formulated to run on the more powerful personal computers now available. The 3-D model was run on a desktop workstation and is not currently practical for field use. A portable version would allow the field engineer to test scenarios which might fit the measured potential profiles. In those areas of interest, more detailed potential measurements could then be performed to confirm the model and locate the active areas while the measurement crew is on-site. With excavation costs on the order of \$1,000 per hole, any techniques that improve the accuracy of excavation location or reduce unnecessary holes will be financially beneficial.

### ACKNOWLEDGEMENTS

The authors would like to thank the management of Ameron for funding this analysis and the management of Arthur D. Little for supporting the preparation and presentation of this paper.

### REFERENCES

- [1] Massachusetts Water Resources Authority, "Request for Proposals for Hultman Aqueduct Risk Analysis and Repair Design," Boston, MA (8/30/94).
- [2] Gouda, V. K. and Mourad, H. M., "Galvanic Cells Encountered in the Corrosion of Steel Reinforcement, Part 1," Corrosion Science, Vol. 14, (11-12), Dec 1974, pp 681-690.
- [3] Gouda, V. K. and Mourad, H. M., "Galvanic Cells Encountered in the Corrosion of Steel Reinforcement, Part 2," Corrosion Science, Vol. 15, (5), May 1975, pp 307-315.
- [4] Gouda, V. K. and Mourad, H. M., "Galvanic Cells Encountered in the Corrosion of Steel Reinforcement, Part 3," Corrosion Science, Vol. 15, (5), May 1975, pp 317-328.
- [5] Gouda, V. K. and Mourad, H. M., "Galvanic Cells Encountered in the Corrosion of Steel Reinforcement, Part 4," Corrosion Science, Vol. 15, (5), May 1975, pp 329-336.
- [6] Hall, S.C. "Analysis of Monitoring Techniques for Prestressed Concrete Cylinder Pipe", Paper #510, Corrosion '94, National Association of Corrosion Engineers, Houston, TX.

# **Corrosion Rate Measurements**

John P. Broomfield<sup>1</sup>

**Field Measurement of the Corrosion Rate of Steel in Concrete using a Microprocessor Controlled Unit with a Monitored Guard Ring for Signal Confinement**

---

**REFERENCE:** Broomfield, J. P., "Field Measurement of the Corrosion Rate of Steel in Concrete Using a Microprocessor Controlled Unit with a Monitored Guard Ring for Signal Confinement," Techniques to Assess the Corrosion Activity of Steel Reinforced Concrete Structures, ASTM STP 1276, Neal S. Berke, Edward Escalante, Charles K. Nmai, and David Whiting, Eds., American Society for Testing and Materials, 1996.

**ABSTRACT:** The principle of corrosion rate measurement by the linear polarisation resistance method is simple. The equipment measures the half cell potential, applies a small current and measures the change in potential. The corrosion rate is proportional to the applied current divided by the potential shift.

Using the technique in the field on reinforced concrete structures is complicated because the area of measurement must be defined and readings fluctuate with the weather conditions.

This paper describes the use of a corrosion rate device in Europe and the USA on bridges, buildings and other structures. Its application for measuring the effectiveness of chloride removal and other rehabilitation techniques is discussed.

**KEYWORDS:** Chloride removal, linear polarisation, corrosion rate measurement, half cell potentials, bridges

---

Corrosion of steel in concrete is a major problem worldwide. A recent estimate in the USA showed that \$200 to \$500 million a year is spent on corrosion proofing and corrosion repair of reinforced concrete bridges and car parking structures against deicing salt induced corrosion [1].

Corrosion of steel in concrete is caused by the breakdown of the natural passivity established when reinforcing steel is surrounded by the highly alkaline pore

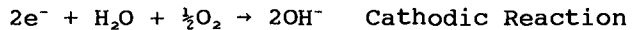
---

<sup>1</sup>Corrosion Consultant, 78 Durham Road, London SW20 OTL, UK

water of the cement matrix. This breakdown is due to either carbonation, or chloride attack.

Carbonation is the result of the reaction between atmospheric carbon dioxide and the pore water. The  $\text{CO}_2$  dissolves in the pore water and forms carbonic acid. This reacts with the alkali and reduces the pH to a level where the passive layer is no longer sustained. Chloride attack is a direct attack upon the passive layer. When the chloride to hydroxyl ratio exceeds 0.7, chloride ions will break down the passive layer and cause corrosion.

The actual corrosion process is electrochemical. At the anode iron dissolves in the pore water forming ferrous ions and liberating electrons, which travel through the reinforcing steel to the cathode where they react with water and oxygen to form hydroxyl ions.



The ferrous ions then go on to react further with oxygen and water to form solid corrosion products (rust).

Corrosion products have a larger volume than the original steel. This leads to the build up of internal stresses and subsequent cracking and spalling of the concrete. The corrosion also decreases the steel cross section. Consequently the load bearing capacity of corrosion damaged structures and their remaining service life is reduced.

#### **CORROSION RATE MEASUREMENT, LINEAR POLARISATION**

There is no single method for accurately measuring corrosion damage. The measurement of half cell potentials is a rapid method of defining areas of corrosion (Fig. 1). It measures the electrochemical potential difference between anodic and cathodic areas by comparison with a standard reference cell. However, the half cell cannot be used to measure the rate of corrosion. It is used to plot isopotential maps that show the most anodic areas of steel. These are the areas most likely to be corroding. Other methods such as hammer sounding, radar or ultrasonic techniques may locate damage, but will not show the rate of deterioration. Cover depth, carbonation depth and chloride content on the concrete will also show areas susceptible to attack but no direct correlation has been found between any of these factors and the amount of corrosion damage.

There are several methods of measuring the true, instantaneous rate of corrosion. Many of these are electrochemical methods. They rely on measuring changes in the half cell potential as it is perturbed, and use electrochemical theory to calculate the corrosion current and hence the rate of corrosion.

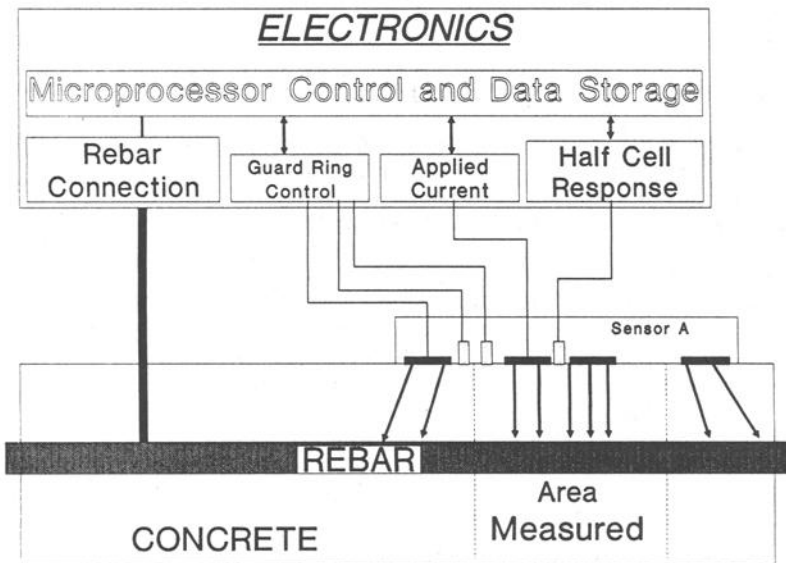
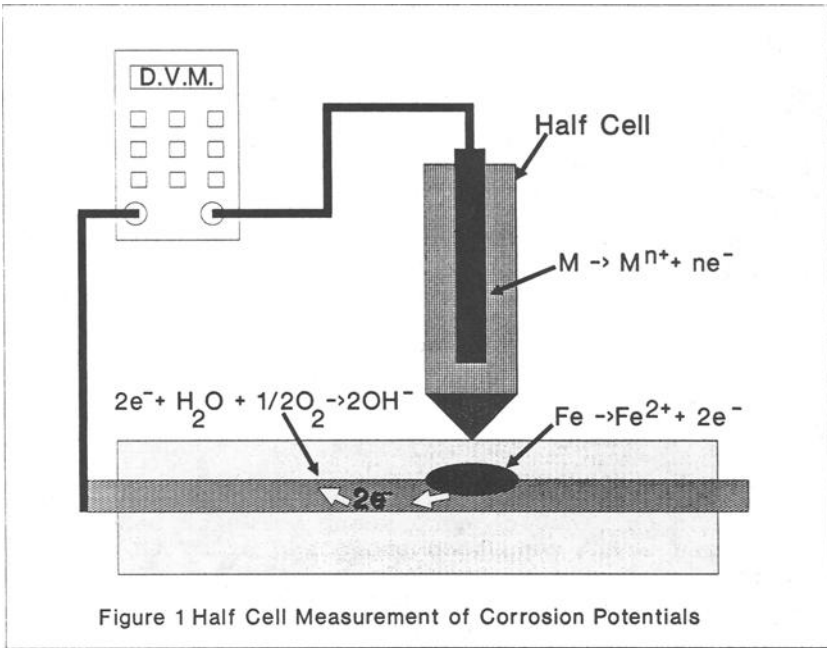


Figure 2 Schematic of Corrosion Rate Device Showing Sensor A

The linear polarisation device applies a small electrical current  $\delta I$  and measures the shift in potential  $\delta E$ . The ratio  $\delta E/\delta I$  is called the polarization resistance  $R_p$ . The polarisation resistance is inversely proportional to the corrosion current  $I_{corr}$ .

$$I_{corr} = B/R_p$$

$$R_p = \delta E/\delta I$$

A linear polarisation device therefore has a half cell to measure the corrosion potential  $E_{corr}$  and the potential shift  $\delta E$ , and a method to apply the electric current  $\delta I$ .  $I_{corr}$  is directly related to the corrosion rate by Faraday's Law which shows that a constant corrosion current of  $1\mu A.cm^{-2} = 11.5\mu m$  steel section loss per year.

The constant B can be measured as it is a function of the Tafel constants of the anodic and cathodic reactions. However this can vary with the amount of anodic and cathodic activity. In this device a constant value of  $B=26mV$  is assigned. As B can vary between 26 and 52 mV this can give some error.

#### GUARD RING CONFINEMENT

The linear polarisation technique is frequently applied to small specimens of known area. When applying it to a network of reinforcing steel we want to make a local measurement and define that locality. The corrosion current  $I_{corr}$  must be associated with a known area to convert to a sensible corrosion rate.

One way of doing this is to use a guard ring. As the current  $\delta I$  is applied from an auxiliary electrode, a concentric guard ring passes a "confining" current that ensures that the current passes into a known area and the change in potential  $\delta E$  is due to that known current passing into a known area.

Most guard rings pass a level of current based on the geometry required to confine the current. This leads to errors when there is high resistivity concrete, variations in potential and activity along the rebar or deep cover.

#### THE GECOR DEVICE

A schematic of the linear polarisation device is shown in Figure 2. It has a control box and logger that applies the current and takes and records the measurements. There are two sensors. Sensor A, shown in the figure, is used to measure  $E_{corr}$  and  $I_{corr}$ . Sensor B (Figure 3) measures concrete resistivity, temperature and relative humidity. The complete system weighs about 5kg and is battery operated.

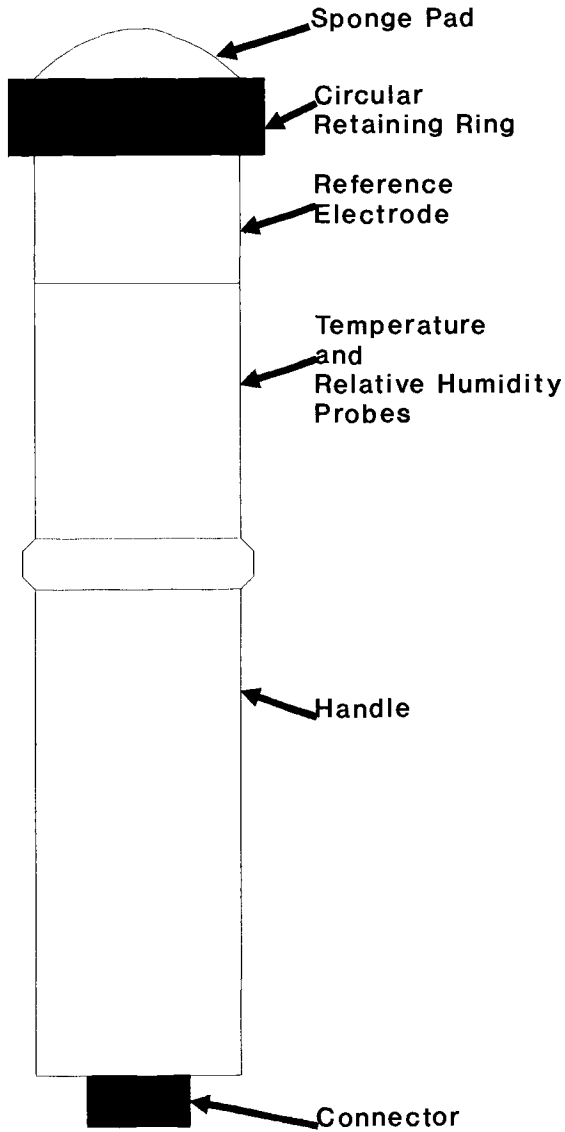


**Figure 3 Schematic of "Sensor B"**

The logger stores 100 sets of readings ( $E_{\text{corr}}$ ,  $I_{\text{corr}}$ ,  $T$  ( $^{\circ}\text{C}$ ) R.H.(%),  $R$  ( $\Omega$ )). The  $I_{\text{corr}}$  reading takes between 2 and 5 minutes, and the hand held sensor A is rapidly moved from location to location for each measurement. A description of the device and its application can be found in [2].

### THE SENSOR CONTROLLED GUARD RING

The device is unique in its ability to accurately confine the area of measurement by using a sensor controlled guard ring. This means that corrosion rate measurements are not carried out over an undefined area, but show the true corrosion rate at the place of measurement [2]. The use of extra half cells within the guard ring ensure that the electric field lines are parallel. Therefore the area measured is precisely the area of steel underneath the 105mm. diameter electrode (Figure 2). This means that the corrosion rate is measured as a current density ( $\mu\text{A}/\text{cm}^2$ ). This can be converted into metal loss by Faraday's law.

The sensor control means that the influence of high resistivity concrete, variation of corrosion rate along the rebar and deep cover are minimised compared to a conventional guard ring.

### CORROSION RATE MEASUREMENT

The system is set up with an electrical connection to the rebar cage and the sensor mounted on the concrete surface with a damp sponge ensuring electrical (ionic) contact. The area of steel beneath the 105mm. diameter electrode must be known, but there are no requirements to mount it over single bars, cross overs or any pre-defined rebar geometry. Measurements can be taken over narrow elements or at corners as long as the sensor electrodes are in contact with the concrete and the area of metal surface is known.

A menu driven system guides the operator through the set up procedure including the entering of the steel surface area. The system will then automatically check for stability of readings, and then automatically calculate  $I_{\text{corr}}$  from the polarisation resistance measurement. This can then be stored with  $E_{\text{corr}}$ . The resistivity, and ambient temperature and relative humidity can also be stored for that location.

It should be noted that the measurement is an instantaneous one (compared with the life of the structure). Any attempt to extrapolate the measurement backward, to estimate steel section loss, or forwards, to predict damage rate, must be done with caution. At the moment there are insufficient data to do this with confidence. However, as the number of structures surveyed increases it should be possible to improve our predictive ability as the variation

of corrosion rate with temperature, relative humidity and with time are more accurately known.

The following broad criteria for corrosion have been developed from field and laboratory investigations with the device

$I_{corr} < 0.1\mu\text{A}\cdot\text{cm}^{-2}$	Passive condition
$I_{corr} 0.1 \text{ to } 0.5\mu\text{A}\cdot\text{cm}^{-2}$	Low Corrosion
$I_{corr} 0.5 \text{ to } 1\mu\text{A}\cdot\text{cm}^{-2}$	Moderate Corrosion
$I_{corr} > 1\mu\text{A}\cdot\text{cm}^{-2}$	High Corrosion Rate

Cracking can occur at 10-100 $\mu\text{m}$ /year depending on geometry, concrete quality, oxygen access (to turn the dissolved iron into a solid corrosion product). This correlates with the transition from moderate to high corrosion given above. In a BRITE/EURAM project [3], Geocisa and Instituto Eduardo Torroja found that cracking due to corrosion occurs when the section loss is in the region 10-30 $\mu\text{m}$  for cover/rebar diameter ratios of 1 to 3.

The interpretation above assumes uniform corrosion. In the case of localized pitting, corrosion rates can be 5-10 times the general corrosion rate [3]

Corrosion rate measurements are affected by temperature and R.H., so the conditions of measurement will affect the interpretation and the limits defined above. The measurements should be accurate to within a factor of two given the variability in the constant "B" discussed above.

## RESISTIVITY, RELATIVE HUMIDITY AND TEMPERATURE MEASUREMENT

### Resistivity

Resistivity is measured by an equation that relates a small electrode to an infinite plane electrode through a medium of resistivity R, where:

$$R = 2 \cdot R_{iR} \cdot D$$

where R = resistivity in  $\text{K}\Omega\cdot\text{cm}$   
 $R_{iR}$  = resistance between rebar network and electrode measured by the iR drop method  
 D = Diameter of electrode

Researchers working with the device in the laboratory [3] have found that when the resistivity is greater than 100 to 200 $\text{k}\Omega\cdot\text{cm}$  you cannot distinguish between active and passive steel and corrosion rate measurement is unnecessary as the rate is so low.

Temperature

Temperature affects corrosion rate directly, as the rate of the oxidation reaction is affected by the amount of heat energy available to drive the reaction. The temperature also affects it indirectly as the concrete resistivity decreases with increased temperature at a constant moisture content. It also affects the relative humidity in the concrete and the mobility of the ions in the pore water. Gowers et al. [4] recently published results showing a strong inverse relationship between temperature and the log of resistivity.

At low temperatures the pore water will freeze and corrosion stops as the ions can no longer move. It should be noted that this will happen well below ambient freezing point as the ions in the pore water depress the freezing point well below 0°C.

One important consequence of this is that corrosion rate measurements can only be directly compared when the measurements are taken at consistent temperatures. One cannot directly compare corrosion rates measured in mid summer with those taken in mid winter if resurveying a structure.

There is no simple calibration available to offset results to allow for temperature. The "B" sensor will measure and record the ambient temperature alongside corrosion rate readings. This can be used to check that repeat measurements are either taken in comparable conditions or that allowances are made for different temperatures.

Relative Humidity

The relative humidity will be a factor in determining how much water there is in the pores to enable the corrosion reaction to be sustained. Chloride induced corrosion is believed to be at a maximum when the RH within the concrete is around 60% [5]. For carbonation there is experimental evidence that the peak is around 95-100% RH [5]. However it is important to recognize that the RH in the pores is not simply related to the atmospheric RH, due to water splash, run off or capillary action, formation of dew, solar heat gain or other factors. Gowers [4] found a weak correlation between ambient RH and resistivity of the concrete.

It should be noted that total desiccation will stop corrosion through moisture starvation while total saturation will stop corrosion through oxygen starvation. A highly saturated structure can corrode rapidly without signs of cracking, as the ferrous ions stay in solution without forming the solid rust that expands and cracks the concrete. A totally saturated structure can reach a very high negative half cell potential (-900mV) without corroding due to oxygen starvation. However, if oxygen then does get access to the steel the corrosion rate will be very high as the steel will have no passive oxide layer to protect it.

The "B" sensor will record ambient relative humidity

and temperature alongside corrosion rate readings. This can be used to check that repeat measurements are either taken in comparable conditions or that allowances are made for different relative humidities and temperatures.

## FIELD MEASUREMENTS

Over 20 structures in USA, Europe & UK have been investigated by several operators of GECOR devices for instance [6 to 10]. The investigations cover both carbonation and chloride induced corrosion. Figure 4 shows the comparison between  $I_{\text{corr}}$  values of carbonation induced and chloride induced corrosion. It can be seen that the  $I_{\text{corr}}$  values are lower for carbonation. For the carbonated structures shown here  $I_{\text{corr}}$  never exceeded  $0.5\mu\text{A}/\text{cm}^2$  (although one or two measurements made more recently show corrosion rates up to  $1\mu\text{A}/\text{cm}^2$ ). This compares with 20% of readings exceeding this value for chloride infested structures and almost 10% greater than  $1.0\mu\text{A}/\text{cm}^2$ .

### Corrosion rates on a corroding bridge and after chloride removal

The Tees Viaduct in northern England is an 18 year old structure with a substructure of reinforced cross heads supported on columns. The deck slabs are supported at expansion joints. Leaking joints have allowed deicing salts to penetrate the cross heads. The rate of ingress appears to have been exacerbated by a porous aggregate that has allowed very rapid build up of chloride (up to 5% chloride by weight of cement) at rebar depth.

The severity of corrosion has lead to extensive rehabilitation. The deck has been repaired, joints sealed and water conducted away from the substructure. The substructure has been surveyed visually and by potential, cover and chloride measurements.

The extent of corrosion is variable. The piers had been ranked by visual inspection into three main groups, ten needing replacement, 37 in need of repair, and the remainder in need of monitoring. Some of the cross heads have now been demolished. Investigation of one pier included the taking of cover measurements, chloride contents and half cell potentials. After demolition the concrete was removed and metal loss measurements made. There was an attempt to correlate the before and after measurements but it is not considered that they could be used for predicting the metal loss of other piers. It was found that the metal loss was less than anticipated despite severe cracking and delamination of the concrete.

On a second pier 26 corrosion rate measurements were taken prior to demolition and damage measurement on the steel. The work was undertaken with an earlier prototype of the Sensor A which required fastening to the beam surface by drilling. This slowed the measurement process, which meant

# DISTRIBUTION OF I<sub>corr</sub> VALUES

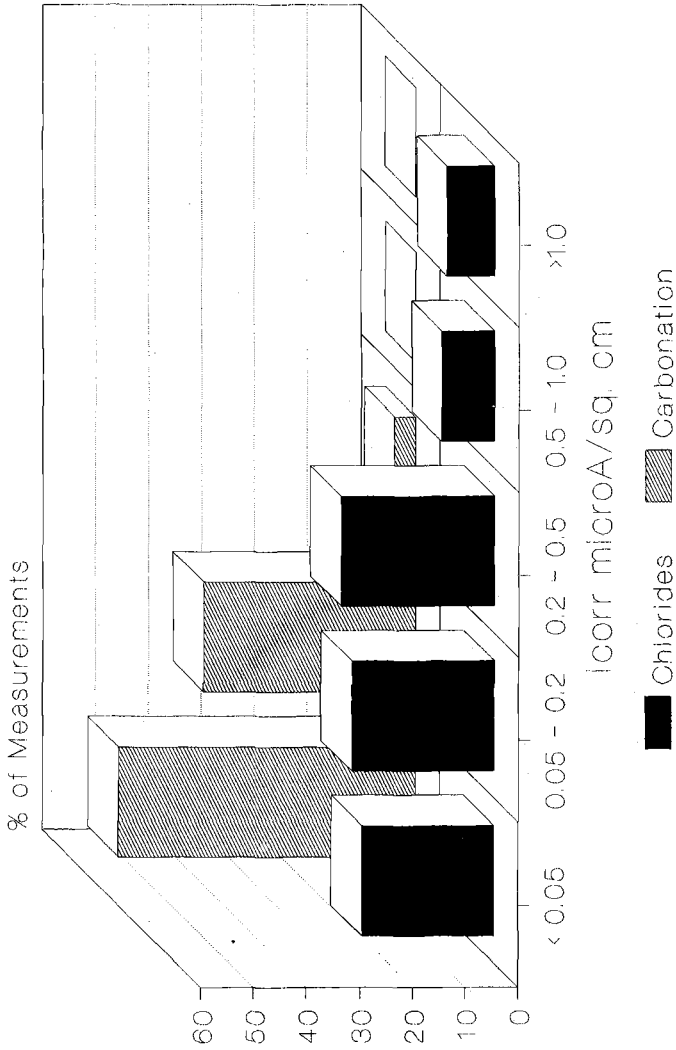


Figure 4 Comparison of Rates due to Chlorides & Carbonation

# Section Loss Versus Icorr Tees Viaduct Bent S11

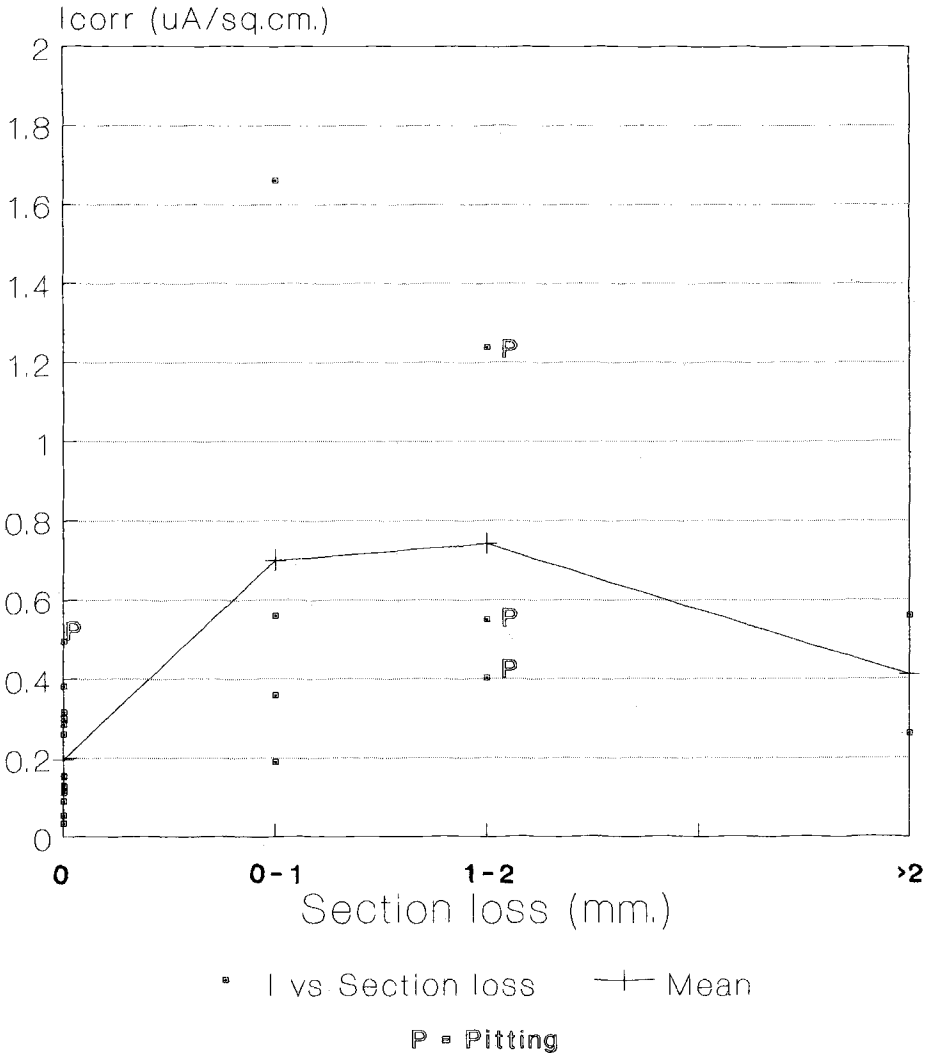


Figure 5 Corrosion Rate versus Section Loss Measurements

that only 26 readings were collected in about 12 hours work on site. Far more readings would now be possible.

It is not possible to correlate exactly the position of the measurement after extraction of the steel, however, Figure 5 shows a plot of  $I_{\text{corr}}$  vs. section loss in mm. on the steel measured after demolition. The figure shows that the highest corrosion rates were at areas of pitting rather than at the areas with greatest section loss. The developers of the device have found corrosion rates five to ten times higher in pits than in uniformly corroding areas. However, this is a very local rate.

This illustrates the problem of simply extrapolating a single corrosion rate measurement to estimate section loss. Repeated surveys with time will give a clear indication of the development of corrosion and enough points to extrapolate the section loss with time. The limited set of measurements taken in this survey reduces the ability to estimate section loss.

#### After Chloride Removal

A section from the centre of one of the demolished cross heads was cut out and taken to a site in Glasgow for the application of a chloride removal trial [10]. After treatment the block remained indoors in an unheated environment. About one year later corrosion rate measurements were taken on the block. These were compared with the results taken from the cross head discussed above. Table 1 summarises the comparison.

Since corrosion rate measurements were not taken on the block before chloride extraction, a direct comparison is not possible. However, corrosion rate measurements were taken on another cross head so some comparison could be made, assuming that the two cross heads were in similar corrosion conditions. "Before and after" half cell surveys were carried out on the block and on the untreated block. Table 1 shows that the untreated crosshead and the block before treatment had very similar half cell readings, supporting the validity of a comparison.

Table 1 shows that the half cell potentials showed a rise from a mean of -331mV (CSE) before treatment to -115mV a month after treatment, -69mV after 2 months and -162mV about 11 months later. The mean corrosion rate on the beam on Tees without chloride removal was  $0.375\mu\text{A.cm}^{-2}$ . One year after treatment the corrosion rate on the other beam was  $0.00283\mu\text{A.cm}^{-2}$ . This is a reduction in mean corrosion rate of a factor of 132.

There are two limitations on this interpretation of the effects of chloride removal:

- 1) We do not know the actual rate of corrosion of the beam tested for chloride removal but believe the two beams to be comparable as the half cell potential data indicate.

**TABLE 1**  
**Summary of Half Cell ( $E_{\text{Coxx}}$ )**  
**and Corrosion Rate ( $I_{\text{Coxx}}$ ) data**  
**From S11 on site and treated Glasgow block**

Tees Viaduct		Glasgow					
S11		1/11/91	25/2/92	4/3/92	14/12/93 (After)		
$E_{\text{Coxx}}$ (mV)	$I_{\text{Coxx}}$ $\mu\text{A}\cdot\text{cm}^{-2}$	Before $E_{\text{Coxx}}$ (mV)	$E_{\text{Coxx}}$ (mV)	$E_{\text{Coxx}}$ (mV)	$E_{\text{Coxx}}$ (mV)*	$I_{\text{Coxx}}$ $\mu\text{A}\cdot\text{cm}^{-2}$	
Mean	-373	-331	-115	-69	-162	0.00283	
Max	-545	-571	-333	-210	-273	0.125 (0.094)**	
Min	-110	-94	-17	6	-155	0.0005***	
No.	30	55	66	70	61	10	

\*Converted from a Ag/AgCl cell reading to copper/copper sulphate by adding (-)100mV (Ag/AgCl calibrated to saturated calomel range (SCE)).

\*\*Larger reading incorrect due to lack of signal confinement by GECOR 6

\*\*\*Many readings were impossible due to high resistance and low corrosion rate. This was the lowest recordable reading.

- 2) The treated beam was kept indoors and therefore not exposed to direct moisture ingress, nor any further salt ingress (although none of the substructure should receive further salting after sealing the joints).

The beam has now been moved back to the Tees Viaduct site and will be tested at regular intervals to monitor the corrosion rates.

The sensitivity of the device at low corrosion rates was important in this investigation as it allowed a true assessment of the corrosion rate after chloride removal.

### CONCLUSIONS

1. A corrosion rate device has been developed that measures the corrosion rate over a defined area of steel embedded in concrete.
2. The device has been applied to over 20 structures in USA, Europe & UK which have been investigated by a number of operators of GECOR devices.
3. For carbonated structures  $I_{corr}$  rarely exceeded  $0.5\mu\text{A}/\text{cm}^2$ . This compares with 20% of readings exceeding this value for chloride contaminated structures and almost 10% greater than  $1.0\mu\text{A}/\text{cm}^2$ . However, the amount of corrosion damage on carbonated structures shows that despite the lower corrosion rate carbonation will still lead to significant deterioration.
4. In a survey on the Tees Viaduct in the UK it was found that corrosion rates are highest in areas of pitting compared with areas of generalized corrosion. Corrosion rates in pitted areas are 5 to 10 times those in areas of generalised corrosion.
5. A comparison of corrosion rates on a crosshead exposed to deicing salt ingress and a comparable section of crosshead 12 months after chloride removal treatment showed a reduction of mean corrosion rate by a factor of 132. However, this was not a direct comparison as the "before and after" measurements were not taken on the same specimen. They were comparisons of corrosion rates on the treated block against corrosion rates on a crosshead in service with similar "before treatment" half cell potentials. Also the treated block had been stored indoors after treatment.

## ACKNOWLEDGEMENTS

The author is grateful J Rodríguez (Geocisa, Spain) for his help in preparing this paper. The GECOR 6 device was developed by Geocisa in collaboration with CENIM (S. Feliú and J.A. González) ICCET (C. Andrade).

## REFERENCES

- [1] National Research Council - Transportation Research Board. "Highway Deicing - Comparing Salt and Calcium Magnesium Acetate." Special Report 235, Washington DC 1991.
- [2] Feliú S., González, J.A., Feliú D. Jr., and Andrade, C. "Confinement of the electrical signal for in situ measurement of polarization resistance in reinforced concrete structures" ACI Materials Journal Sept/Oct. 1990 pp. 457-460.
- [3] Rodríguez, J., Ortega, L.M., García, A.M., Johansson, L., Peterson, K. "On site corrosion rate measurements in concrete structures using a device developed under Eureka Project EU-401" Proc. of International Conf. on Concrete Across Borders Vol. 1, Odense, Denmark, June 1994 pp. 171-185.
- [4] Gowers, K.R.; Millard, S.G.; Bungey, J.H. "The Influence of Environmental conditions upon the measurement of concrete resistivity for the assessment of corrosion durability" Proc. Non-Destructive Testing in Civil Engineering, Ed. J.H. Bungey, Liverpool April 1993, Vol 2. pp 551-566.
- [5] Tuutti, K.; "Corrosion of Steel in Concrete". Publ. Swedish Cement & Concrete Research Institute, Stockholm. 1982.
- [6] Fliz, J.; Sehgal, A.; Li, D.; Kho, Y-T; Pickering, H.; Osseo-Asare K.; Cady P.D. Condition Evaluation of Concrete Bridges Relative to Reinforcement Corrosion - Volume 2: Method for Measuring the Corrosion Rate of Reinforcing Steel; 1992.
- [7] Andrade, C., Alonso, C., Ortega, L.M., García, A.M. "On-site monitoring of concrete repairs by polarization resistance" Proceedings of International RILEM/CSIRO/ACRA Conference on Rehabilitation of Concrete Structures, Melbourne, Australia, September 1992 pp 51-60.

- [8] Broomfield, J.P. Rodríguez, J., Ortega, L.M. and García, A.M. "Corrosion Rate Measurements in Reinforced Concrete Structures by a Linear Polarization Device," Concrete Bridges in Aggressive Environments, Philip D. Cady International Symposium Ed. Richard E. Weyers, Publ. ACI SP-152 1994, pp 163-181.
- [9] Rodríguez J., Ortega, L.M., Garcia A.M. "Assessment of structural elements with corroded reinforcement" Proceedings of International Conference on Corrosion and protection of Steel in Concrete" Sheffield U.K. July 1994. pp. 171-185.
- [10] Buenfeld, N.R. and Broomfield, J.P. "Effect of Chloride Removal on Rebar Bond Strength and Concrete Properties" in "Corrosion and Corrosion Protection of Steel in Concrete, Ed. R.N. Swamy, Publ. Sheffield Academic Press, UK 1994, pp 1438-1460.

## **ELECTROCHEMICAL METHODS FOR ON-SITE DETERMINATIONS OF CORROSION RATES OF REBARS**

---

**REFERENCE:** Feliú, S., González, J. A., and Andrade, C., “**Electrochemical Methods for On-Site Determinations of Corrosion Rates of Rebars,**” Techniques to Assess the Corrosion Activity of Steel Reinforced Concrete Structures, ASTM STP 1276, Neal S. Berke, Edward Escalante, Charles K. Nmai, and David Whiting, Eds., American Society for Testing and Materials, 1996.

**ABSTRACT:** A review on the available electrochemical methods is presented for the on-site determination of rebar corrosion rate. In real size structures the methods available at present may be classified in three groups: A) Confinement of the applied electrical signal, B) Measurement of the lateral spreading of the electrical signal and C) Minimization of this lateral spreading. From these three alternatives, the first one has been implemented in a device that is now currently used for on-site measurements. This device is based in a "controlled" guard ring. In real size structures, the normal values of corrosion rates recorded are of the same order of magnitude of those previously measured in laboratory experiments. The levels are classified in: negligible, low, moderate and high.

The gaps in the knowledge which still need to be investigated are also, commented: 1) unconfined measurements, 2) effect of counterelectrode size, 3) the true meaning of the corrosion rate measured, 4) constant B value, 5) current distribution around rebar perimeter 6) relation between mean corrosion rate and maximum pit depth and 7) identification of local corrosion. Finally, the role of embedded sensors on the monitoring of rebar corrosion risk, is mentioned.

**KEYWORDS:** rebar, corrosion, measurements, electrochemical, methods, on-site.

---

<sup>1</sup> Professor, Centro Nacional de Investigaciones Metalúrgicas, CSIC, Gregorio del Amo, 8, 28040 Madrid, Spain.

<sup>2</sup> Professor, Institute of Construction Science "Eduardo Torroja", CSIC, Serrano Galvache, sn., 28033 Madrid, Spain.

The measurement of  $E_{corr}$  (Rest or Corrosion Potential) is the method most frequently used in field determinations because of its simplicity. From these measurements, potential maps are drawn which reveal those zones that are most likely to undergo corrosion in the active state (ASTM C876-91. Standard Test Method for Half Cell Potentials of Uncoated Reinforcing Steel in Concrete). However, such measurements have a rather qualitative character which may make data difficult to be interpreted [1,2]. Figure 1 shows that corrosion potential is a poor indicator of corrosion activity.

The application of quantitative electrochemical methods to real structures in the field is hindered by a number of factors, most of which arise from the fact that the applied electric signal decreases gradually from the auxiliary counter electrode (CE) [3,4]. Most of the laboratory methods for measuring  $I_{corr}$  entail a prior measurement of the  $\Delta E/\Delta I$  ratio, with  $\Delta E$  being a small potential perturbation on the freely corroding reinforcement and  $\Delta I$  the recorded current per unit area of electrode surface. Provided the electric signal spreads uniformly throughout the working electrode (WE), the  $\Delta E/\Delta I$  ratio defines the polarization resistance ( $R_p$ ) which is required for calculating the corrosion rate, from the well-known Stern-Geary equation [5].

$R_p$  laboratory measurements with small specimens provide a simple method for obtaining a quantitative index for concrete deterioration because a uniform distribution of current is reached. Kinetic estimations are obtained from using either  $R_p$  values, measured under small DC polarization or  $R_T$  ones obtained from Electrochemical Impedance Spectroscopy (EIS) [6]. This last technique has proved to be a powerful tool for investigating corrosion mechanisms, although it requires more expensive instrumentation and larger measurement times than DC measurements, particularly with small corrosion rates, which call for very low frequencies [7].

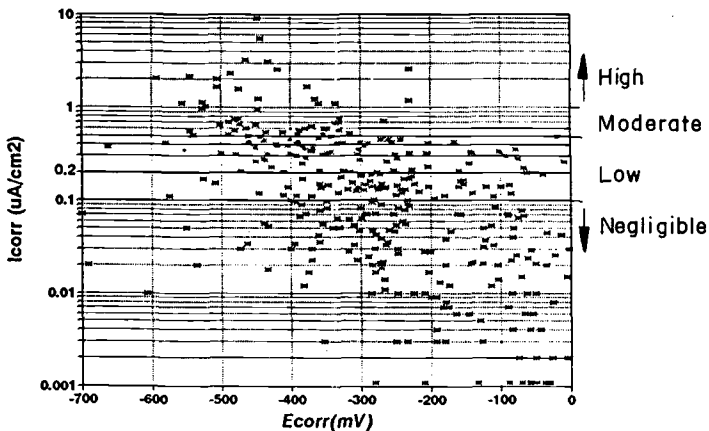


FIG. 1. Plot of data from on-site measurements from many of real structures. Scatter of points shows that  $E_{corr}$  is not an accurate indicator of reinforcement corrosion rate ( $I_{corr}$ ).

### Possibilities of Corrosion Rate on-site measurements

Direct estimations of true  $R_p$  values from  $\Delta E/\Delta I$  ratio are usually unfeasible in large structures, where the applied electric signal tends to decrease with increasing distance from the CE rather than spread uniformly across the WE. Therefore, the action of the electric signal cannot be related to any specific WE (working electrode) zone. Hence,  $\Delta E/\Delta I$  measurements on large structures by use of a small CE provide an apparent polarization resistance ( $R_p^{app}$ ) that differs from the true  $R_p$  value depending on the experimental conditions [3,4].

If the metal is actively corroding and  $R_p$  is low, the current applied from a small CE located in the concrete surface is drained very efficiently by the rebars and it tends to confine itself on a small surface area. Conversely, if the metal is passive and  $R_p$  is high, the current applied tends to spread far away (e.g., around 50 cm) from the application point. Therefore, almost any electrochemical method may provide reliable corrosion rates for actively corroding reinforcement, and all of them pose some difficulties in estimating the typically very low corrosion rates of passive reinforcement.

Methods to determine  $R_p$  in large structures of reinforced concrete can be classified in three groups:

- A. Confinement of the applied electrical signal.
- B. Measurement or estimation of the lateral spreading of the electric signal.
- C. Minimization of the effect of the lateral spreading of the electric signal.

Examples of type A methods are (i) the potentiostatic guard ring and (ii) the sensorized galvanostatic guard ring [8]. Among methods B, mention will be made to those resulting from application of transmission line models [3,4]. Finally, the use of counter electrodes of very large size, or of increasing size to extrapolate the results to infinite size (9,10), belong to method C.

One of the most widely adopted solutions to limit the current lines from the CE to the WE is the guard ring, whereby attenuation of the applied signal is minimized by using a ring shaped CE, surrounding the main electrode (Fig. 2). This way, the current field lines that originate from the latter are confined within a known area of the reinforcement.

However, accomplishing efficient confinement may be difficult [11,12]. A new possibility using the principle of the guard ring has been published by the authors [8]. The method used a galvanostatic pulse and the confinement of the signal is followed by two "extra" reference electrodes, located between central and guard counter (Fig. 3).

It is also possible to obtain rapid information on reinforcement corrosion rate by applying potentiostatic or galvanostatic short pulses [2,13]. However, this information may be not very reliable with passive reinforcements, and these procedures call for further investigation to solve the field work problems posed by the uneven distribution of the current between the small CE placed at the concrete surface and reinforcements.

Only qualitative information can be obtained from these pulses up the moment.

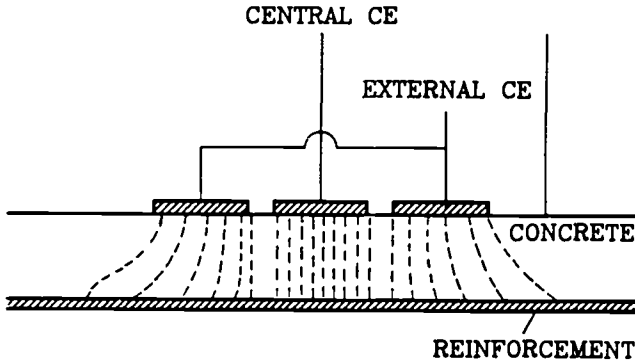


FIG. 2. Confinement of current lines from central counter electrode due to the action of external counter electrode.

Considering the value of  $\Delta E/\Delta I$  without any mathematical correction will give erroneous values of the corrosion rate. Despite this, it is used in some of the techniques now available for the on-site measurements. If the corrosion is generalized, better estimation of  $I_{corr}$  is obtained by a) determining the "critical distance" over which the signal really propagates [3, 4] or b) by extrapolating the result obtained by using several counter electrodes of increasing sizes [9].

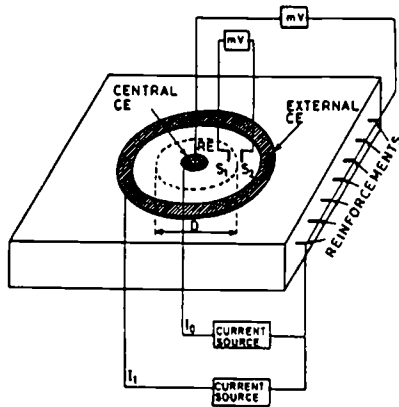


FIG. 3. Arrangement of electrodes in the sensorized confinement method.

**GAPS ON KNOWLEDGE AND RESEARCH NEEDS**

If a constant B value of 26 mV is used the maximum error expected in  $I_{corr}$  value is of a factor of two. Sources of higher errors are discussed below:

### Use of guard ring

In applying the guard ring technique to passive rebars the measurements may be adversely effected by the tendency of the electric signal to exceed the confinement area, mainly when the classical potentiostatic system is used [11]. It is essential to make sure that a good electric contact is obtained by all the points of the guard ring with the concrete surface. With the sensorized galvanostatic guard ring, the electric field from the central CE is equilibrated with that from the guard ring using two reference electrodes placed on the concrete surface. However, it may be not certain that the same balance is exactly kept at the rebar level (below the concrete cover). On the other side, measurements are sensitive to a lack of uniformity in the rebar-concrete properties (e.g., concrete moistening or rebars distribution). Obviously, all these problems can distort some measurements if a correct confinement is not achieved.

### Errors arising from unconfinement of the electrical signal

As has been mentioned  $R_p^{app}$  values measured under unconfined-signal conditions can differ considerably from  $R_p$  values obtained by using confined signals [10].  $R_p$  cannot be calculated directly by multiplying  $R_p^{app}$  by a given coefficient since such a coefficient would change with the experimental conditions (rebar activity, concrete electric resistivity, structure and reinforcements geometries, and concrete cover thickness). The lack of universality of the  $R_p/R_p^{app}$  ratio precludes the establishment of reliable correlations between data obtained with and without a guard ring (Fig. 4).

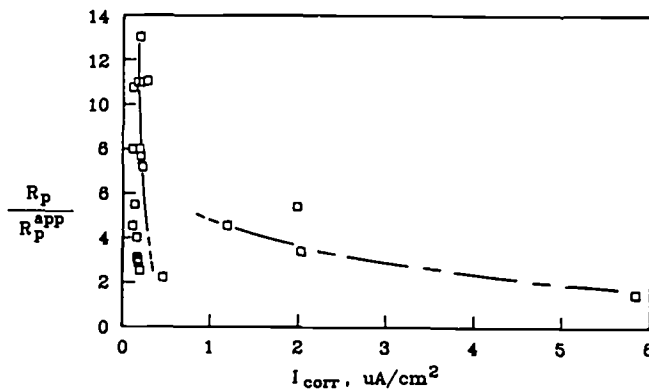


FIG. 4. Variation of the ratio of the true polarization resistance ( $R_p$  measured with confined signal) and the apparent polarization resistance ( $R_p^{app}$  measured without signal confinement) with the corrosion density,  $I_{corr}$ , as calculated from true  $R_p$ . CE size  $50\text{cm}^2$ .

Other procedures use equivalent circuits to model the behaviour of electric signals on reinforced concrete in order to derive equations that provide  $R_p$  from  $R_p^{app}$ .

The problem may lie then in the model selected, which may differ from the real system. The use of the transmission line is a rough approximation, not always appropriate depending on the system geometry.

**Effect of the CE size**

Even if a fairly large CE is used,  $R_p$  may be significantly different from  $R_p^{app}$ , and the apparent values obtained may be too small. For concrete slabs made of mortar containing no chloride, the error factor ( $R_p/R_p^{app}$ ) has been found to easily exceed 100, whereas for chloride containing slabs (actively corroding) were of about 10 or less [10]. The error factor depends not only on the CE size, but also on other variables, as rebar activity and concrete resistivity. Figure 5 obtained from the data of Ref. 11 shows this behaviour. A CE of medium size (500-1000cm<sup>2</sup>), which is fairly easy to handle, can provide  $R_p^{app}$  values with an error factor less than 2 for active rebars. On the contrary, in passive rebars the  $R_p^{app}$  values obtained may be considerably different from the true ones.

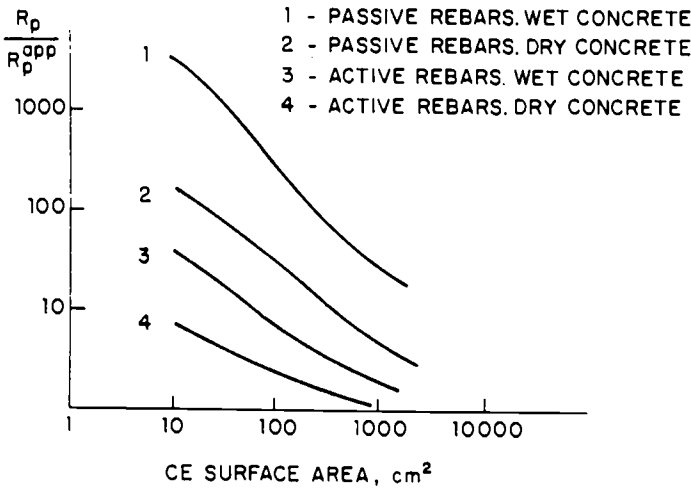


FIG 5. Variation of the error factor ( $R_p/R_p^{app}$ ) with CE surface area.

The inaccuracy in on-site  $R_p$  measurements cannot be overcome by simply using a large enough CE, since local corrosion areas or abrupt changes in corrosion activity along rebars could never be identified.

**Other questions affecting accuracy of measurements**

Besides the questions posed before, there are other sources of uncertainty for a precise determination of  $I_{corr}$  of rebar in concrete. Among them mention will be made of:

True meaning of the measured magnitude. The results of conventional  $R_p$  measurements in the laboratory or in the field will be dependent on the polarization time allowed before taking a reading or on the chosen frequency for A.C. measurements [14]. Despite the use of rather long polarization times (e.g., 15-30 s), only apparent  $R_p$  values may be obtained since the current response does not fully achieve the steady state [6,15]. Similarly, frequencies of 10 or 5 mHz, or lower, may be still far from those necessary to pick up completely the system response. Obviously, this behaviour casts doubts on the magnitude that should really be inserted in the Stern-Geary equation.

Comparison of  $I_{corr}$  data from  $R_p$  measurements obtained with small specimens and gravimetric data has shown an acceptable reliability of the former [16,17] if scan rates between 5-10 mV/min or waiting times longer than 30s are used. However, larger problems may come from A.C. measurements, where impedance values at 10 mHz or 5 mHz provide  $I_{corr}$  values markedly higher than the real ones for passive rebars [18], and values at lower frequencies must be made that extend excessively the testing time.

Constant B. Pioneer investigations [16, 19] showed a good agreement between the electrochemical and gravimetric  $I_{corr}$  measurements in rebars, provided that values of  $B= 26$  mV for active rebars and 52 mV for passive rebars were introduced in the Stern-Geary equation. Other studies [17,20] have confirmed these values or modified them slightly. Although there is a need for much further research for a precise knowledge of the B values appropriate to the different conditions, for practical purposes and when the rebar activity is previously unknown, the B value may be assumed as 26 mV accepting an error factor of about 2.

Current distribution around the rebar circumference. Difficulties have been mentioned for  $R_p$  measurements which arise from a non-uniform distribution of the applied current lengthwise along the rebars. However, in the case of current distribution around the rebar circumference, current uniformity is usually taken for granted. This point has been questioned in a recent paper [21], which suggests that most of the current applied from the CE goes to the reinforcement upper half facing the CE. This would result in a calculated value of  $I_{corr}$  that is twice that occurring. However, a new paper [22] rather supports the first idea, so it seems justified to consider all the rebar perimeter for approximate estimations in practice.

Maximum depth of corrosion pits. The calculated values of  $I_{corr}$  are average values referred to the overall reinforcement surface. The integration of these values over the exposure time allows one to estimate an average penetration of corrosion ( $P_{av}$ ), but it does not inform at all about the maximum penetration ( $P_{max}$ ) of the deepest pits when the attack is very uneven. For life predictions, the  $P_{max}$  value is of more interest than the average value, when the mechanical weakening of the structure is affected by the bar section loss in those places where corrosion is intensified.

$P_{max}$  could be estimated from  $I_{corr}$  provided that a ratio (R) between  $P_{max}$  and  $P_{av}$  could be established. R values ranging from about 4 to 8 in natural corrosion of reinforced concrete have been measured [23]. This finding is of a great practical importance to predict residual life of chloride-contaminated concrete structures. It can

be expected that pit growth proceeds 4-8 times or so more rapidly than the instantaneous  $I_{corr}$  (average rate) measured. Similarly, the maximum total depth of localized attack will exceed by about 4-8 times the estimated average general penetration deduced from loss in weight after a given exposure time.

Identification of active corrosion areas. Identifying areas of active corrosion may help to avoid local section losses in rebars. The suitability of different electrochemical methods for detecting boundaries of active-passive areas has been studied in a recent paper [24]. A beam with one half of its length made of mortar containing 3%  $CaCl_2$  and the other half of non-chloride mortar was used. Thus, rebar corrosion activity changed along the two portions, with a transition point in the middle of the beam. It was found that  $R_p$  measurements made under confined conditions allowed to clearly distinguish such a transition point between active and passive areas, whereas other measurements made under unconfined-signal conditions lead to spurious conclusions and preclude a clear distinction.

## CORROSION RATE VALUES OBTAINED IN ON-SITE MEASUREMENTS

Based on the confinement of the current signal, a portable device has been developed [25] and a patent shared with a private company has been applied. The method uses a galvanostatic pulse and the confinement of the signal is controlled by two extra reference electrodes located between central and guard counter. One of the prototypes developed was tested at Penn State within the tasks of the SHRP Project C-101 [26].

The said corrosion-rate-meter has been used in a great number of structures with very different typologies and under a variety of conditions and variety of climatic environments. From these measurements it has been concluded that the chloride-contaminated structures in general exhibit higher corrosion rates than structures suffering corrosion due to carbonation.

Corrosion rates higher than  $1 \mu A/cm^2$  are seldom measured, values between 0.1- $1 \mu A/cm^2$  being the most frequent. When the steel is passive very low values (smaller than 0.05- $0.1 \mu A/cm^2$ ) are recorded. Table 1 present the ranges of  $I_{corr}$  values found in the laboratory and in real size structures measured on-site. With respect to these ones, the following classification is proposed:

TABLE 1. Levels of corrosion rates measured in laboratory and on-site.

Corrosion rate ( $\mu A/cm^2$ )	Corrosion level
< 0.1	negligible
0.1 - 0.5	low
0.5 - 1	moderate
> 1	high

A comparison of on-site  $I_{corr}$  values to electrical resistivity is presented in Fig. 6. This comparison has allowed the authors to also rank the resistivity values as is described in table 2.

TABLE 2. Levels of concrete resistivity regarding risk of corrosion

Resistivity ( $k\Omega \cdot cm$ )	Corrosion risk
>100-200	- Negligeable corrosion. Too dry concrete
50 - 100	- Low corrosion-rate.
10 - 50	- Moderate to high corrosion when steel is active.
<10	- Resistivity is not the controlling parameter of the corrosion rate.

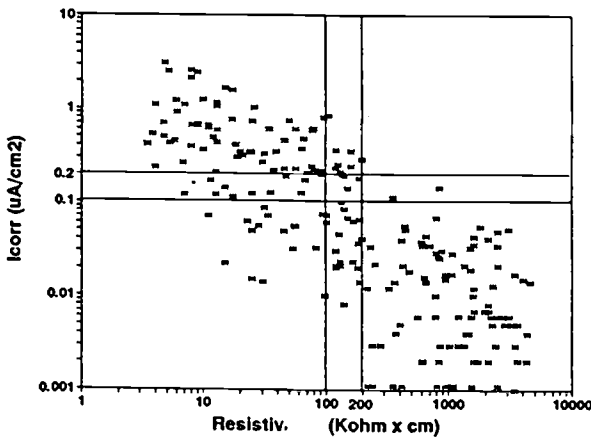


FIG. 6. Comparison of electrical Resistivity and  $I_{corr}$  values measured on-site.

### Embedded sensors

Embedded sensors have been used to monitor concrete structures [27]. These are usually based on the embedment of small pieces of normal steel or stainless steel, or special reference electrodes [28]. These sensors are placed using different cover depths.

The sensors are used to monitor the corrosion potential,  $E_{corr}$ , and resistivity variation due to the daily humidity cycles, or to measure of  $R_p$ .

The monitoring of the depassivation of the sensors embedded at different depths enable the early detection of future distress and to predict the advance of chloride or carbonation front. However, they may not reflect what may happen in a continuous

rebar, as they do not take into account possible galvanic effects with other parts of the structure.

## CONCLUSIONS

The measurement on-site of the corrosion state of the concrete reinforcement has been tried by using different electrochemical techniques. From the extensive work carried out until now by the authors the main conclusions that may drawn up are:

- 1) Methods based on linear Polarization technique are the most suitable to be applied on-site. However, care has to be taken to refer the  $R_p$  value to the steel surface really polarized.
- 2) True  $R_p$  values can be obtained by confining the current applied by means of a sensorized control of the confinement carried out through a guard ring. By means of this method the values of  $E_{corr}$ , electrical resistivity  $R_e$ , and  $R_p$  obtained in real concrete structures are similar to those obtained in small specimens in the same conditions.

## ACKNOWLEDGEMENTS

The authors appreciate the financial support given by the CICYT of Spain. To the research also, thanks are due to GEOCISA (Spain) for supplying information regarding GECOR-6 measurements in real structures.

## REFERENCES

- [1] Escalante, E., Corrosion of Reinforcement in Concrete, C.L. Page, K.W.J. Treadaway and P.B. Bamforth (Eds.), SCI, Elsevier Applied Science, London, 1990, pp. 281-292.
- [2] Elsener, B and Böhni, H. Corrosion Rates of Steel in Concrete, N.S. Berke, V. Chaker and D. Whiting (Eds.), ASTM STP 1065, 1990, pp. 143-156.
- [3] Feliú, S., González, J.A., Andrade, C. and Feliú, V., "On-site determination of the Polarization Resistance in a reinforced concrete beam," Corrosion, **44**, 761 (1988).
- [4] Feliú, S, González, J.A., Andrade, C. and Feliú, V., "Determining polarization resistance in reinforced concrete slabs"., Corrosion Sci., **29**, 105 (1989).
- [5] Stern, M., and Geary, A.L., "Electrochemical polarization: I. A theoretical analysis of the shape of polarization curves", J. Electrochem. Soc., **104**, 55 (1957).

- [6] Andrade, C., Castelo, V., Alonso, C. and González, J.A., "The determination of the corrosion rate of steel embedded in concrete by the  $R_p$  on A.C. Impedance methods," ASTM-STP 906, 1986, pp. 43-64.
- [7] John, D.G, Searson, P.C. and Dawson, J.L. "Use of AC impedance technique in studies on steel in concrete in immersed conditions" *Br. Corros. J.*, Vol. 16 n° 2, (1981).
- [8] Feliú, S., González, J.A., Feliú, S.Jr., and Andrade, C., "Confinement of the electrical signal or in-situ measurement of Polarization Resistance in concrete structures", *Corrosion 90*, NACE Annual Conference, 1990. Paper 142.
- [9] Feliú, S., González, J.A., Escudero, M.L. and Andrade, C., "Influence of counter electrode size on the on-site measurement of polarization resistance in concrete structures", *Corrosion 90*, NACE Annual Conference, 1990. Paper 142.
- [10] Feliú, S., González, J.A. and Andrade, C., "Errors in the on-site measurements of rebar corrosion rates arising from signal unconfinement", P.D. Cady Symposium, Minneapolis, Minnesota, ACI SP-151, 1993, pp-183-195.
- [11] Feliú, S., González, J.A., Escudero, M.L., Feliú, S. Jr. and Andrade, C., "Possibilities of the guard ring for the confinement of the electrical signal in polarization measurement of reinforcements," Corrosion, **46**, 1015 (1990).
- [12] P.D. Simon - Status report on the development of a field instrument using the polarization resistance method for measuring the rate of corrosion of reinforcing steel in concrete - NACE Annual Conference - Corrosion 89, paper no. 380 - New Orleans, (1989).
- [13] Newton, C.J. and Sykes, J.M., "Effect of mix specifications on corrosion of steel in mortars immersed in chloride solutions", Corrosion Sci., **28**, 1051 (1988).
- [14] Feliú, S., Galván, J.C., Feliú, S. Jr., Simancas, J., Bastidas, J.M., Morcillo, M. and Almeida, E., "Differences between apparent polarization resistance values obtained in the time and frequency domains", J. Electroanalytical Chem., in press.
- [15] Millard, S.G. and Gowers, K.R., "Resistivity assessment of in-situ concrete: the influence of conductive and resistive surface layers", Proc. Inst. Civil Engrs. Struct. & Bldgs, **94**, 1992, paper 9876, pp.389-396.
- [16] Andrade, C. and González, J.A., "Quantitative measurements of corrosion rate of reinforcing steels embedded in concrete using polarization resistance measurements," Werkst. Korros., **29**, 515 (1978).
- [17] González, J.A. and Andrade, C., "Effect of carbonation, chlorides and relative humidity on the corrosion of galvanized rebars embedded in concrete," Br.

Corros. J., 17, 21 (1982).

- [18] Feliú, S., González, J.A. and Andrade, C. to be published.
- [19] González, J.A., Algaba, S. and Andrade, C., "Corrosion of Reinforcing bars in carbonated concrete", Br. Corros. J., 15, 138 (1980).
- [20] Hladky, K., John, D.G. and Dawson, J.L. "Development in rate of corrosion measurements for reinforced concrete structures", Proc. Conf. Corrosion 89, New Orleans, LA, April 1989 NACE, Paper 169/1.
- [21] Sehgal, A., Li, D., Kho, Y.T., Osseo-Asare, K. and Pickering, H.W., "Reproducibility of Polarization Resistance measurements in steel-in-concrete systems", Corrosion, 48, 706 (1992).
- [22] Feliú, S., González, J.A. and Andrade, C., "Effect of current distribution on corrosion rate measurements in reinforced concrete", Corrosion, vol.51, nº 1 (1995) 79-86.
- [23] González, J.A., Andrade, C., Alonso, C. and Feliú, S., "Comparison of rates of general corrosion and maximum pitting penetration on concrete embedded steel reinforcements", Cement and Concrete Research, vol. 25, no.2 (1995) 257-264.
- [24] González, J.A., Benito, M., Rodríguez, J. Andrade, C. and Feliú, S., "Suitability of various corrosion assesment methods for identifying active and passive zones in reinforced concrete", Corrosion, vol. 51, no. 2 (1995) 145-152.
- [25] GECOR (Corrosion Rate Meter), GEOCISA, Los Llanos de Jerez, 10. (28820) Coslada, Madrid, Spain.
- [26] Strategic Highway Research Program , Project C101, Contract SHRP-87-C101, National Research Council, Washington, D.C., 1992.
- [27] Schiessl, P. and Raupach, M., "Monitoring system for the corrosion risk of steel in concrete structures", Concrete International, July (1992) 52-55.
- [28] Klinhoffer, O., "In-situ monitoring of reinforcement corrosion by means of electrochemical methods", Symposium on Corrosion and Corrosion Protection of Steel in concrete. Sheffield Academic Press. R.N. Swamy Ed. Sheffield July 1994.

Al Ghorbanpoor,<sup>1</sup> and Shan Shi<sup>2</sup>

**ASSESSMENT OF CORROSION OF STEEL IN CONCRETE STRUCTURES BY MAGNETIC BASED NDE TECHNIQUES**

---

**REFERENCE:** Ghorbanpoor, A. and Shi, S., "Assessment of Corrosion of Steel in Concrete Structures by Magnetic Based NDE Techniques," Techniques to Assess the Corrosion Activity of Steel Reinforced Concrete Structures, ASTM STP 1276, Neal S. Berke, Edward Escalante, Charles K. Nmai, and David Whiting, Eds., American Society for Testing and Materials, 1996.

**ABSTRACT:** Corrosion damage of steel in concrete structures is a major concern. NDE techniques based on variations in induced magnetic fields due to loss of steel have been shown to be an effective tool. This paper includes results from laboratory investigation, field tests, and numerical analysis based on this concept. Test specimens included reinforcing bars and prestressing cables with simulated flaws as well as flaws from real corrosion. Variations in the magnetic field were recorded as electrical signals that were characterized to aid in the detection of corrosion and evaluation of the condition of steel in concrete. It was found that the amplitude of the signals could be related to the extent of the corrosion. Loss of cross sectional area in bars and cables of approximately 3 percent could be detected by the technique. The results of a finite element analysis yielded a good agreement with those from the experiment. The technique offers significant capabilities for field assessment of the condition of steel in concrete structures.

**KEYWORDS:** corrosion, magnetic field, NDE, concrete, reinforcing bars, prestressing cables, signal processing, finite element analysis, laboratory tests, field tests

---

**INTRODUCTION**

Corrosion of steel in concrete structures has been a major concern of owners and practicing engineers for the past several decades. As primary load carrying components, the reinforcing bars and prestressing cables must be in good condition at all times to allow safe use of the structures. High strength reinforcing steel is commonly used in concrete, and therefore, there is a higher susceptibility to stress corrosion cracking and hydrogen embrittlement. Deterioration and eventual failure of one or more of the bars or cables in a member could result in failure or collapse of the member or the structure.

---

<sup>1</sup>Professor, Department of Civil Engineering and Mechanics, University of Wisconsin-Milwaukee, P.O. Box 784, Milwaukee, WI 53201.

<sup>2</sup>Graduate Student, Department of Civil Engineering and Mechanics, University of Wisconsin-Milwaukee.

Evaluation of in-service concrete structures, i.e., bridges, parking structures, etc., over the last few decades has shown a growing evidence of premature deterioration of these structures due to corrosion of reinforcing steel. Several failures and collapses of concrete structures have been reported which were associated with the corrosion of reinforcing or prestressing steel in concrete. Presence of chlorides in concrete is a major source of corrosion of steel reinforcement. Premature bridge deck deterioration occurs in the northern "snow belt" regions of the U.S. where the 1950's "clear roads year round" policy has forced the highway departments to significantly increase the use of de-icing salts. Bridge decks with a design life expectancy of at least 40 years have required major repairs in less than 10 years, and often complete replacement in about 15 years of service [1]. Additionally, many structures located in coastal zones have experienced corrosion problems due to ocean spray and air-born marine salts.

A large number of studies have been conducted to understand the corrosion phenomenon in in-service concrete structures subjected to aggressive environments and to develop methodologies to control the rate of corrosion. The root of the corrosion problem in concrete structures is known to be an electrochemical process involving the breakdown of the protective concrete environment surrounding the steel. The primary factor for initiating the corrosion process is the intrusion of chlorides in concrete, which leads to the development of corrosion cells if a continuous supply of oxygen is provided.

While valuable information with regards to the corrosion activity and factors responsible for corrosion has been obtained from studies performed in the last few decades, little is found in the available literature on reliable and effective assessment of the condition of existing in-service structures. At the present time, there is no routine nondestructive method of inspection available to individuals responsible for maintaining concrete structures that allows reliable assessment of the condition of steel reinforcement in concrete. Recent developments relevant to the concept of variations in an induced magnetic field, as a result of corrosion of steel in concrete, have shown that it is possible to develop a nondestructive testing capability that will permit reliable field assessment of the condition of reinforcing steel in concrete structures.

#### **MAGNETIC BASED NDE CONCEPT AND DEVELOPMENT**

The magnetic based NDE concept for assessing the condition of steel in concrete structures utilizes the ferromagnetic property of the steel to detect perturbances of an externally applied magnetic field due to presence of flaws in the steel. For magnetic field strength below saturation, the following relationship holds;

$$B = \mu \cdot H \quad (1)$$

where

B	=	total magnetic flux density, Wb/m <sup>2</sup> (or tesla),
$\mu$	=	material magnetic permeability, Wb/Am (or H/m), and
H	=	magnetic field strength or intensity, A/m.

It has been shown that flux intensity in steel is a function of the magnetic field strength and material properties (Eq. 1). When an external magnetic field with sufficient strength is applied near a reinforced concrete member, some of the atomic dipoles of reinforcing steel become aligned with the field and the steel becomes magnetized. The concrete remains relatively unaffected. When the strength of the

externally applied field is adequately large, complete alignment of the atomic dipoles will result which is known as magnetic saturation of the steel. Additional field strength beyond the level causing saturation will have no influence on the magnetization of the steel. If the direction of the applied magnetic field is set to be collinear with the longitudinal reinforcing steel in concrete, the flux will be concentrated and magnified in the steel. Any change in the cross sectional area of the steel at any point will cause a flux leakage or fringing, where the continuous flux lines within the steel will be forced into the medium surrounding the flaw. Detection devices, i.e., Hall probes, may be used in the vicinity of the flaw to measure and record the perturbation of the magnetic field as an electrical charge. If the magnetic source and sensors are moved along the length of the concrete member, the signature is then recorded as a continuous signal that can be analyzed to obtain information relevant to the location and extent of the flaw (Fig. 1). Signal features such as the amplitude (A) and peak-to-peak separation (p), as shown in the figure, are used to characterize them. Flux leakage usually results in the development of a three dimensional perturbation of the magnetic field in the vicinity of the flaw. The three dimensional perturbation of the field may be measured by using an array of sensors (Fig. 2). The amplitude of the perturbation is normally associated with the flaw size. It is important to note that other factors also have significant influence on the magnitude of the perturbation. These factors are strength of the magnetic source, distance between the magnet and the steel, and distance between detecting sensors and the steel. However, it is possible to keep the effect of these factors constant, and correlate the amplitude of the magnetic signals to flaw size by performing a system calibration.

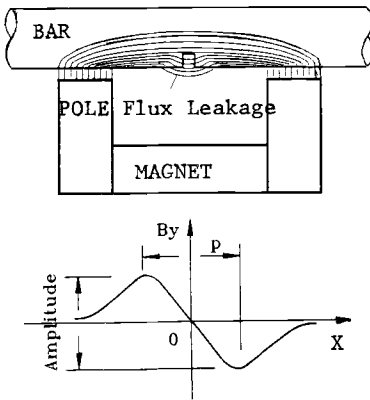


FIG. 1--Magnetic flux leakage and signal.

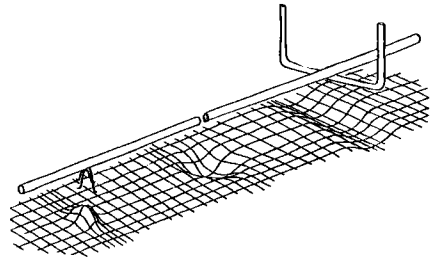


FIG. 2--Three-dimensional variation of magnetic field.

The Hall probes used in a magnetic based NDE system function under the principle of Faraday's law, or;

$$F = iLB$$

(2)

where

$i$	=	a charge moving along the length of a planar conductor,
$L$	=	length of the conductor,
$B$	=	magnetic flux perpendicular to the plane of the conductor, and
$F$	=	force (voltage) exerted on $i$ due to $B$ .

A voltage,  $V_H$ , is developed in a direction perpendicular to  $L$  which will be proportionate to the magnitude of the magnetic field normal to the plane of the sensor. The measured voltage, or the electrical signal, at a point includes the effects from both the adjacent ferromagnetic components and flaws. The ferromagnetic components may include steel element of interest, adjacent steel reinforcement, stirrups, steel chairs, and other metallic artifacts. Therefore, an appropriate analysis approach for the examination of these electrical signals becomes very important.

In general, the signal analysis for this application has been shown to be most effective when they are dealt with in the time domain. Examination of these signals in the frequency domain normally yields no advantage. In addition to the visual examination of the signals, either a two- or three-dimensional analysis method may be used. One two-dimensional method includes a simple subtraction technique where point-by-point subtraction is performed on two signals recorded by two different sensors. The effects from most ferromagnetic artifacts will be eliminated in the resulting signal after the subtraction. Another two dimensional method of signal analysis is a technique based on the correlation concept. Here, a recorded signal is compared, point-by-point, with a mathematically defined ideal flaw signal. A perfect match is represented by +1.00 and a total mismatch is indicated by 0.00. A signal that is a mirror image of the ideal flaw signal is represented by -1.00. A statistical analysis on experimental findings permits an accept/reject criteria to be established based on the correlation values that will be assigned to signals recorded during a NDE test of reinforced concrete structures. The three dimensional analysis method is based on the examination of the three dimensional perturbation of the magnetic field at a point of interest (Fig. 2). Here, a series of sensors located on a horizontal plane and at a close spacing must be used to minimize the error of approximation of the continuous magnetic field. Recorded signals from all the sensors are analyzed together to extract information on the condition of the member at any point. The method offers superior analysis capability where flaws in a steel bar or cable can be easily differentiated from the effects of ferromagnetic artifacts in concrete such as stirrups.

## EXPERIMENTAL STUDY

### Test Procedure

Two prototype systems based on the concept of variation of magnetic field were used in this study to determine their capability in detecting simulated flaws, as well as flaws from real corrosion, in reinforcing bars and prestressing cables. The first system included an electromagnet, as the magnetic source, and was developed in the late 1970's [2]. The second system utilized a relatively light weight permanent magnet and was developed in 1991 to provide improvement by using state-of-the-art equipment and software [3]. This system was developed for laboratory use only. Lack of funding did not allow for further development to make the system suitable for field use. Results of laboratory tests showed similar flaw detection capabilities for the

two systems, except the later system offered more reliable and convenient use with faster data analysis.

In order to establish a data base of magnetic variation (MV) signals, full-length reinforcing bars and prestressing cables with flaws of various sizes and shapes were inserted in pre-made longitudinal holes provided in a 6.1- m long concrete beam. The beam's cross sectional dimensions were 0.61 m X 0.61 m. Flaws were created in steel bars and cables by removing steel equivalent to 7 to 91 percent of the cross sectional area. The beam included 27 longitudinal full-length holes that were located at different positions along the depth and width of the cross section (Fig. 3). Permanent reinforcing steel in the beam included only one row of 5 No. 6 bars at 220 mm from the underside of the beam and No. 3 stirrups spaced at 394 mm along the length of the beam. The first half-length of the beam contained inverted "U" type stirrups along the centerline of the section. The stirrups had short (25 mm) horizontal legs. The second half-length of the beam included rectangular stirrups that extended the entire width of the beam. It was determined that no effect from the inverted "U" type stirrups could be observed on the magnetic signals if the flawed bar was located within 150 mm from each side face of the beam. Due to the relatively large distance from the underside of the beam, the effect of the longitudinal No. 6 bars on the magnetic signals from the flawed bars and cables was insignificant and was neglected in the analysis. Magnetic variation tests were performed from the underside of the beam along its length and the relevant signals associated with the flaws in the bars and cables were recorded and analyzed. The bars and cables were placed in the longitudinal holes located at various distances from the underside of the beam to determine the effect of distance between the magnetic source/sensors and flaws. In addition, the volume of undamaged steel surrounding flawed bars and cables were varied to determine their effect on the relevant signals.

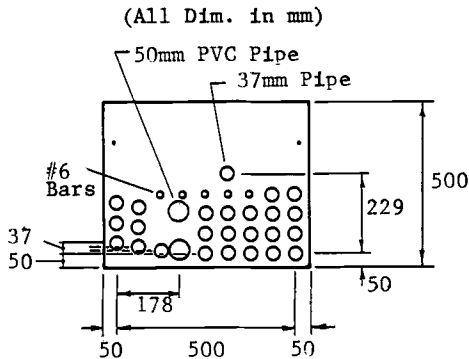


FIG. 3--Cross section of the concrete beam used in the laboratory.

An accelerated corrosion test of reinforcing bars and prestressing cables in a concrete slab was performed to determine the effect of flaws, from real corrosion, on the magnetic signals. Two independent electrical cells were made using the bars and cables in the slab. A 9% sodium chloride solution was applied to two areas of the slab every week (4 days of ponding and 3 days of air drying) for a period of 14 months. The corrosion activity in the slab was monitored by using the Half-Cell Potential technique, following the ASTM Designation C876-87, [4] and by performing monthly tests using the magnetic method. The magnetic signals for all monthly tests were recorded, analyzed and compared with each other for the entire corrosion test period, as well as with a

reference signal recorded prior to the start of the corrosion test. At the end of the corrosion test period, bars and cables were removed from the slab and corrosion flaws were measured and correlated with the results of the magnetic tests.

Test Results

A recorded signal from one sensor for a reinforcing bar, which included various flaw sizes and was located 50 mm from the underside and 100 mm from the side of the beam, is shown in Fig. 4a. In the figure, flaw indications can be clearly distinguished for cross sectional losses larger than approximately 20 percent. The effect of the rectangular stirrups in the second half-length of the beam can also be seen in the signal. An enhancement of the signal analysis may be made by using the correlation method (Fig. 4b). It can be seen in Fig. 4b that flaw indications for the bar are observed for all flaw sizes, including those with smaller than 12 percent loss of area. However, it is shown that the correlation amplitudes are relatively small for flaw sizes smaller than approximately 20 percent of the cross sectional area of the bar.

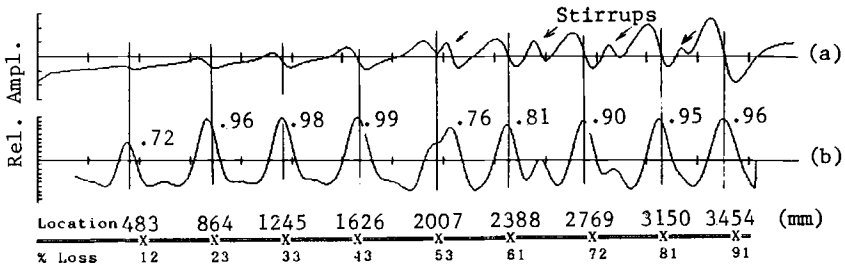


FIG. 4--MV signal analysis for a bar with multiple flaws.  
 (a) Magnetic variation signal, (b) correlation analysis

Additional enhancement may be made by performing the correlation analysis on a signal that has been constructed by subtracting the signals recorded by the first sensor from the signal recorded by a second sensor located directly 25 mm below the first one (Fig. 5). It has been shown that more reliable signal interpretation can be made using this technique.

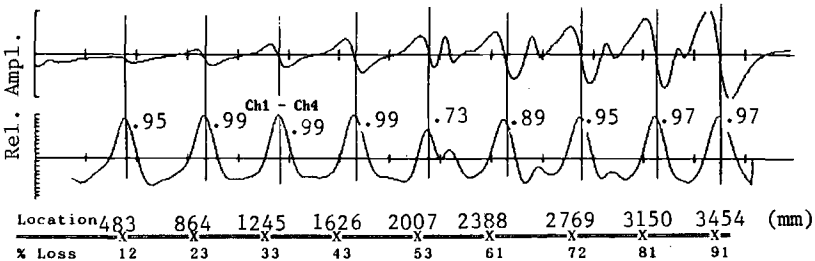


FIG. 5--MV signal analysis (data subtraction & correlation).

When concrete components with heavy reinforcing steel are tested and the magnetic signals are analyzed using the correlation method, erroneous results may be obtained due to the influence of the ferromagnetic

artifacts. In order to analyze magnetic signals in such cases, it is advantageous to examine the three-dimensional magnetic field variation (Fig. 2). A simplification may be made by examining a two-dimensional profile of the signal amplitudes from multiple sensors at any point of interest along the length of the scan (Fig. 6). An array of sensors located at close spacing, i.e., 12 mm, and along a line perpendicular to the direction of the scan are used to record these signals. Transverse profiles at any interval along the scan length may be constructed. Typical flaw and stirrup profiles from a six-sensor array are shown in Fig. 6.

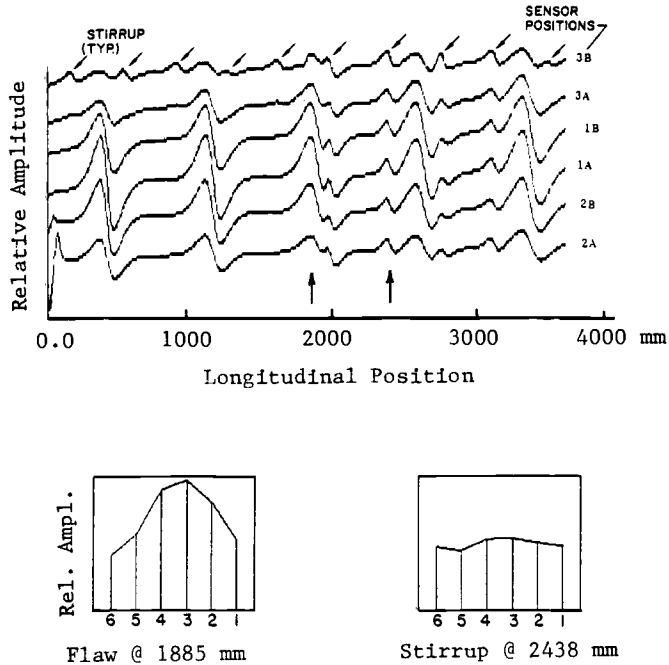


FIG. 6--Two-dimensional Profile analysis using six sensors.

Among various factors that influence the magnetic signals, the effects of the flaw size and distance between the flaw and the source/sensor are the most significant. Figs. 7 and 8 show the results of laboratory tests to determine variation of the amplitudes of magnetic signals due to different flaw sizes and due to distance between the flaw and the source/sensors, respectively. It can be seen from the figures, that for either small flaw sizes or relatively large distances between the flaw and source/sensors, the signal amplitudes become very small. This makes the interpretation of the magnetic signals very difficult if only the signal amplitude is considered. Empirical relationships, based on this study's experimental data, for the relative amplitude of the magnetic signal as a function of the variations in the volume (size) of flaw and in the distance between the flaw and source/sensors may be given as;

$$A_r = \left( \frac{V_2}{V_1} \right)^{1.1} \quad (3)$$

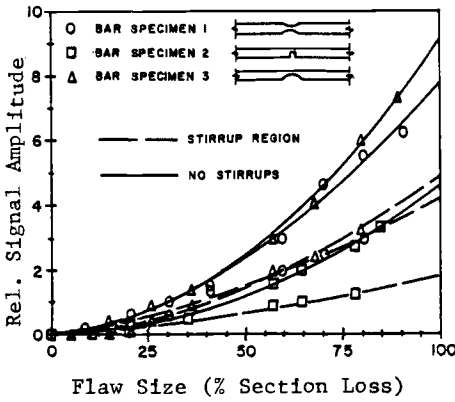


FIG. 7--MV of signal amplitude vs. flaw type and size.

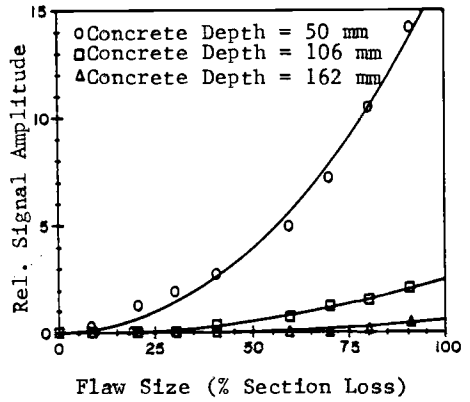


FIG. 8--MV of signal amplitude vs. flaw size and conc. cover.

and

$$A_r = \left( \frac{D_2}{D_1} \right)^{2.8} \tag{4}$$

where

- $A_r$  = relative signal amplitude,
- $V_2/V_1$  = ratio of two flaw sizes, where  $v_1$  and  $v_2$  are flaw volume specified as percentage of the cross sectional area of the reinforcing bar or cable,
- $D_2/D_1$  = ratio of two distances between the flaw and the source/sensor, where  $D_1$  and  $D_2$  must be smaller than 150 mm.

Eqns. 3 and 4 agree with the theoretical solution available for a simplified case of a spherical void embedded in a ferromagnetic medium [5]. It is shown that the amplitude of the magnetic variation signatures proportionate directly to the flaw volume and inversely to the cube of the distance between the flaw and the source/sensor, or;

$$A = (0.8587) \mu H \left( \frac{\mu_o - \mu}{\mu_o + 2\mu} \right) \frac{a^3}{d^3} \tag{5}$$

where

- A = amplitude of the magnetic variation signature at a flaw,
- $\mu_o$  = magnetic permeability of free space (air),  $4\pi \times 10^{-7}$  (H/m),

a = flaw size, and

d = distance between flaw and point of interest (location of source/sensor).

It was found, during this study, that due to small signal amplitudes associated with small flaw sizes or large distances between flaw and source/sensors, it is advantageous to perform an examination of the three-dimensional variation of the magnetic field to make a more reliable assessment of the condition of the steel reinforcement in concrete. This proved to be a more advantageous method when real corrosion flaws in the bars and cables were monitored during the laboratory accelerated test of the concrete slab. An examination of the magnetic signals for a corroded region of the slab at one and at fourteen months clearly indicated the presence of corrosion in the bars and cables. Fig. 9 shows a superimposed view of the results for the two tests for a reinforcing bar. In the figure, the relative changes in the signals indicate corrosion pitting related cross sectional losses equivalent to 7 to 9 percent. A closer examination of the results for other bars and prestressing cables indicated that cross sectional losses equivalent to approximately 3 percent could be identified using the three-dimensional variation of the magnetic field.

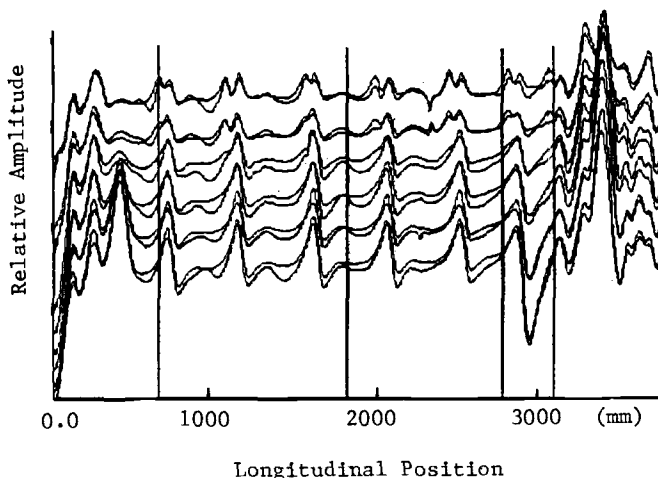


FIG. 9--Superimposed view of MV data for tests at 1 and 14 months.

#### FIELD STUDY

Several MV tests were conducted to evaluate the applicability of the magnetic variation technique under field conditions. Reinforced, prestressed, and post-tensioned concrete bridge structures with a possibility for corrosion problems were chosen for the tests. Only the magnetic system with the electromagnet [2] was used during the field tests. Although the use of the system in the field introduced some installation and setup difficulties and was time consuming, it offered valuable information on the condition of the steel inside concrete that could not otherwise be obtained.

For the bridge structures tested, no indications of major corrosion or fracture of steel reinforcing elements in the concrete were observed as a result of the field tests. Field verifications were made by exposing the reinforcing steel in concrete and inside of post-

tensioning ducts at several random locations to visually assess the condition of the steel. In all cases, close agreement existed between the results of the MV field tests and the actual condition of the steel in the concrete. A composite plot of the magnetic signals from four sensors for a 14-m long section of a post-tensioned concrete girder is shown in Fig. 10. Locations and spacing of the steel stirrups in the girder are shown in the figure without any indications for discontinuities or flaws.

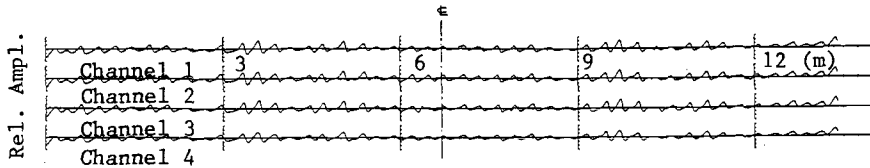


FIG. 10--Field MV signals from 4 sensors for a 14-m long section of a post-tensioned concrete girder.

#### FINITE ELEMENT ANALYSIS

Analytical approaches were used to compare the results with those from the experiment and develop methodologies that could be utilized to aid in the design of magnetic based NDE systems. Closed form solutions exist only for simple geometries, and for most real applications one has to revert to numerical approaches such as the finite elements or the boundary elements techniques. Theoretical basis for analysis of magnetic problems by the finite elements method is well documented in the literature [6]. A commercially available finite element code, ANSYS, was used in this study to obtain solution to the three-dimensional problem of magnetic variation as a function of loss of cross section of steel reinforcing bars due to corrosion.

The following assumptions were made in the finite element analysis: only one reinforcing bar with flaw was considered, flaw in the bar included either complete fracture or partial loss of section of different magnitudes, the bar was placed in the air, the magnetic permeability for the air and concrete was the same, static magnetic analysis was considered without the effects of time-dependency, and the hysteresis effect of the magnetic material was ignored. The B-H curves for both the reinforcing steel bar and the magnet poles are shown in Fig. 11. The coercive, or the demagnetization, force for the magnet used in this study was chosen as 320,000 A/m with a relative magnetic permeability ( $\mu/\mu_0$ ) of 1.0. This magnetic force is equivalent to the intensity of a permanent magnet that produces a magnetic flux density of 0.1 tesla in the air between and at the highest elevation of the poles. Element type used in the analysis included an eight-node three-dimensional solid element with three degrees of freedom per node. The medium, or the air, surrounding the magnet and steel bar was modeled using the same solid element described earlier. The surrounding medium was extended beyond the steel bar for a distance equivalent to three times the distance between the bar and the top of the poles of the magnet.

Fig. 12 shows the geometrical configuration of the problem considered. The geometry shown in the figure, is identical to that of the NDE system developed using an electromagnet. For simplification, advantage was taken of the symmetric property of the problem and only one-half of the geometry was included in the analysis. At the plane of symmetry, all flux lines were set to lay perpendicular to the plane.

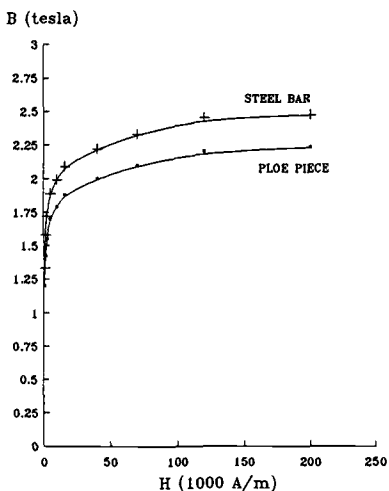


FIG. 11--B-H curves for steel bar and magnet poles.

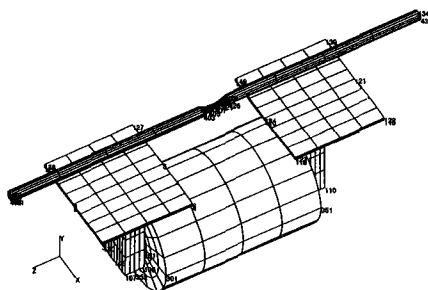


FIG. 12--FE model used in the study.

Various conditions with respect to the size of the flaw and distance between the bar and source/sensor were considered to develop a data base to aid in the construction of a design guideline for magnetic based NDE systems. Table 1 shows the various conditions considered in the analysis.

TABLE 1-- Flaw types and sizes evaluated in the FE analysis

Flaw Type	Flaw Size	Concrete Cover (mm)
Complete Fracture	<u>Gap Size (mm)</u>	50 106 162
	25 50 75 100	
Partial Loss of Section	<u>% of Loss</u>	50 106 162
	25 50 75	

The results of the finite element analysis include the distribution of the magnetic flux density in the bars and magnet components in different orientations and the magnitude of the flux leakage at the vicinity of discontinuities in the bar. Figs. 13 and 14 show the flux density distribution in the magnet and steel bar along the longitudinal axis of the bar, and the flux leakage in a transverse direction within the medium surrounding the steel bar, respectively. As shown in Fig. 13, the flux density in the bar is concentrated and approaching a high value of approximately 2.6 tesla. On the other hand, the flux leakage density in the air surrounding the flaw is in the order of less than 0.2 tesla. It should, however, be noted that flux leakage densities as low as approximately 0.001 tesla can be easily detected. These results agree well with those from the experimental data of this study. The flux leakage in the transverse direction is of primary interest since it corresponds to the component of the field that is normally measured during experiments and real tests. A curve may be

constructed from calculating the magnitudes of the flux leakage at several points at both sides of a flaw. This curve is similar to the magnetic variation signal obtained from an actual experimental or field test (Fig. 1).

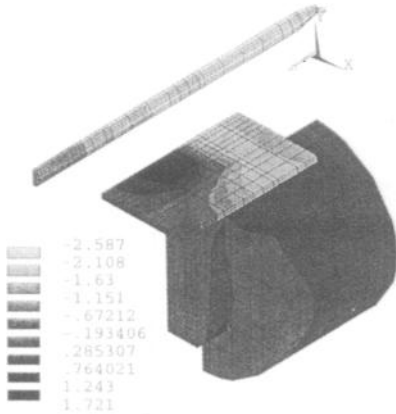


FIG. 13--Mag. flux distribution along the axis of the bar.

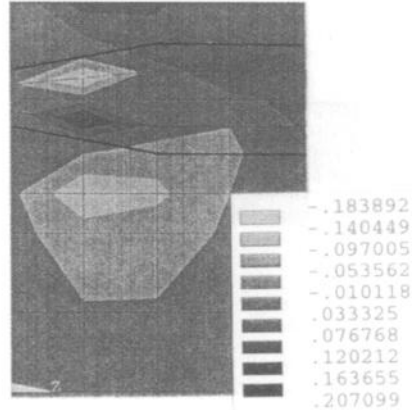


FIG. 14--Flux leakage in the air around the flaw.

Repeating the analysis for various variables, such as flaw sizes and distances between the bar and source/sensor, yields results that lead to the construction of a series of design curves, Figs. 15 and 16. These curves indicate changes in the magnitude of the amplitude of the magnetic variation signals as a function of the signal peak-to-peak separation and the above stated variables. Data obtained from the experimental part of this study, for similar conditions, agree well with the results shown in Fig. 15. No experimental data was available to correspond with those shown in Fig. 16. However, the results from both the finite element and experimental studies indicate that with increasing gap sizes for a complete fracture of a bar, the amplitude of the magnetic variation signals decreases after an initial rapid increase. This appears to be caused due to an increase in the reluctance of the magnetic circuit as the air gap size increases. As a result, a greater portion of the flux is passed in the air directly between the poles causing lower flux flow in the bar. The curves shown in Figs. 15 and 16 may be used during experimental studies or real tests in the field to determine the size and location of flaws in concrete. Magnetic signal peak separation and amplitude values can be readily obtained from the test results which can lead to the estimation of the flaw size and depth within concrete using the given design curves.

## CONCLUSIONS

Based on the evaluation of the results from the analytical, experimental, and field studies of this work it is shown that a reliable and effective assessment of the condition of reinforcing steel in concrete members may be made using NDE techniques based on the variation of an induced external magnetic field. It was found that cross sectional losses equivalent to approximately 3 percent could be detected reliably. The technique shows significant promise and relevant hardware

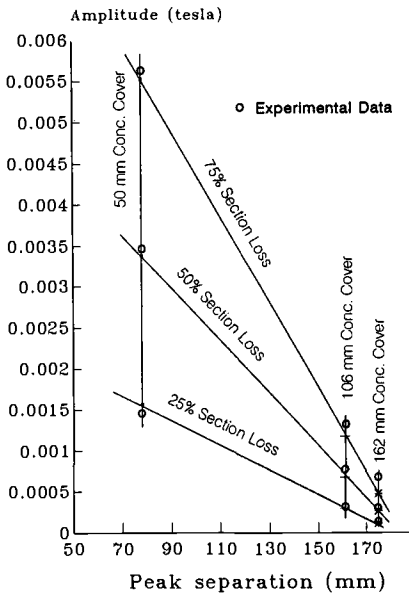


FIG. 15--Design aid to estimate flaw size and position. (FE and Exp. data)

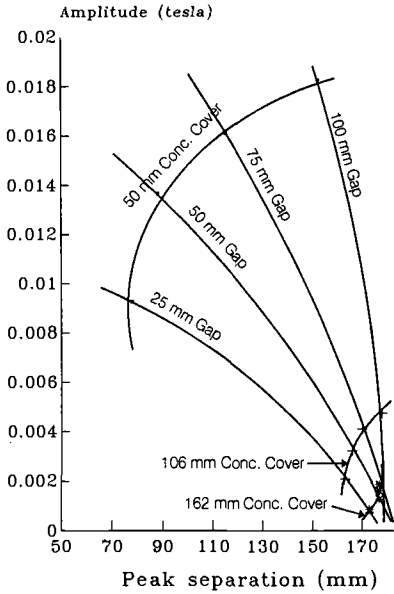


FIG. 16--Design aid to estimate flaw size and position. (FE data)

systems should be developed to take advantage of this capability for field assessment of the condition of reinforcing steel in concrete structures.

#### REFERENCES

- [1] "Solving Corrosion Problems of Bridge Surfaces Could Save Billions," Report to the Congress of the United States by the Comptroller General, Washington, D.C., 1979.
- [2] "Operator's Manual for Concrete Bridge Inspection System," FHWA Contract No. DTFH61-80-C-00002, Southwest Research Institute, San Antonio, Texas, 1981.
- [3] Ghorbanpoor, A., Steber, G. R., and Shew, T. E., "Evaluation of Steel in Concrete Bridges: *The Magnetic Field Disturbance (MFD) System*," Final Report No. FHWA-SA-91-026, Federal Highway Administration, Washington, D.C., 1991.
- [4] "Standard Test Method for Half-Cell Potentials of Uncoated Reinforcing Steel in Concrete," ASTM Designation C876-87. Annual Book of ASTM Standards, The American Society for Testing and Materials, Vol. 4.04, 1987, pp563-570.
- [5] Kraus, J.D., "Electromagnetics," McGraw-Hill, New York, 1984, pp 538-541.
- [6] Bathe, K. J., "Finite Element Procedures in Engineering Analysis," Prentice-Hall, New Jersey, 1989.

David Whiting<sup>1</sup> and Mohamad A. Nagi<sup>2</sup>

## **TESTS FOR EVALUATION OF THE EFFECTIVENESS OF PENETRATING SEALERS IN REDUCING PENETRATION OF CHLORIDES INTO CONCRETE**

---

**REFERENCE:** Whiting, D. and Nagi, M. A., "Tests for Evaluation of the Effectiveness of Penetrating Sealers in Reducing Penetration of Chlorides into Concrete," Techniques to Assess the Corrosion Activity of Steel Reinforced Concrete Structures, ASTM STP 1276, Neal S. Berke, Edward Escalante, Charles K. Nmai, and David Whiting, Eds., American Society for Testing and Materials, 1996.

**ABSTRACT :** A pair of rapid tests for evaluation of the effectiveness of penetrating sealers in preventing corrosive chloride ions from penetrating concrete have been developed. The tests are designed to yield an indication of the relative performance of a sealer as compared with unsealed concrete. The first test is based on measurement of electrical resistance between two small electrodes created on a concrete surface by use of a highly conductive spray-applied coating. A criterion of 200 k-ohms after 4 minutes of test was selected for differentiating between effective and ineffective sealers. The second test is based on absorption of water into the concrete surface over a four minute period. Development and field trials of the two tests are described. The tests are applicable to both horizontal and vertical surfaces. Applications for the tests include quality control of sealer application, qualification of sealers under field conditions, and monitoring of sealer performance over time in a nondestructive manner.

**KEY WORDS :** Absorption, concrete, corrosion, electrical resistance, permeability, sealers

---

Penetrating sealers are coming into increased use as a low-cost method for reducing ingress of moisture, chlorides, and other deleterious, corrosion-inducing substances into reinforced portland cement concrete structures. While a 50:50 mixture of boiled linseed oil and mineral spirits has been a traditional choice, it is no longer widely used. The practice

---

<sup>1</sup> Senior principal engineer and <sup>2</sup> research engineer, respectively. Construction Technology Laboratories, 5420 Old Orchard Road, Skokie, IL 60077.

of sealing has increased appreciably in recent years, and a variety of newer proprietary sealants are now available. The most commonly used are penetrating sealers based on silanes, siloxanes, epoxies, acrylics, stearates, and silicates and take the form of solvent-based or aqueous solutions which are generally spray applied to concrete surface at rates ranging from 2.5 to 5.0 m<sup>2</sup>/L. Sealers in this class generally penetrate more than 2 mm below the immediate concrete surface. Most sealers are not permanent, and periodic reapplications are necessary to maintain protective properties. These sealers can vary widely in their effectiveness, and rapid field techniques are needed to assess their ability to protect concrete.

Considerable laboratory testing on effectiveness of sealers has been carried out. In a study [ 1 ] funded by the National Cooperative Highway Research Program (NCHRP), a large number of sealers of various generic types were subjected to a battery of test procedures developed by the researchers. The procedures used in this report which have evolved into common use primarily utilize the ingress of chloride solutions (and subsequent chloride ion analyses) into the concrete as a measure of sealer effectiveness. In this respect, they are similar in principle to AASHTO T 259 procedures [ 2 ], although sample geometry, conditioning, and exposure differ enough so that substantially different findings may occur when the methods are applied to the same materials. Other laboratory evaluations of sealers using various techniques have been carried out by the Alberta Department of Transportation [ 3,4 ], the Ontario Ministry of Transportation [ 5 ], and a number of State highway agencies [ 6,7,8 ]. To-date, there has been no standardization activity in this area by ASTM.

A number of field studies of the effectiveness of penetrating sealers have also been reported. Rasouljan, et. al. [ 9 ] periodically obtained cores from five structures treated with silanes in 1981 and allowed to weather in northern and marine environments for 4 years. Results indicate that absorptions of cores gradually increased with time and were not much less than control (unsealed) samples in some cases. Depth of penetration of silanes was found to be 2 mm at most. In a somewhat more extensive study, the Minnesota Department of Transportation [ 10 ] evaluated nine products on a bridge deck overlaid in 1983 with low-slump dense concrete. After 3 years of sampling, the most effective products included an oligomeric alkoxy-silane and a penetrating epoxy. Other products lost effectiveness within the 3 year test period. A similar study was carried out by the Pennsylvania Department of Transportation [ 11 ], in which seven sealants were applied to the deck, sidewalks, and parapets of a bridge constructed in 1984. Sampling for chloride contents spanned a 4 year period. Only one penetrating sealer (a resin in mineral spirit formulation) was found to be as effective as conventional linseed oil treatment in reducing chloride ion penetration when compared to untreated sections. In view of these somewhat conflicting results, it is apparent that a rapid means of determination of sealer effectiveness via an in-situ non-destructive test is sorely needed. Development of two such field methods is the subject of this paper, which is taken from a report published by the Strategic Highway Research Program [ 12 ]. Only summary results are presented in this paper, readers wishing to access the full set of data generated during the SHRP study are advised to obtain the referenced SHRP report.

## LABORATORY RANKING OF SEALER EFFECTIVENESS

### Preparation of Test Specimens

Test specimens were prepared for two purposes. First, to serve as concrete substrates onto which sealers could be applied and subsequently tested using laboratory procedures in common practice, such as NCHRP 244 Series II [ 1 ] and AASHTO T 259 [ 2 ]. Secondly, the sealed concrete specimens were also used for development and trial of the two new field test procedures.

The mix proportions for the test concrete are shown in Table 1. Aggregates used were a chloride-free siliceous gravel having a maximum size of 19 mm and a chloride-free siliceous sand with a fineness modulus of 3.0. A Type I (low alkali) cement was used in the mixtures. A 2 percent aqueous solution of neutralized Vinsol resin was used as an air-entraining admixture. All mixtures fell within the selected slump range of  $75 \pm 25$  mm and  $6 \pm 1.5$  percent air content.

TABLE 1 -- Mixture proportions for concrete test mixtures.

Quantities, kg/m <sup>3</sup>					
Cement	Sand	Gravel	Water	Water - Cement Ratio	Admixture mL/kg
270	878	1046	136	0.50	3

Two types of concrete test specimens were cast. The first type, produced primarily for NCHRP 244 Series II testing, consisted of 100 mm cubes. The second type, produced for AASHTO T 259 ponding and for evaluation of prototype field methods, consisted of 305 x 305 x 75 mm slabs. A total of six batches of concrete were prepared with six cubes and two slabs being produced from each batch. All specimens were covered with wet burlap and polyethylene sheeting immediately after casting and finishing was completed. After 24 hours all specimens were demolded and placed into separate heavy-duty polyethylene bags for a period of 28 days. After this storage period, one-half of the specimens were placed into an environment maintained at  $23 \pm 1.7$  °C and  $50 \pm 5$  percent relative humidity. This was denoted as "Set A". The remaining specimens ("Set B") were removed from the storage bags and subjected to one of the following moist cycles, depending on whether cubes or slabs were used. Cubes were placed into a moist room of the type used to cure concrete specimens for a 8 hour period at weekly intervals. When not in the moist room they were stored in the same environment as Set A. Slabs were placed on masonry blocks in a horizontal position, and the top surfaces covered with wet burlap and soaked twice during one day at weekly intervals. The burlap covering was removed the day following each soaking day in the cycle. All specimens were given a light sandblast (just enough to remove surface paste) 14 days after removal from the polyethylene bags. Cubes were sandblasted on all faces, slabs were sandblasted on the finished face only.

Five penetrating sealers were chosen for use in the development program. These were coded from 1 through 5. Generic descriptions of the sealer compositions were provided by manufacturers. The sealers were chosen so as to represent the most commonly used types of penetrating sealers. Materials which function primarily as surface

coatings, or materials whose primary application is for sealing of cracks were not included in the program. Sealer codes and generic descriptions are given in Table 2.

TABLE 2 -- Penetrating sealers used in method development.

Code	Generic Description
1	40% isobutyltrimethoxy silane in isopropanol
2	20% oligomeric alkyl-alkoxysiloxane in mixture of mineral spirits, naphtha, and diacetone alcohol
3	40% alkylalkoxy silane in water
4	water-based sodium silicate solution
5	two-component solvent-based epoxy penetrant
6	control - no sealer applied

All sealers were brush applied, the brush being pre-saturated with sealer prior to application to reduce errors due to retention of sealer on the brush. Sealers 1, 2, 3, and 5 were applied in single coats. Sealer 4 was applied in 2 coats, the surface being allowed to dry between coats. Application rate for sealers 1, 2, and 3 was 3.0 m<sup>2</sup>/L and for sealers 4 and 5 was 3.7 m<sup>2</sup>/L. For set A specimens, sealers were applied 21 days after removal from the polyethylene bags. For set B specimens, sealers were applied 15 weeks after commencement of the moist cycling regimen.

#### NCHRP 244 Series II Testing

Series II testing was applied to cubes prepared from Set A and Set B concretes. Testing was initiated on Set A specimens ten days after application of sealers. Testing was initiated on Set B specimens after an additional five moist cycles had been accrued subsequent to application of sealers. Series II procedures were followed for all specimens. Rankings were established based on mass of chloride ion penetrating the specimens over the 42 day exposure period. Complete test data are given in the full SHRP report [ 12 ] on which this paper is based.

For Set A, the following ranking, in order of sealer effectiveness, was assigned.

Sealer 2 > Sealer 1 > Sealer 3 > Sealer 5 > Sealer 4 > Control

For Set B, the following ranking, in order of sealer effectiveness, was assigned.

Sealer 1 ≈ Sealer 3 > Sealer 2 > Sealer 5 > Sealer 4 > Control

In both cases, the most effective sealers were of the alkyl-alkoxy silane and siloxane categories. Epoxy was generally less effective by a factor of 2 or more, and silicate was essentially ineffective, differing only marginally from behavior of unsealed specimens.

### AASHTO T 259 Testing

AASHTO T 259 testing, commonly referred to as "90 day ponding", was applied to slabs prepared from Set A concretes. After 90 days of ponding a 3% sodium chloride solution on the slab surfaces the solution was removed, and drill samples obtained and analyzed for total chloride content. The following ranking, in order of sealer effectiveness, was assigned.

Sealer 1 > Sealer 3 > Sealer 2 > Sealer 5 > Sealer 4 > Control

While position of individual sealers within the rankings differ between the T 259 and Series II results, the relative performance of the broad classes of sealers remains the same. That is, silanes and siloxanes reduce chloride penetration more than the epoxy and silicate sealers tested. These results, then, were used as bases of comparison for results obtained from the more rapid field techniques under development.

## **SURFACE ABSORPTION TEST DEVELOPMENT**

### Test Device

The device used for surface absorption testing of sealed concretes was based on equipment used for RILEM procedure II.4 [ 13 ] for testing water resistance of masonry units. The device used for testing horizontal surfaces consists of a polycarbonate water reservoir having a 75mm diameter contact area with the concrete surface. A capillary tube having a 3mm inner diameter is threaded into the top end of the reservoir. The cell is affixed to the concrete surface by using a blend of modeling clay and axle grease ( 5 gm grease to 50 gm clay) rolled into a cylindrical shape and cut and fit to the circumference of the bottom of the cell. A version of the device which could be used for testing vertical surfaces was also constructed. Detailed drawings of both devices are given in the SHRP report [ 12 ].

The test is conducted by allowing water to flow from an external reservoir into the base unit until the water column is filled to a height of approximately 400 mm. The intake tube is then closed, and the column drop monitored as a function of time over a 10 minute period.

### Results

A series of Set A slabs was conditioned at pre-selected temperatures and subjected to the surface absorption testing. Results are given in Table 3.

TABLE 3 -- Results of surface absorption testing at various temperatures.

Sealer	Column drop (mm) in 4 minutes at indicated temperature			Column drop (mm) in 10 minutes at indicated temperature		
	3 °C	23°C	40 °C	3 °C	23°C	40 °C
none	49	45	30	92	80	55
1	1	7	1	3	10	2
2	1	6	2	3	7	4
3	3	13	2	5	17	2
4	35	30	22	70	50	43
5	5	7	6	11	13	12

The results follow the general trends seen in the comparison testing, with the exception that the epoxy sealant (sealer 5) was somewhat more effective in this test than in the tests carried out on cube specimens. However, the distinction between the unsealed concrete, concrete sealed with an ineffective product (sealer 4), and concrete treated with penetrating sealers is readily discernable.

Though there are some differences caused by temperature, the general pattern of the data remains fairly consistent. Examination of the results led to the following suggested preliminary criteria for interpretation of test results, with those values obtained using either silicate or no sealer being representative of "poor" sealers, and those values obtained using the other 4 sealers being chosen as representative of "good" sealers:

Column Drop (mm) in 4 Minutes

<10: Good Sealer  
>20: Poor or no Sealer

Column Drop (mm) in 10 Minutes

<20: Good Sealer  
>40: Poor or no Sealer

## ELECTRICAL RESISTANCE TEST DEVELOPMENT

### Test Equipment and Procedure

Electrical resistance testing has been used to assess the integrity of membranes applied to bridge deck surfaces. In this test procedure, covered by ASTM Test Method for Electrical Resistivity of Membrane-Pavement Systems (D 3633), a copper plate is placed onto a wetted sponge placed on the surface of the deck. An electrical connection is made to the reinforcing steel in the top mat of the deck. The electrical resistance between the top mat and the copper plate is then measured by an ohmmeter. A high value (typically greater than 500 k-ohm) indicates that the membrane is functioning essentially as a dielectric material. Attempts to apply this technique to surfaces treated with penetrating sealers has not been successful, primarily because only a very small thickness of concrete is actually affected by the sealer, and the total resistance measured mainly reflects the resistance of the body of unsealed concrete. A technique more sensitive to the sealed surface zone of the concrete was needed.

It was felt that by placing relatively thin electrodes a small distance apart on the surface of the concrete, the effective volume of measurement could be confined to the near surface zone. To evaluate this configuration, two strip electrodes were created on a concrete surface by masking off an area 3 mm wide by 100 mm long, and creating two 6 mm wide strips of silver conductive paint (spray applied) on either side of this strip. The paint was applied in three layers, drying for 5 minutes between each layer using a 1500W hand-held dryer. Low end-to-end resistance ( $< 50$  ohms) of the paint strips were achieved after surface temperatures reached  $50^{\circ}\text{C}$ . Resistance across the 3 mm wide concrete test area was then measured using a soil resistance meter (maximum range = 1.1 meg-ohm) in 2-pin mode. Because of the high readings obtained (normally in excess of 100 k-ohm), lead resistance was negligible. The test area was then wetted with a hand-held sponge for a period of five minutes and excess water removed from across the 3 mm strip with a towel to prevent shorting of the electrodes. Five minutes after initial contact of the surface with water the first readings were taken. Readings were taken over a test period of four minutes.

The technique was applied to Set A and Set B slabs. Results are shown in Figures 1 and 2. For control and Sealer 4 slabs resistance remains fairly constant at low values for the four minute test period. For slabs treated with the more effective sealers resistance rises quickly to a high value. We have interpreted this behavior as representing evaporation of the small amount of water which penetrates (or initially forms a very thin film) on the concrete surface. The less water that penetrates, the more quickly it can evaporate from the surface, and the more rapid the resistance rise.

To examine the applicability of the test to specimens which have been exposed to deicing or marine salts, resistance gages were applied to a series of test slabs previously ponded with 3% sodium chloride solution for 90 days. The behavior of resistance versus time for these slabs is shown in Figure 3. As in the testing on specimens not exposed to chloride salts, both control and slabs treated with sealer 4 showed low resistance throughout the test period. In this case the slab treated with sealer 5 (epoxy-based sealer) also exhibited resistance levels below 200 k-ohms throughout the period of test. This variable performance of epoxy had been noted previously, and might be due to the fact that it is not a true penetrating sealer, as significant amounts of material remain on the surface. This may form a variable surface depending on application technique and inhomogeneities in the surface.

From analysis of these data, it was found that if a criterion of 200 k-ohm at 4 minutes were selected, acceptable sealers (i.e. sealers 1, 2, and 3) would exhibit values exceeding this criterion in 97 percent of the cases included. Therefore a criterion of at least 200 k-ohm after 4 minutes of drying was selected as the value to use when interpreting results results obtained using this electrical resistance test.

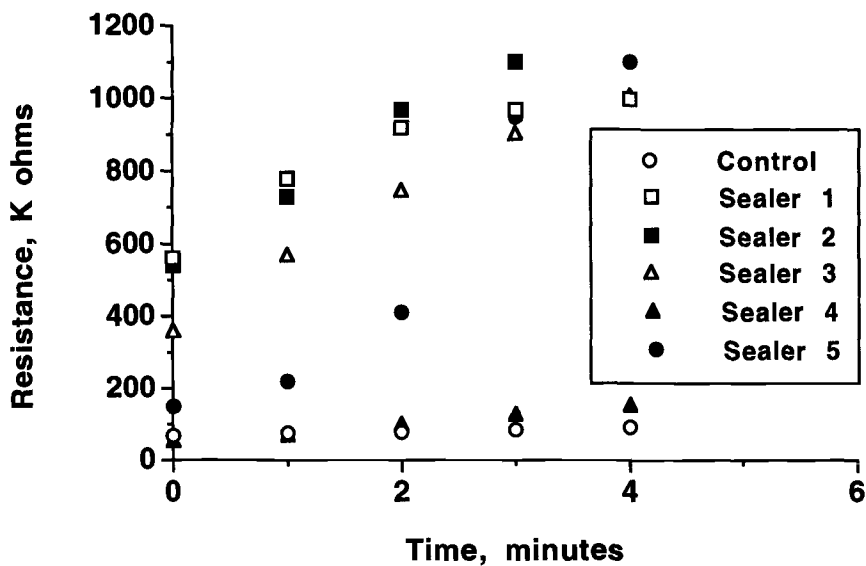


FIG. 1 -- Electrical resistance test results on Set A slabs.

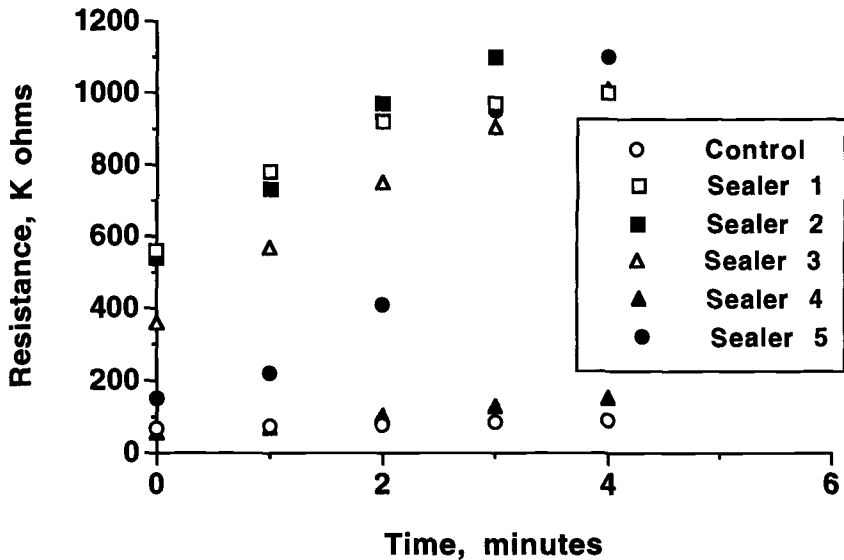


FIG. 2 -- Electrical resistance test results on Set B slabs.

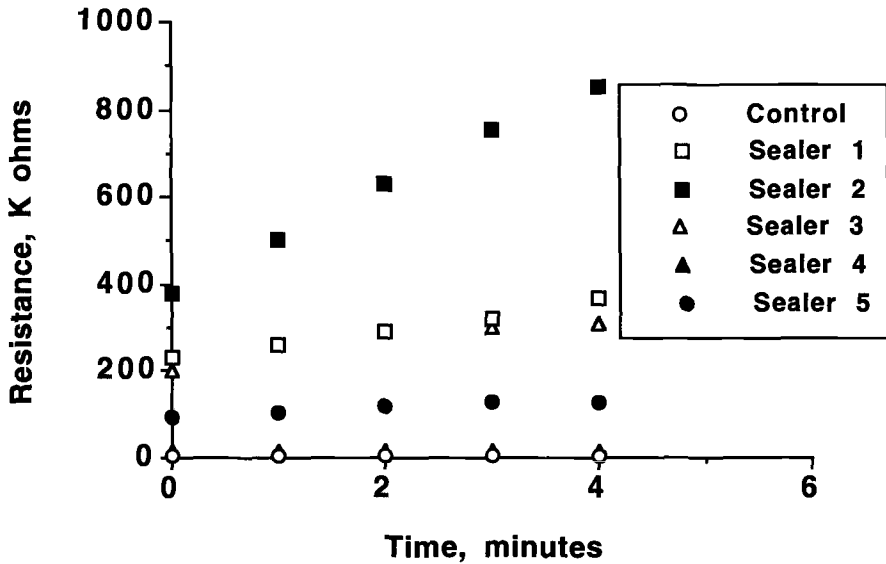


FIG. 3 -- Electrical resistance test results on slabs exposed to 3% sodium chloride solution.

## FIELD EVALUATIONS

In order to evaluate the techniques under actual test conditions, and to obtain some indication of their ability to discriminate between effective and non-effective sealers on actual structures, a series of field trials was carried out. The primary purpose of these field trials was to evaluate the applicability of the methods under a variety of conditions to be expected in the field. Due to the absence of standard field techniques for assessing the on-site effectiveness of penetrating sealers, it was not possible to make an absolute assessment of the accuracy of the methods in the field. Field trials were carried out under winter, spring, and summer conditions. Trials carried out under winter conditions in Vermont were unsuccessful, due to the inability of achieving a seal to the surface with the surface absorption method, and the high winds and cold substrate temperatures which prevented formation of adequate silver surface electrodes for the electrical resistance technique. Subsequent trials were carried out on bridges on Rt. 101 in Santa Barbara, California and I35E in St. Paul, Minnesota under more temperate conditions.

### Rt. 101 - Santa Barbara County, California

Penetrating sealers had been applied to a series of bridge structures in Santa Barbara County which had experienced distress due to alkali-silica reactivity (ASR). The intent was to reduce the interior relative humidity by allowing the sealer to transmit water vapor to the relatively dry ambient environment, while at the same time preventing liquid water from

entering the concrete during exposure to direct rainfall. The sealers were applied to the bridge support and substructures in 1988 and 1989, 2 to 3 years prior to testing. Three bridges on Route 101 were selected for testing. Illustrative field data on one of these structures are given in this paper, more detailed results can be found in the full SHRP report [ 12 ].

The first bridge selected carried Hollister Avenue over Rt. 101. During testing weather was clear, with average daytime temperature of about 18 °C and light winds. A total of eight locations were tested, which included tests on three of the piers, a concrete beam, and a wingwall. Results are presented in Table 4.

TABLE 4 -- Results of surface resistance testing at Hollister Avenue bridge.

Location	Resistance at 4 minutes, k-ohms
1 -Pier No. 1	340
2 -Pier No. 2	330
3 -Pier No. 2	950
4 -Pier No. 1	330
5 -Beam	58
6 -Beam	23
7 -Pier No. 3	240
8 -Wingwall	20

All 4-minute readings obtained on the piers exceeded the criterion of 200 k-ohms, indicating that the sealer was applied in these locations and should be effective. Readings obtained on the beam and wingwall indicate that the sealer had not been applied in these locations.

The surface absorption device was also tested at this site. Because water is used for both test methods, and because inadvertent wetting prior to test may interfere with each test, test locations for the absorption test were located a short distance away from those used for the resistance testing. Results are presented in Table 5.

TABLE 5 -- Results of surface absorption testing at Hollister Avenue bridge.

Location	Drop in capillary column (mm) at time indicated	
	4 minutes	10 minutes
1-Pier No. 1	5	9
2 -Pier No. 2	8	13
3 -Pier No. 2	13	51
4 -Pier No. 1	7	16
5 -Beam	14	34
8 -Wingwall	8	12

At location 3, while resistance readings were very high and indicated a particularly effective application, absorption results were indicative of a marginal or poor sealer. Close inspection of the test area after tests were completed indicated the presence of surface voids which may have led to the high results. At location 8 the resistance test indicated that no sealer had been applied, while the absorption test indicated the presence of sealer. The absorption test was carried out at a location considerably removed from the resistance test,

as it was necessary to carry out testing simultaneously in this area. It is possible that the applicators had simply not applied sealer to the location used for the resistance test.

### I 35E, St. Paul, Minnesota

The Minnesota Department of Transportation [ 10 ] evaluated nine sealer products on a bridge deck in St. Paul, Minnesota overlaid in 1983 with low-slump dense concrete. The bridge is located on I35E over Jefferson Avenue in St. Paul. The left (passing) lanes on both north and southbound sections were treated with the penetrating sealers the year following initial construction. A description of the products applied to the test sections is given in Table 6.

TABLE 6 -- Description of products applied to test sections on St. Paul bridge deck.

Product Description	Test Sections
40% Alkyl-alkoxy silane in ethanol Modified fluorosilicate in water	TS2, <u>TS18</u> TS10, <u>TS16</u>
Alkoxy-silane prime coat with methyl methacrylate polymer top coat	TS11, <u>TS17</u>
20% oligomeric alkoxy-silane in mineral spirits	TS8, <u>TS13</u>
20% methyl methacrylate-ethyl acrylate copolymer in toluene and xylene	<u>TS21</u>
50% solids epoxy (2-part)	TS4, <u>TS12</u>
40% alkyltrialkoxo silane in isopropanol	TS6, <u>TS22</u>
Alkyl-alkoxy silane	TS9, <u>TS15</u>
5% sodium methyl silanolate	TS5, <u>TS20</u>
Control (no sealer)	TS7, <u>TS14</u> , <u>TS19</u>

During the testing the weather was clear, with high temperatures near 30 °C. Temperature of the deck surfaces exposed to sun ranged from near 27 °C early in the day to over 38 °C in the early afternoon. Because of the hot deck surface, problems were encountered in application of the surface absorption method. Apparently, the high deck temperatures caused expansion of the water in the measurement column during the course of the test, resulting in near zero (and even negative) column drops. While resistance gage tests could be carried out the first day of testing, work with the surface absorption device was suspended until the following day, when testing was carried out earlier in the day to avoid the peak temperatures of the afternoon. Additionally, during the second day of testing the high deck temperatures on sections TS 20 and 21 resulted in unusually rapid heating of the resistance gages immediately after drying was initiated. This resulted in damage to the gages on these sections, and no readings were obtainable. Results of surface resistance testing on the eleven test sections selected are given in Table 7. Two sets of the silver electrode gages were applied to each section tested.

TABLE 7 -- Results of surface resistance testing at St. Paul bridge.

Location	Resistance at 4 minutes, k-ohms	
	Gage No. 1	Gage No. 2
TS 12	160	16
TS 13	172	150
TS 14 (control)	160	140
TS 15	470	160
TS 16	240	200
TS 17	145	182
TS 18	120	210
TS 19 (control)	155	120
TS 22	190	105

Most of the readings fall within the region (less than about 200 k-ohms) characterized by untreated concretes. This would indicate either that sealers had deteriorated over time, were initially ineffective, or that they had been worn away under traffic over the seven year exposure period. No distinction could be made between performance of the individual sealers, as all had apparently failed by this point in time.

On the second day, tests were carried out using the surface absorption device on nine of the test sections. Results are presented in Table 8.

TABLE 8 -- Results of surface absorption testing at St. Paul bridge.

Location	Drop in capillary column (mm) at time indicated	
	4 minutes	10 minutes
TS 13	4	5
TS 14	5	7
TS 15	6	7
TS 16	5	8
TS 17	3	4
TS 18	6	8
TS 19 (control)	4	7
TS 20	4	5

Results for all sections tested were very similar. Sealed sections performed no better than the control, corroborating results obtained using the resistance gages and substantiating the conclusion that the sealers were no longer effective on these test sections. However, all results obtained using the absorption device were very low, and indicative of properly sealed concrete, even for the control section. This discrepancy can be explained by the fact that the concrete used to place this deck was a low slump concrete with water-to-cement (w/c) ratio near 0.35, designed to reduce infiltration of chlorides into the deck. All previous work with the absorption device had been on more conventional concretes with higher w/c ratios. Therefore, this is seen as a limitation of the absorption technique, as the criteria established can only be applied if the concrete is of a conventional mix design.

## CONCLUSIONS

The two test methods developed are applicable under both laboratory and field conditions. While not nearly as quantitative as standard laboratory techniques, the new methods are able to rank sealers in approximately the same order of effectiveness towards reduction of chloride ion ingress as long term testing. The major advantages of the new methods are that they can be used on in-place concrete structures, and are relatively simple and inexpensive to conduct.

There are a number of limitations which must be considered when attempting to carry out the testing under field conditions. Both methods require an initially dry surface, therefore the methods cannot be carried out under wet conditions. This is not a large problem with the resistance method, as drying is included as a standard part of the method. Under extremely cold conditions the clay/grease seals used to affix the surface absorption reservoirs to the surface do not bond properly, and it is difficult to achieve a good seal. Likewise, the conductive paint used in the resistance method dries very slowly in cold conditions, and the drying regimen may need to be lengthened. Conversely, a hot surface may cause expansion of the water in the capillary column and lead to erroneous readings. Drying of the conductive paint in the resistance method must be carefully monitored under hot conditions, else temperature excursions above the recommended surface drying temperature may be experienced. Finally, windy conditions may make it difficult to apply uniform coatings of paint, and may require the use of more paint than originally intended.

## ACKNOWLEDGEMENTS

This research was funded by the Strategic Highway Research Program (National Research Council), through a subcontract from the Pennsylvania State University. The publication of this article does not necessarily indicate approval or endorsement by Penn State, the National Academy of Sciences, the United States Government, or the American Association of State Highway Transportation Officials, (or its member states), of the findings, opinions, conclusions, or recommendations either inferred or specifically expressed herein. The authors would like to thank Dr. Philip D. Cady for advice and encouragement throughout the course of the study.

## REFERENCES

- [ 1 ] Pfeiffer, D.W. and Scali, M.J., "Concrete Sealers for Protection of Bridge Structures," NCHRP Report 244, Transportation Research Board, Washington, DC, December 1981.
- [ 2 ] "Standard Method of Test for Resistance of Concrete to Chloride Ion Penetration," AASHTO Designation: T259-80 (1990), pp. 769-770, American Association of State Highway and Transportation Officials, Standard Specifications for Transportation Materials and Methods of Sampling and Testing, Part II-Methods of Sampling and Testing, Washington, D.C., 1990.
- [ 3 ] Carter, P.D. and Forbes, A.J. "Comparative Evaluation of the Waterproofing and Durability of Concrete Sealers," ABTR/RD/RR-86/09, Alberta Transportation Research and Development Branch, Final Report 1984-86, October 1986.
- [ 4 ] Carter, P., "The Use of Penetrating Sealers on Concrete Bridge Decks", in Structural Materials, Proceedings of the Sessions Related to Structural Materials, ASCE

Structures Congress, San Francisco, CA May 1-5, 1989, J.F. Orofino, ed. pp. 292-302.

- [ 5 ] Rollings, R.M. and Chojnacki, B. "A Laboratory Evaluation of Concrete Surface Sealants-Phase II," MI-127, Ministry of Transportation of Ontario, November 1988.
- [ 6 ] Petty, D.A., "Laboratory Evaluation of Cement Concrete Sealers," Commonwealth of Massachusetts, Department of Public Works, Research and Materials Section, 1986.
- [ 7 ] Fernandez, N. "Evaluation of the Performance of Concrete Sealers," Iowa Transportation Department, Materials Section, February 1988.
- [ 8 ] Rutkowski, T.S. "Evaluation of Penetrating Surface Treatments of Bridge Deck Concretes," Final Report Research File No. 81-5, Research Unit, Materials Section, Division of Highways and Transportation Facilities, Wisconsin Department of Transportation, November 14, 1988.
- [ 9 ] Rasoulian, M., Burnett, C., and Desselles, R., "Evaluation of Experimental Installation of Silane Treatment on Bridges," FHWA /LA-87/207, Louisiana Department of Transportation and Development, Final Report, September 1981-April 1986.
- [ 10 ] Hagen, M.G., "Special Study 367- Extended Evaluation of Selected Experimental Bridge Deck Protective Systems-Concrete Sealers for Bridge Decks," Final Report, Physical Research Section, Office of Materials, Research, and Standards, Minnesota Department of Transportation, February 1988.
- [ 11 ] Ballew, J.W. and Highlands, K.L., "Evaluation of Protective Coatings to Reduce Penetration of Bridge Surfaces", Final Report, FHWA-PA-89-002+83-41, Engineering Technology Division, Bureau of Bridge and Roadway Technology, Pennsylvania Department of Transportation, February, 1989.
- [ 12 ] Whiting, D., Ost, B., Nagi, M., and Cady, P.D., "Condition Evaluation of Concrete Bridges Relative to Reinforcement Corrosion. Vol. 5: Methods for Evaluating the Effectiveness of Penetrating Sealers", SHRP-S-327, Strategic Highway Research Program, Washington, D.C., 1993.
- [ 13 ] "Recommended Tests to Measure the Deterioration of Stone and to Assess the Effectiveness of Treatment Methods", Test No. II.4, Water Absorption Under Low Pressure (Pipe Method), Materials and Structures, Vol. 13, No. 75, pp. 201-205, May-June, 1980.

Steven J. Ford<sup>1</sup> and Thomas O. Mason<sup>2</sup>

## COMBINED BULK AND INTERFACIAL STUDIES OF THE CEMENT/STEEL SYSTEM BY IMPEDANCE SPECTROSCOPY<sup>3</sup>

---

**REFERENCE:** Ford, S. J. and Mason, T. O., "Combined Bulk and Interfacial Studies of the Cement/Steel System by Impedance Spectroscopy," Techniques to Assess the Corrosion Activity of Steel Reinforced Concrete Structures, ASTM STP 1276, Neal S. Berke, Edward Escalante, Charles K. Nmai, and David Whiting, Eds., American Society for Testing and Materials, 1996.

**ABSTRACT:** Three arcs, corresponding to the bulk, interfacial, and electrode responses, are apparent in the impedance spectrum of cement paste / reinforcing steel systems. The 3-point impedance technique, without potentiostat, is capable of simultaneously and continuously monitoring these three responses over several orders of frequency (MHz-mHz). The high frequency (MHz) bulk arc provides such parameters as diffusivity and permeability of the paste, which in turn have implications for the ingress of corrosive species, such as chloride ions, known to greatly affect the corrosion rate of reinforcing steels. The double layer arc (Hz) provides insight into the nature of the near interfacial zone of the paste/ steel system, where the higher degree of porosity may affect corrosive behavior. The low frequency (mHz) electrode arc is related to the passive nature of the steel. Oxide film thickness can be inferred, as well as corrosion rates in active, passive, and pitting regimes.

**KEYWORDS:** impedance spectroscopy, cement, steel, diffusion, permeability, passivation, corrosion

---

<sup>1</sup>Research Assistant, Materials Science and Engineering Department, Northwestern University, Evanston, IL 60208.

<sup>2</sup>Professor, Materials Science and Engineering Department, Northwestern University, Evanston, IL 60208.

<sup>3</sup>This work supported by the Center for Advanced Cement-Based Materials under NSF grant DMS-91-20002.

Advances in impedance spectroscopy (IS) for the study of corrosion and materials microstructure are brought to bear on the study of the cement/steel system. IS reveals the condition of the interface, including the corrosion rate, as well as information concerning the microstructure (porosity, interconnectivity) of the cement. From the latter, transport properties important to steel reinforced concrete durability--i.e., diffusivity and permeability--can be estimated. Impedance spectroscopy is thus, a powerful tool for probing the overlayers and interfaces associated with steel reinforcements.

Recently, we have investigated the use of 3-point IS, without a potentiostat, over 10 orders of magnitude in frequency from mHz to 10 MHz. In Nyquist format (-imaginary vs. real impedance) three arcs are obtained in non-corroding steel/cement systems--an extremely large low frequency (Hz-mHz) electrode arc, a second, intermediate frequency (Hz) interfacial arc, and a smaller high frequency (kHz-MHz) bulk arc. From the impedance spectrum, the cement resistivity can be established. If saturated, the interconnectivity of the pore structure can be determined. Meaningful comparisons can be made with respect to the roles of admixtures on microstructure development. Using the Nernst-Einstein and Katz-Thompson equations, ion diffusivity and fluid permeability can be estimated, respectively. The intermediate frequency arc can be related to the role of the cement paste microstructure near the interface on the charge transfer/double layer process. From the electrode arc, the existence or absence of a passive oxide film can be immediately established. In addition, its materials aspects--thickness, dielectric constant, and resistivity--can be inferred. Using the Stern-Geary equation and published Tafel constants for iron, the rate of corrosion can be estimated on the basis of electrode resistance. The onset of pitting and active corrosion can be readily detected with IS.

In this paper we present a brief review of impedance spectroscopy, with past and present work using this technique to study the corrosive nature of cement-based systems. Because microstructural features on all levels in this system affect corrosion of reinforcing steel, it is obvious that the ability to monitor the complete system is advantageous for the study of these materials. The effect of changes in the different microstructural features, to the corrosion of reinforcing steel is presented.

## IMPEDANCE SPECTROSCOPY

### Theory

Impedance spectroscopy (IS) is an experimental technique which is becoming increasingly prevalent in the study of materials. The technique involves applying a sinusoidal excitation signal to the specimen of interest and recording the time-varying response. This is repeated over a large range of frequencies, and the gain and phase angle differences are analyzed. The impedance is analogous to the resistance in DC electrical measurements, and is governed by Ohm's law of the form:

$$V(t) = I(t) \bullet Z(\omega) \quad (1)$$

where  $V(t)$  and  $I(t)$  are the time varying voltage and current respectively, and  $Z(\omega)$  is the frequency dependent impedance. Because the impedance is a complex function, it can be divided into components as follows:

$$Z(\omega) = Z'(\omega) + jZ''(\omega) \quad (2)$$

where  $Z'(\omega)$  and  $Z''(\omega)$  are the real and imaginary parts of the total impedance  $Z(\omega)$ . A plot of these components in the real-imaginary plane is often used to analyze the response of a system. An example of a typical response is shown in Figure 1, for a simple, yet widely observed equivalent circuit network composed of a resistor and capacitor in parallel. The values for the circuit elements and other important system parameters are depicted in Figure 1 and are described below:

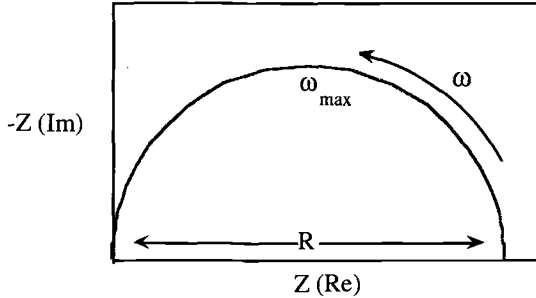


**FIG. 1.** Nyquist plot of a simple equivalent circuit consisting of a resistor and capacitor in parallel.

$R$  - The resistance of the system is defined by the diameter of the semicircle in the Nyquist plot.

$\omega_{\text{max}}$  - The frequency maximum of the impedance arc is the point at which the imaginary component is greatest. This value, in conjunction with the arc diameter, allow calculation of the capacitance of the system from the equation:

$$\omega_{\text{max}} = (RC)^{-1} \quad (3)$$

These values then allow the calculation of other material parameters such as resistivity, dielectric constant, and relaxation time.

Because the relaxation times for electrochemical and bulk reactions differ by orders of magnitude, IS is able to discern the responses, and a complete view of the system is possible. This does not mean, however, that the results are unambiguous. Often, when relaxation times are not vastly different, responses overlap one another and deconvolution is necessary. Arcs can also be suppressed below the real axis, in which case Eq.(3) is not strictly valid, and a "pure" capacitance value cannot be obtained.

### Application

In most solid state applications, IS measurements are made using a standard two electrode configuration in which the response signal is measured through the same electrodes used to apply the excitation signal. As described elsewhere [1], this approach has two main flaws with respect to analyzing the paste/steel system. First, the high frequency response is skewed by the presence of inductive effects from the leads which occur in the same frequency range ( $\approx$ MHz). This error can be reduced using a nulling procedure described elsewhere [2], but can seldom be entirely eliminated. The second limitation, however, is more directly relevant to the study of the corrosion of reinforcing steel. Because the impedance spectrum reflects the response of the complete system, both electrodes make contributions, and the electrode arc becomes a convolution of the two

responses. As can be seen in Figure 2, the assumption that the two electrodes are identical is not always appropriate, and analysis of the system is hindered.

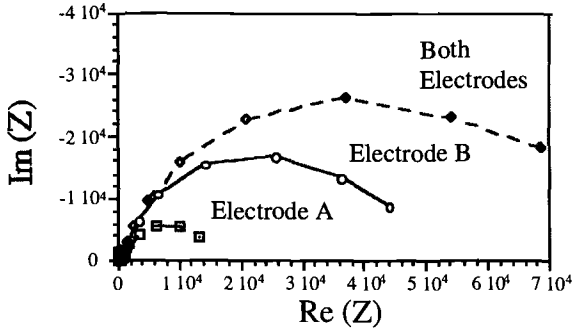


**FIG. 2.** Nyquist plot showing the response of an OPC/steel system, with dissimilar electrodes. Individual electrodes (A and B) were measured in 3-point configuration.

Three terminal measurements have been performed in the past, using a potentiostat, making analysis of a single electrode possible. A problem arises, however, when analyzing the paste/steel system, because potentiostats often interfere with high frequency IS measurements and limit the frequency range to below 50 or 100 kHz. Unfortunately, bulk cement responses occur in the MHz range, making a complete characterization of the system impossible. Recently, we have investigated the use of a three terminal technique without potentiostat [3]. This allows measurement of paste/steel systems over a frequency range of ten orders of magnitude (10 MHz - 1 mHz), encompassing the bulk and electrode effects. A typical 3-point impedance spectrum of an OPC paste with embedded, low carbon steel electrodes and a water to cement ratio (w/c) of 0.4, is shown in Figure 3. Three arcs are apparent, whose origins will be discussed more fully below.

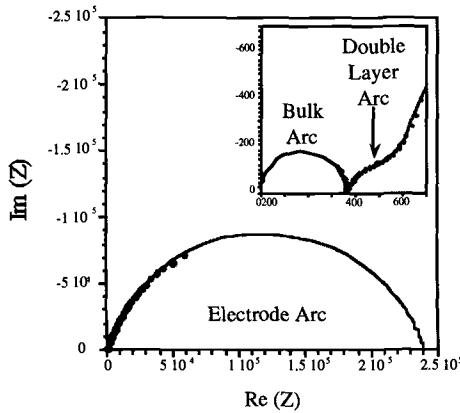


**FIG. 3.** Typical impedance spectrum for the cement paste/reinforcing steel system shown in Figure 4.

## EXPERIMENTAL PROCEDURE

Cement paste specimens were prepared with Type I OPC and distilled water. Specific water to cement ratios were obtained by mixing appropriate weights of OPC and distilled water in a Hobart planetary mixer for fifteen minutes at low speed. The paste was then cast in rectangular Plexiglas molds with dimensions  $2.54 \times 2.54 \times 10 \text{ cm}^3$  as shown in Figure 4. C-1018 steel electrodes of dimensions  $0.25 \times 1.90 \times 3.85 \text{ cm}^3$  were polished to a  $6 \mu\text{m}$  finish and cast in the paste perpendicular to the long axis of the bars. A geometric area of approximately  $5 \text{ cm}^2$  was immersed in the paste. The specimens were cured at 100% relative humidity in a chamber attached to the front of the impedance analyzer, ensuring a saturated microstructure.

Measurements were made with a Solartron 1260 Frequency Response Analyzer, with Z60 data collection software[4]. Coaxial cables with alligator clips were used for electrode connections, which were kept to a minimum length to reduce inductive effects. Copper wire, pressed into the surface of the specimens, was used as a reference electrode for 3-point measurements. The excitation signal was applied through the Generator Output and Input Current ports, and the "hi" and "lo" voltage ports were used as the sensing electrode connections. Excitation signals were kept to a minimum ( $<25 \text{ mV}$ ), and a frequency range from 10 MHz to 1 mHz was used for most measurements.

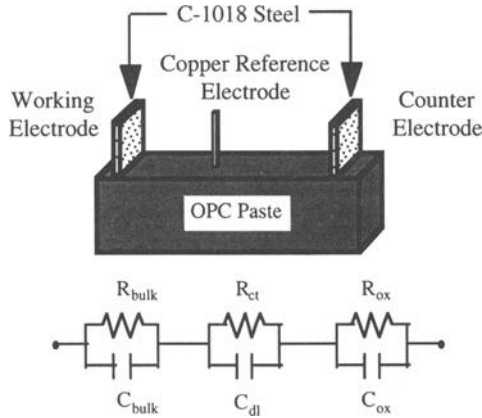


**FIG. 4.** Schematic of the cement paste bars used in the IS studies along with a simple equivalent circuit model representing the system.

## THE BULK ARC

The study of bulk properties is important in corrosion research, as it is the matrix through which corroding species must travel. Ingress of  $\text{H}_2\text{O}$ ,  $\text{CO}_2$ , and  $\text{Cl}^-$  to the reinforcing steel surface, are all contributing factors to the corrosion of reinforcing steel in cementitious systems. It would therefore be helpful to understand the transport properties in this class of materials. Impedance spectroscopy allows these properties to be monitored in-situ, in a non-destructive, non-invasive manner [5-10].

The low frequency intercept of the bulk IS arc, as shown in Figure 3, can be used to determine important engineering parameters such as permeability and diffusivity.

Microstructural changes during hydration can be monitored and characterized by the conductivity ( $\sigma$ ):

$$\sigma = \frac{l}{RA} \quad (4)$$

where  $l$  and  $A$  are the appropriate geometric factors and  $R$  is the bulk resistance. These parameters can then be used to characterize the bulk paste system.

One parameter of interest, because of its relation to the ingress of corrosive species, is diffusivity. The Nernst-Einstein equation, relating diffusivity and the normalized conductivity, is as follows:

$$\frac{\sigma}{\sigma_0} = \frac{D}{D_0} \quad (5)$$

where  $D$  is the diffusivity of the species of interest, and  $D_0$  is the intrinsic diffusivity in pure  $H_2O$  [11]. Thus, given the conductivities of the bulk material and pore solution, we can predict  $D$  for any ion, based upon published values of  $D_0$ .

Another important property of cementitious systems is permeability. It is a major consideration for durability predictions due to freeze/thaw cycles, as well as relating the ease by which corrosive species can migrate to the reinforcing steel surface. The Katz-Thompson equation has been used to predict the permeability of these systems, with input parameters from mercury intrusion porosimetry (MIP), as well as impedance spectroscopy. The relation, presented below, was initially developed for porous rocks [12], but has correlated well with cement paste systems [13].

$$k = \frac{1}{226} d_c^2 \frac{\sigma}{\sigma_0} \quad (6)$$

Here,  $k$  is the absolute permeability,  $d_c$  is a threshold pore diameter,  $\sigma$  is the total conductivity, and  $\sigma_0$  is the conductivity of the pore solution. Pore solution conductivity,  $\sigma_0$ , is determined in parallel measurements by expressing pore fluid and immediately measuring its conductivity [14]. Alternatively,  $\sigma_0$  can be estimated to  $\approx 10\%$  given the initial cement composition [15]. The threshold pore diameter is determined by MIP as the inflection point where mercury fully intrudes and percolates the paste. IS is used to determine the conductivities, with the predicted permeabilities agreeing with those measured by standard experimental values within an order of magnitude [13].

## THE INTERMEDIATE FREQUENCY ARC

Several researchers have described the existence of an intermediate frequency arc in corroding systems [16-19]. Previous reports have suggested that this arc is the response of corrosion products formed in the pores of cement systems [19]. We have shown, however, that this arc exists in synthetic pore solutions in the absence of paste [1], which suggests that it is associated with the charge transfer / double layer response. The presence of this response in passive systems also suggests that active corrosion need not be present for the feature to be observed [1, 18].

On the other hand, the intermediate frequency response mimics that of the bulk. As can be seen in Figure 5, the charge transfer resistance follows the same trend with hydration as does the bulk resistance. In contrast, the arc diameter in synthetic pore

solutions remains essentially constant with time [1]. Therefore, it would seem that the microstructure of the paste in the near interfacial zone has a direct effect on the intermediate frequency arc. This may explain why prior workers have attributed this arc to corrosion products formed near the interface.

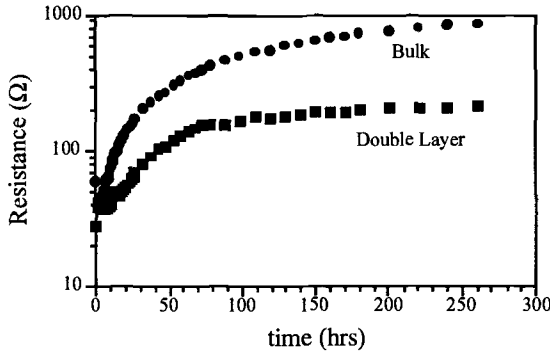


**FIG. 5.** Resistance versus time plots for the bulk and double layer arcs. Specimens were low carbon steel electrodes in normal OPC pastes with  $w/c = 0.4$ .

A simplified microstructural model is presented in Figure 6 to account for the similarity in the bulk and intermediate frequency responses with time. The impedance response of the system is measured via the conductive pore phase, so that, as the volume fraction of capillary porosity decreases with hydration, the effective area of pores adjacent to the interface also decreases. Similarly, corrosion products near the interface of actively corroding steel can modify the local microstructure and therefore, the intermediate frequency arc. The microstructure in the interfacial zone has

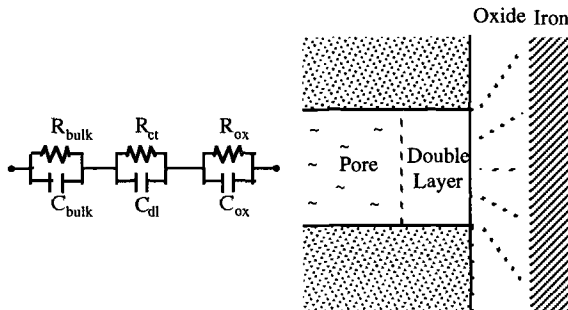


**FIG. 6.** Microstructural model for the OPC/steel system with an equivalent circuit network for modeling the typical impedance response of Figure 3.

been shown to be quite different from that of the bulk by several researchers [20, 21]. A higher degree of porosity has been shown to exist, which would have implications for the corrosion of reinforcing steel in cement paste, in that the diffusion of corrosive species could be much faster along this interface. Further studies of the intermediate frequency arc are ongoing in an attempt to quantify these observations.

**THE ELECTRODE ARC**

The low frequency impedance arc is of greatest interest in the study of corrosion in the cement paste/reinforcing steel system. Saturated cementitious materials are ideal hosts for reinforcing steels, providing a highly passivating environment. Problems arise when the matrix is subjected to wet/dry cycles and chloride ion ingress. Using impedance spectroscopy, the corrosive behavior of steel reinforcement under various environmental conditions can be assessed.

In the highly alkaline environment of cement pastes, a passive oxide film forms on the steel surface [22, 23]. This adherent film acts as a barrier to corrosion, slowing the process by several orders of magnitude. Using the Stern-Geary equation to relate the corrosion current,  $I_{corr}$ , and the polarization resistance,  $R_p$  [24]:

$$I_{corr} = \frac{b_a b_c}{2.303(b_a + b_c)} \frac{1}{R_p} \tag{7}$$

(where  $b_a$  and  $b_c$  are the anodic and cathodic Tafel slopes) in conjunction with Faraday’s law, the corrosion rate of the steel can be determined from IS measurements of  $R_p$ :

$$mpy = \frac{I_{corr} M}{neAN\rho} = \frac{8017}{AR_p} \tag{8}$$

using the appropriate values for iron. Here,  $M$  is the molecular weight,  $n$  is the number of equivalents,  $e$  is the electronic charge,  $A$  is the corroding area,  $N$  is Avagadro’s number, and  $\rho$  is the density of the material. Values obtained from IS show that it is quite easy to distinguish between the active and passive state. Corrosion rates on the order of 0.01 mils per year (mpy) are obtained for passivated iron in saturated cementitious systems assuming  $R_p \approx R_{OX}$ , while rates more than two orders of magnitude higher have been seen in cases where active corrosion is occurring [25]. Localized corrosion rates may be orders of magnitude higher still because the area undergoing pitting corrosion is so much smaller.

As stated above, a passive oxide film is thought to form on the steel surface in high pH environments (i.e. cement pore fluid). It is, however, very difficult to ascertain the exact structure of this film. Many hypotheses have been made ranging from single to multi-layered structures composed of iron oxides and hydroxides [23, 26, 27]. Impedance spectroscopy can be used to monitor this film more closely, in an attempt to determine its structure and its response to admixtures and different environments. Assuming a dielectric constant of 10 for the iron oxide, the thickness of this layer can be estimated based upon the electrode arc capacitance, as shown in Figure 7.

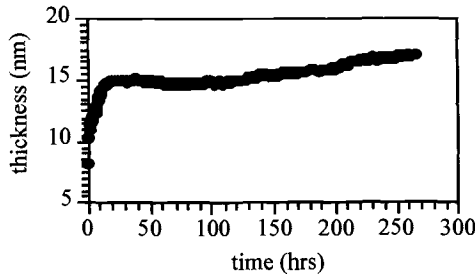


**FIG. 7.** Oxide thickness versus time for a low carbon steel in an OPC paste of  $w/c = 0.4$ .

It is stressed that this is at best an approximation, given the typical depression of the electrode arc and the supposed multilayer nature of the oxide film. The adherent film forms very rapidly, and stabilizes at a value of approximately 15 nm, consistent with prior reports [28, 29].

The transition from passivation, through pitting, to active corrosion can be readily followed using impedance spectroscopy. It is known that chloride salts greatly increase the corrosion of steel in concrete, although the mechanism by which this occurs is still unclear. As shown in Figure 8, the addition of  $\text{Cl}^-$  to a system where steel is immersed in synthetic pore solution greatly alters the impedance response of the steel. Initially, the pore solution simulates that of an OPC paste of  $w/c = 0.5$  at 100 hrs [2]. Upon addition of 2% NaCl by weight at  $t = 0$ , the resistance of the steel interface decreases rapidly. The decreasing electrode resistance signals the pitting of the oxide film and the onset of active corrosion.

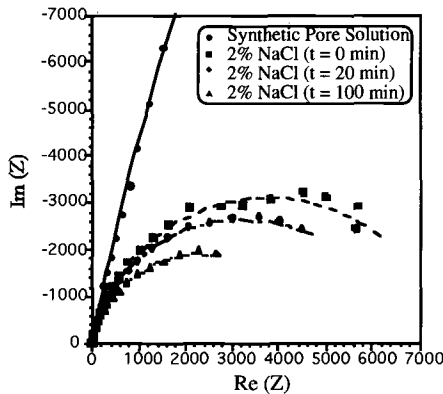


**FIG. 8.** Impedance spectra for a low carbon steel submerged in synthetic pore solution with NaCl additions.

## STEEL IN MORTARS AND CONCRETES

Current work is focused on extension of 3-point IS to the more complex mortar and concrete systems. Each of the three impedance arcs in the typical cement paste/reinforcing steel spectrum is expected to be altered by the addition of aggregates into the matrix.

In mortars and concretes, the paste is a continuous, porous body, surrounding the individual aggregate particles. Microstructurally, transition zones have been observed surrounding these particles [21]. Changes in the bulk arc are being examined to determine changes in such parameters as permeability and diffusivity with respect to the percolation of these near interfacial zones. The intermediate frequency double layer arc may also be affected by these changes, and may give even more insight into the microstructural nature of the transition zone.

Work focused on the electrode response will monitor the passive oxide layer with addition of aggregate particles in combination with various mineral and chemical admixtures including corrosion inhibitors. Changes in oxide chemistry and thickness will be emphasized to determine the effect of these additions on the corrosion resistance of reinforcing steels.

## CONCLUSIONS

Impedance spectroscopy is a useful tool for monitoring the corrosion rate of steel reinforcement in cement-based materials. In addition, such parameters as bulk paste diffusivity and permeability, interfacial zone porosity, and passive oxide thickness can be determined and related to the corrosive nature of a system before corrosion occurs. The study of these basic microstructural components can lead to a better understanding of the paste/steel system as a whole, and thus, to the underlying causes of reinforcement corrosion and to strategies for reducing this problem.

## REFERENCES

- [1] S.J. Ford, "Passivation Studies of the Cement Paste/Reinforcing Steel System Using Impedance Spectroscopy," M.S. Thesis, Dept. of Mat. Sci. and Eng., Northwestern University, Evanston, IL (1994).
- [2] B.J. Christensen, "Microstructure Studies of Hydrating Portland Cement-Based Materials using Impedance Spectroscopy," Doctoral Thesis, Dept. of Mat. Sci. and Eng., Northwestern University, Evanston, IL (1993).
- [3] S.J. Ford, T.O. Mason, B.J. Christensen, R.T. Coverdale, H.M. Jennings, and E.J. Garboczi, "Electrode Configurations and Impedance Spectra of Cement Pastes," Journal of Materials Science, **30**, 1217-1224 (1995).
- [4] Scribner Associates, Charlottesville, VA 22901 (1994),
- [5] W.J. McCarter, and R. Brousseau, "The A.C. Response of Hardened Cement Paste," Cement and Concrete Research, **20**(6), 891-900 (1990).
- [6] K. Brantervik, and G.A. Niklasson, "Circuit Models for Cement Based Materials Obtained from Impedance Spectroscopy," Cement and Concrete Research, **21**(4), 496-508 (1991).
- [7] C.A. Scuderi, T.O. Mason, and H.M. Jennings, "Impedance Spectra of Hydrating Cement Pastes," Journal of Materials Science, **26**, 349-353 (1991).
- [8] R.T. Coverdale, B.J. Christensen, H.M. Jennings, T.O. Mason, D.P. Bentz, and E.J. Garboczi, "Interpretation of Impedance Spectroscopy of Cement Paste via Computer Modelling. Part I: Bulk Conductivity and Offset Resistance," Journal of Materials Science, **30**(3), 712-719 (1995).
- [9] P. Gu, P. Xie, Y. Fu, and J.J. Beaudoin, "A.C. Impedance Phenomena in Hydrating Cement Systems: Frequency Dispersion Angle and Pore Size Distribution," Cement and Concrete Research, **24**(1), 86-88 (1994).
- [10] P. Gu, P. Xie, J.J. Beaudoin, and R. Brousseau, "A.C. Impedance Spectroscopy (I): A New Equivalent Circuit Model for Hydrated Portland Cement Paste," Cement and Concrete Research, **22**(5), 833-840 (1992).

- [11] E.J. Garboczi, "Permeability, Diffusivity, and Microstructural Parameters: A Critical Review," Cement and Concrete Research, **20**(4), 591-601 (1990).
- [12] A.J. Katz, and A.H. Thompson, "Quantitative Prediction of Permeability in Porous Rock," Physical Review B, **34**(11), 8179-8181 (1986).
- [13] B.J. Christensen, R.T. Coverdale, R.A. Olson, S.J. Ford, E.J. Garboczi, H.M. Jennings, and T.O. Mason, "Impedance Spectroscopy of Hydrating Cement-Based Materials: Measurement, Interpretation, and Application," Journal of the American Ceramic Society, **77**(11), 2789-2804 (1994).
- [14] B.J. Christensen, T.O. Mason, and H.M. Jennings, "Influence of Silica Fume on the Early Hydration of Portland Cements Using Impedance Spectroscopy," Journal of the American Ceramic Society, **75**(4), 939-45 (1992).
- [15] H.F.W. Taylor, "A Method for Predicting Alkali Ion Concentrations in Cement Pore Solutions," Advances in Cement Research, **1**(1), 5-17 (1987).
- [16] G. Reinhard, U. Rammelt, and K. Rammelt, "Analysis of Impedance Spectra on Corroding Metals," Corrosion Science, **26**(2), 109-120 (1986).
- [17] L. Lemoine, F. Wenger, and J. Galland, "Study of the Corrosion of Concrete Reinforcement by Electrochemical Impedance Measurement", N.S. Berke, V. Chaker, and D. Whittings, Eds., Corrosion Rates of Steel in Concrete, American Society for Testing Materials, Philadelphia (1990), ASTM STP 1065, pp. 118-133.
- [18] D.G. John, P.C. Searson, and J.L. Dawson, "Use of AC Impedance Technique in Studies on Steel in Concrete in Immersed Conditions," British Corrosion Journal, **16**(2), 102-106 (1981).
- [19] L. Hachani, C. Fiaud, E. Triki, and A. Raharinaivo, "Characterisation of Steel/Concrete Interface by Electrochemical Impedance Spectroscopy," British Corrosion Journal, **29**(2), 122-127 (1994).
- [20] M.N. Al Khalaf, and C.L. Page, "Steel/Mortar Interfaces: Microstructural Features and Mode of Failure," Cement and Concrete Research, **9**(2), 197-208 (1979).
- [21] A. Bentur, S. Diamond, and S. Mindess, "The Microstructure of the Steel Fibre-Cement Interface," Journal of Materials Science, **20**, 3610-3620 (1985).
- [22] M.J.N. Pourbaix, Thermodynamics of Dilute Aqueous Solutions, Edward Arnold & Co., (1949).
- [23] J.E.O. Mayne, J.W. Menter, and M.J. Pryor, "The Mechanism of Inhibition of the Corrosion of Iron by Sodium Hydroxide Solution," Journal of the Chemical Society, **46**(3), 3229-3236 (1950).
- [24] M. Stern, and A.L. Geary, "Electrochemical Polarization I. A Theoretical Analysis of the Shape of Polarization Curves," Journal of the Electrochemical Society, **104**(1), 56-63 (1957).

- [25] P. Rodríguez, E. Ramírez, and J.A. González, "Methods for Studying Corrosion in Reinforced Concrete," Magazine of Concrete Research, **46**(167), 81-90 (1994).
- [26] K. Noda, T. Tsuru, and S. Haruyama, "The Impedance Characteristics of Passive Films on Iron," Corrosion Science, **31**, 673-687 (1990).
- [27] F.P. Glasser, and K.K. Sagoe-Crentsil, "Steel in Concrete: Part II Electron Microscopy Analysis," Magazine of Concrete Research, **41**(149), 213-220 (1989).
- [28] H.H. Uhlig, and W.R. Revie, "Theories of Passivity," Corrosion and Corrosion Control: An Introduction to Corrosion Science and Engineering, John Wiley & Sons, New York, pp. 69-72 (1985).
- [29] H.A. Miley, and U.R. Evans, "The Passivity of Metals. Part VIII. The Rate of Growth of Oxide Films on Iron," Journal of the Chemical Society, **33**(2), 1295-1298 (1937).

## **Case Studies**

Paul D. Krauss<sup>1</sup> and Charles K. Nmai<sup>2</sup>

**PRELIMINARY CORROSION INVESTIGATION OF PRESTRESSED CONCRETE PILES IN A MARINE ENVIRONMENT: DEERFIELD BEACH FISHING PIER**

---

**REFERENCE:** Krauss, P. D. and Nmai, C. K., “Preliminary Corrosion Investigation of Prestressed Concrete Piles in a Marine Environment,” Techniques to Assess the Corrosion Activity of Steel Reinforced Concrete Structures, ASTM STP 1276, Neal S. Berke, Edward Escalante, Charles K. Nmai, and David Whiting, Eds., American Society for Testing and Materials, 1996.

**ABSTRACT:** Between the Fall of 1991 and Spring of 1992, a new fishing pier was constructed in Deerfield Beach, Florida, to replace a badly deteriorated pier that was demolished. The precast, prestressed concrete piles used in the construction of the new pier contained a water-based organic corrosion inhibitor consisting of amines and fatty acid esters. This inhibitor offers corrosion protection by reducing chloride ingress and by forming a protective film at the surface of embedded steel. In the Fall of 1993, a preliminary corrosion investigation of the piles was performed to assess the performance of the concrete used in the construction of the pier and to establish baseline values for future investigations. The techniques used included visual and half-cell potential surveys, and determination of chloride ion contents. Chloride ion contents at the reinforcing steel level were found to be well below that which would induce corrosion. Other types of testing and analytical techniques that may be used in future investigations to assess the performance of the piles and to predict their useful service life are also discussed.

**KEYWORDS:** chloride ions, concrete, corrosion, diffusion, half-cell potentials, marine environment, piles, prestressing strands, service life, visual survey

---

<sup>1</sup>Consultant, Wiss, Janney, Elstner Associates, Inc., 330 Pfingsten Road, Northbrook, IL, 60062  
<sup>2</sup>Technical Manager, Master Builders, Inc., 23700 Chagrin Blvd., Cleveland, OH 44122

Reinforced concrete marine structures are highly vulnerable to corrosion due to chloride ion attack, the severity of the attack being dependent on among other factors the prevailing climatic conditions. For example, reinforced concrete specimens exposed to a marine intertidal zones at Port Hueneme, California, were observed to have about one-third less corrosion compared to companion specimens at Key West, Florida [1]. The difference in the rate of corrosion was attributed to the lower water temperature of 56 to 64 °F (13 to 18 °C) at Port Hueneme compared to 78 °F (26 °C) at Key West [1].

The aggressiveness of the warm marine environment in Florida has led to the premature deterioration of numerous bridges and buildings along the coastline [2,3]. It has been reported that in the absence of special design procedures, typical Florida marine substructures exhibit visible signs of corrosion distress within about 12 years of exposure [2]. An investigation of a badly deteriorated fishing pier in Deerfield Beach, Florida, in 1988 indicated chloride ion contents ranging from 34 to 58 lb/yd<sup>3</sup> (20 to 34 kg/m<sup>3</sup>) in piles, and 20 to 41 lb/yd<sup>3</sup> (12 to 24 kg/m<sup>3</sup>) in bent caps [4]. The fishing pier was demolished and between the Fall of 1991 and Spring of 1992, a new fishing pier was constructed to replace it.

The new Deerfield Beach fishing pier consists of precast concrete compression piles, precast concrete pile bents, precast concrete beams and a wooden deck. The compression piles were 18 in. (460 mm) square in section and had a concrete cover of 3 in. (75 mm) over No. 5 gage spiral ties that encased twelve 9/16 in. (14 mm) diameter prestressing strands. The concrete mixture used in the manufacture of the piles contained 726 lb/yd<sup>3</sup> (431 kg/m<sup>3</sup>) of a Type I/II cement, 159 lb/yd<sup>3</sup> (94 kg/m<sup>3</sup>) of a Class F fly ash and 1 gal/yd<sup>3</sup> (5 L/m<sup>3</sup>) of a water-based organic corrosion inhibitor consisting of amines and fatty acid esters. As shown in Table 1, the specified water-cementitious materials ratio was 0.34 and the specified 28-day compressive strength was 5000 psi (34.5 MPa). Actual 28-day compressive strengths reportedly averaged 7000 to 7500 psi (48.3 to 51.7 MPa). The water-based organic corrosion inhibitor was not used in the pile bents and the beams.

A preliminary corrosion investigation of the piles was performed in the Fall of 1993 to assess the performance of the organic corrosion inhibitor-treated concrete and to establish baseline values for future investigations. The investigation consisted of a visual survey, a limited half-cell potential survey, drilling for concrete powder samples for chloride content determination, and coring to obtain samples for petrographic examination of the concrete and chloride content determination. The findings of this investigation are presented in this paper. Also included is a discussion of other testing procedures and analytical techniques that may be used in future investigations to assess the performance of the piles in the aggressive Florida marine environment.

**TABLE 1 -- Concrete Performance Data**

Cement, Type I/II	726 lb/yd <sup>3</sup>
Fly Ash, Class F	159 "
Fine Aggregate	940 "
Coarse Aggregate	1590 "
Water	300 "
Air-Entraining Admixture	0.5 fl oz/cwt
Retarding Admixture	2.0 "
High-Range Water-Reducing Admixture	12.0 "
Water-Based Organic Corrosion Inhibitor	1.0 gal/yd <sup>3</sup>
Water-Cementitious Materials Ratio	0.34
Slump	3 ± 1 in
Air Content	3 ± 1.5 %
28-day Compressive Strength	7000 - 7500 psi

(1 in. = 25.4 mm; 145 psi = 1 MPa; 1 lb/yd<sup>3</sup> = 0.7646 kg/m<sup>3</sup>; 1 gal/yd<sup>3</sup> = 5.0 L/m<sup>3</sup>; 1 fl oz/cwt = 65.2 mL/100 kg)

## VISUAL SURVEY

In situations where examination of the surface of a reinforced concrete member is feasible, a visual survey is often useful in that it provides a quick assessment of distress within the member. Such distress is usually manifested in the form of rust staining on the surface, cracking and spalling. Depending on the extent of deterioration, "sounding" with a hammer can also be used to determine the presence and, to a degree, the extent of subsurface delaminations.

The first ten rows of piles, pile cap bents, and beams of the Deerfield Beach fishing pier nearest the beach were visually surveyed at close range from the beach and from the water. Because the pier extends several hundred feet into the sea, a boat was rented for use in surveying the end of the pier. Unfortunately, choppy waves prevented close inspection or sampling of the concrete near the end of the pier.

In general, the concrete was observed to be in excellent condition. The aesthetics of the piles were, however, marred by epoxy drippings and rust staining caused by exposed lift points, temporary supports, and steel plates fixed to the piles during construction. The outlines of the temporary steel plates were clearly visible and the rust stains, which did not originate from within the piles, could be easily removed from the surface by scraping. Rust staining caused by miscellaneous steel pieces in the concrete such as chair tips, small pieces of metal debris and lift points were also visible. Stains due to metal debris were limited to the bottom side of the piles as cast and could also be easily

removed by scraping. Larger areas of rust staining due to exposed metal pieces were observed on piles near the end of the pier.

Several piles also had rust stains near the top of the piles, in areas that appear to be associated with lifting hooks that were cut or burned off but not patched with epoxy. None of the observed rust stains in the fishing pier, which had been exposed to the marine environment for less than two years at the time of the investigation, could be related to corrosion of the embedded reinforcing steel or prestressing strands. This was confirmed later when coring exposed a section of the No. 5 gage spiral steel used for confinement of the concrete core. By means of a flashlight it was determined that the exposed wire was not corroding.

Local areas of chipped concrete, most likely due to handling, were also observed as were fine cracks on the top surface, as cast, of some of the piles. It is speculated that the cause of these fine cracks may be related to finishing or curing. Because of the fineness of the cracks and the corrosion-resistant high quality concrete used in casting the piles, a significant decrease in durability is not anticipated.

### HALF-CELL POTENTIAL SURVEY

A limited half-cell potential survey was performed on the center pile in the third row of piles to establish baseline readings. A silver-silver chloride reference half-cell electrode was used to obtain readings at each of several elevations on the east and west faces of the pile. The ground elevation was approximately 14 ft 9 in. (4.5 m) from the bottom of the pile cap. A measurement was taken 3 in. (75 mm) from each edge such that the silver-silver chloride half-cell electrode was directly over a corner strand, based on the reinforcing details obtained for the piles. The ground connection was made to a spiral steel that was exposed when a core sample was obtained from this pile.

The measured half-cell potentials (Table 2 and Fig. 1) show that potentials were high near ground elevation. This is not uncommon for noncorroding structures that are in contact with the sea or soil. The potentials decreased smoothly toward the pile cap, and at each elevation were consistent. Although the high potentials recorded near ground elevation are close to the free corrosion potential of steel exposed to seawater, approximately -670 mV versus the silver-silver chloride (Ag-AgCl) electrode [5], they are not an indication of active corrosion within the pile, but rather the saturation of the concrete due to direct contact with the seawater and the high electrical conductivity of the saltwater. This is supported further by the fact that there were no large deviations or sharp gradients in the measured potentials that would indicate active corrosion.

It should also be noted that the general criteria for interpretation of half-cell potentials measured in accordance with ASTM C 876, *Standard Test Method for Half-Cell Potentials of Uncoated Reinforcing Steel in Concrete*, are applicable only to structures that are not in direct contact with soil or seawater. In situations where oxygen

availability may be limited, such as in very wet concrete, the ASTM C 876 criteria have been reported to be unsatisfactory [6]. Under such conditions, potentials that are numerically greater than that which would typically indicate corrosion activity, can be obtained for noncorroding reinforcement.

**TABLE 2 -- Half-Cell Potentials for Center Pile, Bent 3**

ELEVATION (ft)	Half-Cell Potential (volts vs. silver-silver chloride)			
	EAST FACE		WEST FACE	
	North End	South End	North End	South End
11	-0.140	-	-	-
10	-0.174	-0.160	-	-
9	-0.184	-0.213	-	-
8	-0.213	-0.256	-	-
7	-0.252	-0.235	-0.218	-0.224
6	-0.255	-0.281	-0.241	-0.248
5	-0.288	-0.335	-0.301	-0.321
4	-0.346	-0.445	-0.357	-0.358
3	-0.484	-0.490	-0.474	-0.486
2	-0.564	-0.587	-0.560	-0.574
1	-	-	-0.620	-0.612

(1 ft = 0.3048 m)

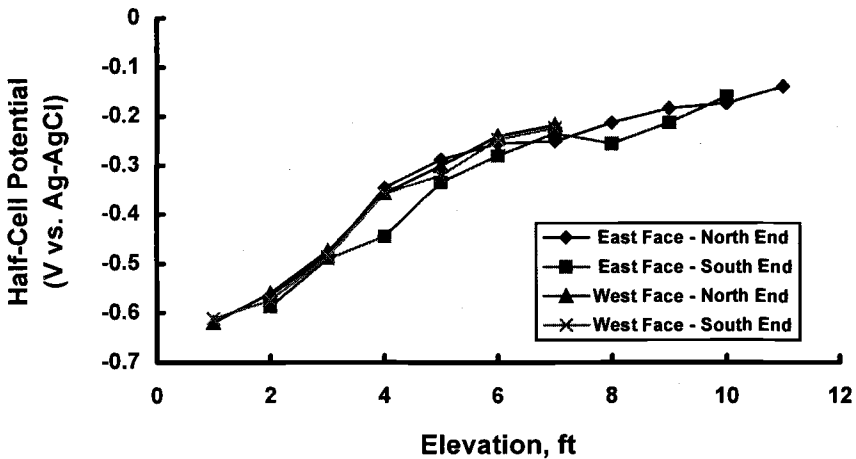


FIG. 1 -- Half-Cell Potential Data for Center Pile of Bent 3

## DETERMINATION OF CHLORIDE ION CONTENTS

Powder samples for chloride analysis were obtained by successive drilling with a rotary impact drill from four different locations. The first sample, designated B1C-E2, was obtained from the center of the east face of Bent 1 pile cap, 2 in. (50 mm) from the bottom of the cap. The second sample was taken from the east face of the center pile of Bent 1, two feet (0.6 m) below the pile cap. This sample was designated P1C-E2. Samples P2C-E3 and P2C-E7 were taken from the east face of the center pile of Bent 2, three and seven feet (0.9 and 2.1 m) below the bottom of the pile cap, respectively. The location from which P2C-E7 was taken is wetted by the sea during high tide. The other locations would be directly wetted only during extreme high tides or storms. They are, however, on the east faces exposed directly to the sea breeze.

To obtain the chloride profile at each location, powder samples were obtained at 3/4 in. (19 mm) depth intervals to a total depth of 3 in. (75 mm), the thickness of the concrete cover. The first 1/4 in. (6 mm) from the surface was, however, discarded. Also, the powder sample at each depth was obtained by combining powder samples from four adjacent 5/8 in. (16 mm) diameter holes. The chloride ion contents were determined by using an acid-soluble potentiometric titration procedure similar to ASTM C 1152, *Standard Test Method for Acid-Soluble Chloride in Mortar and Concrete*.

In addition to analyzing the powder samples, chloride ion contents were also determined from three 2 in. (50 mm) diameter cores that were taken from the piles. Core #1 was taken from the east face of the center pile of Bent 1 approximately one foot (0.3 m) below the bottom of the pile cap. This area is not in the tidal splash zone, however, direct contact with seawater during very high tides or storms is likely. Cores #2 and #3 were taken from the east face of the center pile of Bent 3, 7 ft 9 in. (2.4 m) and 9 ft 3 in. (2.8 m) from the bottom of the pile cap, respectively. This area is exposed repeatedly to wetting and drying due to intense splashing during high tide and drying during low tide. It is anticipated that the area from which Cores #2 and #3 were taken represent the most severe exposure for chloride intrusion and chloride-induced corrosion. A section of the No. 5 gage spiral steel was exposed at a depth of 3-3/8 in. (86 mm) when Core #2 was taken, thus verifying that the depth of concrete cover was as specified. As mentioned earlier, the wire was not corroding.

The chloride data, which are presented in Table 3, show that chloride ion contents decreased sharply with depth. The chloride ion content at the 1/4 to 3/4 in. (6 to 19 mm) depth was generally between 0.15 and 0.28 percent, except for P2C-E3 which was 0.417 percent. The higher chloride ion content at P2C-E3 may be explained by the fact that this section is subjected to more wetting and drying, and as such more capillary suction, compared to the section around P2C-E7 which may not experience much drying because of the extent of wetting during high tide. Differences in the amount of wetting and drying experienced may also explain why the chloride ion contents from Core #1, from the center pile of Bent 1, were slightly higher than those obtained from Cores #2 and #3 from the center pile of Bent 3.

**TABLE 3 -- Chloride Analysis Data**

SAMPLE ID	ACID-SOLUBLE CHLORIDE ION CONTENT (% by weight of concrete)			
	$1/4 - 3/4$ in.	$3/4 - 1$ in.	$1\frac{1}{2} - 2\frac{1}{4}$ in.	$2\frac{1}{4} - 3$ in.
<b><u>Powder Samples</u></b>				
B1C-E3	0.253	0.046	0.038	0.019
P1C-E2	0.165	0.019	<0.007	0.011
P2C-E7	0.231	0.046	<0.007	<0.004
P2C-E3	0.417	0.063	0.011	0.010
<b><u>Core Samples</u></b>				
Core #1	0.280	0.038	<0.007	<0.004
Core #2	0.202	0.012	<0.007	<0.007
Core #3	0.160	0.008	<0.007	<0.007

(1 in. = 25.4 mm)

The data also show that the chloride ion contents of the samples from the pile cap of Bent 1, B1C-E3, were greater than those from the pile directly below it, P1C-E2. The samples from the pile cap also had the highest chloride contents at the 1-1/2 to 3 in. (38 to 75 mm) depths compared to all the other samples including the cores taken from the splash zone area of the center pile of Bent 3. Of the members sampled, the pile cap is the least likely to have direct contact with seawater because it is above the high tide level. Therefore, the limited sampling indicates that the pile cap may be more permeable to chloride ingress compared to the piles.

A water-based organic corrosion inhibitor was used in the concrete for the piles but not in that for the pile caps. This inhibitor has been reported to function by reducing the ingress of chloride ions into concrete and by forming a protective film at the surface of embedded steel [7]. Therefore, the difference in the chloride ion contents of the samples from the piles and the pile cap may be attributed to the use of this inhibitor in the concrete for the piles. A plot of the average chloride ion content versus depth for all the samples obtained from the piles (that is, for the concrete treated with the water-based organic corrosion inhibitor) is shown in Fig. 2.

Also shown in Fig. 2 is the chloride ion content that would be required to initiate corrosion of mild steel embedded in plain concrete (dotted line), based on the generally accepted corrosion threshold value of 0.2 percent acid-soluble chlorides by weight of cement, and the cement content of the concrete mixture (see Table 1). The figure shows that the chloride ion content at a depth of 3 in. (75 mm), which is the depth to the reinforcing steel in the piles, is well below that which would induce corrosion of mild steel in plain concrete. As will be discussed later, prestressing strands such as that used in the piles can tolerate much higher concentrations of chloride ions without corroding.

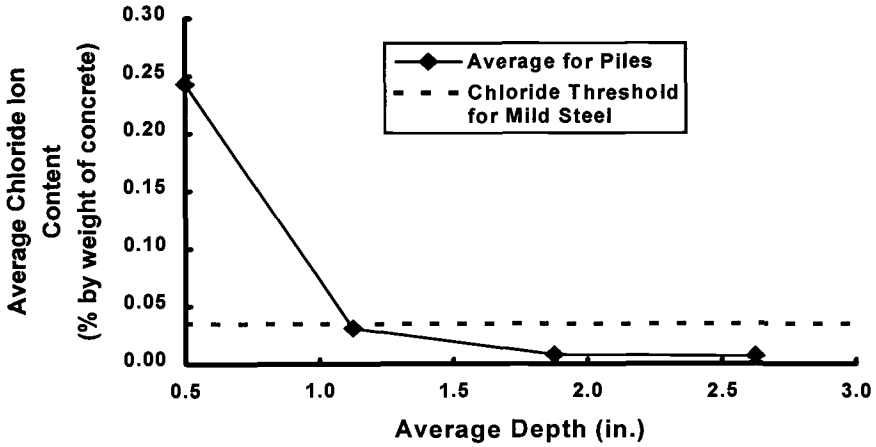


FIG. 2 -- Average Chloride Ion Content for Pile Samples

**PREDICTION OF USEFUL SERVICE LIFE**

The useful service life of a reinforced concrete structure in a marine environment is a function of several factors including chemical attack of the concrete by the seawater and corrosion of the embedded reinforcing steel. However, in the discussions that follows, only deterioration due to chloride-induced corrosion of the reinforcement will be considered.

For a reinforced concrete structure, the useful service life due to chloride-induced corrosion will be the sum of the initiation period and the number of years before deterioration reaches an accepted damage level [8]. The initiation period is dependent on how long it takes for chloride ions to build up to the threshold value for steel. It is influenced by several factors, some of which are described below.

Concrete Cover

The thicker the concrete cover, the longer it will take for chloride ions to penetrate to the level of the reinforcing steel; and hence, the longer the time to corrosion initiation. As verified during coring, the piles had a concrete cover of 3 in. (75 mm).

Permeability of the Concrete

The permeability of the concrete is influenced by the mixture proportions, in particular, the amount and type of cement and pozzolanic material used, the water-cementitious materials ratio, and the degree of curing. Admixtures such as the water-based organic

corrosion inhibitor will also reduce concrete permeability. The less permeable the concrete, the longer it will take for chloride ions to penetrate to the level of the reinforcing steel; and hence, the longer the time to corrosion initiation. Chloride ions can also be bound in the concrete matrix, the degree of binding being dependent on the type and amount of cement and pozzolanic material used.

Petrographic examination of cores obtained from the piles revealed that the cement paste was dark gray, hard and dense, and that the concrete had a low water-cementitious materials ratio and was of good quality. Therefore, it is expected that the concrete will have low permeability.

### Chloride Threshold Value

The chloride threshold value is dependent on the type of steel reinforcement, the binder system and also the presence, if any, of a corrosion inhibitor in the concrete mixture. It is generally accepted that the chloride threshold value for mild steel in plain concrete is within the range of 1.2 to 1.5 lb/yd<sup>3</sup> (0.7 to 0.9 kg/m<sup>3</sup>) of concrete. Although this value is often assumed to be applicable to prestressing strands, time-to-corrosion studies have shown that the chloride threshold for unstressed prestressing strands may be as much as six times that for mild steel [9]. This may be due to a couple of factors. First, prestressing strands have a smooth drawn surface that is less susceptible to corrosion. Second, prestressing strands may possess an unintentional corrosion protection system imparted by lubricants that are commonly used to coat them during the manufacturing process. The lubricants are typically zinc phosphate or calcium stearate materials.

The use of a corrosion inhibitor in the concrete mixture will also increase the chloride threshold value. The increase, however, will be dependent on the type and amount of inhibitor used. Because the piles for the Deerfield Beach Fishing Pier are reinforced with prestressing strands and were manufactured from concrete containing a corrosion inhibitor, the chloride threshold, though unknown, is expected to be much higher than 1.5 lb/yd<sup>3</sup> (0.9 kg/m<sup>3</sup>).

### Chloride Exposure Conditions

For a given concrete in a marine environment, the amount of chloride ions that will penetrate the concrete is influenced by several factors including: proximity to the seawater; surface chloride ion concentration; concentration of chloride ions within the concrete; and wetting and drying conditions at the affected area, which will influence the transport mechanism for the chloride ions. Whereas diffusion may be the transport mode in the submerged area, in the splash zone area it is more likely a combination of absorption, capillary suction and diffusion. A reasonable estimate of the time to corrosion initiation in the piles can be obtained by using analytical techniques such as the standard solution for Fick's diffusion equation for a semi-infinite slab, Eq. 1.

$$C = C_o \{1 - \text{erf}[x / (2\sqrt{D_{\text{eff}} \cdot t})]\} \quad (\text{Eq. 1})$$

where,  $C$  = chloride ion concentration at time,  $t$ , and depth,  $x$ ,  
 $C_o$  = surface chloride ion concentration, and  
 $D_{\text{eff}}$  = effective chloride diffusion coefficient.

This process requires knowledge of the thickness of the concrete cover, the chloride diffusion coefficient for the concrete, and the chloride threshold value. For a given chloride distribution, an effective chloride diffusion coefficient can be determined using the above equation. The chloride build up over time at the level of the reinforcing steel can then be predicted, and from that the time to corrosion initiation. The Deerfield Beach Fishing Pier piles will be sampled at periodic intervals to determine chloride levels and the chloride diffusion coefficient over time.

Next, the number of years before deterioration reaches an accepted damage level has to be determined. This value is dependent on several factors, the most important of which are rate of corrosion and what is considered acceptable with regard to damage. Several electrochemical devices for determining the rate of corrosion in field structures have been developed [10-13]. Some of these are based on the linear polarization and at least one is based on the principle of superimposed current pulses of high and low frequency with current confinement. These devices have been reported to give comparable qualitative results for actively corroding structures. However, significant differences in magnitude of measured corrosion currents can be obtained [14].

An acceptable damage level has to be established for a realistic estimation of service life. The criteria selected may be based on aesthetic or structural considerations depending on the intended use of the structure. Also, it should be dependent on the type of structure or member; for example, prestressed versus nonprestressed. This is because whereas a certain percentage reduction in steel area may be tolerable in a nonprestressed structure, such reduction in a prestressed concrete structure can lead to catastrophic failure. Currently, no universally-accepted criteria for damage exist. It is expected, however, that as a result of increased focus on service life prediction for reinforced concrete structures, criteria will be developed in the near future.

## SUMMARY

A preliminary corrosion investigation of piles used in the construction of the Deerfield Beach Fishing Pier was performed to assess the performance of the concrete and to establish baseline values for future investigations. Visual and half-cell potential surveys, and sampling for determination of chloride ion contents were performed. Half-cell potentials were found to be high near ground level decreasing toward the top of

pile. In general, the readings were consistent at each elevation and produced a smooth mostly linear curve over the height surveyed. The readings did not indicate corrosion. This was confirmed by a section of the No. 5 gage spiral steel exposed during coring that was examined and found not to be corroding.

Chloride data indicate that the pile cap samples had the highest chloride contents at the 1-1/2 to 3 in. (38 to 75 mm) depths compared to all the pile samples. The piles were fabricated from concrete containing a water-based organic corrosion inhibitor, which also reduces chloride ingress into concrete. The pile caps do not contain this inhibitor. The limited data indicates that the pile cap, which also has the least exposure to saltwater splash, may be more permeable than the piles. Chloride data from this investigation as well as future ones will be used to determine an effective chloride diffusion coefficient for the concrete to facilitate prediction of the time to corrosion initiation in the piles.

## REFERENCES

- [1] Burke, D.F., "Performance of Epoxy-coated Rebar, Galvanized Rebar, and Plain Rebar with Calcium Nitrite in a Marine Environment," Corrosion and Corrosion Protection of Steel in Concrete, Vol. 2, R. Narayan Swamy, Ed., Sheffield Academic Press, July 1994, pp. 1254 - 1266.
- [2] Sagues, A., Powers, R., and Zayed, A., "Marine Environment Corrosion of Epoxy-Coated Reinforcing Steel," Corrosion of Reinforcement in Concrete, C. Page, K. Treadaway and P. Bamforth, Eds., Elsevier Appl.Sci., London-NewYork, 1990, pp. 539-549.
- [3] Scannell, W.T., and Sohahngpurwala, A.A., "Rehabilitation of Reinforced Concrete Balconies on a Multi-Story Condominium in South Florida," Paper No. 202, CORROSION 92, NACE, 1992, 16 pp.
- [4] City of Deerfield Beach, "Engineering Report - Structural Investigation of the Deerfield Beach Fishing Pier," CH2M Hill Report on Investigation of Deerfield Beach Fishing Pier, Oct. 1988, 13 pp.
- [5] Fidjestol, P., and Nilsen, N., "Field Test of Reinforcement Corrosion in Concrete," Performance of Concrete in Marine Environment, SP-65, American Concrete Institute, Detroit, Michigan, Aug. 1980, pp. 205-221.
- [6] Sharp, J.V., Figg, J.W., and Leeming, M.B., "The Assessment of Corrosion of the Reinforcement in Marine Concrete by Electrochemical and Other Methods," Concrete in Marine Environment - Proceedings of the Second International Conference, SP-109, St. Andrews by-the-Sea, Canada, V.M. Malhotra, Ed., Aug. 1988, pp. 105-125.

- [7] Nmai, C.K., Farrington, S.A., and Bobrowski, G.S., "Organic-Based Corrosion-Inhibiting Admixture for Reinforced Concrete," *Concrete International*, American Concrete Institute, Vol. 14, No. 4, April 1992, pp. 45-51.
- [8] Tuutti, K., "Service Life of Structures with Regard to Corrosion of Embedded Steel," Performance of Concrete in Marine Environment, SP-65, American Concrete Institute, Detroit, Michigan, Aug. 1980, pp. 223-236.
- [9] PROTECTIVE SYSTEMS FOR NEW PRESTRESSED AND SUBSTRUCTURE CONCRETE, U.S. Department of Transportation, Federal Highway Administration, Report No. FHWA/RD-86/193, April 1987, 126 pp.
- [10] Clear, K.C., "Measuring Rate of Corrosion of Steel in Field Concrete Structures," Concrete Bridge Design and Maintenance: Steel Corrosion in Concrete, Transportation Research Record 1211, pp. 28-37.
- [11] Andrade, C., Castelo, V., Alonso, C., and Gonzalez, J.A., "The Determination of the Corrosion Rate of Steel Embedded in Concrete by the Polarization Resistance and AC Impedance Methods," Corrosion Effect of Stray Currents and the Techniques for Evaluating Corrosion of Rebars in Concrete, ASTM STP 906, V. Chaker, Ed., American Society for Testing and Materials, Philadelphia, 1986, pp. 43-63.
- [12] Feliu, S., Gonzalez, J.A., Feliu, S., Jr., and Andrade, M.C., "Polarization Resistance in Reinforced Concrete," *ACI Materials Journal*, Vol. 87, No. 5, Sep./Oct. 1990, pp. 457-460.
- [13] Matsuoka, K., Kihira, H., Ito, S., and Murata, T., Paper No. 121, Presented at NACE Corrosion '87, National Association of Corrosion Engineers, Houston, TX, 1987.
- [14] SHRP-S/FR-92-104, "Condition Evaluation of Concrete Bridges Relative to Reinforcement Corrosion - Volume 2: Method for Measuring the Corrosion Rate of Reinforcing Steel," Strategic Highway Research Program, National Research Council, Washington, D.C., 1992, 105 pp.

Alberto A. Sagiúés<sup>1</sup> and Rodney G. Powers<sup>2</sup>

## **FIELD EXPERIENCE WITH REBAR PROBES TO MONITOR PERFORMANCE OF SPRAYED ZINC GALVANIC ANODES ON CONCRETE**

---

**REFERENCE:** Sagiúés, A. A. and Powers, R. G., “**Field Experience with Rebar Probes to Monitor Performance of Sprayed Zinc Galvanic Anodes on Concrete,**” Techniques to Assess the Corrosion Activity of Steel Reinforced Concrete Structures, ASTM STP 1276, Neal S. Berke, Edward Escalante, Charles Nmai, and David Whiting, Eds., American Society for Testing and Materials, 1996.

**ABSTRACT:** Sprayed zinc galvanic anodes have shown promise as low-cost alternatives to simple gunite repair or even impressed current systems for corrosion-damaged marine substructure of bridges. Because the anodes are permanently connected to the rebar assembly at many points, it is not normally possible to deenergize the anode for measurement of steel polarization and current delivery. Field performance of these systems has been monitored with short embedded rebar probes fitted with external switchable connections. This has allowed for current density, depolarization decay, and polarized potential measurements as a function of time. The anode current delivery has also been measured with isolated cutout anode regions “windows”, and in one case with a specially designed, fully disconnectable anode. The results of the different means of evaluating system performance over several years are compared for various field installations in Florida. The relative merits of the monitoring methods and the information they provide on the corrosion condition of the steel are analyzed.

**KEYWORDS:** corrosion, concrete, cathodic protection, probes, polarization decay, errors, anodes

---

## **INTRODUCTION**

Sprayed zinc galvanic anodes have been used in recent years for the control of corrosion of reinforcing steel in marine substructures [1-3]. An advantage of these anodes is that, unlike in the case of impressed current systems, it is not necessary for adequate operation to remove random short circuits between the anode and the

---

<sup>1</sup>Professor, Department of Civil Engineering and Mechanics, University of South Florida, Tampa, FL 33620.

<sup>2</sup>Assistant State Corrosion Engineer, Materials Office, Florida Department of Transportation, 2006 N.E. Waldo Rd., Gainesville, FL 32601.

reinforcing steel, thus avoiding a time consuming and expensive procedure. Indeed, the sacrificial anode installation can often be made by directly spraying zinc over the exposed steel in a spall area after cleaning the surface [4]. The simplicity resulting from having a permanently and redundantly connected anode gives rise to some performance monitoring problems. Because the anode cannot be easily disconnected from the structure steel, conventional current delivery and steel depolarization measurements to determine protection efficiency are usually not feasible.

Alternative procedures to permit monitoring of the anode performance have been developed at several field installations described in detail elsewhere [1]. Measurements of anode current density delivery were conducted by isolating small portions of the anode, called "windows", 30 cm by 30 cm in size (900 cm<sup>2</sup>, ~1 ft<sup>2</sup>). A window was made on the already deposited anode (typically 0.4 mm thick) by making a shallow cut around the window perimeter with a 6 mm wide concrete saw blade. The window was then connected to the rest of the anode (and hence to the reinforcing steel) by means of a short stainless steel strap and bolted contacts. The current delivered by the window could then be measured directly by temporarily removing the strap and inserting a low resistance (<5Ω) ammeter. Division of the current by the window area yielded the effective current density delivered by the anode window. Since the anodes were placed on flat concrete surfaces or on relatively large diameter structural elements, the current flow was approximately uniform toward the underlying reinforcing steel. For most of the structural elements tested, the ratio of the area of underlying steel to the area of concrete surface was approximately 1:1, so that the anode current density was also approximately equal to the steel current density. The concrete cover was typically 5 cm to 10 cm (2 in to 4 in).

The effectiveness of a cathodic protection system is often assessed by means of a depolarization test. In such test the steel is temporarily disconnected from the anode, and the potential of the disconnected steel is monitored as a function of time. The potential of the steel is expected to shift toward more noble values because the cathodic current is no longer present. The extent of the shift in the noble direction is then indicative of the amount of polarization provided by the cathodic protection system. Shifts exceeding 100 mV during a period of several (typically 4) hours are commonly interpreted as being indicative of adequate protection [5]. Useful measurements of steel depolarization by disconnecting only a window and monitoring the potential of the steel underneath are not possible, because enough residual current from the surrounding anode regions would remain to make the test uncertain. To permit evaluation of the protective action of the galvanic systems, short independent rebar probes were embedded in the concrete at the time of anode application.

The probes consisted of a short segment of #4 (12.7 mm diameter) plain steel rebar, with a No. 14 insulated copper strand wire electrically connected by crimping to one of the ends of the rebar segment. The wire connection end and the opposite end were coated with an epoxy potting compound, leaving exposed 2 in<sup>2</sup> (6.3 cm<sup>2</sup>) of the lateral rebar surface. The probes were installed by first drilling a 2 inch (5 cm) diameter hole perpendicular to the concrete surface using a hollow core drill, to the

depth desired for the probe. The core was then broken off to obtain a flat hole bottom. The probe was positioned parallel to the hole bottom (Figure 1). The hole was then filled with mortar using silica sand, type II cement, and a water/cement ratio near 0.4, to obtain a low-slump mix that would not spill easily from the hole. Seawater was used for the mix, resulting in an as-cast chloride content of about 4 to 8 Kg/m<sup>3</sup> (7 to 14 pounds per cubic yard, pcy), representative of that of the surrounding concrete.

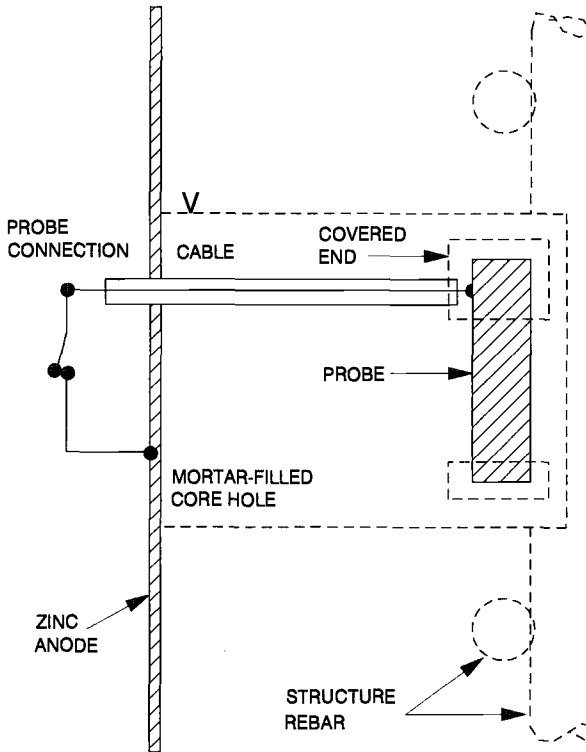


FIG. 1-- Rebar probe installation.

Probes and test windows of the types described above were installed at test locations of four bridges in the Florida Keys, and another bridge in Tampa Bay (see Table 1). Three of the bridges in the Florida Keys were built using epoxy-coated rebar (ECR), which had undergone severe corrosion by the time of the anode installation [6]. The remaining bridges used conventional plain rebar and were also experiencing corrosion damage at the time of anode installation. A detailed description of the systems is given in References 1 - 3.

Table 1-- Field Installations

BRIDGE	BRIDGE LOCATION	ANODE INSTALLATIONS	REBAR TYPE
NILES CHANNEL (NC)	U.S. 1 (FLORIDA KEYS)	COLUMNS, STRUTS	ECR
SEVEN MILE (SM)	U.S. 1 (FLORIDA KEYS)	COLUMNS, STRUT	ECR
LONG KEY (LK)	U.S. 1 (FLORIDA KEYS)	STRUT	ECR
BAHIA HONDA (BH)	U.S. 1 (FLORIDA KEYS)	COLUMNS, STRUT	PLAIN
HOWARD FRANKLAND (HF)	I 275 (TAMPA BAY)	PILE CAP BEAMS UNDERDECK	PLAIN

In the HF bridge one of the pile caps and an underdeck segments were carefully processed to permit disconnection of the entire anode from the structure steel, thus allowing for direct determination of polarization effects and comparison with the test window and rebar probe behavior.

## RESULTS

### Current density of test windows and rebar probes.

Figure 2 shows the current densities (averaged for all the probes at each of the test sites) measured at various times over a period of two years for the bridges in the Florida Keys. The graph compares the current densities of the probes with the current densities of the adjacent test windows. The diagonal line corresponds to ideal 1:1 correlation between both measurements. The overall averages for the BH and NC bridges fall close to the ideal correlation, but the probe current densities for the LK and SM bridges are on average one order of magnitude greater than the corresponding test window values. Figure 3 shows a similar comparison for the data from the HF bridge. Because the system had been in operation for approximately only one year, the data shown are only for the last set of field measurements, which were taken near the end of the year. The results in Figure 3 are for individual window locations, as well as for the two locations where the entire anode could be disconnected. With the exception of one beam structural element (set of three data at the upper left corner), the probe and test window current densities tended on average to be within a factor of two of each other. A similar degree of agreement existed with the entire anode-disconnectable elements (labeled DECK and STRUC).

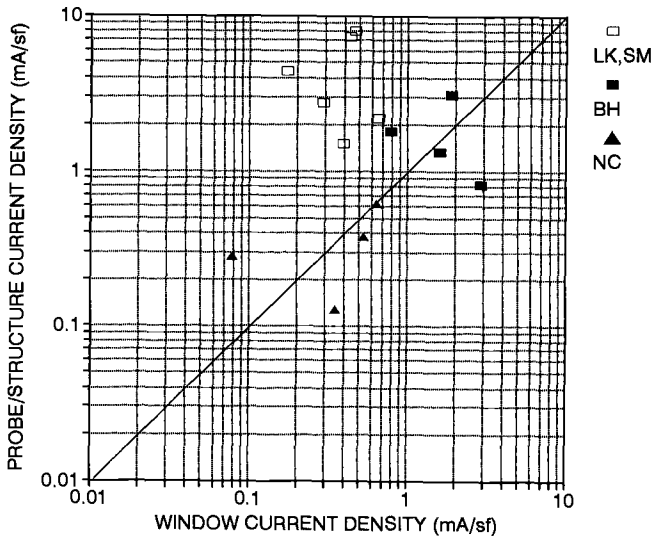


FIG. 2-- Rebar probe and test window current densities, Florida Keys bridges.  
 $1 \text{ mA/sf} = 1.08 \text{ } \mu\text{A/cm}^2$

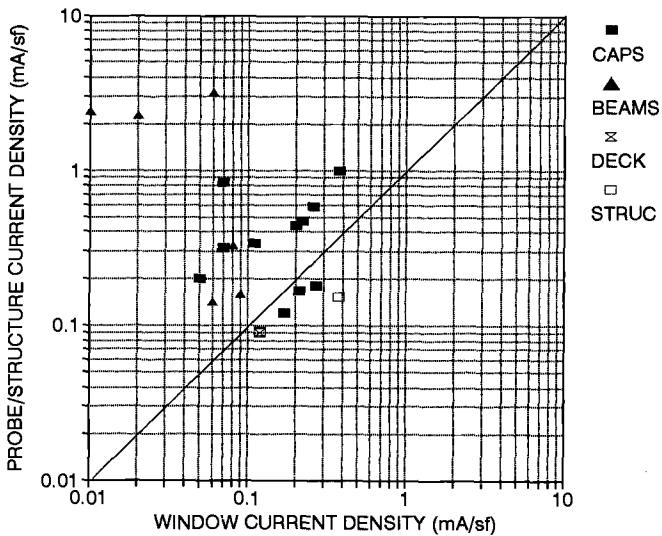


FIG. 3-- Rebar probe and test window (or entire rebar assembly for Deck and Structure portion of a selected element) current densities, Howard Frankland bridge.  
 $1 \text{ mA/sf} = 1.08 \text{ } \mu\text{A/cm}^2$

Polarization decay measurements.

Figure 4 shows the polarization decay measurements (times ranging from 1 h to 24 h following disconnection of the probe) as a function of probe current density for all the locations tested. The values for the HF bridge are for individual probes after about one year of testing; the values for the Florida Keys bridges are averaged for each structural element and taken at various times over a two year test period. The values designated HF STR correspond to both the deck and pile cap that had disconnectable anodes. The large majority of the tests show depolarization values that exceed 100 mV. The extent of depolarization increased with current density in both the HF and Florida Keys locations. A straight-line fit of the results in the potential-logarithm of current density plot yielded slopes of about 60 mV/decade and 100 mV/decade for the Florida Keys and Howard Frankland locations respectively. The polarization decay values of the elements with disconnectable anodes were generally comparable with those of the rebar probes.

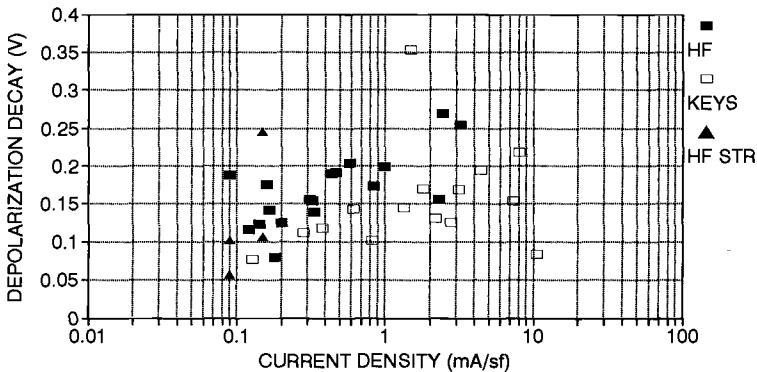


FIG 4-- Depolarization of rebar probes at Howard Frankland and Keys locations (HF, KEYS) and entire rebar assembly for Deck and Structure portion of a selected element of the HF bridge (HF STR) as a function of current density.  $1 \text{ mA/sf} = 1.08 \mu\text{A/cm}^2$

## DISCUSSION

Because the ratio of steel surface area to external concrete surface area is approximately 1:1 in the structures examined, comparison of anode current density to probe current density can be made directly, in the manner shown in Figures 2 and 3. In the Florida Keys location with plain rebar (BH), the probe and window current densities were reasonably similar, considering the scatter expected from field measurements and characteristic of most electrochemical corrosion evaluations. Two of the three remaining Florida Keys locations showed probe current densities that were much greater than those of the test windows. This is not surprising because those

three structures contained ECR, which is expected to sustain a lower current density than uncoated steel as the protective current must be delivered only at points where coating breaks are present. Thus in those structures the plain steel probes tended to receive a greater current density than the average value for the rest of the structure. The plain steel probes under those conditions serve only as a means of monitoring the anode ability to deliver current, but cannot provide a quantitative indication of the amount of polarization to the corroding ECR structure. In principle, short segments of ECR could be configured like the plain steel probes and serve for these structures. However, the corrosion mechanism of ECR is complex [6] and corrosion may require a long time to develop. Therefore, it is not clear whether small ECR probes could provide a sufficiently useful representation of the condition of the surrounding material.

In the HF location the current densities were generally smaller, reflecting the moderate degree of corrosion encountered in the portions of that structure that were examined [3]. The probes and reinforcing steel were plain rebar, and agreement between window and probe current densities was reasonable with the exception of a set of three probes from one of the beams. Examination of the field data failed to reveal a reason for the discrepancy in that beam. Agreement between the current densities of the test windows with those of the structural elements with fully disconnectable anodes was also reasonable.

The amount of depolarization obtained with the test probes followed the expected trends (increasing with magnitude of the current density) and was of the order typically encountered in impressed current systems for reinforcing steel with similar current densities [7]. There was good agreement with the behavior of the entire anode/structure depolarization when similar tests were performed with the elements were disconnection of the entire assembly was possible. The magnitude of the depolarization was suggestive of adequate polarization performance in most cases [1]. The approximate potential-log current density slopes were on the order of those expected for situations where cathodic oxygen reduction is present, as would be expected for cathodic protection of steel in concrete [8].

The results presented above suggest that the probes and test windows provided a useful means of assessing the system performance for situations such as the present one when complete anode disconnection is not feasible. The scatter of the results suggests that multiple probes should be placed in any system to be characterized, and that caution should be used when interpreting the results.

Caution is in order also when considering the absolute potentials of the probes, as measured by an electrode placed on the external concrete surface. Even with simple steel configurations and without external anodes, the measured steel potential may be sensitive to the exact placement of the reference electrode tip and on the condition of the concrete surface [9]. Additional complications exist for the present system. Figure 5 is a schematic of a sacrificial CP system for which a potential measurement is performed. When the anode is connected to the structure, the electrochemical circuit includes the current  $I$  (shown as an electronic current, direction

opposite to conventional current) through the wire connecting anode with steel, and the return ionic current  $I$  (shown as a net negative ion current) through the concrete.  $V_{cs}$  is the potential of the concrete immediately next to the steel, and  $V_{ca}$  the concrete potential at the external concrete surface. All potentials are given in the scale corresponding to the reference electrode used.  $V_{ca}$  and  $V_{cs}$  differ from each other by an amount equal to  $I R$ , where  $R$  is the resistance of the intervening concrete between the anode and the steel. The voltmeter reads a potential  $V_r$  (which in the connected system is the same whether the  $+$  lead of the voltmeter is connected to the steel or to the anode, assuming that the connecting wire has negligible resistance).

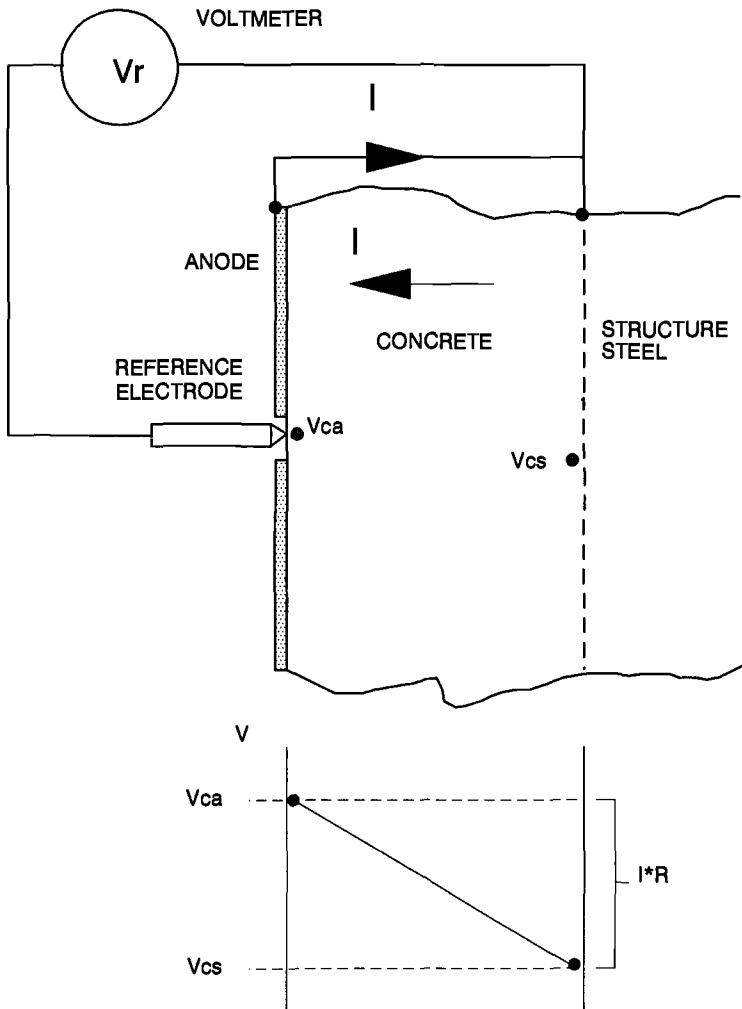


FIG 5-- Schematic for the evaluation of potential measurements of a system in which the entire steel assembly can be disconnected from the anode.

To illustrate the behavior of a rebar probe during a polarization decay test, assume first that the connection between anode and the entire steel structure could be broken at will. Before the connection is broken:

$$I R = I R_o \quad (1a)$$

$$V_{cs} = V_{cs_o} \quad (1b)$$

$$V_{ca} = V_{cs_o} + I R_o \quad (1c)$$

$$V_r = -V_{cs_o} + I R_o \quad (1d)$$

Immediately after disconnection (the "instant-off" condition) and with the voltmeter always connected to the anode:

$$I R = 0 \quad (2a)$$

$$V_{cs} = V_{cs_o} \quad (2b)$$

$$V_{ca} = V_{cs_o} \quad (2d)$$

$$V_r = -V_{cs_o} \quad (2e)$$

After depolarization:

$$I R = 0 \quad (3a)$$

$$V_{cs} = V_{cs_{dep}} \quad (3b)$$

$$V_{ca} = V_{cs_{dep}} \quad (3c)$$

$$V_r = -V_{cs_{dep}} \quad (3d)$$

Therefore, the change in  $V_r$  during the polarization decay test is

$$\Delta V_r = -\Delta V_{cs} \quad (4)$$

and the voltmeter registers the true polarization decay at the steel surface. Also, the voltmeter reading following instant-off corresponds to the true potentials at the steel-concrete interface.

When only a small portion of the steel (the rebar probe) can be disconnected, conditions are different than in the previous case. See Figure 6. The + lead of the voltmeter is now connected to the rebar probe.  $V_{cs1}$  is the potential of the concrete immediately next to the probe.

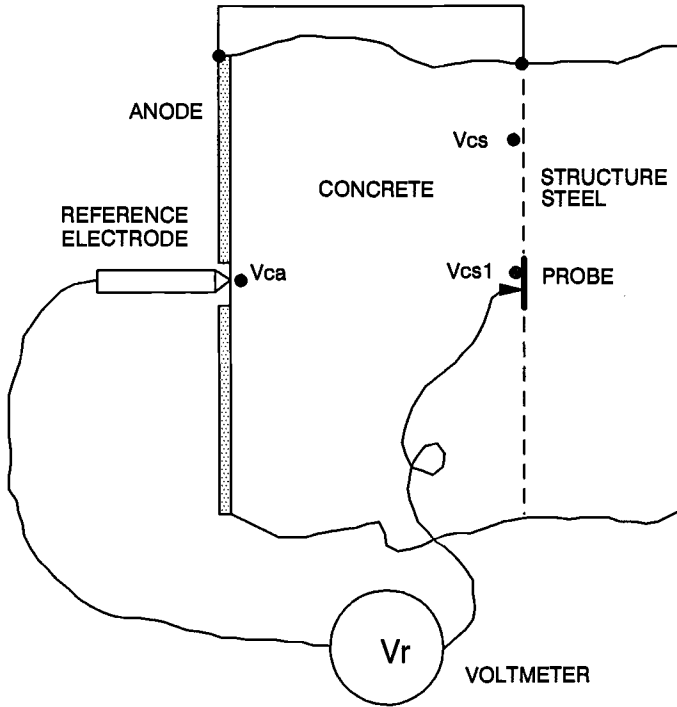


FIG 6-- Schematic for the evaluation of potential measurements of a system in which only the rebar probe can be disconnected from the rest of the system.

Before disconnecting the rebar probe from the rest of the anode-structure:

$$I R = I R_o \tag{5a}$$

$$V_{cs1} = V_{cs} = V_{cs1_o} = V_{cs_o} \tag{5b}$$

$$V_{ca} = V_{cs1_o} + I R_o \tag{5c}$$

Immediately after disconnection of the probe from the rest of the system (the "instant-off" condition) and with the voltmeter always connected to the probe:

$$I R = (I - I_p) R \approx I R_o \text{ (since } I_p \ll I) \tag{6a}$$

$$V_{cs1} \approx V_{cs1_o} + I R_o \tag{6b}$$

$$V_r \approx -V_{cs1_o} + I R_o \tag{6c}$$

After depolarization:

$$I R \approx I R_o \quad (7a)$$

$$V_{cs1} = V_{cs1_{dep}} \quad (7b)$$

$$V_{ca} \approx V_{cs1_{dep}} + I R_o \quad (7c)$$

$$V_r \approx -V_{cs1_{dep}} - I R_o \quad (7d)$$

As a result, the change in  $V_r$  during the polarization decay test is:

$$\Delta V_r \approx -\Delta V_{cs1} \quad (8)$$

and the voltmeter registers approximately the true polarization decay of the rebar probe surface. However, the voltmeter reading following instant-off is still affected by the overall IR drop of the system because disconnecting the probe changes very little the overall current across the concrete cover between the external surface and the rebar mat. This is substantiated by measurements of the potential change upon disconnection of the entire anode in the components so fitted of the HF bridge. IR drop there was in the order of 100 to 300 mV. Disconnection of rebar probes caused instantaneous potential changes of only typically 3 mV. As a result of this effect, depolarization tests with the rebar probes are reasonably accurate but the measured instant-off potentials of the rebar probes are typically 100 to 300 mV more negative than the actual value polarized potential of the probes.

This paper is limited to the suitability of the rebar probes and test windows to assess system performance. For information on the overall effectiveness of the sacrificial sprayed anode cathodic protection systems, the reader is referred to References 1- 4.

## CONCLUSIONS

1. The rebar probes could be installed easily and reliably under field conditions in a variety of marine bridge substructures.
2. Current density delivery to the probes was reasonably comparable to the anode current density and to the structure steel current density in plain rebar systems with steel-concrete surface ratios approaching 1:1. The current density of the plain rebar probes exceeded significantly that of the surrounding reinforcing steel in epoxy-coated rebar systems.
3. Field polarization measurements were successfully conducted with the rebar probes over a period of several years.
4. The instant-off potential reading with the rebar probes still includes most of the

overall IR drop of the system.

5. The IR drop remains nearly constant during the polarization decay test of the probes, so that the actual decay of the probe can be measured with sufficient accuracy.

## ACKNOWLEDGMENT

This investigation was supported by the Strategic Highway Research Program, Contract SHRP ID-024, the National Cooperative Highway Research Program, Contract NCHRP-92-ID024B, and the Florida Department of Transportation. The findings and opinions in this paper are those of the authors and not necessarily those of the supporting agencies.

## REFERENCES

- [1] Sagüés A. A. and Powers, R.G., "Sprayed-Zinc Sacrificial Anodes for Reinforced Concrete in Marine Service", Paper No. 515, Corrosion/95, NACE International, Houston, 1995.
- [2] Sagüés, A. and Powers, R., "Low-Cost Sprayed Zinc Galvanic Anode for Control of Corrosion of Reinforcing Steel in Marine Bridge Substructures", Final Report, Contract No. SHRP-88-ID024, Strategic Highway Research Program, Washington, 1993.
- [3] Sagüés, A. and Powers, R., "Sprayed Zinc Galvanic Anode for Corrosion Protection of Marine Substructure Reinforced Concrete", Volumes I and II, Final Report, NCHRP Contract NCHRP-92-ID024B, National Cooperative Highway Research Program, National Research Council, Washington, D.C., 1995.
- [4] R. Kessler and R. Powers, "Zinc Metallizing for Galvanic Cathodic Protection of Steel reinforced Concrete in a Marine Environment", Paper No. 324, Corrosion/90, NACE International, Houston, 1990.
- [5] J.Bennett, J. Bartholomew and T. Turk, "Cathodic Protection Criteria Related Studies Under SHRP Contract", Paper No. 323, Corrosion/93, NACE International, Houston, 1993.
- [6] Sagüés, A., Powers, R. and Kessler, R., "Corrosion Processes and Field Performance of Epoxy-Coated Reinforcing Steel in Marine Substructures", Paper No. 299, Corrosion/94, National Association of Corrosion Engineers, Houston, 1994.
- [7] Broomfield, J., "Results of a Field Survey of Cathodic Protection Systems on North American Bridges", Paper No. 204, Corrosion/92, NACE, Houston, 1992.
- [8] Bartholomew, J. et al, "Control Criteria and Materials Performance Studies for Cathodic Protection of Reinforced Concrete", Report SHRP-S-670, Strategic Highway Research Program, National Research Council, Washington, 1993.
- [9] Bennett, J. and Mitchell, T., "Reference Electrodes for use with Reinforced Concrete Structures", Paper No. 191, Corrosion/92, NACE International, Houston, 1992.

William J. Brickey<sup>1</sup>

## **A CASE STUDY: ASSESSMENT OF ICE RINK REFRIGERANT TUBING CORROSION USING HALF CELL TECHNIQUES**

---

**REFERENCE:** Brickey, W. J., "A Case Study: Assessment of Ice Rink Refrigerant Tubing Corrosion Using Half Cell Techniques," Techniques to Assess the Corrosion Activity of Steel Reinforced Concrete Structures, ASTM STP 1276, Neal S. Berke, Edward Escalante, Charles K. Nmai, and David Whiting, Eds., American Society for Testing and Materials, 1996.

**ABSTRACT:** This paper describes a corrosion study performed on an ice rink. The purpose of the study was to evaluate the extent and increase in corrosion of low carbon steel refrigeration tubes and the reinforcing steel embedded in a concrete slab-on-grade. A copper-copper sulfate half cell was used in the assessment. Chemical analyses, microscopic examinations and destructive examinations were used to supplement and confirm the results of the half cell testing.

An increase in corrosion activity was determined by comparing the results of half cell surveys conducted in 1989 and 1990. The cause of the corrosion activity was determined from chemical analyses, microscopic examinations and destructive techniques.

**KEY WORDS:** Corrosion, chlorides, half cell potential surveys

There has been much written on the subject of embedded reinforcement corrosion, especially chloride induced corrosion associated with chloride containing concrete ingredients and de-icing salts. During the literature search phase of the study to determine the cause of ice rink refrigerant tubing corrosion, no information could be found about similar studies. This paper describes the results of a corrosion study where the primary embedded steel being studied is not reinforcing steel and the chloride is from a source other than concrete ingredients or de-icing salts.

---

### **Background**

The subject ice rink is located outdoors on a college campus in western North Carolina. At the time of the study, the rink was approximately 5 years old. Construction drawings

---

<sup>1</sup> William J. Brickey, P.E., Managing Principal, Law Engineering and Environmental Services, Inc., 4634 South 36th Place, Phoenix, AZ 85040

indicated that the ice rink floor was a 75mm thick reinforced concrete slab-on-grade with approximate plan dimensions of 42 meters by 26 meters.

Supply and return headers for the R-22 refrigerant were located within thickened edges constructed monolithically with the concrete slab at the short dimension ends of the ice rink. Refrigerant tubing, spaced 100mm on center, was placed between two layers of reinforcement. The bottom layer of reinforcement consisted of No. 4 bars spaced 450mm on center in both directions. A 6X6-10/10 welded wire fabric was used for the top layer of reinforcement. Refrigeration tubes were specified as 16mm outside diameter, 1.25mm wall thickness ASTM A53 material. A longitudinal cross section of the ice rink is shown in Figure 1.

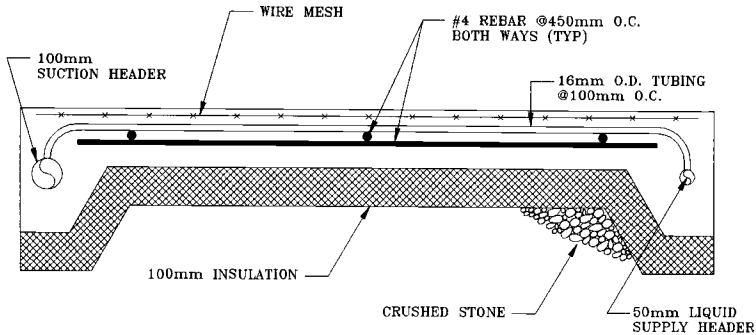


FIG. 1 --Longitudinal cross section of ice rink.

The ice rink was constructed in 1984. Loss of refrigerant reportedly began within a few years of construction and progressively increased over the next several years. In November, 1989, a half cell potential survey of the concrete rink floor was performed. The results of the survey were used to select repair areas where corroded refrigeration tubes were removed and replaced. These repairs were made just prior to opening the rink for the winter 1989/90 season.

Leaks continued throughout the winter 1989/90 season. A second half cell potential survey of the concrete rink floor was performed in October/ November 1990. The results of this half cell potential survey and subsequent repair attempts revealed that the corrosion problem had become more extensive. After failed attempts to repair the rink, a study was performed to determine the cause of the corrosion and the feasibility of repair.

### Study Procedures

Visual, non-destructive, destructive, and chemical methods were used to define the extent and cause of refrigerant tubing corrosion. The non-destructive methods consisted of obtaining half cell potential survey data and locating embedded steel using magnetic techniques. Destructive methods included removing concrete cover over embedded steel

that had been previously located using the non-destructive magnetic methods and drilling concrete cores from the ice rink floor. Concrete cover and core samples were returned to the laboratory where they were visually examined and tested for water soluble chlorides. The laboratory examinations included a microscopic examination of polished sections prepared from concrete cores and examinations of refrigerant tubing samples with the unaided eye and at low magnifications.

### Half Cell Potential Survey Results

The half cell potential surveys were performed in November 1989 and October/November 1990. A copper-copper sulfate half cell was used and the test was conducted in accordance with ASTM Standard Test Method for Half Cell Potentials of Uncoated Reinforcing Steel in Concrete (C 876-87). Half cell measurements were initially made on a 2.7 meter (9 feet) grid pattern. Additional measurements were made at core and concrete cover sampling locations and between selected grid points to better define the areas where the probability of corrosion was high.

The data were analyzed using procedures outlined in ASTM C 876. Equipotential contour maps developed from the 1989 and 1990 data are shown in Figures 2 and 3, respectively. The percentage of half cell potential readings more negative than -0.35 volts (high corrosion probability) and less negative than -0.20 volts (low corrosion probability) were also determined for both the 1989 and 1990 data. This information is summarized in Table 1.

TABLE 1 -- Summary of half cell potential readings.

Survey date	Number of Readings	Readings Less Negative Than - 0.20 Volts, %	Readings More Negative Than - 0.35 Volts, %
1989	185	62	8
1990	186	51	11

### Visual Condition Survey Observations

The condition of the rink was visually assessed approximately one month after the second half cell survey had been completed (November 1990). Repairs were being made to the rink at the time of the visual condition survey.

The concrete had been chipped away in the repair areas located at the refrigerant supply and return ends of the rink. Within these repair areas, sections of corroded tubing had been replaced with new tubing. Connections between the existing and replacement tubing were made with ferrule type connectors. Tubing samples removed from repair

areas were moderately to severely corroded. The reinforcing steel in the repair areas was moderately corroded.

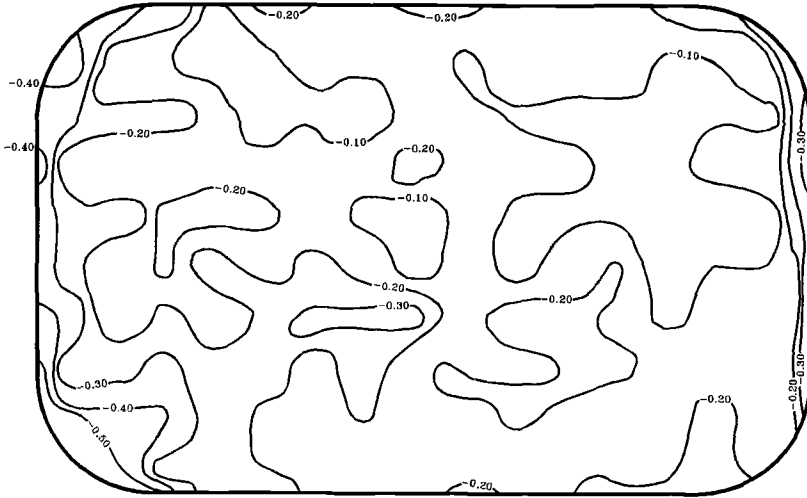


FIG. 2 --Equipotential contour map - 1989 survey (potential values are expressed in volts).

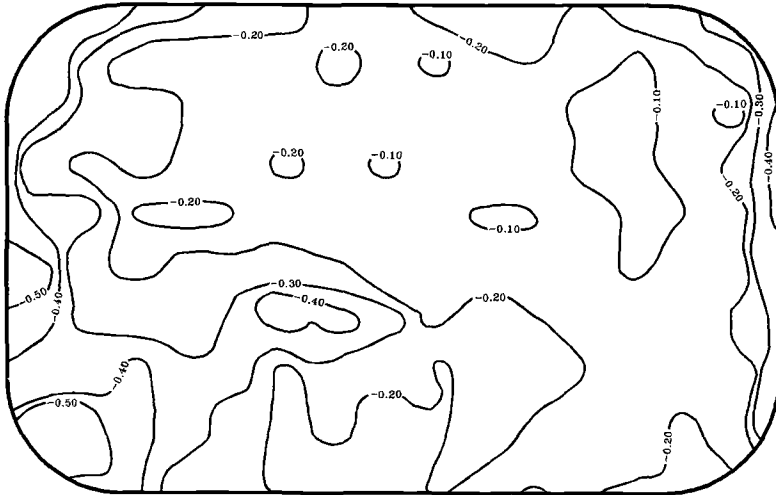


FIG. 3 --Equipotential contour map - 1990 survey (potential values are expressed in volts).

After measuring the voltage potential, the concrete cover over the tubing and wire mesh was chipped away at five test pit locations. Half cell potentials were more negative than  $-0.35$  volts at three of the test pit locations and less negative than  $-0.29$  volts at the

remaining two locations. The tubing and reinforcing steel was moderately corroded at the locations where the half cell potentials were more negative than -0.35 volts. Very slight to no corrosion was observed at locations where the potentials were less negative than -0.29 volts.

In the repair areas, the concrete cover over the tubing ranged from 19mm to 35mm and averaged approximately 25mm. The cover over the wire mesh was generally less than 12mm. The total concrete thickness was approximately 140mm.

Water ponded in many low spots on the rink. It was estimated that the ponding covered more than 30 percent of the rink surface.

### Chemical Analyses of Concrete Samples

Seven samples of the concrete from various locations and depths were tested for pH and the presence of water soluble chlorides. The water soluble chloride analyses were performed in accordance with AASHTO Standard Method of Sampling and Testing for Total Chloride Ion in Concrete and Concrete Raw Materials (T 260-84). The results of the testing are presented in Table 2.

TABLE 2 -- Results of chloride analyses (percent water soluble chlorides are stated as a percentage of an estimated cement content of 312kg per cubic meter of concrete).

Sample Type	Depth, mm	Potential, Volts <sup>1</sup>	pH	Percent Chlorides
Test Pit	0 - 25	-0.48	12.2	0.02
Test Pit	0 - 25	0.56	12.1	0.08
Core	0 - 25	-0.20	12.2	0.16
Core	25-50	-0.63	12.2	0.40
Core	50-75	-0.51	12.2	0.51
Core	50-125	-0.63	12.2	0.37
Repair area debris	75-150	N/A	12.1	0.66

<sup>1</sup> Potential measurements made on surface of ice rink

The chemical analyses revealed that the pH of the concrete was slightly low and most of the samples contained excessive quantities of water soluble chlorides. The percent water soluble chlorides by weight of cement ranged from 0.08 to 0.66 and averaged 0.33. Samples obtained adjacent to or below the tubing had 0.37 to 0.66 percent water soluble chlorides by weight of cement. The concrete cover samples tested had water soluble chloride concentrations ranging from 0.02 to 0.16 percent by weight of cement.

### Laboratory Examination of Concrete and Tubing Samples

Samples of the concrete and corroded tubing were visually examined in the laboratory. Polished sections prepared from two cores were microscopically examined in accordance with ASTM Standard Practice for Petrographic Examination of Hardened Concrete (C 856-83) procedures. The tubing samples were examined with the unaided eye and at low magnifications; (10X or less).

The overall quality of the concrete was judged to be fair based on observations made during the microscopic examinations. The concrete around the reinforcing steel and refrigerant tubes was well compacted. The concrete was air entrained and appeared to be well proportioned. The total air content was estimated to be 5 to 7 percent. The paste was judged to be moderately hard and the water cement ratio was estimated to range from 0.55 to 0.60. The concrete was not significantly carbonated; treating freshly fractured faces with phenolphthalein revealed that the depth of carbonation did not exceed 3mm.

Iron oxide staining was observed in the concrete surrounding the tubing and reinforcing bars and moderate corrosion was observed on the lower half of the reinforcing bars that were cut by the coring process. Severe pitting, which is indicative of micro cell type galvanic corrosion [1], was observed on the reinforcing bars and tubing samples examined. The sections of tubing that had been removed and replaced were slightly to severely corroded. The severity of the corrosion ranged from slight to extensive pitting. In some cases, the pits had penetrated the tube walls.

### Discussion

Reinforcing bars and other ferrous metals embedded in concrete are normally protected from corrosion by a protective layer of iron oxide. In order for corrosion to occur, the steel must be depassivated. Depassivation can occur in the presence of chloride ions or by carbonation of the concrete cover [2]. The results of this study revealed that the depth of concrete carbonation had not yet reached the refrigeration tubing. In fact, the depth of carbonation had not exceeded 3mm in any of the samples examined. However, high levels of water soluble chlorides (0.37 to 0.66 percent by weight of cement) were found in the concrete surrounding the refrigerant tubes and No. 4 reinforcing bars. Currently, it is believed that chloride ion concentrations in excess of 0.2 percent by weight of cement will lead to corrosion of embedded steel, if oxygen and moisture are present [1].

Based on the results of the study, the primary cause of corrosion was attributed to the presence of objectionable quantities of chlorides in the concrete surrounding the refrigerant tubes and reinforcing steel. It was further concluded that the chloride source was not from the mix ingredients (aggregates, cement, water or admixtures) or de-icing salts. These conclusions are based on the variations of water soluble chlorides throughout the depth profile of the slab. It was postulated that the chloride concentrations would have been more uniform if the chloride source was from the mixture ingredients.

The use of de-icing salts would have resulted in high chloride concentrations in the concrete cover material where this study found the chloride concentrations to be the lowest.

After some research [3], it was postulated that the chlorides were introduced into the concrete as a byproduct of the decomposition of the R-22 refrigerant. An R-22 refrigerant molecule, or monochlorodifluoromethane contains 1 chlorine atom, 1 hydrogen atom and two fluorine atoms attached to one carbon atom. In the initial stages of refrigerant decomposition, the carbon-chloride bonds, which are weaker than the carbon-fluorine bonds, were broken in the highly alkaline concrete environment. The chlorine was replaced by hydroxyl and released as chloride ions into the concrete. This reaction is shown in Figure 4.

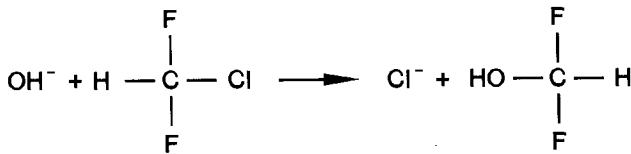


FIG. 4 --Decomposition of R-22 refrigerant.

The corrosion problem is more severe and was first detected at the supply and return ends of the rink. Voltage potentials in these areas were more negative than -0.35 volts, which, according to the ASTM C 876 evaluation criteria, indicated that the probability of corrosion is high. It is believed that the corrosion began at the supply and return ends of the rink because leaks were present in the connections between the refrigerant tubes and the supply and return headers prior to concreting the rink, or they developed shortly after placement of concrete.

A comparison of the equipotential contour maps from 1989 and 1990 revealed that the high corrosion probability areas had increased in size. This increase in corrosion is presented graphically in Figure 5. The increase in corrosion activity can also be seen by examining the data in Table 1. The percentage of voltage potential readings indicating a high probability of corrosion (more negative than -0.35 volts) increased from 8 percent in 1989 to 11 percent in 1990 and the percentage of readings indicating a low probability of corrosion (less negative than -0.20 volts) decreased from 62 percent in 1989 to 51 percent in 1990. This rapid increase in corrosion activity was attributed to additional refrigerant leaks that developed when corrosion pits began to penetrate the refrigerant tube walls, thereby exposing the surrounding concrete to more chlorides.

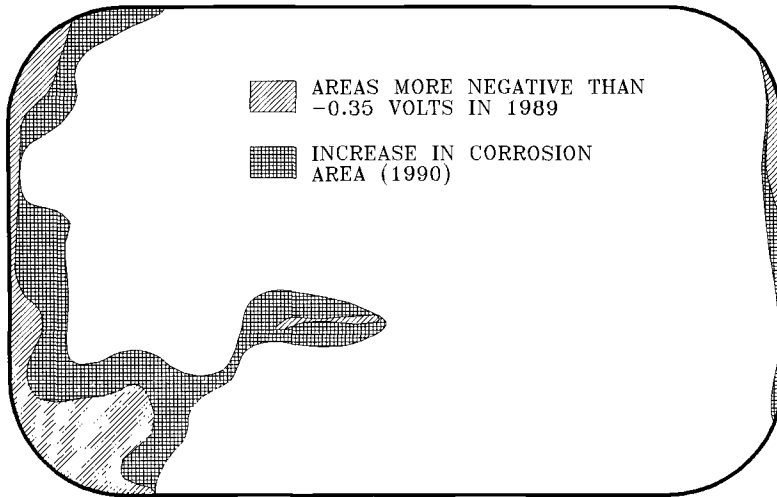


FIG. 5 --Areas of corrosion indicated by 1989 and 1990 survey data.

It was determined that repair of the rink would require that all concrete containing excessive chloride levels be removed. In addition, it would be necessary to confirm that the connections between the refrigeration tubes and supply and return headers were not leaking. Refrigerant leaks through other tube connections and corroded tubes would also have to be identified and repaired. Based on these requirements and the past performance of attempted repairs, it was determined that a satisfactory repair of the rink was not feasible.

### References

- [1] Fraczek, J., "A Review of Electrochemical Principles as Applied to Corrosion of Steel in a Concrete or Grout Environment", Corrosion Concrete, and Chlorides - Steel Corrosion in Concrete: Causes and Restraints, ACI SP - 102, 1987.
- [2] ACI Committee 222, Corrosion of Metals in Concrete, ACI 222R-89, American Concrete Institute, Detroit, 1989, pp 3-8.
- [3] Morrison and Boyd, Organic Chemistry, Allyn And Bacon, Inc., 3rd Edition, 1973, p. 457.

ISBN 0-8031-2009-5